699-70-3

Cassini Program Environmental Impact Statement Supporting Study

Volume 3: Cassini Earth Swingby Plan

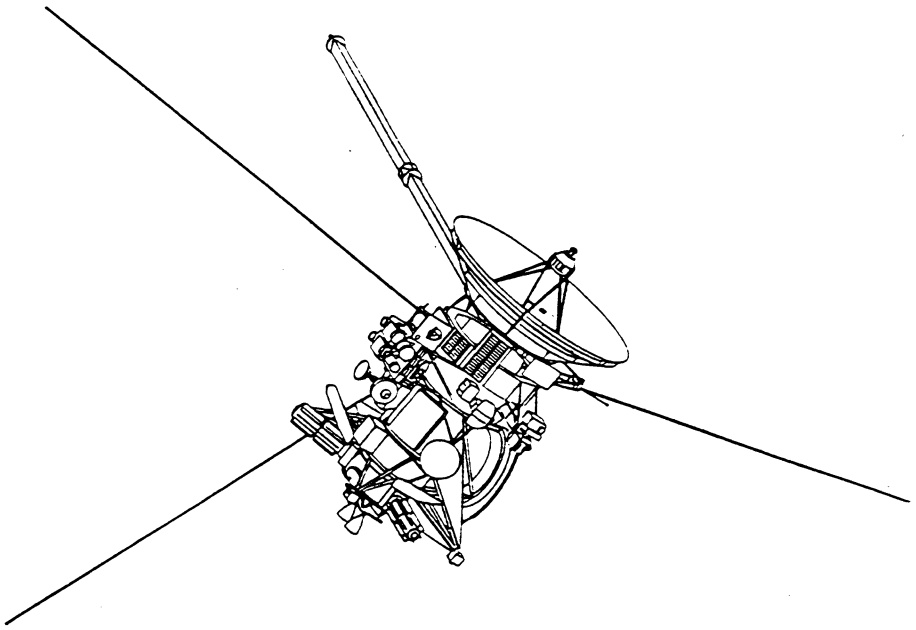

November 18, 1993

JPL
Jet Propulsion Laboratory
California Institute of Technology

JPL D-10178-3

CONTENTS

LIST OF FIGURES

LIST OF TABLES

GLOSSARY OF TERMS AND ACRONYMS

Acronyms and Abbreviations

AACS	Attitude and Articulation Control Subsystem
APP	Automated Picture Planning
ATLO	Assembly, Test, and Launch Operations
AU	Astronomical Unit
BIH	Bureau International de l'Heure
CAPS	Cassini Plasma Spectrograph
CDA	Cosmic Dust Analyzer
CDS	Command and Data Subsystem
CIRS	Composite Infrared Spectrometer
DCS	Data and Computing Services
DOI	Distributed operations Interface
DPTRAJ	Double Precision Trajectory
DSM	Deep Space Maneuver
DSN	Deep Space Network
EFC	Engineering Flight Computers
EIS	Environmental Impact Statement
EPS	Electronic Packaging Subsystem
FSO	Flight Systems Operations
FST	Facility Science Team
HGA	High Gain Antenna
HPOC	Huygens Probe Operations Center
IDRSPS	Intermediate Data Records Stripper Processing System
INMS	Ion and Neutral Mass Spectrometer
IRU	Inertial Reference Unit

ISS	Imaging Science Subsytem
ISS NAC	Imaging Science Subsytem, Narrow Angle Camera
ISS WAC	Imaging Science Subsytem, Wide Angle Camera
LEM	Lower Equipment Module
JPL	Jet Propulsion Laboratory
LGA	Low Gain Antenna
MAG	Magnetometer
ME	Main Engine
MEA	Main Engine Actuator
MET	Mission Elapsed Time
MIF	Micrometeoroid Induced Failure
MIMI	Magnetospheric Imaging Experiment
MIMI HEMS	Magnetospheric Imaging Experiment, Charge-Energy-Mass Spectrometer
MIMI LEMMS	Magnetospheric Imaging Experiment, Low Energy Magnetospheric Measurement System
MLI	Multilayer Insulation
MMH	Monomethyl Hydrazine
Monte Carlo	Statistical simulation technique used to analyze random or probabilistic processes
MOPS	Maneuver Operations Program
MPVT	Mission Planning Virtual Team
N_{CASE}	Number of long-term Monte Carlo cases (initial trajectory states at spacecraft failure times)
N_{CRX}	Number of Earth torus crossings encountered in a long-term Monte Carlo cases
NASA	National Aeronautics and Space Administration
NTO	Nitrogen Tetroxide
ODP	Orbit Determination Program

ONP	Optical Navigation Program
ONIPS	Optical Navigation Image Processing System
$P_F(i)$	Probability of failure for the ith failure mode
P_I	Probability of Earth impact
$P_{I/CRX}$	Probability of Earth impact given that the spacecraft has passed through Earth's torus
$P_{I/F}(i)$	Probability of a resultant Earth impact trajectory given an occurrence of the ith failure mode
$P_{NR}(i)$	Probability of no recovery given the failure mode a the time to impact
PCA	Pressurant Control Assembly
PDF	Probability Density Function
PDS	Project Data System
PIA	Propellant Isolation Assembly
PMS	Propulsion Module Subsystem
PMSEA	Propulsion Module Subsystem, Electronics Assembly
PPS	Power and Pyrotechnics Subsystem
RCS	Reaction Control System
REA	Rocket Engine Assembly
RFEA	Radio Frequency Electronics Assembly
RFIS	Radio Frequency Instrumentation Subsystem
RFS	Radio Frequency Subsystem
RHU	Radioisotope Heater Unit
RPWS	Radio and Plasma Wave Science
RTG	Radioisotope Thermoelectric Generator
RTO	Real Time Operations
S/C	Spacecraft
SCAS	Science Calibration Subsystem

SOI	Saturn Orbit Insertion
SSA	Sun Sensor Assemblies
SSDPS	Solar System Data Processing System
SSR	Solid State Recorder
SVS	Simulation and Verification Services
SVT	Sequence Virtual Team
S/W	Software
TCM	Trajectory Correction Maneuver
TDS	Tracking and Data System
torus	A doughnut-shaped volume, in this report the volume swept out by the Earth in its orbit
UEM	Upper Equipment Module
ULO	Uplink Operations
USS	Upper Shell Structure
UT1	Universal Time
VDM	Valve Driver Module
VEEGA	Venus-Earth-Earth-Gravity-Assist
VIMS	Visible and Infrared Mapping Spectrometer
VIMS IR	Visible and Infrared Mapping Spectrometer-Infrared
VLBI	Very Long Baseline Interferometry
VVEJGA	Venus-Venus-Earth-Jupiter-Gravity-Assist
WRT	With Respect To

OVERVIEW

O.1 INTRODUCTION

The Cassini mission requires trajectories that use planetary swingbys to achieve the necessary energy and orbit shaping to reach Saturn. The proposed baseline trajectory for Cassini is a Venus-Venus-Earth-Jupiter-Gravity-Assist, (VVEJGA) transfer to Saturn. The launch period for this opportunity is in October 1997. As the name implies, the VVEJGA trajectory, makes use of four gravity-assist planetary swingbys between launch from Earth and arrival at Saturn. This use of planetary gravity assists reduces launch energy requirements, compared to other Earth-Saturn transfer modes, and allows the spacecraft to be launched by the Titan IV (SRMU)/Centaur. Direct Earth-Saturn transfers with this launch vehicle are not possible for Cassini.

The baseline plan calls for the Cassini spacecraft to use Radioisotope Thermoelectric Generators (RTGs) to supply electrical power. Therefore, precautions must be taken to ensure that an inadvertent reentry into the Earth's atmosphere, defined for this report as Earth impact, does not occur in the course of performing the Earth swingby. The situation is analogous to previous missions where navigation techniques and mission operations were designed to ensure either Earth impact avoidance (Galileo mission to Jupiter) or Mars protection from microbiological contamination (Mariner and Viking missions to Mars).

Design precautions must also be taken to preclude Earth impact resulting from loss of control of the spacecraft during interplanetary cruise. If the spacecraft were to drift in its orbit around the Sun, Earth impact could result. decades to millennia later after many spacecraft revolutions around the Sun,

In order that an accidental Earth impact not be a credible event, the Cassini Project has levied the following design requirement in its Project Policies and Requirements Document.

> *" Following injection, the probability of Earth impact by the spacecraft shall not exceed 10^{-6} taking into account potential failures."*

To satisfy this requirement an assessment of the Earth impact probability has been performed. The probability of Earth impact is presented as a probability density function (PDF) over the model uncertainty rather than a worst-case value. The advantage of such an approach is to provide information about the uncertainty of the estimation of the Earth impact probability. The above requirement is interpreted to be that the expected value of the Earth impact probability, from injection to 100 years beyond the nominal Saturn encounter date, shall not exceed 10^{-6}.

This report documents a study that has been performed to determine the necessary actions in spacecraft, ground system, and navigation desing to ensure that the probability of Earth impact satisfies the design requirement. Also included is a quantitative assessment of the probability of Earth impact, including uncertainties in the assessment process. This report serves several useful purposes. First, it develops and exercises the approach to be used in the Earth swingby strategy. This provides an early understanding of the Earth impact probability and enables identification of possible failure modes specific to the baseline spacecraft design. Second, it allows the Project to conduct trades among possible measures that reduce Earth impact probability early in the spacecraft and navigation design process. Third, it demonstrates that the navigation strategy will result in a probability of Earth impact that meets the Project's requirement.

O.2 METHODOLOGY

The Earth impact probability is composed of short-term and long-term components. The short-term component is the contribution resulting from the navigation of the Earth swingbys for a given trajectory. The long-term component is the contribution to a disabled spacecraft drifting in orbit about the Sun that could reencounter the Earth sometime beyond the nominal Saturn encounter date. For this analysis, the possibility of impact during the 100 years is considered.

For either component, the Earth impact probability, or P_I, may be expressed as:

$$P_I = \sum_i P_F(i) * P_{\frac{I}{F}}(i) * P_{NR}(i)$$

where

P_I = probability of Earth impact

$P_F(i)$ = probability of failure for ith failure mode

$P_{\frac{I}{F}}(i)$ = probability of a resultant Earth impact trajectory given an occurrence of the ith failure mode

$P_{NR}(i)$ = probability of no recovery given the failure mode and the time to impact - this probability is conditional on the occurrence of the failure and on the spacecraft being on an impact trajectory resulting from the failure

This relationship illustrates several important concepts. First is that there are a number of failure modes that contribute to Earth impact probability. One objective of this study is to identify these failure modes. The $P_{I/F}$ and P_{NR} terms acknowledge that not all failures place the spacecraft on an impacting trajectory nor affect the capability to achieve a successful and safe Earth swingby. An example is the Galileo high gain antenna anomaly that resulted in only a partial deployment of the antenna. This failure did not prevent the precise delivery of the Galilleo spacecraft at the second Earth swingby.

In order to keep the short-term impact probability low, a trajectory-biasing strategy is used to reduce $P_{I/F}$. During most of Cassini's inner solar system journey, the spacecraft is on a trajectory that, without further maneuvers, would miss the Earth by tens of thousands of kilometers. The spacecraft is placed on a trajectory passing through the required Earth swingby point just 10 days prior to the encounter.

A trajectory-biasing strategy selected to control the short-term probability, while affecting the long-term probability, cannot be used to control the long-term probability. Over a long time scale**,** the impact probability is dominated by third-body perturbations to the spacecraft trajectory and by accidental planetary gravity-assist swingbys. Therefore, the long-term Earth impact probability is controlled by designing the spacecraft and mission operations such that the failure probabilities are low.

The P_{NR} term in the impact probability equation factors in the spacecraft's ability to recover and successfully apply a corrective maneuver after a failure. If a failure does not completely incapacitate the spacecraft, then the normal course of action is to accurately determine the spacecraft trajectory and, if required, command a recovery sequence to modify the trajectory and avoid Earth impact.

The Earth impact probability is evaluated for two trajectories. The first trajectory is the primary VVEJGA trajectory. The second trajectory considered in this study is the backup Venus-Earth-Earth-Gravity-Assist (VEEGA) trajectory. The launch period for this trajectory is in March/April 1999.

O.3 FAILURE MODE ANALYSIS

In general, all failures can be classified into three categories: environmentally induced failures, internal spacecraft failures, and ground induced failures. These types of failures can result in an anomalous ΔV (spacecraft velocity change) that could place the spacecraft on an Earth impacting trajectory, and a subset of these failures could prevent the spacecraft from being recovered after being placed on an Earth impact Trajectory.

Of all the failure modes identified in this study, only micrometeoroid-induced tank rupture is a significant contributor the short-term Earth impact probability. The spacecraft design do include components to provide protection froat micrometeoroids, but there are particles with sufficiently high energies to damage the spacecraft. A rupture of a propellant or a pressurant tank will cause an anomalous ΔV and may cause loss of spacecraft commandability. The contribution to Earth impact probability from all other failure modes is more than an order of magnitude less than that from micrometeoroid-induced failures. Other failure modes include stuck-open thruster valves, main engine valve failures, accelerometer failures, main engine gimbal actuator failures, and anomalous Sun searches due to stellar reference unit or inertial reference unit failures. Attitude and Articulation Control Subsystem (AACS) and Command and Data Subsystem (CDS) flight software coding errors are the spacecraft software contributors to Earth impact probability.

Loss due to spacecraft system internal failures is the dominant failure mode for the long-term Earth impact probability. These failures include design and implementation errors, common-mode failures, electronic parts failures, hardware failures, and software errors.

Ground-induced errors are errors made on the ground by the spacecraft controllers, which are then sent to the spacecraft and executed. Two categories of ground-induced errors are erroneous ground commands and navigation design errors. These potential errors are insignificant contributors to Earth impact probability.

For those failures which do not completely disable the spacecraft, additional failures are required to prevent recovery. Until the spacecraft is close to Earth swingby, only new failures which comopletely diasable the spacecraft need to be considered, for other failures can be diagnosed and collected with sufficient time renaming to make another recovery attempt. The primary spacecraft disabling features are micrometeoriod hits and spacecraft system internal failures. For initial failures that occur very close to swingby, there is not enough time to detect the failure and take corrective action. Between these two periods, there is a period before the Earth swingby when there is only time to make one recovery attempt; any subsequent failure is conservatively assumed to abort recovery attempts. The majore contributors during this period are ground failures preventing successful execution of a recovery maneuver and a spacecraft failure requiring ground intervention.

O.4 SHORT-TERM EARTH IMPACT PROBABILITY

The primary objective of the navigation strategy between launch and the Earth swingby is to satisfy the Earth impact probability requirement while delivering the spacecraft to the necessary Earth swingby aimpoint. To calculate the probability of Earth impact requires a knowledge of three factors: the failure probabilities and associated ΔVs, the uncertainties in the navigation process, and the characteristics of the spacecraft trajectory. For the purpose of defining an Earth swingby navigation strategy, steps have been taken to minimize the effect of both failures and navigation uncertainties. The navigation strategy focuses on specifying and controlling the spacecraft trajectory conditions given the failure probabilities and navigation uncertainties.

In general, the impact probability decreases as the swingby altitude increases, so that impact avoidance requirements could be satisfied by simply raising the swingby altitude. However, specific swingby conditions are needed to shape the trajectory, and the spacecraft cannot carry sufficient propellant to replace this effect (except possibly for a very small bias). Fortunately, there would be enough propellant to bring the trajectory in towards the Earth in several steps before the swingby.

In order to calculate a PDF for the short-term Earth impact probability it is necessary to perform a Monte Carlo simulation for both the primary and backup mission trajectories. The mean values for the resulting distributions are $2.0X10^{-7}$ and $6.1x10^{-7}$, respectively.

O.5 LONG-TERM EARTH IMPACT PROBABILITY

The short-term impact analysis establishes that the probability of Earth impact during a targeted Earth swingby is extremely small. However, if the spacecraft becomes uncommandable before Saturn orbit insertion (SOI) and does not impact the Earth during a targeted swingby, there is still a remote possibility that long-term perturbations to the orbit could cause the spacecraft to eventually reencounter the Earth. The long-term analysis computes the probability of Earth impact at a non-targeted swingby from the time of spacecraft failure to 100 years beyond the planned SOI date.

The choice of 100 years is a reasonable benchmark. For trajectories for which long-term impact is possible, the mean time to impact is estimated to range from 10^5 to beyond 10^6 years, but the opportunity for impact is greatest during the first few centuries following injection. The likelihood of impact is greater in the centuries immediately following injection since the spacecraft is targeted for at least one Earth swingby during the interplanetary cruise, resulting in a spacecraft orbit which is initially in the vicinity of Earth's orbit. Long-term perturbations tend to move the spacecraft orbit away from its initial orientation.

To have chosen a longer time reference, a thousand years for example, would have been overly conservative when combined with the short-term risk involving plutonium-238. The hazards associated with plutonium-238 decrease with time. The half-life of plutonium-238 is 88 years; that is to say, the hazard decreases by half every 88 years.

To compute the probability of Earth impact, a knowledge of the spacecraft failure probabilities and associated ΔVs, the uncertainties in the navigation process, and the long-term motion of the spacecraft is required. Only those failures which cause the spacecraft to become uncommandable with no chance of recovery are appropriate for the long-term analysis.

Since a single trajectory propagation would not be representative of the range of possible spacecraft trajectories that could result given a failure at any time during interplanetary cruise, a Monte Carlo analysis was performed using thousands of trajectories considering a wide range of failure times and associated ΔVs. Associated with each case is an initial spacecraft orbital state which is perturbed by navigation uncertainty and any Δvs associated with the failure. Each state is then propagated for 100 years for use in the analysis.

To determine the probability of Earth impact given a failure, use was made of a large body of work refined over the past forty years to estimate the probability of impact by Earth-crossing asteroids. Existing theory which was applicable to lifetime analysis of asteroids and comets was modified to apply to this spacecraft impact analysis. In this method, the number of passages of the spacecraft through the Earth torus (the region of space swept out by the Earth as it orbits the Sun) are used to compute the probability of Earth impact. For an impact to occur, the spacecraft must cross through the Earth torus, and at the time of the crossing, the Earth must be at a position within the torus to cause impact.

The number of torus crossings for all Monte Carlo cases were computed by propagating the initial conditions for each case using a high-precision numerical integration program, and then counting each passage through the Earth torus. For a given torus crossing, Earth-crossing asteroid theory was used to analytically compute the probability of the Earth being in the position required for Earth impact. An uncertainty analysis was performed to yield probability distributions for both the number of torus crossings per case and the probability of Earth impact given a torus crossing. These distributions were combined with the spacecraft failure distribution to yield a PDF for the long-term Earth impact probability.

The mean long-term Earth impact probability for 100 years is 3.7×10^{-8} for the primary mission and 3.6×10^{-7} for the backup mission. The impact probability is larger for the backup mission due to the longer cruise duration and the different interplanetary trajectory

characteristics. An important result is that for failures occurring during the latter half of interplanetary cruise on both missions, in nearly all cases, the spacecraft is quickly ejected from the solar system by a strong Saturn gravity assist, thus precluding any possibility of Earth impact.

As a point of interest, a subset (~20%) of all the Monte Carlo cases was also propagated for 1000 years to study the very long-term probability of Earth impact. The same methodology used for the 100-year cases was used for these 1000-year cases. The mean probability of Earth impact over 1000 years is ~2.5 times higher for the primary mission and ~1.5 times higher for the backup mission than that for a l00-year time period.

0.6 EARTH IMPACT PROBABILITY ASSESSMENT

The Project requirement on the Earth Swingby Plan is that the probability of Earth impact be less than or equal to one in a million (10^{-6}). A number of parameters can be used to describe the characteristics and interpretation of a PDF (or of a complementary cumulative probability curve). The "expected value" of a random variable is expressed by the mean of the probability distribution. Thus, the Project requirement that the probability of Earth impact be less than or equal to 10^{-6} has been considered met when the mean of the assessed probability distribution is less than or equal to 10^{-6}.

The total Earth impact probability distribution is the probabilistic sum of the short-term and long-term Earth impact probability distributions. A 1,000-trial Monte Carlo simulation was used to perform this probabilistic summation. The PDF and complementary cumulative probabilities for the primary and backup trajectories are presented in Figures O-1 thru O-4. The mean values of these distributions are 2.4×10^{-7} for the primary trajectory and 9.7×10^{-7} for the backup trajectory. Since the mean of both distributions is less than 10^{-6}, the Project Earth swingby requirement is satisfied for both missions. For reference, Figures O-2 and O-4 also indicate values below which 90% of the possible Earth impact probabilities lie.

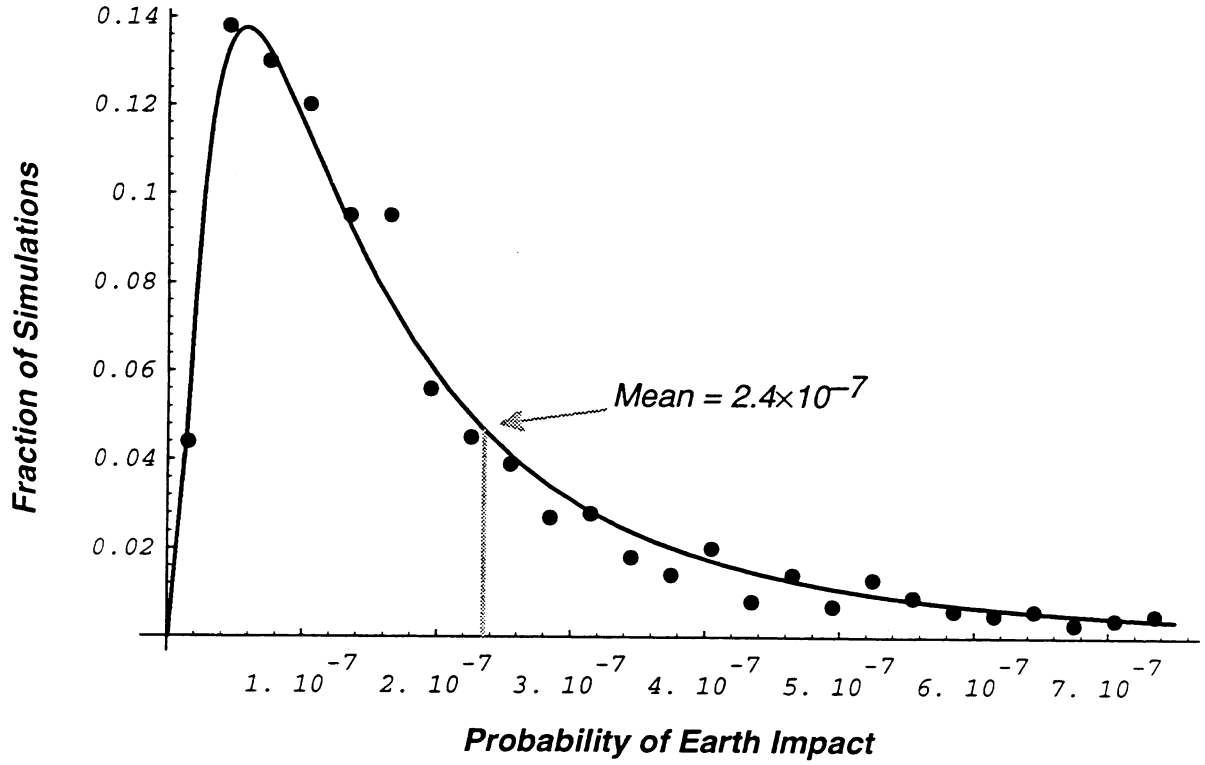

Figure 0-1 Primary Mission Probability Density Function

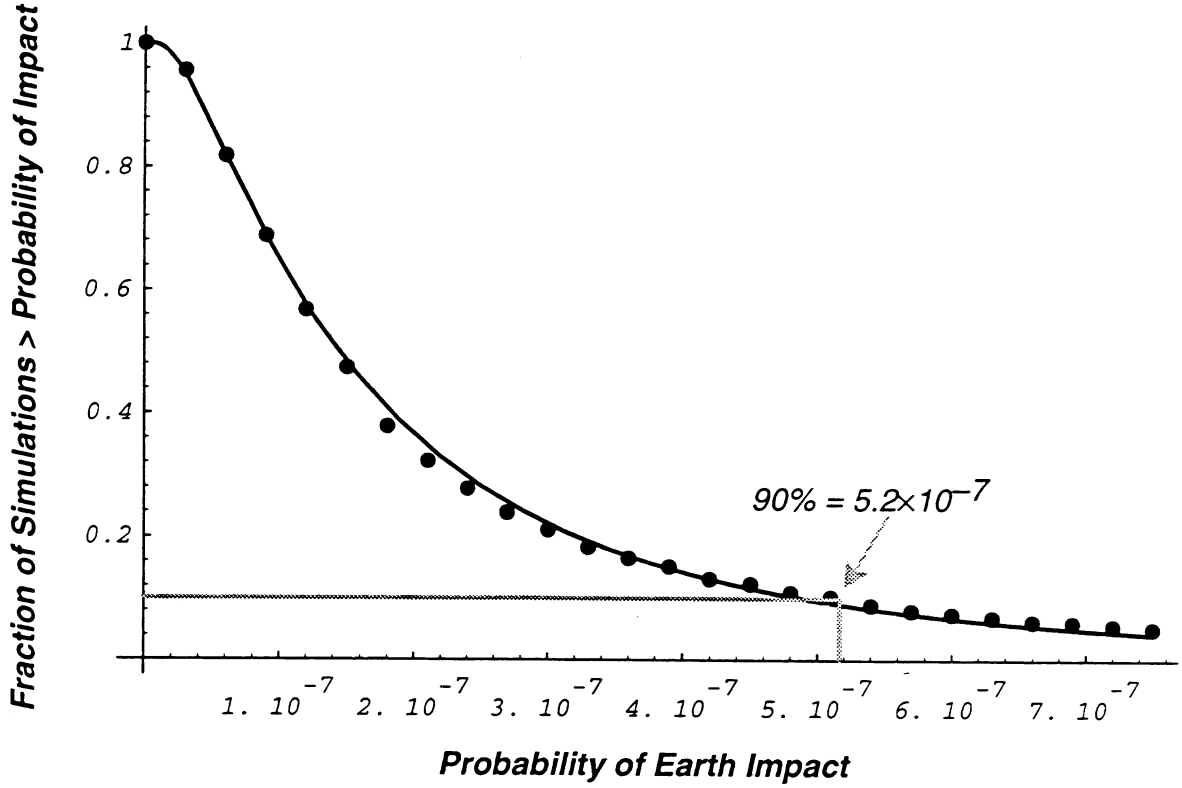

Figure 0-2 Primary Mission Complementary Cumulative Probability

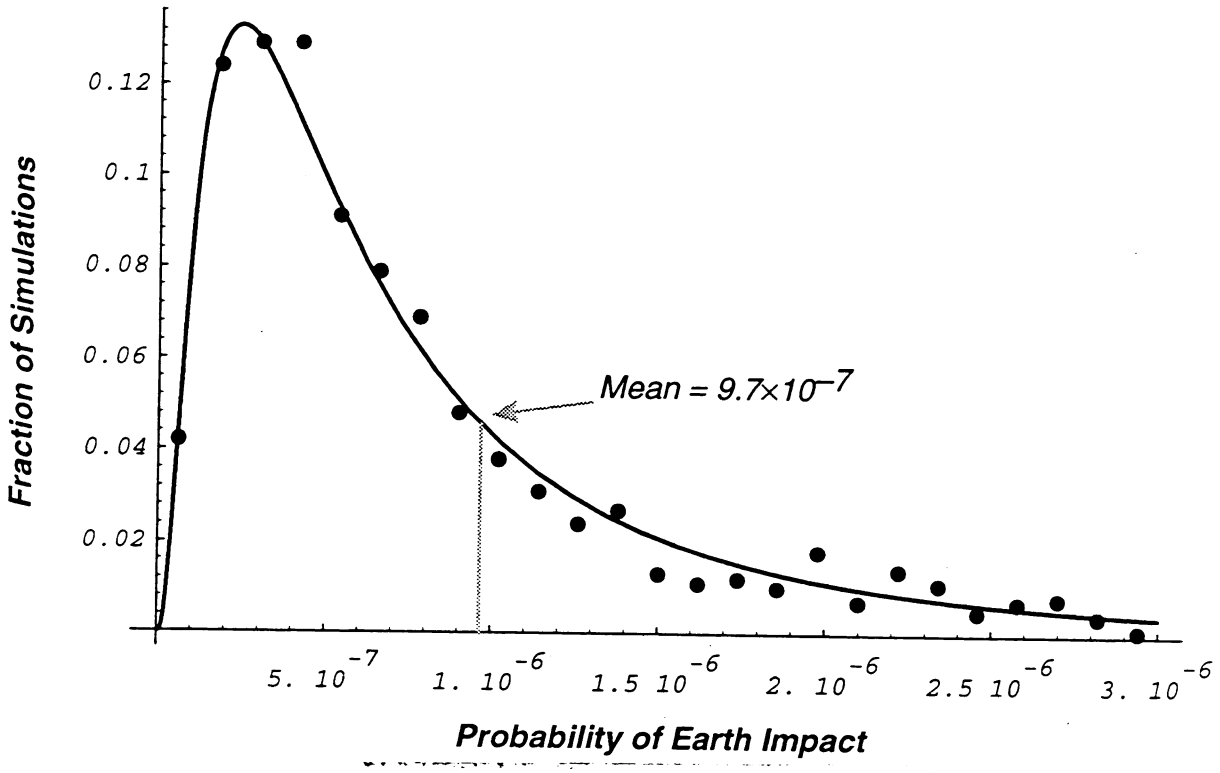

Figure 0-3 Backup Mission Probability Density Function

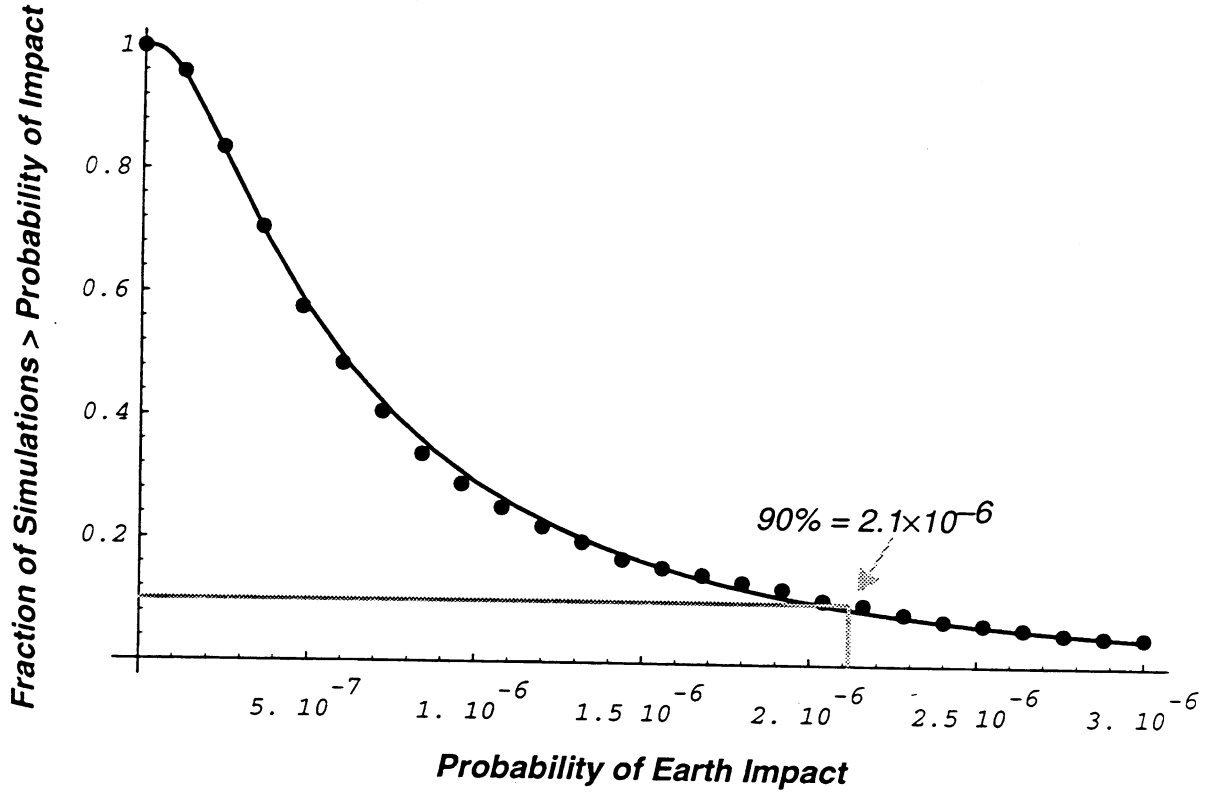

Figure 0-4 Backup Mission Complementary Cumulative Probability

SECTION 1

INTRODUCTION

1.1 PURPOSE OF THE STUDY

Volume 3 is one of four documents that the Cassini Project at the Jet Propulsion Laboratory (JPL) has compiled to support the preparation of an Environmental Impact Statement (EIS) for the Cassini Program by the National Aeronautics and Space Administration (NASA). Volume 1 describes the primary and backup Cassini missions, the science objectives, the Cassini spacecraft, and the Titan IV (SRMU)/Centaur launch vehicle. The focus of Volume 2 is on identifying and characterizing potential mission and power alternatives, and then comparing those alternatives with the Cassini baseline mission. Volume 3, this volume, assesses the probabilities of inadvertent spacecraft reentry into the Earth's atmosphere after successful injection onto the interplanetary transfer. An executive summary covering Volumes 1-3 is given in Volume 4.

In this report, the term "Earth impact" is defined as the reentry of the spacecraft into the Earth's atmosphere at an entry angle sufficient for capture. Similarly, the term “impacting trajectory” refers to a trajectory on which the spacecraft, if unattended, would reenter the Earth's atmosphere. If the spacecraft is on an impacting trajectory, there are in most cases weeks to years before impact would occur, during which time corrective action could be taken to avoid impact.

The Cassini mission requires trajectories that use planetary swingbys to achieve the necessary energy and orbit shaping to reach Saturn. The use of planetary gravity assists allows spacecraft launch by a Titan/Centaur launch vehicle. Gravity-assist trajectories to Saturn that only use Venus or Jupiter swingbys are more expensive, have much longer transit times and return less science. They are examined and documented in Volume 2.

The baseline plan calls for the Cassini spacecraft to use RTGs to supply electrical power. Therefore, precautions must be taken to ensure that an inadvertent reentry into the Earth's atmosphere does not occur during the Earth swingby. The situation is analogous to previous missions where navigation techniques and mission operations were designed to ensure either Earth impact avoidance (Galileo mission to Jupiter) or Mars protection from microbiological contamination (Mariner and Viking missions to Mars).

Design precautions must also be taken to preclude Ear impact resulting from loss of control of the spacecraft during interplanetary cruise. If the spacecraft were to drift in orbit around the Sun, Earth impact could result decades to millennia later, after many spacecraft revolutions around the Sun.

This report documents a study that has been performed determine the necessary actions in spacecraft, ground system, a navigation design to ensure that the probability of Earth impact is made very small. This report also provides a quantitative assessment of the probability of Earth impact, including, uncertainties in the assessment process. This report is designed to achieve several purposes. First, it develops and exercises t approach to be used in the Earth swingby strategy, thereby providing an early understanding of the Earth impact probability and enabling identification of possible failure modes specific the baseline spacecraft design. Second, it allows the Project t conduct trades among possible measures that reduce Earth impact probability early in the spacecraft and navigation design process. Third, it demonstrates that the navigation strategy will result a probability of Earth impact that satisfies the Project requirement.

The spacecraft design for this study is based on a July 1, 1993 configuration date. Design changes after this date will be monitored to ensure that the Earth swingby requirement not violated.

This volume does not address the case of Earth impact as a result of failures during the launch phase or the question possible health consequences in the unlikely event that an inadvertent impact does occur. These questions will be addressed as part of the Environmental Impact Statement.

1.2 ORGANIZATION OF THE DOCUMENT

The document is structured in a manner that reflects analysis process. Section 2 outlines the technical approach use in this study. High-level flow diagrams are provided to illustrate the methodology. A description of several of the major Project areas that are relevant to the Earth Swingby Plan is given in Section 3. The baseline spacecraft and mission is discussed, although not at the same level of detail as in Volume 1. An overview of the navigation system and the uplink process is also provided for background information.

A summary of the failure mode analysis is contained in Section 4 and Appendices A and B. This material discusses fail causes and their consequences and whether recovery is possible. Probability values and the resulting ΔV, along with their uncertainties, are assigned to each failure mode. In addition, Section 4 contains the analysis of the probability of no recovery in cases when initial failure does not preclude recovery.

Section 5 describes the plan for navigating the Cassini spacecraft past the Earth for the primary and backup trajectories. A design strategy is developed, incorporating the failure mode information, to reduce the probability of inadvertent Earth impact. This probability is termed the short-term impact probability since it concerns the time period of the nominal Earth swingbys.

The Earth impact probability over time periods much greater than the nominal trajectories is called the long-term impact probability and is treated in Section 6. The time period examined for the long-term impact probability of a disabled spacecraft is 100 years. An even greater time period of 1000 years is also addressed.

The total Earth impact probability is the statistical combination of the short-term and long-term impact probabilities. This is presented in Section 7. The answer is presented as a probability distribution function that accounts for uncertainties in both the process and mathematical models used in the process.

The technical analysis for this study was nearly completed when communications were lost with the Mars Observer spacecraft several days before Mars orbit insertion. At this time no official findings have been presented to explain the loss of the spacecraft. Appendix C handles this issue in a generic but useful manner and discusses the implications of the Mars Observer event to the findings in this study.

This past August, during the annual Perseids meteor shower, the Russian space station Mir 1 is said to have experienced as many as 60 to 70 micrometeoroid hits. Since the Cassini swingbys for the primary and backup trajectories also occur in August, an assessment of the environmental implications of the Perseids meteor shower for Cassini is in progress and reported in Appendix D.

There is a small probability of about 0.003 that a Centaur failure will occur which results in a reduced injection burn that does not achieve the required departure launch energy. The spacecraft is on an Earth escape trajectory, but does not have the required launch energy to go to Venus. A long-term Earth impact probability results from this failure and is discussed in Appendix E.

SECTION 2

METHODOLOGY

2.1 INTRODUCTION

In order that an accidental Earth impact not be a credible event, the Cassini Project has levied the following design requirement in its Project Policies and Requirements Document:

> *" Following injection, the probability of Earth impact by the spacecraft shall not exceed 10^{-6} taking into account potential failures."*

For this study, Earth impact is defined as reentry at an entry angle greater than or equal to 7 degrees at a reference entry altitude of 122 km (76 mi). Entry angles of less than 7 degrees are assumed to be too shallow for entry into the atmosphere.

To satisfy this requirement, an assessment of the Earth impact probability has been performed. The probability of Earth impact is presented as a probability density function over the model uncertainty. The advantage of such an approach is to provide information about the uncertainty of the estimation of the Earth impact probability. The above requirement is interpreted to be that the expected value (mean) of the Earth impact probability from injection to 100 years beyond the nominal Saturn encounter date shall not exceed 10^{-6}.

The overall methodology for determining Earth impact probability is given in Figure 2-1. The Earth impact probability is composed of short-term and long-term components. The short-term component is the contribution resulting from the navigation of the Earth swingbys for a given trajectory. The long-term component is the contribution due to a disabled spacecraft drifting in orbit about the Sun that could reencounter the Earth sometime in the next 100 years.

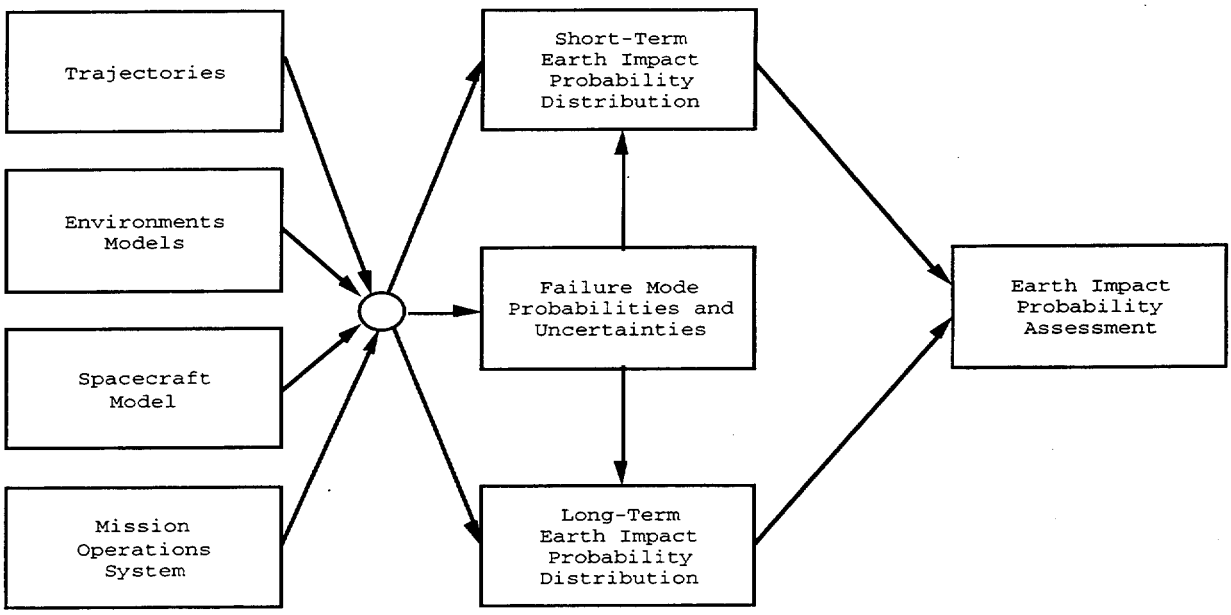

Figure 2-1 Earth Impact Probability Assessment Methodology

An important defining equation for Earth impact probability is as follows:

$$P_I = \sum_i P_F(i) * P_{\frac{I}{F}}(i) * P_{NR}(i)$$

where

P_I = probability of Earth impact

$P_F(i)$ = probability of failure for ith failure mode

$P_{\frac{I}{F}}(i)$ = probability of a resultant Earth impact trajectory given an occurrence of the ith failure mode

$P_{NR}(i)$ = probability of no recovery given the failure mode and the time to impact – this probability is conditional on the occurrence of the failure and on the spacecraft being on an impact trajectory resulting from the failure

This equation illustrates several important concepts. First is that there are a number of failure modes that contribute to Earth impact probability. One objective of this study is to identify all these failure modes. The $P_{I/F}$ and P_{NR} terms acknowledge that not all failures place the spacecraft on an impacting trajectory nor affect the capability to achieve a successful and safe Earth swingby. An example is the Galileo high gain antenna anomaly that resulted in only a partial deployment of the antenna before reaching the second planned Earth swingby. This failure did not prevent the precise delivery of the Galileo spacecraft at the second Earth swingby.

To keep the short-term impact probability acceptably low, a trajectory biasing strategy is used to reduce $P_{I/F}$. During most of Cassini's inner solar system journey, the spacecraft is on a trajectory that, without further maneuvers, would miss the Earth by tens of thousands of kilometers. The spacecraft is placed on a trajectory passing through the required Earth swingby point 10 days prior to the encounter. A trajectory-biasing strategy selected to control the short-term probability, while affecting the long-term probability, cannot be used to control the long-term probability. Over a long time scale, the impact probability is dominated by third-body perturbations to the spacecraft trajectory and by accidental planetary gravity-assist swingbys. Therefore, the long-term Earth impact probability is controlled by designing the spacecraft and mission operations to minimize failure mode probabilities.

The P_{NR} term in the impact probability equation factors in the spacecraft's ability to recover and successfully apply a corrective maneuver after a failure. If a failure does not completely incapacitate the spacecraft, then the normal course of action is to accurately determine the spacecraft trajectory and, if required, command a recovery sequence to correct the trajectory and avoid Earth impact.

The failure mode analysis for this study considered three types of failures; environmentally induced spacecraft failures, spacecraft failures, and ground-induced errors. These failures may impart a velocity change to the spacecraft, thus altering its trajectory. For an Earth impacting trajectory to result from a velocity change, the velocity change must be of sufficient magnitude and in the necessary direction.

Earth impacting trajectories can also result from uncertainties in the normal operation of the spacecraft and navigation system. For example, the actual velocity change achieved during a maneuver will differ slightly from the desired change. Likewise, the actual state (position and velocity) of the spacecraft will differ from the state estimated by the navigation system. Both of these uncertainties, if large enough and uncorrected, could lead to Earth impact. These are not failures, but expected variations in the operation of the systems.

The Earth impact probability is evaluated for two trajectories. The first trajectory is the proposed baseline Venus-Venus-Earth-Jupiter-Gravity-Assist (VVEJGA) trajectory. The launch period for this trajectory is in October 1997. The trajectory for the opening day of the launch period was selected for evaluation of the short-term impact probability, since the Earth swingby is at the minimum allowed swingby altitude of 500 km (311 mi). Trajectories for days later in the launch period with swingby altitudes greater than 500 km are less demanding with respect to the short-term Earth impact probability. The long-term impact probability, which is insensitive to trajectory variations across the launch period, was evaluated for a trajectory with a launch date in the middle of the launch period.

The second trajectory considered in this study is the backup Venus-Earth-Earth-Gravity-Assist (VEEGA) trajectory. The launch period for this opportunity is in March/April 1999. The opening day of the launch period was selected for evaluation for both the short-term and long-term impact probabilities. The second Earth swingby altitude of 500 km is constant across the launch period, and the first Earth swingby altitude is at its minimum value on the opening day. It is therefore assumed that the Earth impact probability has very little launch day dependence for this opportunity, with the opening day tending to be the highest.

2.2 SHORT-TERM EARTH IMPACT LOGIC DIAGRAM

To provide a clear understanding of the scenarios that might lead to Earth impact, logic diagrams have been developed for both short- and long-term Earth impact. The short-term Earth impact logic diagram is provided in Figure 2-2. This logic diagram shows only the contributing failure modes to the short-term Earth impact probability, with the significant contributors in bold. Each of the failure modes identified are discussed in detail in Section 4. The specific subsection location is also provided in the logic diagram.

Starting from the top, the logic diagram shows that for Earth impact to occur that it is necessary for the spacecraft to be on an impacting trajectory followed by an inability to change the trajectory. The left-hand branch indicates that there are two ways for the spacecraft to be placed on an impacting trajectory. The first way is the occurrence of an anomalous ΔV with the exact magnitude and direction to place the spacecraft on an impacting trajectory. The second way is due to the normal uncertainties in the orbit determination and maneuver execution process.

The causes of an anomalous ΔV are placed in three categories; (1) micrometeoroid induced rupture of either the bipropellant, hydrazine, or helium tanks, (2) an unplanned firing of the main engine or thrusters due to either an anomalous Sun search or erroneous ground command, and (3) a planned firing of the main engine or thrusters, but in the wrong direction or with the wrong magnitude. Five failure modes, as indicated in the logic

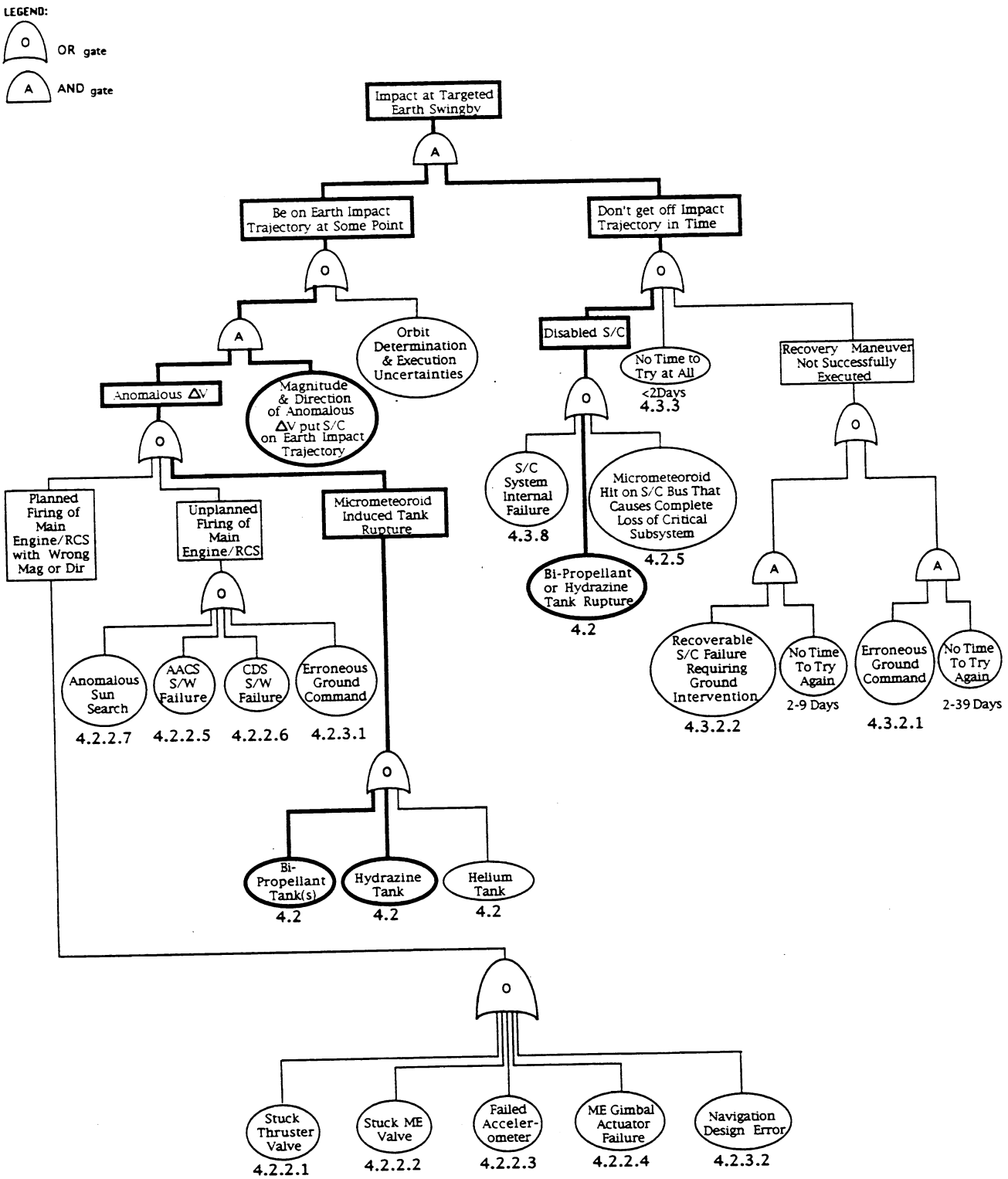

Figure 2-2 Short-Term Earth Impact Probability Logic Diagram

diagram, have been identified that provide a contribution to Earth impact probability from an erroneous planned main engine or thruster firing.

The right-hand branch of the logic diagram illustrates the reasons for not being able to get off an Earth impacting trajectory. The first reason is that the spacecraft is uncommandable. This could be due to (1) a micrometeoroid hit on the spacecraft bus that causes complete loss of a critical subsystem, (2) a bipropellant or hydrazine tank rupture, or (3) a spacecraft system internal failure. A second cause for remaining on an Earth impacting trajectory is that there is not enough time remaining before Earth impact to design and implement a recovery maneuver. A third reason for not avoiding Earth impact is that a recovery maneuver was not successfully executed and there is not enough time to attempt another. An unsuccessful recovery maneuver could be due to a recoverable spacecraft failure requiring ground intervention or an erroneous ground command.

A number of other spacecraft failures, not shown in the logic diagram, were also considered which do not significantly affect the total probability. These include: (1) rupture of the bipropellant tanks due to overpressurization caused by excessive heat input, (2) radiation, (3) charging, (4) erroneous star identification prior to a maneuver, (5) simultaneous main engine valve and latch valve failure, and (6) memory failure. In addition, there were several ground failures that were also considered that did not significantly affect the total impact probability, These include uplink transmission error and erroneous file transmission.

2.3 LONG-TERM EARTH IMPACT LOGIC DIAGRAM

The logic diagram for the long-term Earth impact scenarios is given in Figure 2-3. The two required conditions for long-term impact are an uncommandable spacecraft anytime before SOI (see left-hand branch of logic diagram) and satisfaction of orbit geometry and phasing requirements for Earth impact (see right-hand branch of logic diagram). The dominant scenario for long-term Earth impact is in bold.

The left-hand branch of the logic diagram is further subdivided according to whether the failure mode leading to spacecraft non-commandability resulted in an anomalous ΔV being applied to the spacecraft. only a micrometeoroid-induced tank rupture results in an anomalous ΔV. Failure modes not resulting in an anomalous ΔV include spacecraft system internal failures and micrometeoroid hits on the spacecraft bus that cause complete loss of a critical subsystem.

Once the spacecraft has been disabled, an Earth impact will only occur if specific orbit geometry and phasing requirements are satisfied. The geometry condition to be satisfied

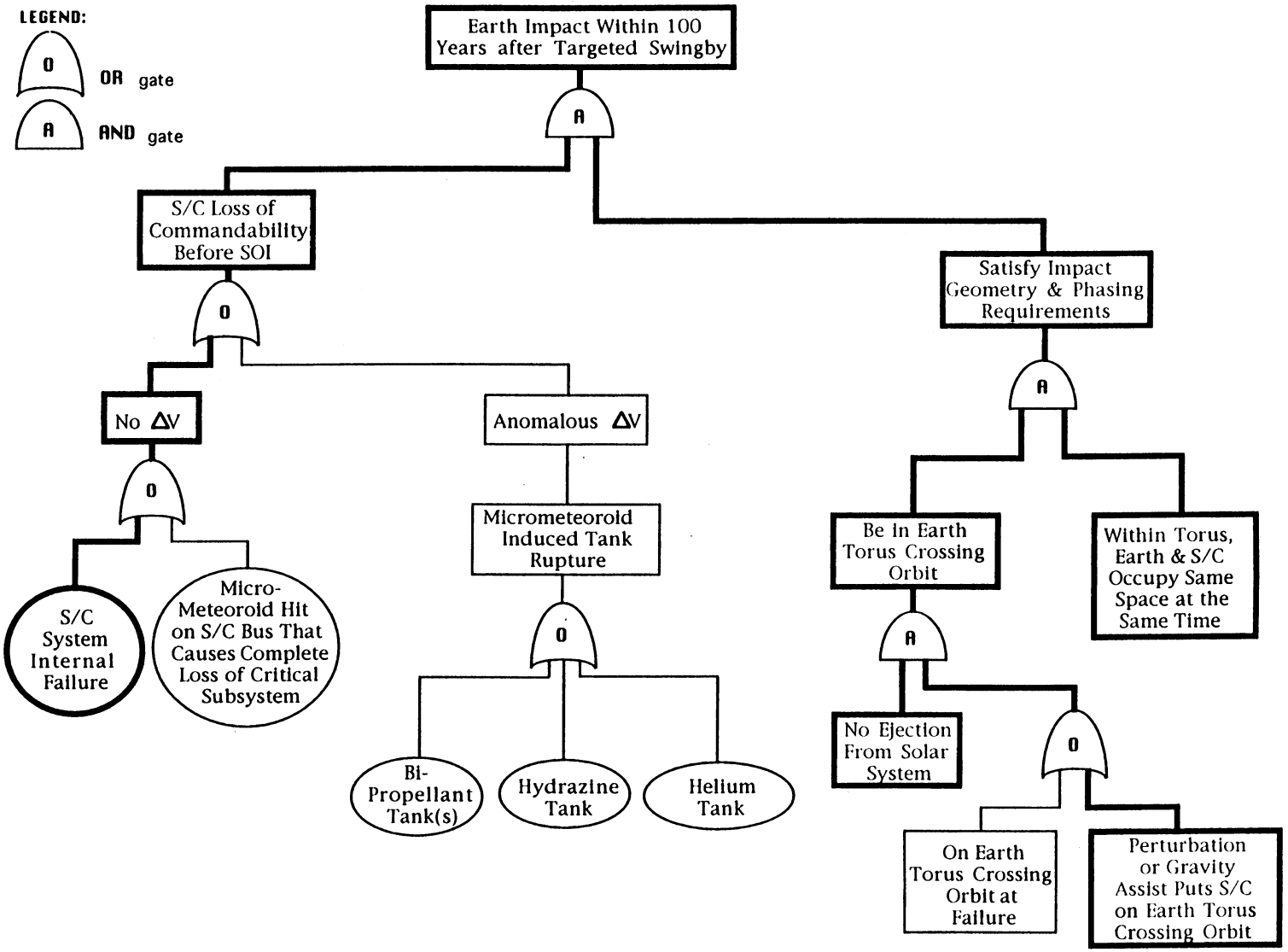

Figure 2-3 Long-Term Earth Impact Probability Logic Diagram

is that the spacecraft be on an Earth-torus-crossing orbit. The Earth torus is that region of space swept out by the Earth during its motion around the Sun. If the spacecraft is not in an Earth-torus-crossing orbit at the time of failure, it is possible to be placed in such a configuration at a later time due to third-body perturbations or planetary gravity assists. The final condition to be satisfied is a phasing constraint that requires the Earth to be present when the spacecraft passes through the Earth torus.

2.4 FAILURE MODE ANALYSIS

In general, all failures can be classified into three categories: environmentally induced failures, internal spacecraft failures, and ground induced failures. These failures can result either in an anomalous ΔV, which might place the spacecraft on an Earth impacting trajectory, or may prevent the spacecraft from being recovered after inadvertently being placed on an Earth impact trajectory.

For each significant failure mode identified, three estimates of the probability of occurrence are provided. The first estimate is the best estimate and represents the most accurate estimation of the failure rate. There is believed to be a 50-50 chance of the real value being higher or lower than the best estimate. The other two values attempt to quantify the uncertainty associated with the best estimate. The 90 percentile value represents the value that is believed to have a 90% chance of being greater than the true value. It is thus a conservative estimate of the failure probability. The 10 percentile value represents the non-conservative end of the uncertainty. There is only a 10% chance that the true value will be below the 10 percentile value. There are also some uncertainties in the ΔV estimates associated with some failures. A similar process was used to quantify these uncertainties.

Of all the failure modes identified in this study, only micrometeoroid-induced tank rupture contributes significantly to the short-term Earth impact probability. The spacecraft design does include components to provide protection from micrometeoroids, but there are particles with sufficiently high energies to damage the spacecraft. A rupture of a propellant or a pressurant tank will cause an anomalous ΔV, and may cause loss of spacecraft commandability or spacecraft incapacitation. A micrometeoroid impact on the electronic bus structure will impart only a negligible ΔV, but may cause loss of spacecraft commandability. The contribution to Earth impact probability from all other failure modes is several orders of magnitude less than that from micrometeoroid-induced failures. other failure modes include .stuck-open thruster valves, main engine valve failures, accelerometer failures, main engine gimbal actuator failures, and anomalous Sun search due to stellar reference unit or inertial reference unit failures. AACS and CDS flight software coding errors are the spacecraft software contributors to Earth impact probability.

Loss due to spacecraft system internal failures is the dominant failure mode for the long-term Earth impact probability. These failures include design and implementation errors, common mode failures, cascading failures, electronic parts failures, hardware failures, and software errors.

Ground-induced errors are errors made on the ground by the spacecraft controllers, which are then sent to the spacecraft and executed. Two categories of ground induced errors are erroneous ground commands and navigation design errors. Since the spacecraft software assumes that all validity checks are done on the ground, if an erroneous V command is transmitted, it will be executed. In the case of a navigational design error, a single error is made in one of the parameters for a planned maneuver during the design process prior to the sequence generation cycle.

The failure modes analysis also includes a calculation of the probability of no recovery. For catastrophic failures, which preclude the execution of subsequent maneuvers, the value of P_{NR} is Set to 1. In particular, P_{NR} is 1 for all of the failures involved in the long term impact probability.

For those failures that put the spacecraft on an impacting trajectory, but do not preclude the execution of subsequent maneuvers, the key determining factor as to whether the spacecraft could in fact be maneuvered off the impacting trajectory is the time left before swingby, not the cause of the initial failure. Three time periods were identified: before E-39 days, between E-39 and E-2 days and between E-2 and E-0 days. Failure modes were identified for each period and probability estimates were made for each, to be used for all recoverable failures causing the spacecraft to go on an impacting trajectory during that period.

The reasons for no recovery during each of the periods is shown in Figure 2-2 and listed in Section 2.2.

2.5 SHORT-TERM IMPACT PROBABILITY

The primary objective of the navigation strategy between launch and the Earth swingby is to satisfy the Earth impact probability requirement while delivering the spacecraft to the necessary Earth swingby aimpoint. To calculate the probability of Earth impact requires a knowledge of three factors: the failure probabilities and associated ΔVs, the uncertainties in the navigation process, and the characteristics of the spacecraft trajectory. For the purpose of defining an Earth-swingby navigation strategy, steps have been taken to minimize the effect of spacecraft failures and navigation uncertainties. The navigation strategy focuses on specifying and controlling the spacecraft trajectory conditions given the failure probabilities and navigation uncertainties.

In general, the impact probability decreases as the swingby altitude increases, so that impact avoidance requirements could be satisfied by simply raising the swingby altitude. However, specific swingby conditions are needed to shape the trajectory, and the spacecraft cannot carry sufficient propellant to replace this effect (except possibly for a very small bias). Fortunately, there would be enough propellant to bring the trajectory in towards the Earth in several steps before the swingby.

The technique is to partition the trajectory into segments. The trajectory on each segment is targeted to swingby conditions that yield an acceptable impact probability under the conditions expected during that segment. Due to the navigational uncertainties and trajectory dynamics, this strategy allows at least the final segment to be targeted to the desired swingby conditions. Prior segments are targeted to biased aimpoints that, if uncorrected, have higher swingby altitudes. The trajectory segments are joined by required spacecraft maneuvers. Prior to launch, analysis is performed to determine both the duration and swingby conditions for each segment. After launch, the spacecraft is controlled to meet these conditions.

The following general method is used to calculate the short-term Earth impact probability- for both the primary and backup trajectories. For each significant failure mode it is necessary to compute the probability of impact given failure. Given values for three confidence levels (10%, 50%, and 90%) for navigation uncertainties (consisting of orbit determination and execution errors) and three variations of failure ΔV; the impact probability given failure is computed along the trajectory at either maneuvers or discrete time steps, depending upon the failure mode. The result is nine variations of fractional impact probability as a function of time.

In order to generate a PDF for the short-term Earth impact probability, a Monte Carlo simulation was performed with random selections from each of the three terms ($P_{I/F}$, P_F, and P_{NR}) required to calculate Earth impact probability. For the probability of impact given failure ($P_{I/F}$), a random selection is made from one of the nine fractional impact probability vectors. The probability of failure (P_F) is sampled at three discrete probability levels, 10%, 50%, and 90%, representing the best estimate of the failure probability and the upper and lower values. For the micrometeoroid impact induced failure, the probability of failure is given as a continuous distribution. The probability of not being able to accomplish a recovery maneuver (P_{NR}) is also sampled at the 10%, 50%, and 90% probability levels.

The Monte Carlo process simulates the results for a large number of missions. Each simulated mission is broken down into a number of time steps. After sampling each of the three

individual factors, they are multiplied together to obtain a probability of impact, P_I, for the failure mode during the time interval. These individual impact probabilities are then summed over both the duration of the mission segment and across all of the failure modes to obtain the total distribution of the probability of impact for the mission segment.

2.6 LONG-TERM IMPACT PROBABILITY

The short-term impact analysis establishes that the probability of Earth impact during a targeted Earth swingby is extremely small. However, if the spacecraft becomes uncommandable before SOI and does not impact the Earth during a targeted swingby, there is still a remote possibility that long-term perturbations to the orbit could cause the spacecraft to eventually reencounter the Earth. The long-term analysis computes the probability of Earth impact at a non-targeted swingby from the time of spacecraft failure to 100 years beyond the planned SOI date.

To compute the probability of Earth impact, a knowledge of the spacecraft failure probabilities and associated ΔVs, the uncertainties in the navigation process, and the long-term motion of the spacecraft is required. Only those failures which cause the spacecraft to become uncommandable with no chance of recovery are appropriate for the long-term analysis. The P_{NR} term is therefore equal to 1 for the long-term analysis. The long-term impact probability is dominated by secular third-body perturbations to the spacecraft trajectory and by accidental gravity-assist swingbys. Therefore, the primary way to control the long-term Earth impact probability is to minimize the spacecraft failure probabilities.

The following method is used to compute the long-term Earth impact probability for both the primary and backup trajectories. Since a single trajectory propagation would not be representative of the range of possible spacecraft trajectories that could result given a failure at any time during interplanetary cruise, a Monte Carlo analysis was performed using thousands of trajectories considering a wide range of failure times and associated ΔVs. The primary and backup Cassini trajectories were each evaluated using ~5000 failure cases. Associated with each case is an initial spacecraft orbital state, which is perturbed by navigation uncertainty, and any ΔVs associated with the failure. Each state is then propagated for 100 years in the analysis.

Spacecraft failure probabilities were used to compute a probability distribution of failure (P_F term) representative of the entire interplanetary cruise for each mission. The failure probability distribution was obtained by randomly sampling the cumulative failure probability distributions as many times as required until ~5000 failure times during cruise were obtained.

To determine the probability of Earth impact given a failure, $P_{I/F}$, use was made of a large body of work refined over the past forty years to estimate the probability of impact by Earth-crossing asteroids. In this method, the number of passages of the spacecraft through the torus swept out by the Earth as it orbits the Sun are used to compute the probability of Earth impact. For an impact to occur, the spacecraft must cross through the Earth torus and, at the time of the crossing, the Earth must be at a position within the torus to cause impact. The term PI/F is computed as the product of two terms: 1) the expected number of torus crossings by the spacecraft per Monte Carlo case (N_{CRX}/N_{CASE}), and 2) the probability that the Earth occupies the same portion of the torus as the spacecraft at the time the spacecraft crosses the torus ($P_{I/CRX}$).

The number of torus crossings for all Monte Carlo cases were computed by propagating the initial conditions for each case using a high-precision numerical integration program and counting each passage through the Earth's torus. This procedure was used rather than the analytical model for long-term orbital motion used by most Earth-crossing asteroid analysis since the analytical expressions proved inadequate for the Cassini time frame and orbital characteristics. An uncertainty on the number of torus crossing per case was determined, and a distribution for this term constructed (assuming a normal distribution).

Standard Earth-crossing asteroid theory was applicable and therefore used to compute the $P_{I/CRX}$ term. The value of $P_{I/CRX}$ is slightly different for each torus crossing, and thus an average value was used to compute a best estimate value for the entire mission. An uncertainty in the value of $P_{I/CRX}$ was estimated and a distribution for this term constructed assuming a log-normal distribution.

The distributions for the N_{CRX}/N_{CASE} and $P_{I/CRX}$ terms were combined with the distribution for the $P_F(i)$ term to yield a PDF for the long-term Earth impact probability, P_I. The velocity vector of the spacecraft relative to the Earth was estimated at each torus crossing, assuming that the Earth was in the position required for impact, in order to estimate the likely range of entry velocities and entry latitudes for the long-term. The entry latitude distribution can be estimated given the likely range of magnitudes and declinations of the Earth-relative velocities. An entry angle distribution was computed assuming that the spacecraft aimpoint is equally likely to lie anywhere within the Earth impact circle.

A subset (~20%) of the Monte Carlo cases was also propagated for 1000 years to study the very long-term probability of Earth impact. The same methodology as used for the 100-year propagation was used for these 1000-year cases.

2.7 EARTH IMPACT PROBABILITY ASSESSMENT

The Project requirement on the Earth Swingby Plan is that the probability of Earth impact be less than or equal to one in a million (10-6). A number of parameters can be used to describe the characteristics and interpretation of a PDF (or of a complementary cumulative probability curve). The "expected value" of a random variable is expressed by the mean of the probability distribution. Thus, the Project requirement that the probability of Earth impact be less than or equal to 10^{-6} has been considered met when the mean of the assessed probability distribution is less than or equal to 10^{-6}.

The total Earth impact probability distribution is the probabilistic sum of the short-term and long-term Earth impact probability distributions. A 1000-trial Monte Carlo simulation was used to perform this probabilistic summation. The mean of the total Earth impact distribution was compared to 10^{-6} to determine if the Project Earth impact requirement was satisfied for both the primary and backup trajectories.

SECTION 3

PROGRAM DESCRIPTION

3.1 CASSINI ORBITER DESCRIPTION

The Cassini spacecraft is a three-axis stabilized spacecraft, and is depicted in two views in Figure 3-1. It acts as a platform for five remote sensing, six fields and particles and radio science experiments, and as a carrier for the Huygens Probe. The spacecraft measures 8 meters (26.2 ft) in height and 4 meters (13.1 ft) in diameter. The spacecraft with science instruments and Huygens Probe will have an approximate dry mass of 2520 kg (5560 lbs). Up to 3000 kg (6614 lbs) of bipropellant and 132 kg (291 lbs) of monopropellant will be carried to perform maneuvers and attitude control.

The main body of the spacecraft can be described as a stack of modules. These consist of the Lower Equipment Module (LEM) containing the reaction wheels, the Propulsion Module, the Upper Equipment Module (UEM) containing the Upper Shell Structure,(USS) and the electronics bus, and the High Gain Antenna (HGA). Attached to this stack are the Remote Sensing Pallet on which the remote sensing instruments are mounted, the Fields and Particles Pallet for the fields and particles instruments, the Huygens Probe, the magnetometer boom, and other spacecraft components.

The origin of the spacecraft coordinate system is on the centerline of the spacecraft on a plane defined by the interface between the Upper Shell Structure and the Engineering Bus. The Remote Sensing Pallet is mounted along the +X side of the spacecraft, the magnetometer boom defines the +Y axis, and the main engine nozzles nominally point along the +Z axis. Figure 3-1 graphically illustrates the coordinate system.

3.1.1 Orbiter Subsystems

The Cassini Orbiter contains 12 engineering sub-systems. The spacecraft functional block diagram (Figure 32) illustrates how these various subsystems interact. A description of each engineering subsystem is provided below.

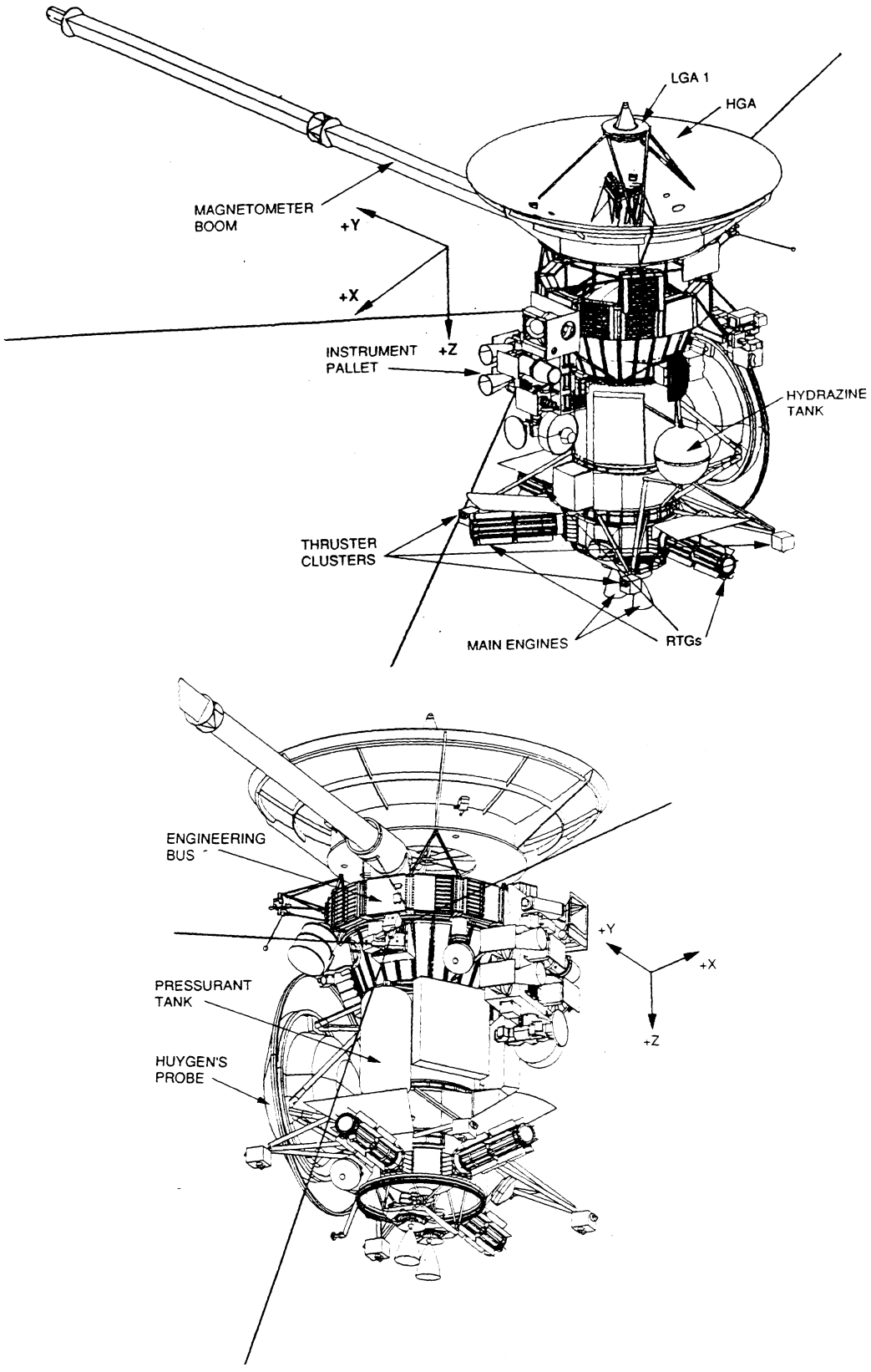

Figure 3-1 Cassini Spacecraft

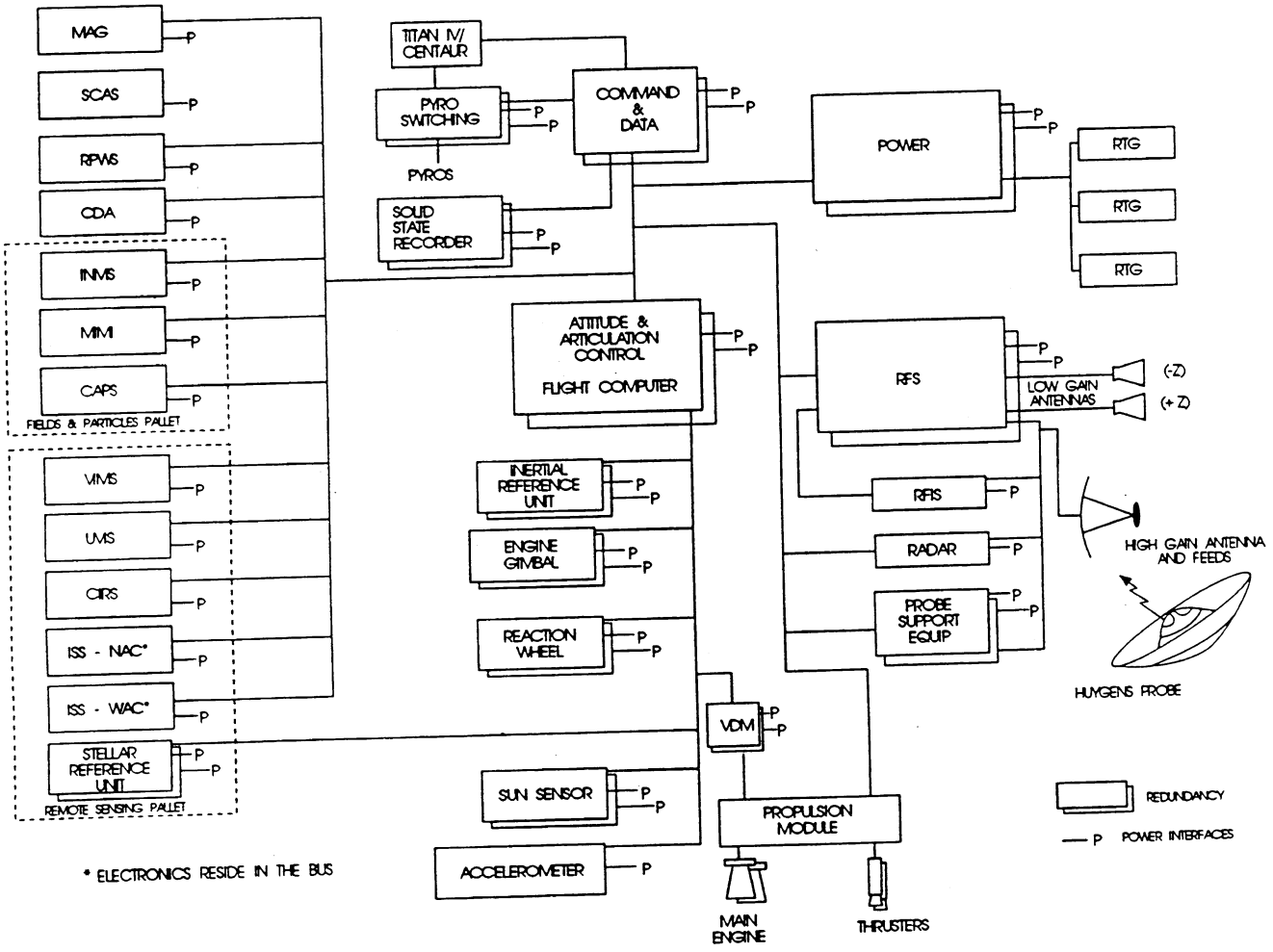

Figure 3-2 Cassini Spacecraft Functional Block Diagram

3.1.1.1 Structure Subsystem. The Structure Subsystem provides mechanical support and alignment for all flight equipment, including the Huygens Probe. It also provides attachment points for handling, provides an equipotential container, acts as an electrical grounding reference, and provides protection from radiation and meteoroids. The structure consists of the UEM (which includes the 12-bay electronics bus assembly), the instrument pallets, the magnetometer boom, and the LEM. It also includes all of the brackets and structure for integrating the Huygens Probe, the HGA, the main rocket engines, and other equipment. The spacecraft electronics bus houses much of the various engineering subsystems, electronics, including the Command and Data Subsystem, the Radio Frequency Subsystem, and the Attitude and Articulation Control Subsystem.

3.1.1.2 Radio Frequency Subsystem. The Radio Frequency Subsystem (RFS) provides the telecommunications link between the spacecraft and the ground, and also supports radio science investigations. When sending information to the ground, the RFS produces an X-band carrier, modulates it with data received from the Command and Data Subsystem (CDS), amplifies it using Traveling Wave Tube Amplifiers, and delivers it to one of the spacecraft antennas. When receiving, the RFS accepts X-band ground command/data signals from one of the antennas, demodulates them, and delivers the commands/data to the CDS for storage and/or execution.

3.1.1.3 Power and Pyrotechnics Subsystem. The Power and Pyrotechnics Subsystem (PPS) provides regulated electrical power to space-craft users via a power bus. The power for the spacecraft is provided by three RTGS, located at the bottom of the LEM (See Figure 3-1). The PPS turns loads on and off based upon commands from the CDS. In addition, the PPS provides power to various pyrotechnic devices on command from the CDS.

3.1.1.4 Command and Data Subsystem. The Command and Data Subsystem processes and distributes commands/data received from the ground and collects science and engineering data for transmission to the ground. In addition, it stores both received command and transmission data for later use. The CDS uses one each of the two redundant Solid State Recorders (SSRS) and Engineering Flight Computers (EFC).

CDS software algorithms control the nominal operation of the spacecraft. In addition, the CDS software also contains algorithms that provide fault protection for the spacecraft. Fault protection software ensures that, in the case of a serious fault, the spacecraft will be placed into a safe,-stable, commendable state for a period of at least two weeks without ground intervention required, giving the ground operations teams time to solve the problem and send the spacecraft a new command sequence. If necessary, the fault protection routines autonomously respond to faults needing immediate action.

3.1.1.5 Attitude and Articulation Control Subsystem. The Attitude and Articulation Control Subsystem (AACS) provides dynamic control of the spacecraft in rotation and translation. The AACS contains a suite of sensors that includes redundant Sun Sensor Assemblies (SSA), redundant stellar reference units, a Z-axis accelerometer, and a redundant 3-axis Inertial Reference Unit (IRU). The AACS also contains reaction wheels, actuators for the main rocket engine gimbals, and electronics which control actuation of the Propulsion Module Subsystem (PMS).

Using two redundant EFCS, the AACS processes commands from the CDS, and produces commands to be delivered to AACS actuators and/or PMS valves. The AACS EFCs also contain fault protection algorithms for AACS components.

3.1.1.6 Cabling Subsystem. The Cabling Subsystem consists of all power and data cabling on the spacecraft, except for coaxial cabling and waveguides. It also provides any access and breakouts that are needed during integration and testing prior to launch.

3.1.1.7 Propulsion Module Subsystem. The Propulsion Module Subsystem (PMS) provides thrust and torques to the spacecraft. Under command from AACS, the thrust and torques establish the spacecraft orientation and turning rates, and any required velocity changes.

For attitude control and small ΔV maneuvers, the PMS uses a monopropellant hydrazine system known as the Reaction Control Subsystem (RCS). The system consists of a titanium monopropellant tank, four thruster clusters mounted off the LEM at the base of the spacecraft, controlling valves, tubing, and other miscellaneous components. The monopropellant tank is located on the outside of the central spacecraft body, on the -Y face of the spacecraft (See Figure 3-3). The tank is covered by a 20-layer multilayer insulation (MLI) blanket for thermal control. Each of the clusters contains four 0.67 N (0.15 lbf) thrusters oriented in directions parallel to the spacecraft X and Z axes. The thrusters provide coupled torques about the Z axes, and uncoupled torques about the X and Y axes.

For larger ΔVs, the PMS uses its bipropellant system. Two large titanium bipropellant tanks (containing nitrogen tetroxide (NTO) and monomethyl hydrazine (MMH)) fill the central cylinder of the spacecraft. The tanks are stacked vertically within the cylinder, with the MMH tank on top (See Figure 3-3). The cylinder is made from aluminum and is covered with MLI for thermal control. Thrust is generated with two redundant main rocket engines, each providing a thrust of approximately 490 N (110 lbf). These engines are gimbaled so that, under AACS control during burns, the thrust vector can be maintained through the shifting center of mass of the spacecraft. During a

main engine burn, RCS thrusters are controlled by AACS to maintain the required spacecraft attitude.

P_{MS} valve actuators for the main engines and thrusters operate in response to commands received from AACS.

Both systems are pressurized by the same helium pressurant system, which includes a filament-wound graphite epoxy helium tank, regulators, tubing, and other miscellaneous components. The tank is located on the outside of the central cylinder on the +Y face and is covered by MLI (See Figure 3-3).

A schematic of the PMS is given on Figure 3-4.

3.1.1.8 Temperature Control Subsystem. The Temperature Control Subsystem maintains desirable temperatures for all spacecraft components. Temperatures of the various parts of the spacecraft are kept within required limits by a number of local thermal control techniques. Where needed, commandable electric heaters are used to keep components within required limits. Automatically adjusted reflective louvers on the electronics bus help control temperature within the bus. Radioisotope Heater Units (RHUs) and Variable Radioisotope Heater Units (VRHUs) are used where heat input is needed and where RHU radiation will not interfere with spacecraft or instrument functions. Multilayer insulation blankets cover much of the spacecraft and its equipment. Temperature sensors are located at many sites on the spacecraft, and their measurements are used by the CDS to provide commands to electric heaters.

During the near-Sun portion of the trajectory, the central portion of the spacecraft is shaded by pointing the HGA (-Z axis) towards the Sun; the HGA is large enough to provide shade for the entire spacecraft body including the Huygens Probe.

3.1.1.9 Devices Subsystem. The Mechanical Devices Subsystem provides the hardware needed to perform deployments and separations. Some of these devices include pyrotechnic separation devices for separation of the spacecraft from the launch vehicle, springs to provide the impulse to separate the spacecraft from the launch vehicle, a self-deploying 10.5-meter (34.4 ft) coiled longeron mast stored in a canister for the two magnetometers, and electrostatic discharge covers over inflight separation connectors. In addition, the devices subsystem provides an articulation system for the backup reaction wheel assembly and louvers and variable RHUs for temperature control.

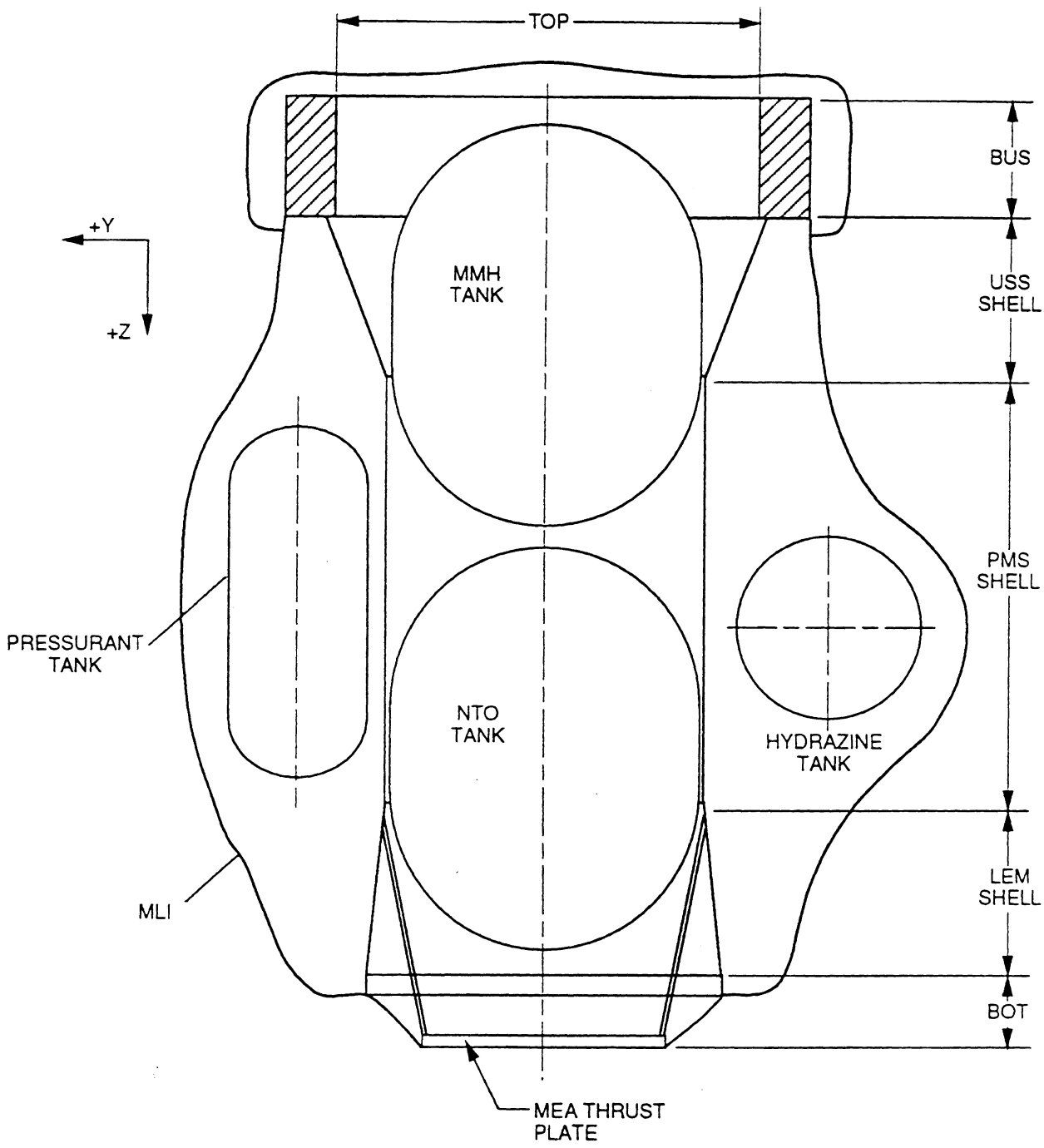

Figure 3-3 Propellant Tank Configuration

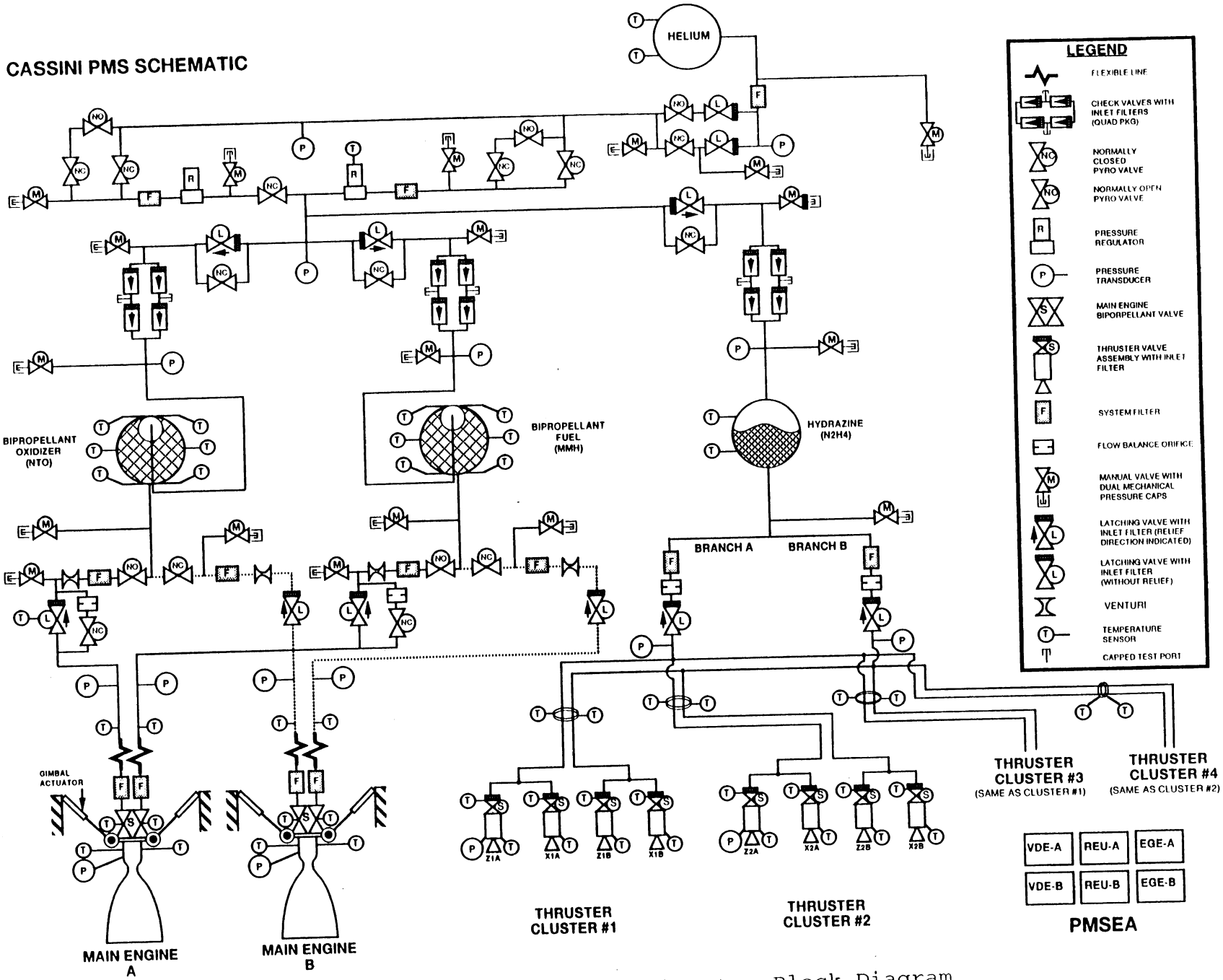

Figure 3-4 Propulsion Module Subsystem Block Diagram

3.1.1.10 Electronic Packaging Subsystem. The Electronic Packaging Subsystem (EPS) provides the electronics packaging for most of the spacecraft in the form of the 12-bay electronics bus (see Figure 3-5). The bus is made up of bays containing standardized, dual-shearplate electronics modules.

3.1.1.11 Solid State Recorder Subsystem. The Solid State Recorder Subsystem (SSR) is a solid-state memory that stores science data and engineering measurements. Once data is stored, it can be retrieved for transmission to the ground or for onboard processing. The data is stored and retrieved on command from the CDS.

3.1.1.12 Antenna Subsystem. The Antenna Subsystem consists of the HGA, the two Low Gain Antennas (LGAs), and necessary coaxial cabling. The HGA is used to transmit/receive data at high data rates, but must be accurately pointed at the Earth when transmitting. The HGA is also used by the RADAR and radio science experiments for science purposes. The LGAs receive/transmit data at much lower rates, but each provides nearly hemispherical coverage. The coverage from the two LGAs allows the spacecraft to receive commands from nearly any spacecraft orientation during the early portion of the mission (prior to the final Earth swingby). One of the two LGAs will be selected when operational constraints prevent pointing the HGA towards the Earth.

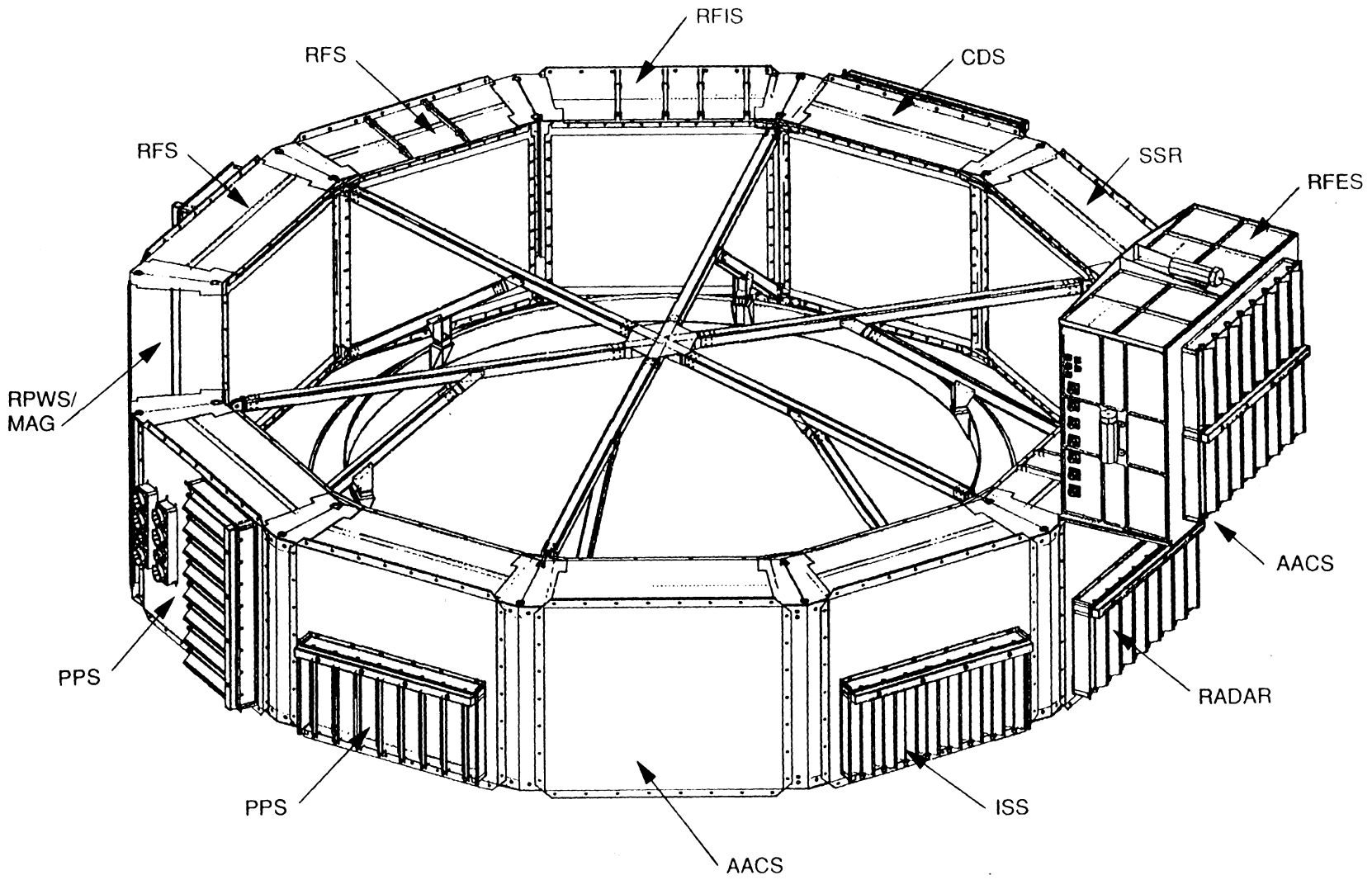

Figure 3-5 Bus Layout

3.2 THE BASELINE CASSINI MISSION DESIGN

3.2.1 The Baseline Primary Mission Design

The baseline Cassini mission is scheduled for launch within a 25-day period beginning October 6, 1997. Using the Titan IV (SRMU)/Centaur launch vehicle, the spacecraft will be injected into a 6.7-year VVEJGA trajectory to Saturn, as shown in Figure 3-6. The first Venus swingby will occur in April 1998. The following December, a maneuver will occur to place the spacecraft on course for the second Venus swingby in June 1999. Due to the Earth's unique orientation relative to Venus during this time period, the spacecraft will be able to fly on to Earth in slightly under two months, where it will obtain another gravity assist in August 1999.

After flying past the Earth, the spacecraft will swing out toward Jupiter, passing through the asteroid belt. Due to limited propellant reserves, lack of adequate ground systems for science support, and the absence of a readily accessible asteroid of appropriate size, an asteroid flyby along the way is not planned. In December 2000, the spacecraft will swing by Jupiter to obtain a fourth and final gravity assist.

For several months prior to arrival at Saturn in June 2004, the spacecraft will perform science observations of the Saturnian system as it draws nearer to its destination. The intensity and pace of observations will increase sharply during the last few days, prior to the execution of the Saturn Orbit Insertion (SOI) burn. The spacecraft's closest approach to the planet during the SOI phase, at about 0.3 Saturn radii [18,000 km (11,000 mi)], is the closest of the entire mission. Because this provides a unique opportunity for observing the inner regions of the ring system and magnetosphere, the roughly 1.5-hour orbital insertion burn will be delayed about 0.75 hours from its optimal point to permit science observations.

After SOI, the spacecraft will swing out to the most distant point in its orbit around Saturn (about 200 Saturn radii [1.2×10^7 km (7.5×10^6 mi)]), and then swing in again to achieve an encounter with Titan in November 2004. About three weeks before Cassini's first flyby of Titan, the spacecraft will release the Huygens Probe, targeted for entry into Titan's atmosphere. Two days after Probe release, the Orbiter will perform a deflection maneuver to be in position to receive scientific information gathered by the Huygens Probe throughout its estimated 2.5-hour parachute descent to Titan's surface. The Orbiter can remain in position to receive information from the battery-powered Probe for up to three hours, which would include data collected at the surface if the Probe survives its landing. All data gathered by the Probe will be stored on the Orbiter for later transmission to Earth.

The spacecraft will then continue on its tour of the Saturnian system, including multiple Titan swingbys for gravity assist and science acquisition. The Titan swingbys and Saturn orbits will be designed to allow maximum science coverage, including the acquisition of science data from Saturn's icy satellites. By the end of the four-year tour, the orbital inclination will have been increased from an initial value of 10.5 degrees to approximately-80 degrees, allowing investigation of the environment at high latitudes. In particular, the spacecraft will investigate the source of the unique Saturn Kilometric Radiation. The 10.7-year nominal mission will then end in June 2008.

3.2.2 The Baseline Backup Mission Design

The backup launch opportunity would be used in the event that a problem should arise with the spacecraft or launch vehicle, causing a delay in the launch date for the primary trajectory, a launch date beyond the primary and secondary launch opportunities. A launch date for the backup trajectory has been scheduled for March 1999, around 17 months after the primary mission launch opportunity. The baseline Cassini backup mission would be able to fulfill scientific goals similar to the primary mission's, including the four-year satellite tour. However, it would take three years longer to reach Saturn. This longer cruise time increases the probability of spacecraft malfunction. The time in storage also provides opportunity for malfunction.

The baseline backup trajectory, as shown in Figure 37, is a 9.8-year VEEGA trajectory. In this trajectory, the gravity-assist sequence begins with a June 2000 swingby of Venus, after which the spacecraft proceeds to Earth for a second gravity assist in August 2001. This second assist propels the spacecraft on a broad, sweeping arc through the asteroid belt. In August 2004, Cassini arrives back at the Earth for a third and final planetary gravity assist. This assist catapults the spacecraft toward Saturn, allowing an arrival at the ringed planet in December 2008. The Probe delivery and tour portions of the mission are very similar to those described for the baseline mission, with the timetable shifted to reflect the 2008 arrival date. The baseline backup mission's arrival date, however, is less desirable than that of the baseline primary. Aside from the four-year delay in science return compared with the baseline, it also offers a much less advantageous geometry of Saturn's rings, both as seen from the Earth and from the spacecraft because of poor lighting for imaging.

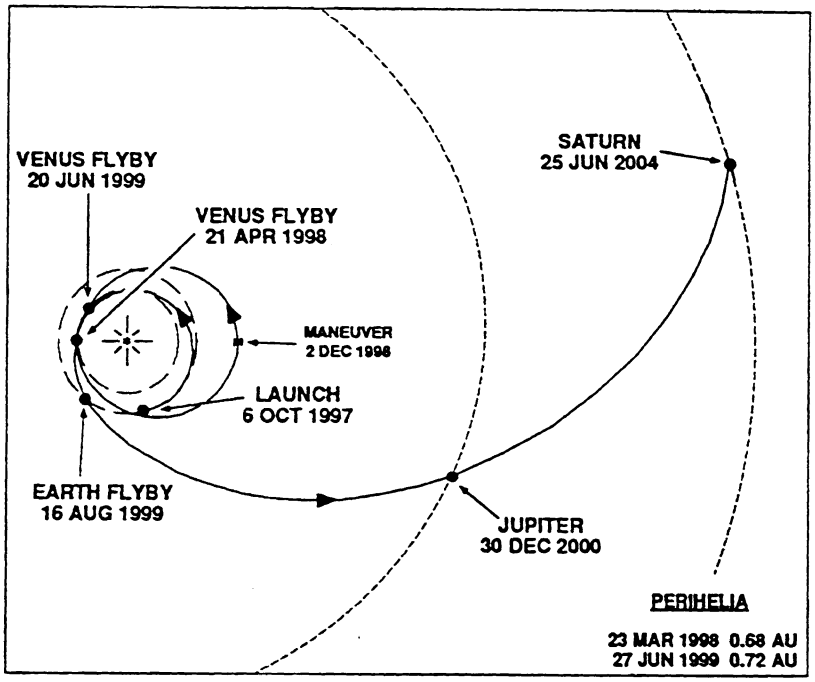

1 AU = 1.496×10^8 km (9.296×10^7 mi)

Figure 3-6 Cassini October 1997 VVEJGA Interplanetary Trajectory

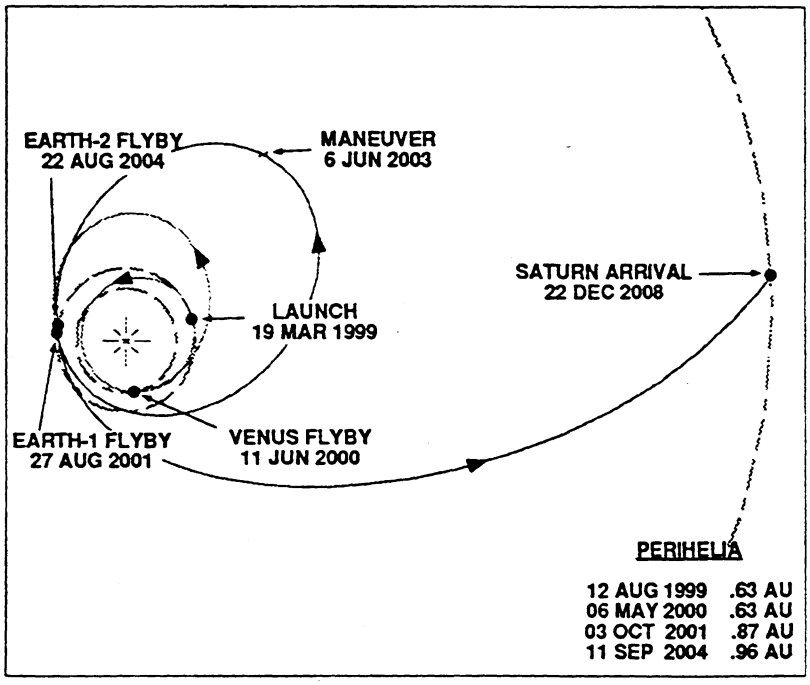

1 AU = 1.496×10^8 km (9.296×10^7 mi)

Figure 3-7 Cassini March 1999 VEEGA Interplanetary Trajectory

3.3 NAVIGATION SYSTEM

3.3.1 Introduction

Navigating the Cassini spacecraft safely past the Earth must be accomplished with great confidence. This subsection contains a review of the navigation task and compares performance history with predictions of current capabilities.

Navigation is defined as the process of locating, predicting, and controlling a flight path in order to achieve mission objectives. A preflight mission design activity provides the baseline trajectory for the spaceflight. Navigation updates the trajectory and provides the tools required to execute the flight. Navigation support for each deep space mission involves a planning phase in which flight accuracy is predicted and the systems to execute the flight are developed, and an operation phase where the actual process of navigation is executed.

There is now an extensive history of deep space navigation. Beginning with the Mariner 2 mission to Venus in 1962, a series of spacecraft were sent to the inner planets to perform remote science sensing during swingby encounters. In the 1970s, the range of navigation applications was expanded to include the delivery of spacecraft to orbit the inner planets-first with the Mariner 9 mission to Mars in 1971, then Mariner 10 to Venus and Mercury in 1974, the Viking missions to Mars in 1976, and finally the Pioneer Program to Venus. In the 1970s the exploration of the outer planets began with the early Pioneers to Jupiter and Saturn, followed by the Voyager Program. These missions have been followed by the Magellan spacecraft to Venus, Galileo to Jupiter and, in 1992, the Mars Observer mission.

Most of these missions have been carried out using the JPL Deep Space Network (DSN) for trajectory measurements and the Ground Data Processing System for guidance. Taken together these comprise the JPL Navigation System, which has evolved over the last three decades. Subsection 3.3.2 describes the elements of the measurement and data processing systems that comprise today's navigation system. A summary is provided of the historical performance achieved with the system during the past three decades of planetary exploration, along with a description of how the system is used operationally.

3.3.2 JPL Navigation System

Figure 3-8 illustrates in schematic form the elements of measurement and computation that comprise the current JPL navigation system to be employed on the Cassini mission. The left side of the diagram shows a spacecraft acquiring optical images of the target body and being tracked by two ground antennas. The right side shows the ground processing system, which models the trajectory motion, estimates the orbit, and computes the flight path corrections.

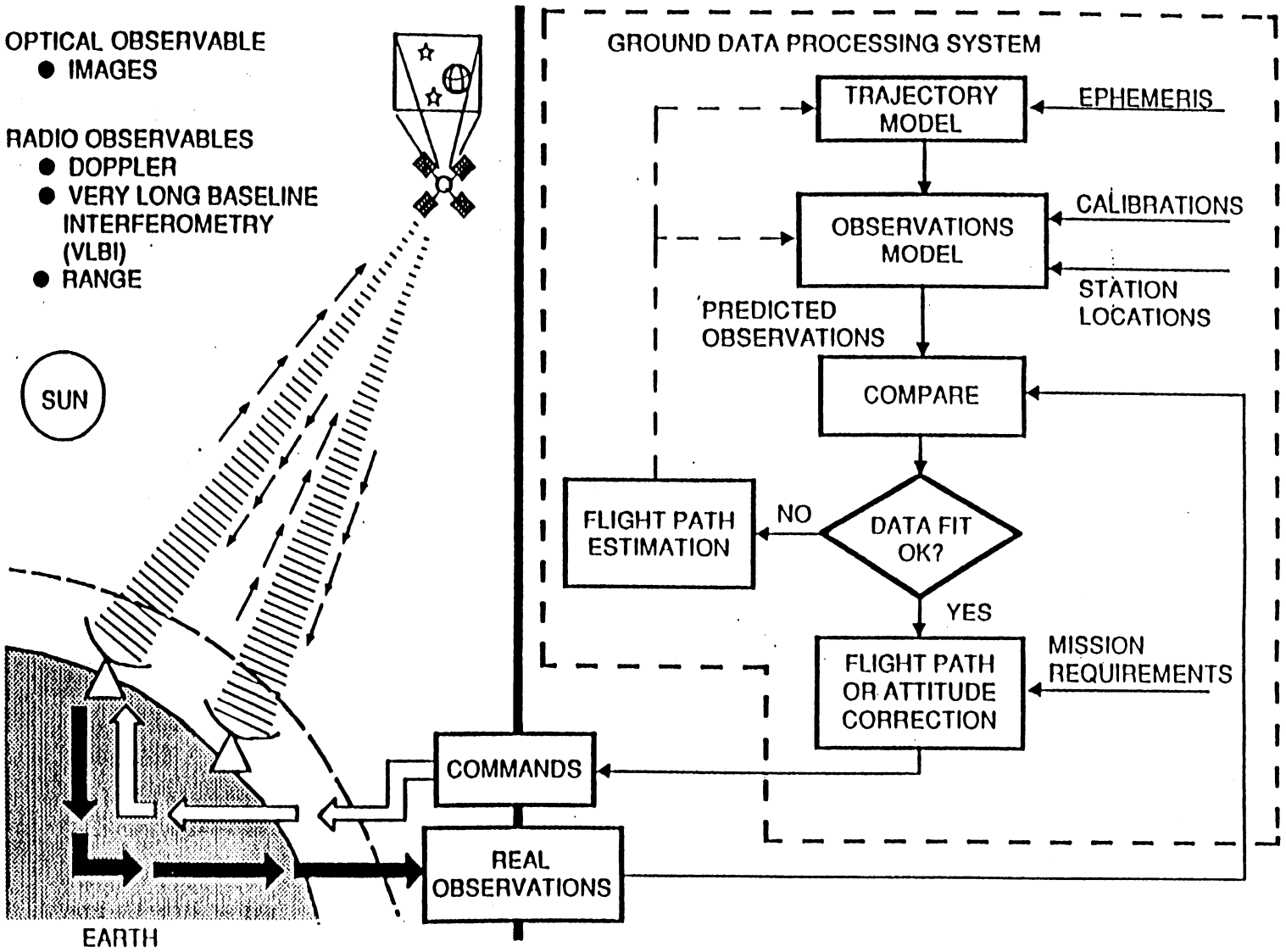

Figure 3-8 Schematic Description of the JPL Navigation System

3.3.2.1 Measurement System. The baseline navigation measurement system of the 1960s consisted of two-way S-band [2.3 GHz (2.3×10^9 cps)] radio Doppler. This system was used to navigate the early Mariner missions to Venus and Mars. Beginning with Mariner 9, two-way, 1 MHz (10^6 cps**)** bandwidth ranging data were also employed. Ranging data were used as supplementary data to Doppler during the planet orbiting phase, when the Doppler data noise increased dramatically near superior conjunction.

Beginning with the Viking mission in 1975, NASA spacecraft transponders transmitted S-band and X-band [8.4 GHz (8.4×10^9 c/s)] downlink to Earth, both signals being coherent with the uplink S-band. Processing the S- and X-band data allowed a calibration of the effects of charged particles on the downlink signal. Mapping methods were employed to infer the effect on the uplink. This dual-frequency technique was used successfully to calibrate both Doppler and range during periods of high activity in the solar plasma and Earth's atmosphere.

The Cassini spacecraft will use an X-band for both uplink and downlink. This system will provide greater Doppler measurement accuracy and is less sensitive to solar plasma and Earth atmospheric effects because these errors are inversely proportional to the square of the frequency.

Optical measurements, acquired from the science cameras on board the spacecraft, have been used on the Mariner 10, Viking, and Voyager missions to improve the target-relative orbit determination accuracy in the final approach stages of their planet and satellite encounters. These optical measurements also are being used on the Galileo mission, and are planned for the Cassini mission beginning with the Saturn approach phase.

A new data type, Very Long Baseline Interferometry (VLBI), was brought into operational use by the Voyager Project for the Uranus and Neptune encounters. Tracking of the spacecraft from two sites separated by a long baseline, and differencing this measurement with a similar VLBI measurement of a nearby quasar yields a precise angular measurement with respect to the well-known quasar positions. VLBI may be used on the secondary or backup missions.

3.3.2.2 Data Processing System. Doppler, range, VLBI, and optical image data are brought to JPL via the DSN tracking stations. A large software system is operated at JPL to determine the spacecraft's orbit and to compute trajectory correction parameters. The elements of the software system are listed in Table 3-1. The size of the entire software set is over a million lines of FORTRAN code.

Table 3-1 Major Software Elements of the JPL Navigation Data Processing System

Program	Function
ODP	Fits data to obtain orbit
DPTRAJ	Integrates trajectory
MOPS	Computes correction maneuver
IDRSPS	Edits and formats radio data
MEDIA	Calibrates radio data
APP	Plans optical navigation pictures
ONIPS	Extracts optical observable
ONP	Computes optical data partials

Newly acquired radio data are first processed in the Intermediate Data Records Stripper Processing System (IDRSPS) Program, where the data from different tracking stations are merged into a single time-sequenced array. After data of poor quality are removed from the array in this system, the array is stored for input to the orbit estimation process.

Two programs are used in the orbit estimation process. First, the Double Precision Trajectory (DPTRAJ) System computes an N-body numerical integration of the trajectory and state transition partials from initial conditions. The numerical integration is performed using a variable order predictor, corrector method. The Orbit Determination Program (ODP) computes simulated observables corresponding to each actual observation based on the trajectory modeled by DPTRAJ, and computes the partial derivatives of the observables with respect to the initial conditions of the trajectory. It may also compute partial derivatives with respect to a multitude of additional trajectory and observation model parameters, such as planet gravity terms, target ephemeris coordinates, spacecraft gas leaks, and tracking station locations. The radio navigation data calibrations are computed using the MEDIA Program and input along with the measured data array. An array of observation residuals is computed and regression analysis is performed to produce a best estimate of corrections to the initial state parameters and the other desired parameters. The product of the process is a numerically integrated trajectory that best fits the observations.

The Automated Picture Planning (APP) Program, Optical Navigation Image Processing System (ONIPS), and Optical Navigation Program (ONP) are all associated with obtaining and preparing the optical navigation data for input to the orbit estimation process.

The best-estimate trajectory serves as the basis for computation of the velocity correction parameters required to correct the flight path to meet the mission target objectives, a computation that is performed by the Maneuver Operations Program (MOPS).

3.3.2.3 Navigation Support Systems. Deep space navigation requires the computation of accurate orbits and targeting corrections. These are made possible by the use of submeteraccurate modeling throughout the navigation processing system and several model support systems, which furnish the data and constants necessary for accurate computation. Submeter modeling is achieved by the use of double precision in all trajectory and observable computations, and by the use of a relativistic light/time solution algorithm in the Doppler and range-observable computations (this takes into account the retardation in the velocity of light by gravity and the transformation from solar system barycentric (center of mass) coordinate time to Earth station proper time). Model support systems provide the location of planets and natural satellites in the solar system, the location of the tracking stations on Earth, variations in the Earth's rotation and orientation, and the effects of transmission media on the radio signal. A description of these support systems is given below:

(1) The Planetary and Satellite Ephemeris System. The ephemeris of a heavenly body is basically a catalogue, in tabular form, of that body's position in space at various time intervals. JPL's planetary ephemerides are derived primarily from optical transit data acquired by the U.S. Naval Observatory over the past century, from radar planet surface-bounce range data obtained by the NASA DSN over the past decade, and from spacecraft range data from past planetary missions. A large data reduction system, the Solar System Data Processing System (SSDPS), is maintained by JPL to process these many observations and produce the world-standard JPL ephemerides, which are accurate to within 0.2 geocentric microradians. Ephemerides for the planets' natural satellites are developed from photographic (astrometric plate) measurements and data from previous missions and are computed in a data reduction system similar to SSDPS.

(2) Tracking Station Locations. Position coordinates of the DSN tracking stations are computed from Doppler navigation data taken from planetary encounters and are tied to the ephemeris used in reducing the data. As a new planetary ephemeris is generated, the locations of the Earth tracking stations are recomputed. Stations are located

relative to the current ephemeris, to an accuracy of better than one meter (3.3 ft).

(3) Universal Time and Polar Motion. Universal Time (UTI) and polar motion data are obtained from the Bureau International de 1'Heure (BIH) in Paris, France, after its reduction of meridian circle data. These Earth rotation variations are stored in computer files in polynomial form and are applied as calibrations to the computed radio observables.

(4) Transmission Media Effects. Tropospheric effects on Doppler and range data are modeled in equation form. Charged particle effects from the Earth's ionosphere are modeled as elevation-dependent daily varying calibrations. In contrast to previous missions which used S-band uplink and S- and X-band Downlink, the Cassini mission will use X-band for both uplink and downlink, thereby reducing the necessity for both ionospheric and solar plasma calibrations.

3.3.2.4 Navigation System operations. The navigation system is operated in support of each deep space mission, both before the actual flight and during the flight. Prior to launch, navigation system software is exercised with simulated data. Covariances generated in these exercises enable the analyst to identify the major error sources for the mission of interest and predict the total achievable mission accuracy, along with the required measurements and their acquisition schedule. Performance constraints on the spacecraft systems, such as total required propellant or maximum allowable gas leakage rates, can also be defined.

During flight, the navigation system is operated to support the actual guiding of the flight profile. The system determines all of the maneuvers that correct the flight path, and furnishes all trajectories used to compute the spacecraft science instrument pointing sequences and spacecraft antenna pointing and turning sequences. Doppler data are processed in the navigation system to investigate spacecraft anomalies, such as abnormal gas leaks, that may affect the flight path. The navigation system predicts the times of all dynamically related mission events such as occultation times. Finally, reconstructed orbits are used to accurately locate the instrument viewing footprints as an aid to the analysis of the science data.

When actual data processing begins, it is conducted as a scientific experiment in which a hypothesized flight path is adopted and tested against the observations. This testing process is patterned after the preflight analysis, is matured well before planetary encounters, and usually involves the following:

(1) Computing a multiplicity of flight path solutions, including:

(a) Solutions for various tracking data arc lengths to examine the distinguishing effect of changing geometry.

(b) Solutions for various choices of data types to examine the degree of compatibility or conflict between data types and establish realistic data weighting policies.

(c) Solutions for various combinations of estimated parameters to detect mismodeled phenomena and establish corrected model parameter values.

(d) Solutions using various data filtering algorithms and a priori statistics on estimated parameters.

(2) Selecting an adopted best-estimate flight path solution strategy from an analysis of the following characteristics of all solutions:

(a) Noise and signatures in the data residuals.

(b) Comparison of the flight path estimates with previcus results.

(c) Compatibility of model parameter estimated values with estimated values from other sources.

(d) Comparison of computed error covariances and error sensitivities to unestimated model parameter errors and stochastic phenomena.

(3) Exercising the adopted strategy to produce the final best-estimate flight path.

The computation of maneuvers is also a complex process. It requires the placing of maneuvers at times that are conducive to minimizing propellant use, satisfying constraints, and achieving high accuracy.

3.3.2.5 Doppler Navigation Performance. One measure of navigation system performance is the statistical accuracy with which navigation delivers a spacecraft to its target. To look at the record of planetary encounter deliveries, it is enlightening to first examine analytically the accuracy that can be achieved from Doppler data received from a station on Earth while tracking

a spacecraft in distant space. This information content can then be compared to actual flight experiences.

In the left half of Figure 3-9 a station on Earth is shown Doppler-tracking a spacecraft at range ρ, with the Earth rotating at rate ω. The Doppler signal is proportional to the spacecraft-station range rate, which follows in time a pattern that closely resembles a sine wave. In the equation within the figure, the topocentric range rate is shown to be approximately equal to the geocentric range rate plus the sinusoidally varying term. The average signal is thus proportional to the geocentric range rate. The amplitude of the sinusoidal term is proportional to the cosine of the geocentric declination.

There are three important points to note concerning the information content of Doppler data in the determination of the position of the spacecraft in the plane perpendicular to the Earth-spacecraft direction (plane of the sky): First, the basic Doppler measurements provide geocentric angle determination, thus the position accuracy of the spacecraft is directly proportional to the geocentric range. Second, the ability of this system to determine declination is inversely related to the sine of the geocentric declination. Therefore, an error in declination is magnified by a factor of the reciprocal of the sine of the declination. This explains the traditional low declination problem often referred to in space navigation literature. Third, the determination of right ascension is not particularly sensitive to variations in geometry. In practice, right ascension is usually determined more accurately than is declination. The third dimension along the Earth-spacecraft direction is measured accurately [i.e., to < 20 m (66 ft)] directly from radiometric range data.

An obvious concern develops with the accuracy of Doppler navigation if the target planet is near zero declination when encountered by the spacecraft. Conceptually, a singularity occurs and Doppler orbit-determination accuracies in declination fall off sharply. For this reason, a new radiometric observation, ΔVLBI, has been developed. If two tracking stations with long north-south baselines, as shown in the right half of Figure 3-9, measure the time delay equivalent to a one-way range difference, errors in the measured range are proportional to the reciprocal of the cosine of the declination, not the reciprocal of the sine. Hence, no singularity occurs at zero declination. The current VLBI system produced angular measurements accurate to 75 Nanoradians.

Figure 3-10 provides the flight record of achievement of deep space radio navigation in terms of the actual delivery error, mapped and adjusted for the differences in declination and range, into equivalent geocentric declination error at 23.5 degree. The error values were derived by selecting from the flight records the best or most credible flight path solution based on data obtained

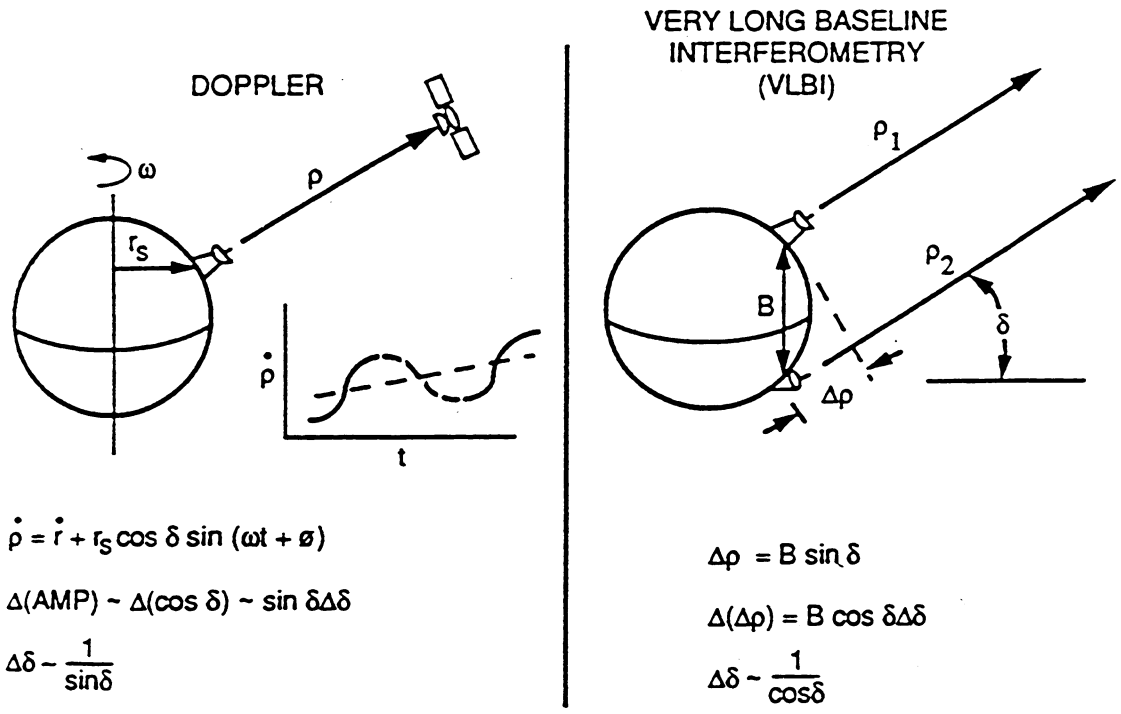

Figure 3-9 Properties of Doppler and ΔVLBI Data as Navigation Measurements

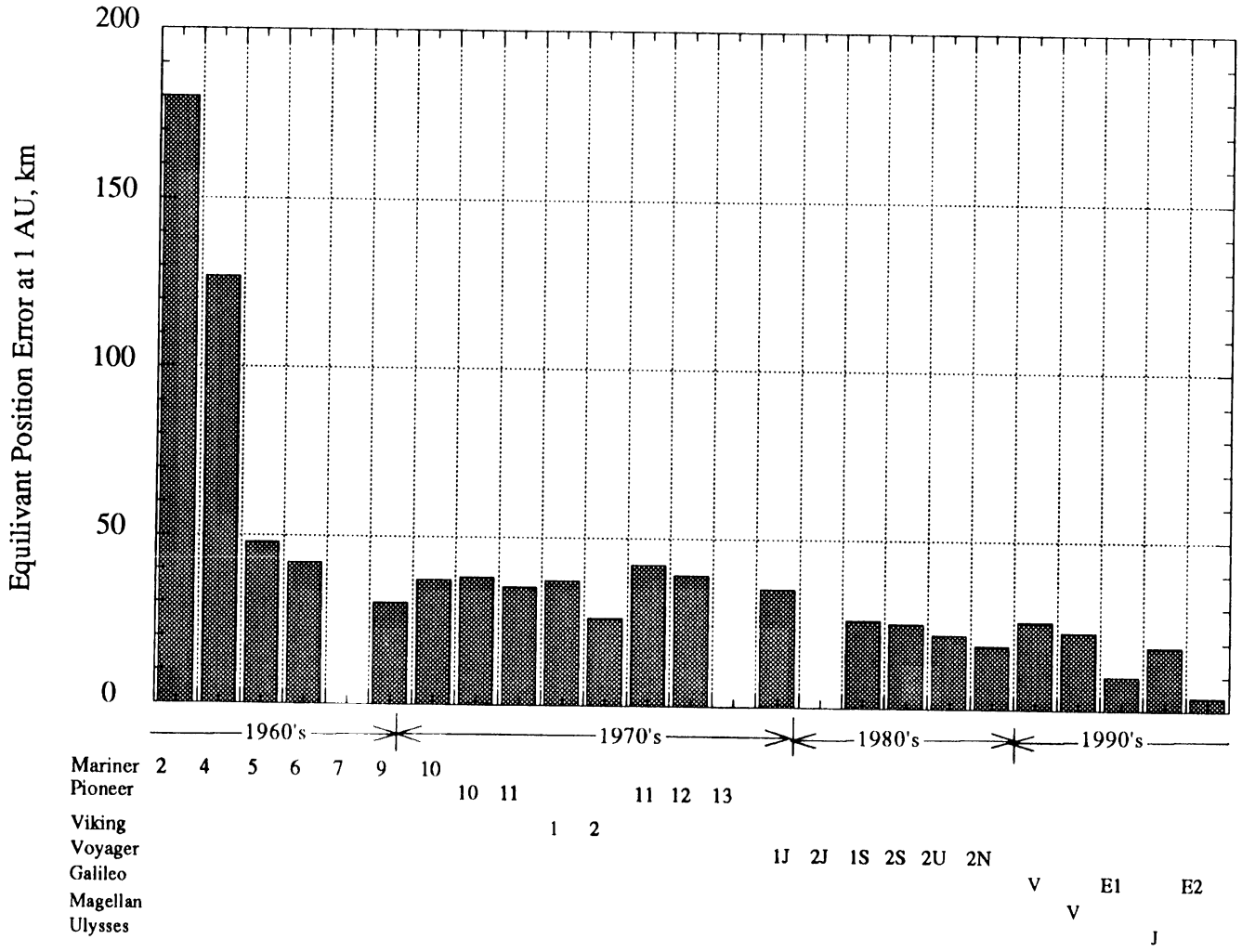

1 AU = 1.496×10^8 km (9.296×10^7 mi)
(1 km = 0.62 mi)

Figure 3-10 Mission-to-Mission Doppler Navigation Performance History - Equivalent Geocentric Declination Error at δ= 23.5 deg

before the spacecraft experienced appreciable effects from the gravity field of the encountered planet, and subtracting the best post-flight orbit solution based on data taken during planetary encounter. Because approach trajectory estimates based on data obtained during encounter are extremely accurate due to the effect of gravity on the spacecraft and the Doppler, this difference represents a good approximation to the actual error in the delivery flight path. As shown in the figure, the delivery errors for Mariners 2 and 4 were relatively large, but later missions have experienced a remarkable consistency in navigation performance. Note also that Doppler navigation systems have delivered spacecraft to distant targets over the past several years with an accuracy of about 0.25 geocentric microradians (at an equivalent declination of 23.5 deg).

The delivery navigation of the voyager encounters with Jupiter (2J), Saturn (lS and 2S), Uranus (2U), and Neptune (2N) were achieved with the aid of optical navigation using the spacecraft camera and were not primarily dependent upon the Doppler navigation accuracy. Therefore, an equivalent radio-only accuracy has been estimated. The Galileo navigation also relies on an accurate ranging system in addition to the Doppler system. This reduces the sensitivity to the geocentric declination and the range, hence these accuracies have not been normalized.

3.3.3 Orbit Knowledge Determination for Earth Swingby

In the pre-launch navigation analysis to support an Earth swingby, covariance analysis is conducted to determine the accuracy to which the spacecraft's state is known as a function of time. Covariance analysis is presented here for the Earth swingby on the prime trajectory. Results for the swingby are based on the spacecraft tracking schedule, which acquires one track of coherent X-band Doppler data per week during cruise. The tracking coverage increases to once per day 90 days prior to encounter and to twice per day 50 days prior to an encounter. Multiple range measurement are obtained during each Doppler track.

In analyzing the swingby, knowledge of the spacecraft's state is derived as a function of time, as are uncertainties in maneuvers, constant and random nongravitational accelerations due to gas leaks, and the component of solar pressure along the Sun-spacecraft line (radial). Incorporated into these derivations are the considered effects of constant errors in tracking station locations, ionosphere, troposphere, Earth's ephemeris, and Earth's gravitational parameter **(μ).** (Error sources not estimated but permitted to influence the covariance are said to be “considered.”) State knowledge is expressed in terms of the Earth encounter B-plane (see Figure 5-1). In terms of the magnitude of the miss vector, B, Figure 3-11 illustrates the typical knowledge uncertainty of the spacecraft position as a function of time relative to Earth encounter. The three-step increases in the curve show the effect of the maneuver execution errors on the predicted delivery accuracy.

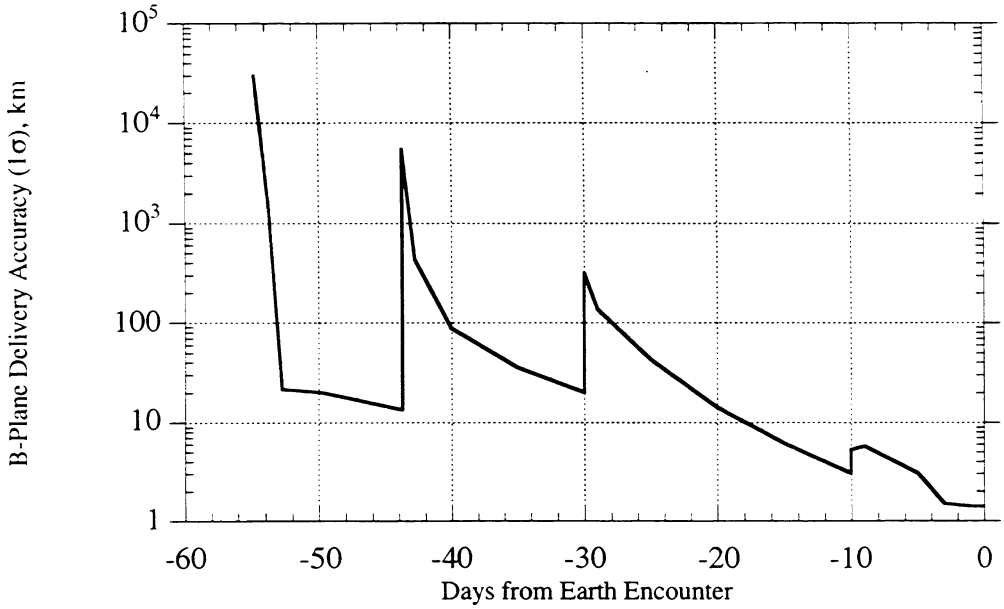

(1 km = 0.62 mi)

Figure 3-11 Typical Spacecraft Knowledge History

3.4 UPLINK PROCESS OVERVIEW

The uplink process for Cassini takes the basic desires of the Cassini Flight Team (Spacecraft, Probe Engineering, Navigation, Mission Design, and Science Teams), generates the spacecraft uplink loads necessary to achieve them, and transmits them to the spacecraft.

There are three basic phases to the process:

(1) Generating and reviewing the desired activities.

(2) Translating the activities into uplink loads and validating them.

(3) Transmitting the uplink loads and ensuring they are correctly received on board the spacecraft.

The same basic process is used for all uplinks, including those to move the spacecraft off an impact trajectory. Under nominal conditions the process takes two months, with the maneuver design process taking one month. For a recovery maneuver during the period close to swingby, the normal schedule would be compressed by conducting more activities in parallel, not by eliminating steps. The nominal Cassini Project operations is designed to be able to

execute a planned trajectory maneuver two days after Titan flyby. Two days is also considered to be the minimum time necessary to do an unplanned recovery maneuver.

3.4.1 Uplink Definitions

3.4.1.1 Command Loads. Most uplink loads to the spacecraft are in the form of a file containing individual commands that are expressed in the form of a numeric operation code plus a number of parameters. There may be restrictions put on the values of the parameters. Some commands may be expanded on-board into a number of sub-operations.

During the command generation process, command operations are referenced using mnemonics, not their numeric forms. This makes it less likely that mistakes will be made and facilitates the review of the command loads. Translation of the commands into numeric (binary) form is done late in the process. The binary commands are aggregated into "packets" of up, to 2000 bits, each of which is then placed in a "frame." A cyclic redundancy check is placed at the end of each packet and frame for error detection. For every 56 bits of the frame, an 8-bit code capable of correcting one error and detecting two errors is then calculated and inserted.

Although all uplink loads are called "command loads" or "command files", some loads might contain new software for an engineering subsystem or instrument, rather than commands. Flight software errors are treated, in this document, as spacecraft failures and will not be considered further here, except to state that the same error detection and correction codes used for the transmission of command loads also apply to software loads.

3.4.1.2 System-Level and Instrument-Internal Commands. There are two types of commands: 1) system-level commands, and 2) instrument-internal commands. System-level commands are those commands that affect the entire spacecraft. All commands to spacecraft engineering subsystems are of this type, along with some instrument commands. Instrument-internal commands affect only the instrument to which the commands are sent. Because instrument-internal commands cannot cause trajectory changes and cannot affect the execution of a recovery maneuver, they will not be considered further. For convenience, therefore, the term "real-time command" will be used in this document to mean "system-level real-time command."

3.4.1.3 Restricted Commands. The system-level commands are further divided into "restricted" and "non-restricted." Restricted commands are those considered to have a significant effect on spacecraft resource usage or to cause a difficult-to-reverse action. Restricted commands will be given extra scrutiny during the command review process. There are two Cassini commands that could cause a change in spacecraft trajectory (7ENGINEBURN and 7RCSBURN); both are defined to be restricted commands.

3.4.1.4 Sequenced Commands. Most of the activity on the spacecraft is controlled from the ground by means of sequences of commands that are uplinked to the spacecraft during one uplink window, but which are to be executed over an extended period.

During cruise, it is expected that a sequence will cover a period on the order of 50 days. These loads are generally quite large, containing up to 300 kilobytes of data.

Many of the commands in the sequence will contain the time at which the command is to be executed. They will be stored in the CDS memory and distributed to the executing subsystem or instrument just prior to the execution time. These commands can therefore be executed only once. Some instrument-internal commands are sent to the instrument immediately upon receipt. Whether they can be executed more than once is dependent on the instrument design; however, by definition these commands cannot affect the Earth swingby trajectory.

The sequence may also include groups of commands that are stored on board, but which do not have assigned execution times. These groups may be executed multiple times, either by other stored commands or by commands sent directly from the ground (real-time commands). Commands which can cause a trajectory change will always be time-tagged.

In the case of maneuvers, a preliminary set of time-tagged commands is included when the sequence is first uplinked. However, the values for the turn commands and burn commands are set to zero. As the time for execution gets closer, recent navigation data are used to finalize the maneuver parameters. Approximately 24 hours prior to the maneuver execution time, the actual values are uplinked, overwriting the previously uplinked commands. After the maneuver has been executed, commands will be uplinked to zero out the maneuver.

The process of developing a sequence is a hierarchical step-wise refinement process. Each step of the process transforms higher-level sequence components into more detailed sequence components until eventually the actual commands to be sent to the spacecraft are generated. The reasons for this approach include the fact that the design of a sequence cannot be done in a single step due to the wide range and number of details that must be dealt with, and the need for effective coordination and communication among scientists and engineers who are not co-located and have different interests, technical backgrounds, and viewpoints.

Prior to launch, there is a period, called Assembly, Test and Launch Operations (ATLO), during which the spacecraft is tested. During ATLO at least three sequences are to be tested. These three sequences are: Launch, Probe Checkout, and Spacecraft Maneuver. The test cases are designed for both nominal and fault cases (e.g., burn longer than maximum burn time) of the sequence.

3.4.1.5 Real-Time Commands. Occasionally commands which are not part of a sequence will be transmitted. These are called “realtime commands.” A real-time command may be designated to be executed immediately upon receipt or it may contain a time tag for delayed execution. A real-time command can execute in parallel with a nominal executing sequence or in the absence of any executing sequence.

Loads containing real-time commands are generally significantly smaller than those containing sequences, since most spacecraft activity is controlled by the sequenced commands.

There are two ways in which real-time commands can be generated. In the course of developing a sequence, it may be determined that there are some commands which should not be included in the stored sequence, but which should be sent from the ground at or closer to the time of execution. These commands are called “planned real-time commands.” Such commands are used to provide a backup to a critical stored command or because the exact execution time or parameters for a command are not known at the time the sequence is generated. Planned real-time commands are generated in parallel with the sequence and are approved at the same time.

Unplanned real-time “commands” are those which are needed to correct trends on the spacecraft and/or to respond to anomalies. A separate generation and approval process is used for unplanned real-time commands, although they undergo most of the same constraint checking and restricted command checking that is done for the planned real-time commands.

3.4.2 Uplink Operations Organization

During the Cruise Phase, which contains the Earth swingby, uplink operations involve planning, sequencing, validating, and then commanding the Cassini Spacecraft to ensure its safe arrival at Saturn. Activities during the Cruise Phase which involve the meeting of science objectives will be considered here only to the extent that they might affect the Earth swingby.

Figure 3-12 shows the operations organization supporting the uplink process during the Cruise Phase.

A downlink process is conducted in parallel with the uplink process. It collects and processes the telemetry from the spacecraft as well as radiometric data on the ground. Inputs from the downlink process are used as appropriate in the uplink process. Examples include the use of trajectory determination data for maneuver design and the use of command receipt verification telemetry to determine if an uplink was successful.

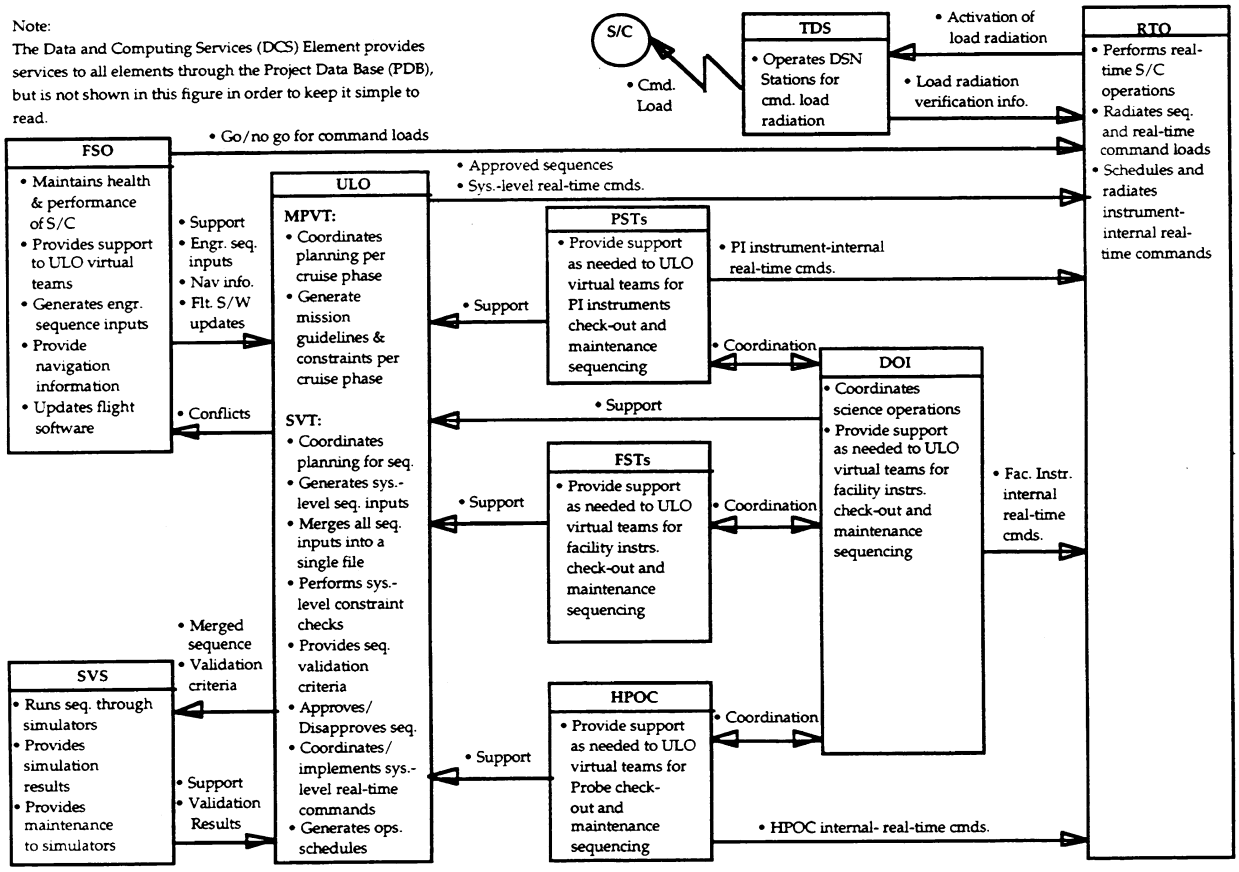

Figure 3-12 Operations Organization, Major Functions, and Interfaces in the Uplink Process

The uplink process is performed by a Sequence Virtual Team (SVT) led by a sequence integration engineer from the uplink operations element and consisting of members from all the other ground system elements (Flight System Operations, Distributed Operations Interface, Simulation and verification Services, RealTime operations, and Science Teams). The Flight System Operations Element contains the navigation analysis and the spacecraft health and monitoring functions.

There will be one "instance" of the SVT for each sequence developed. It comes into existence at the beginning of sequence development and ceases to exist at the conclusion of onboard execution of the sequence. Membership from the different elements may vary between instances, depending on-the spacecraft activities to be performed during the execution period.

The SVT is charged with the responsibility of building the sequence and will contain all the people (skills) needed to build it. Sequence review and approval outside of the SVT will not be required. In addition, the SVT is responsible for all planned and unplanned real-time commands which will be executed during the execution period covered by the sequence.

3.4.3 Uplink Subprocesses

The overall uplink process is divided into seven subprocesses. These seven subprocesses and the major interfaces between them are shown in Figure 3-13.

3.4.3.1 Mission Planning Subprocess. During the Mission Planning Subprocess, the mission plan is updated from launch minus one year to end of mission at established times or if an anomaly occurs that affects the mission objectives. Mission planning ensures that the major science and engineering activities are accounted for and coordinated. Aimpoints for all trajectory correction maneuvers will be established during this subprocess.

3.4.3.2 Sequence Planning Subprocess. Sequence planning converts the mission plan into a more-detailed working timeline, which contains spacecraft and ground resource allocations and identifies windows of time for major activities, such as maneuvers, for the sequence under consideration. Through the duration of the Sequence Planning Subprocess, the working timeline matures to a conflict-free activity plan.

3.4.3.3 Sequence Generation Subprocess. During the Sequence Generation Subprocess members of the SVT generate the subsequences to perform the activities included in the activity plan. Each user checks all internal commands for violations to constraints, guidelines, and/or flight rules. Most of these checks are done by software. In particular, the checks for restricted command usage and command parameter violation are performed by software.

In particular, the sequence generation activity for trajectory change maneuvers starts with a set of inputs, in electronic format, from the navigation design function of the Flight System Operations Element. These electronic inputs are directly input into a program operated by a spacecraft analyst, who is also a member of the Flight Systems operations Element, to define the set of propulsive parameters for the execution of the maneuver. A navigation member of the Flight System Operations Element verifies the range and magnitude of the resulting propulsive parameters and validates the maneuver design.

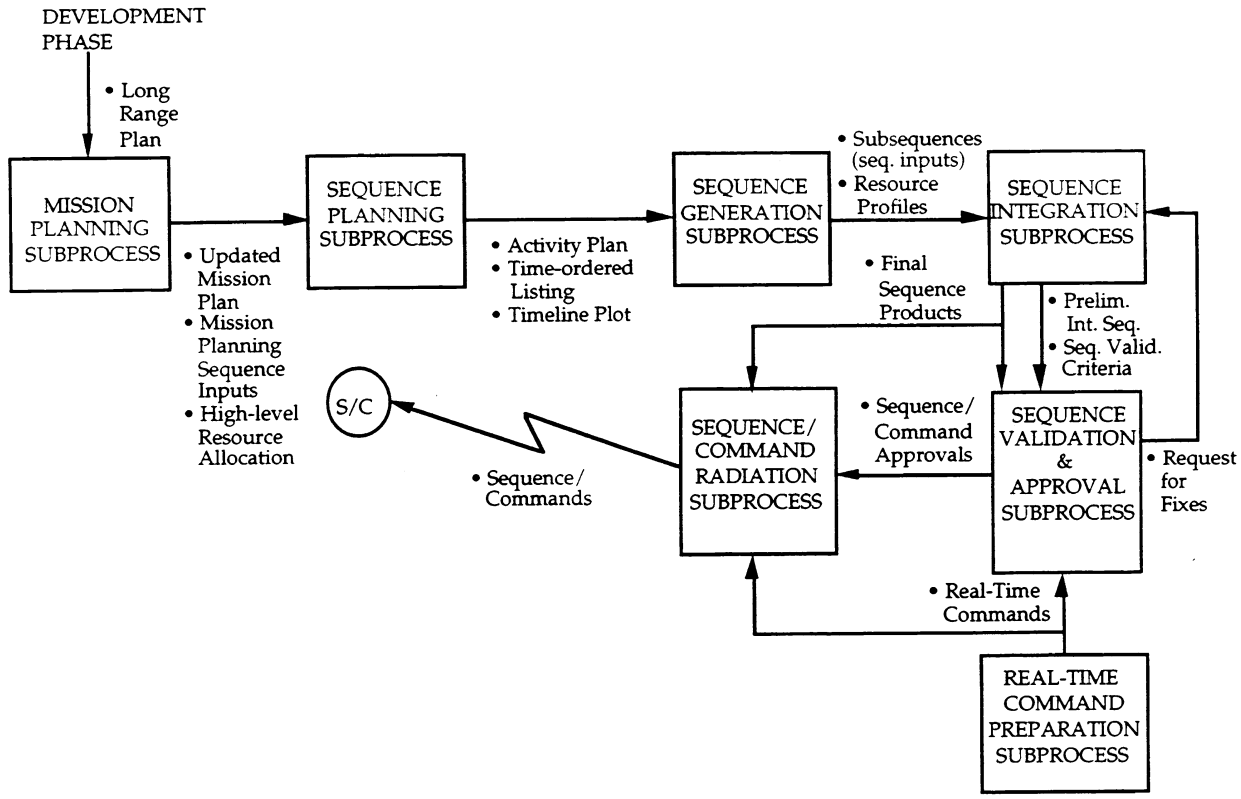

Figure 3-13 Uplink Process Overview for Cruise Operations

Before the Earth swingby maneuver is executed, the flight team will have executed approximately ten trajectory correction maneuvers using the same software and procedures.

Once the maneuver design has been verified, the spacecraft analyst merges the maneuver design with the rest of the engineering inputs (subsequence) and performs final checks of all engineering commands. These final checks include the verification of all guidelines, constraints, and flight rules applicable to maneuvers.

3.4.3.4 Sequence Integration Subprocess. During the Sequence Integration Subprocess all subsequences are merged into a single sequence. At this point, the integrated sequence is checked for system-level violations of constraints, guidelines, and/or flight rules, as well as for usage of restricted commands. Conflicts and violations are identified and resolved by the SVT.

Once all conflicts are considered to be resolved, the SVT merges the final subsequence components into a single working file. Checks for violations to system-level guidelines, constraints, and flight rules and the usage of restricted commands are performed.

The SVT translates the final integrated sequence into its binary representation file, including the incorporation into packets. In addition, the sequence integration subprocess generates the sequence of events for use in configuring the ground systems and monitoring the spacecraft operation.

3.4.3.5 Real-Time Command Preparation Subprocess. The Real-Time Command Preparation Subprocess is used only when it is necessary to generate a command or set of commands that is not part of a nominal executing or to-be-executed sequence. Since the nominal sequencing operations (Sequence Planning, Sequence Generation, and Sequence Integration subprocesses) are not performed during the Real-time Command Preparation Subprocess, the functions performed during this subprocess ensure that all real-time command loads and ground activities are adequately coordinated and implemented relative to the sequence executing on-board the spacecraft.

The need for planned real-time commands is normally identified by the SVT, while the need for unplanned real-time commands is normally identified by the Flight System Operations Element. Once the need is identified, responsibility for the generation, validation and approval is assigned to the SVT responsible for the time period during which the commands will be executed.

As part of the Real-Time Command Preparation Subprocess, the SVT defines the radiation requirements for the real-time command(s), including the command load window(s) placement and duration.

The SVT implements the requested system-level real-time commands and checks them for constraint and/or flight rules violations. Once the file containing the system-level real-time commands is free of implementation errors and free of constraint and flight rules violations, any instrument-internal real-time commands are appended and the file is stored in the Project Data Base. The instrument-internal real time commands will have been validated prior to submission. Modifications to the Sequence of Events are also generated.

3.4.3.6 Sequence/Command Validation & Approval Subprocess. The Sequence/Command Validation & Approval Subprocess ensures that all command loads, whether they contain sequences or real-time commands, are verified for correctness and integrity, validated against intent, and approved for radiation to the spacecraft.

The Sequence/Command Validation & Approval Subprocess tests the Final Integrated Sequence or real-time command load for constraint violations and errors. After sequences or real-time command loads are generated, there is extensive testing (simulation) and review. During the Sequence/Command Validation and Approval Subprocess, the execution of commands may be simulated on a spacecraft hardware test bed and/or software simulator.

The SVT defines the criteria or requirements for testing or validating the command load. If it is decided to validate the command load by analysis, the SVT performs this validation. if the command load is to be simulated, then the SVT decides what type of simulation is needed (functional and software simulation and/or spacecraft hardware simulation). The Simulation and Verification Services Element then runs the command load through the specified simulators). Once the simulation test has been successfully completed, the SVT reviews the test report.

Based on the outcome of the validation process, the sequence integration engineer approves or disapproves the command load. If the command load is approved, then the approval is passed along with, the file to the Sequence/Command Radiation Subprocess. if the command load is disapproved, then the SVT may decide to fix the problem, if time allows it, or not to radiate the command load at all. Additional project personnel will be consulted as needed in making the final decision.

3.4.3.7 Sequence/Command Radiation Subprocess. The Sequence/Command Radiation Subprocess accepts command loads (prepared during Sequence Integration and/or Real-Time Command Preparation) and controls and verifies their radiation to the spacecraft. This subprocess includes incorporating the packets into frames and providing the coding.

Once the command load (final integrated sequence or real-time command(s)) has been approved for radiation to the spacecraft, the Real-Time Operations Element transmits the translated command load to the DSN station responsible for radiating the command load to the spacecraft. Tracking and Data Services Element members configure the DSN station for radiating the command load to the spacecraft. The command load is queued for radiation to the spacecraft by the Real-Time Operations Element. The command load is modulated onto a command sub-carrier and radiated to the spacecraft, with transmission verification being performed (i.e., it is verified that the command bits are being correctly transmitted to the spacecraft).

3.4.3.8 Command Receipt Verification. Upon receipt of the uplink, the spacecraft performs the error correction and detection algorithms. Any uncorrectable frames are rejected and an indication is sent in the telemetry. The Real-Time Operations Element detects the error indication and works with the other Elements to determine what action should be taken.

SECTION 4

FAILURE MODES

4.1 METHODOLOGY

4.1.1 Introduction

This section deals with the different types of failures that could impart an unplanned or anomalous ΔV to the spacecraft, or could cause a loss of spacecraft commandability. The section is divided into two parts: 1) a discussion of those failures that could result in an anomalous ΔV and possibly place the spacecraft on an Earth impact trajectory and 2) those failures that will prevent the spacecraft from being recovered after inadvertently being placed on an Earth impact trajectory. All of the failures in each category are classified into three general categories: environmentally-induced failures (i.e., micrometeoroids), internal spacecraft failures, and ground-induced failures.

4.1.2 Estimate Uncertainties

For each failure mode, the probability of failure (P_F) was estimated using a combination of historical data (where available), analysis (where appropriate), and informed judgments by experienced engineers. However, as the data and processes used to estimate each P_F typically have some levels of uncertainty associated with them, the predicted P_Fs are also somewhat uncertain. These uncertainties were quantified by providing three estimates of the PF for each failure mode (with the exception of micrometeoroids, whose uncertainties were expressed in the form of a probability distribution function). The best estimate of the P_F, $P_{F.50}$, is defined as the point at which there is believed to be a 50-50 chance of the real P_F being higher or lower than the $P_{F.50}$ estimate. The $P_{F.50}$ value is thus the median value of the predicted range of probabilities. The two additional values are used to quantify the uncertainty associated with the best estimate. The 90 percentile value, $P_{F.90}$, represents a conservative upper estimate and $P_{F.10}$ represents an unconservative lower estimate. The real PF has only a 10 percent chance of being higher than $P_{F.90}$ and only a 10 percent chance of being lower than $P_{F.10}$.

Three points were considered sufficient to describe the uncertainties associated with each failure mode. Because there were a large number of inputs to the calculations used to predict the probability distribution of Earth impact, it was expected that the final probability distribution would be well-populated in both tails by the choice of extreme uncertainty values for several inputs. However, one failure mode dominated the short-term model uncertainty (micrometeoroid induced failures), and it was decided to model the uncertainties for that failure mode as a continuous distribution. When the effects of micrometeoroid induced failures are removed from the final probability calculations, the remaining distribution of

points shows that the choice of three points to describe model uncertainty does in fact provide a filled-out distribution.

The placement of the three uncertainty points (10%, 50%, 90%) was chosen so that all of the points contribute significantly to the result. Each point is sampled 30%, 40% and 30% of the time, respectively, to regenerate the standard deviation of a normal distribution with arithmetically spaced point values, or the logarithmic spread of a log-normal distribution with geometrically spaced point values. This choice also gave the experts providing the quantitative failure information familiar confidence levels upon which to base their uncertainty estimates.

A similar process was used to quantify the uncertainties associated with all ΔV estimates. The best estimate of the ΔV produced by a failure, ΔV_{BE}, was assessed by determining what physical process would most likely occur, and then determining the ΔV that would result from that process. Variations in the ΔV, represented by ΔV_{LL1} and ΔV_{LL2}, due to uncertainties in physical process were assessed by varying the parameters used to describe the physical process (e.g., time to respond to a fault, fragmentation particle size, etc.), although a single parameter was usually dominant. The amount of uncertainty associated with the P_F and ΔVs of each failure mode can thus be assessed by examining its three values. Well-understood and predictable failure modes have a narrow range of predicted values, and less well-understood or less predictable modes have broader ranges.

4.1.3 Logic Diagram

All of the failures described in this subsection represent endpoints on the short- and long-term Earth impact probability logic diagrams (Figures 2-2 and 2-3, respectively). The endpoints on each diagram are discussed in this subsection, with the exception of the endpoints dealing with navigational issues, which are discussed separately in Sections 5 and 6. In the short-term diagram, the section associated with each endpoint is noted on the diagram.

4.1.4 Summary of Results

Table 4-1 is a summary of most of the failure data used to predict the short- and long-term Earth impact Probabilities. Probabilities of failure that are functions of mission elapsed time are presented as graphs in the following subsections that describe those probabilities.

Table 4-1 consists of four columns: The failure type, the probability of occurrence, the ΔV effects, and a column identifying whether each failure will prevent subsequent recovery of the spacecraft. The information used to create the data in the table is explained below for each failure mode.

1 m/s = 3.3 ft/s

Table 4-1 Spacecraft and Ground Failure Probabilities and ΔV Effects

(Page 1 of 2)

Failure Mode	Probability of Failure	ΔV	Comments
1) Stuck Open Thruster Valve			
A. Z Thruster			
(1) Mechanical Failure	PF = 3.75E-7/day - 10% PF = 3.75E-6/day - 50% PF = 3.75E-5/day - 90%	Magnitude: Gaussian w/ following parameters Mean = 0.18 m/s, sigma = 0.0015 m/s - 10% Mean = 0.23 m/s, sigma = 0.03 m/s - 50% Mean = 0.28 m/s, sigma = 0.045 m/s - 90% Direction: -Z	Recovery Possible
(2) Electrical Failure	PF = 3.75E-7/day - 10% PF = 3.75E-6/day - 50% PF = 3.75E-5/day - 90%	Magnitude: Uniform w/ following parameters 0.0006 - 0.0012 m/s - 10% 0.006 - 0.012 m/s - 50% 0.06 - 0.12 m/s - 90% Direction: -Z	Recovery Possible
B. X Thruster			
(1) Mechanical Failure	PF = 3.75E-7/day - 10% PF = 3.75E-6/day - 50% PF = 3.75E-5/day - 90%	Magnitude: Gaussian w/ following parameters Mean = 0.088 m/s, sigma = 0.0075 m/s - 10% Mean = 0.11 m/s, sigma = 0.015 m/s - 50% Mean = 0.13 m/s, sigma = 0.023 m/s - 90% Direction: X or -X AND Magnitude: Gaussian w/ following parameters Mean = 0.10 m/s, sigma = 0.009 m/s - 10% Mean = 0.13 m/s, sigma = 0.018 m/s - 50% Mean = 0.16 m/s, sigma = 0.027 m/s - 90% Direction: -Z	Recovery Possible
(2) Electrical Failure	PF = 3.75E-7/day - 10% PF = 3.75E-6/day - 50% PF = 3.75E-5/day - 90%	Magnitude: Uniform w/ following parameters 0.0003 - 0.0006 m/s - 10% 0.003 - 0.006 m/s - 50% 0.03 - 0.06 m/s - 90% Direction: -Z Magnitude: Uniform w/ following parameters 0.0004 - 0.0008 m/s - 10% 0.004 - 0.008 m/s - 50% 0.04 - 0.08 m/s - 90% Direction: -Z	Recovery Possible
2) Stuck Open Main Engine Valve			
A. Mechanical Failure			
(1) Oxidizer Valve	PF = 3.75E-7/day - 10% PF = 3.75E-6/day - 50% PF = 3.75E-5/day - 90%	Magnitude: Gaussian w/ following parameters Mean = 0.032 m/s, sigma = 0.002 m/s - 10% Mean = 0.040 m/s, sigma = 0.004 m/s - 50% Mean = 0.048 m/s, sigma = 0.006 m/s - 90% Direction: -Z	Recovery Possible

1 m/s = 3.3 ft/s

Table 4-1 Spacecraft and Ground Failure Probabilities and ΔV Effects

(Page 2 of 2)

Failure Mode	Probability of Failure	ΔV	Comments
(2) Fuel Valve	PF = 0.13E-7/maneuver - 10% PF = 0.13E-6/maneuver - 50% PF = 0.13E-5/maneuver - 90%	Magnitude: Gaussian w/ following parameters Mean = 0.019 m/s, sigma = 0.001 m/s - 10% Mean = 0.024 m/s, sigma = 0.002 m/s - 50% Mean = 0.029 m/s, sigma = 0.003 m/s - 90% Direction: -Z	Recovery Possible
B. Electrical Failure (Fuel and Oxid. valves remain open)	PF = 0.13E-7/maneuver - 10% PF = 0.13E-6/maneuver - 50% PF = 0.13E-5/maneuver - 90%	Magnitude: Gaussian w/ following parameters Mean = 0.12 m/s, sigma = 0.005 m/s - 10% Mean = 0.15 m/s, sigma = 0.01 m/s - 50% Mean = 0.18 m/s, sigma = 0.015 m/s - 90% Direction: -Z	Recovery Possible
3) Acceleromenter Failure	PF = 6E-6/day between manuevers - 10% PF = 1E-5/day between maneuvers - 50% PF = 1.6E-5/day between maneuvers - 90% PLUS PF = 4.8E-5/day between maneuvers - 10% PF = 8E-5/day between maneuvers - 50% PF = 1.3E-4/day between maneuvers - 90%	Magnitude: Gaussian w/ following parameters Mean = 4% of planned mnvr, sigma = 1.33% of planned mnvr - 10% Mean = 5% of planned mnvr, sigma = 1.67% of planned mnvr - 50% Mean = 6% of planned mnvr, sigma = 2% of planned mnvr - 90% Direction: -Z	Recovery Possible
4) Main Engine Gimbal Actuator Failure	PF = 1.02E-4/maneuver - 10% PF = 1.7E-4/maneuver - 50% PF = 2.72E-4/maneuver - 90%	Magnitude: Gaussian w/ following parameters Mean = 0.004 m/s, sigma = 0.0008 m/s - 10% Mean = 0.013 m/s, sigma = 0.0026 m/s - 50% Mean = 0.026 m/s, sigma = 0.0052 m/s - 90% Direction: Uniform lateral	Recovery Possible
5) AACS Flight Software Error	PF = 5.0E-6/maneuver - 10% PF = 5.0E-5/maneuver - 50% PF = 1.0E-4/maneuver - 90%	(50%) RCS 0.0003 m/s - 10% 0.001 m/s - 50% 0.005 m/s - 90% Direction: Uniform Spherical (50%) Main Engine 0.02 m/s - 10% 0.08 m/s - 50% 0.17 m/s - 90% Direction: -Z	Recovery Possible
6) CDS Flight Software Error	PF < 1E-6/day - 10% PF < 1E-5/day - 50% PF < 1E-4/day - 90%	Magnitude: Last commandedΔV Direction: -Z	Recovery Possible
7) Anomalous Sun Search	PF = 1E-5/maneuver - 10% PF = 1E-4/maneuver - 50% PF = 2E-4/maneuver - 90%	Magnitude: Uniform w/ following parameters 0 - 0.050 m/s - 10% 0 - 0.063 m/s - 50% 0 - 0.76 m/s - 90% Direction: Uniform Spherical	Recovery Possible

4.2 ΔV-INDUCING FAILURES

This section deals with all failures that will induce an unplanned or anomalous ΔV to the spacecraft. These failures include those caused by micrometeoroids, spacecraft failures, and ground system failures. Some of these failures will also cause loss of spacecraft commandability.

4.2.1 MICROMETEOROID-INDUCED FAILURES

Cometary and asteroidal particulates in orbit around the Sun may impact the Cassini spacecraft and cause damage. Although no interplanetary spacecraft is known to have suffered catastrophic micrometeoroid damage, micrometeoroid-induced failures (MIFS) present a potential threat to the Cassini mission. The Cassini design does include components to provide protection against micrometeoroids, but there are particles with sufficiently high energies to damage the spacecraft.

The elements of the spacecraft that are of concern in this analysis are the spacecraft's propellant tanks, pressurant tank, and engineering bus. A rupture of one of the spacecraft's propellant or pressurant tanks due to an MIF would result in an anomalous ΔV being applied to the spacecraft, and may cause further damage to other spacecraft components. An MIF occurring on some of the engineering bus bays could result in loss of both redundant halves of a critical subsystem, which would cause loss of spacecraft commandability.

4.2.1.1 Probability-of Failure Due to Micrometeroids. The method used to predict probabilities of failure due to micrometeoroids consists of three basic steps: 1) modeling the interplanetary particle environment, 2) predicting the numbers, sizes, relative velocities, etc., of particles that will impact the spacecraft on its trajectory, and 3) determining how many of those particles will defeat the spacecraft's micrometeoroid protection and cause damage to critical spacecraft components.

4.2.1.1.1 Micrometeoroid Environmental Model. The interplanetary micrometeoroid environment has been characterized by a model which incorporates up-to-date information from recent space missions and other observations. Neil Divine of JPL used data from radar observations, zodiacal light measurements, particle fluxes from impact detectors aboard the Pioneer 10 and 11, Helios 1, Galileo, and Ulysses spacecraft, and measurements of interplanetary flux near Earth to create a model of the interplanetary meteoroid environment (See Reference 1). The model describes the distribution of interplanetary particles in terms of particle mass, flux (particles/unit area*second), orbital inclination, eccentricity, and perihelion distance. The model includes particles ranging from 10^{-18} to 1.0 gram (3.5×10^{-20} to .035 ounces) in mass and covers the region of space from <0.1 to

20 AU [<1.496xl0^7 to 2.992xl0^9 km (9.296xl0^6 to 1.859xl0^9 mi)]. The Divine model incorporates all of the information available at the time of its conception, and is believed to be more accurate than the standard NASA model published in 1970. The Divine model predicts higher fluences than the NASA model, and has been accepted by the Cassini Project as its official micrometeoroid model. The model has since been validated using more recently available information from the Long Duration Exposure Facility (LDEF).

Man-made Earth orbital debris from low Earth orbit up to geosynchronous orbit does not affect these calculations, and so was not included. For the short-term component, a MIF that near the swingby closest approach cannot result in enough ΔV to get the spacecraft on an Earth-impact trajectory. For the long-term component, so little time is spent in the orbital debris regime (tens of minutes) that is does not add measurably to the total probability of spacecraft loss due to MIF's.

4.2.1.1.2 Particle Count Determination. The basic process used to estimate the number of particle impacts is to multiply the predicted particle fluence (particles/unit area) encountered by the spacecraft on its trajectory by the total exposed area of the spacecraft. The particle fluence is derived from the JPL micrometeoroid environmental model by integrating the predicted flux over the time period of interest. In reality, however, this seemingly simple calculation is extremely complex.

First, the flux predicted by the environmental model and the spacecraft trajectory characteristics both vary as a function of mission elapsed time, and the entire trajectory cannot be modeled sufficiently as a single period of time. Therefore, the mission must be broken into a series of small time steps. Each time step has its own particular predicted fluence which is used to predict the number of particle impacts during that interval.

Second, the fluence of particles seen by a surface of the spacecraft depends upon the relative velocities of the particles with respect to the spacecraft. Assessment of these velocities requires knowledge about the velocity of the spacecraft and the velocities of the particles in inertial space. The spacecraft's velocity was determined by the orbital characteristics of its trajectory. Particle velocities were determined from the orbital parameters specified by the Divine model. Once the inertial velocities were determined, software was the used to predict the velocities of the particles with respect to the spacecraft as the spacecraft travels along its trajectory.

Third, the particle fluence encountered by a surface of the spacecraft depends upon the orientation of the surface with respect to the velocity of the spacecraft. The orientation of each surface of the spacecraft is dependent upon the orientation of the spacecraft as a whole, which in turn is dependent upon the

location of the spacecraft in its trajectory. During the early portions of both trajectories (i.e., before the final Earth swingby), the HGA will nearly always be pointed towards the Sun to maintain thermal control. However, for most of the mission, the roll orientation of the spacecraft (i.e., the rotation about the Z axis) is not currently specified. For this case, the predicted fluence for a surface normal to the Z axis is an average of the flux components from all directions about the roll axis.

However, during the near-Earth portion of each trajectory, the short-term probability of Earth impact is particularly sensitive to micrometeoroid impacts. Surfaces on the side of the spacecraft pointed in the direction of motion, also called the ram direction, will see more impacts than will surfaces pointed away from the direction of motion. From a period from E30 to E-0 days, the spacecraft will be oriented with the Probe in the ram direction to use the Probe as a shield against the micrometeoroids approaching from the ram direction (where number of impacting particles and relative particle velocities will be highest). During this period, the fluence seen by a given surface will be a function of the surface's orientation about the roll axis (i.e., the fluence is not averaged about the roll axis).

This Probe pointing strategy will only marginally increase the risk of micrometeoroid damage to the Probe. The risk can be ameliorated, if necessary, by orienting the Probe away from the ram direction during a period when micrometeoroid impacts on the spacecraft do not present a possibility of short-term Earth impact.

For both Cassini trajectories (primary and backup), fluences for the entire mission were calculated for both the unspecified and Probe-pointed orientations (with data for the Probe-pointed case being used only for the E-30 to E-0 day period).

Fourth, to predict whether a particle of a specific size and speed will defeat the spacecraft's micrometeoroid protection, the angle at which the particle hits the spacecraft surface (relative to the local surface normal) must be known. Due to spacecraft geometry, particles with the same heliocentric direction of motion will impact different sections of the spacecraft with different impact angles (see Figure 4-1). To calculate the local angle of impact for each surface, information about particle directions of motion was combined with knowledge about the spacecraft orientation and geometry for each section. In addition, the effective surface areas were reduced to account for the foreshortened area as seen from the particle's velocity vector.

Fifth, the micrometeoroid model predicts a broad range of particle masses and relative velocities (direction and speed), which can occur in any combination. To permit numerical calculations, each particle parameter was divided into ranges.

For each time step, fluences were predicted for each possible permutation of particle mass, direction, and speed ranges, with the total fluence being a summation of all of the permutations. Thus, for each time step there is a three dimensional matrix predicting the fluence seen during that interval.

4.2.1.1.3 Spacecraft Protection Evaluation. Once the fluence was predicted as a function of particle mass, impact direction, and impact speed for each time step, it was possible to predict the number of particles which could cause critical damage to the spacecraft.

Micrometeoroid protection for the tanks is provided by the multilayer insulation (MLI) blankets used to control the temperature of the spacecraft. These blankets act as a bumper which disintegrates incoming micrometeoroids and in some cases convert the debris to liquid or gas, thereby spreading their momentum over a larger area (see Figure 4-1). The bipropellant tanks are further protected, in most cases, by the cylindrical support shell. Protection for the bus **is** provided by MLI blankets and the dual shearplate structure used to house spacecraft electronics.

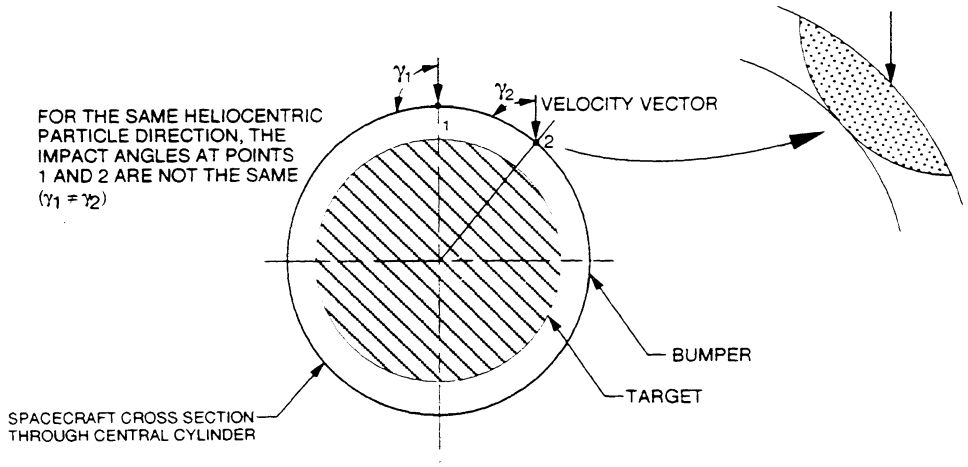

Figure 4-1 Micrometeoroid Protection System

Because different sections of the spacecraft have different levels of micrometeoroid protection, the spacecraft was divided into several regions for the purpose of determining the vulnerability of the spacecraft to micrometeoroids. These sections include the upper shell structure (USS), the propulsion module shell (PMS), the lower equipment module (LEM), the upper and lower tank domes (TOP and BOT), the monopropellant hydrazine tank, the helium pressurant tank, and the engineering bus. This division is illustrated in Figure 4-2.

The protection associated with each section is a function of many factors, including the thickness of the blankets, the spacing of the blankets from the inner (target) surface, and the material properties of the inner surface. Hypervelocity impact analysis software was created to model the effects of a micrometeoroid impact using relationships derived by Hallock Swift (see Reference 2).

For each type of protection, it was necessary to determine the smallest mass particle that would cause critical damage for each incidence angle and impact speed permutation. Once these masses were known, the surface area of each section vulnerable to each permutation of particle mass, speed, and impact angle was calculated. These vulnerable areas were then multiplied by the fluence predicted for each permutation to obtain the total number of MIFs for each section. The number of failures for each section were then added together to obtain the total number of failures for the entire spacecraft for that time step.

4.2.1.1.4 Micrometeoroid Failure Model Calibration. Once the MIF probabilities were completed, the results were calibrated to reflect the experience of other JPL interplanetary missions. The models used to predict MIFs for Cassini were applied to the two voyager and one Galileo spacecraft to predict the number of MIFs these spacecraft would expect to date. Other spacecraft were considered, but were not included in this database because they would not have significantly altered the results, due to relatively short flight times in high micrometeoroid danger areas. It must be noted that no interplanetary spacecraft have suffered catastrophic micrometeoroid damage.

The data used for the calibration considered the differences in these other spacecraft's trajectories, configurations, and degrees of micrometeoroid protection. For these missions, the expected number of MIFs is approximately 1, with a $P_{F.90}$ value of approximately 2. Review of the Voyager and Galileo flight experience indicates that the actual number of MIFs was zero. As described in Appendix A, Bayes' theorem was used to correct the Cassini estimates based upon this data.

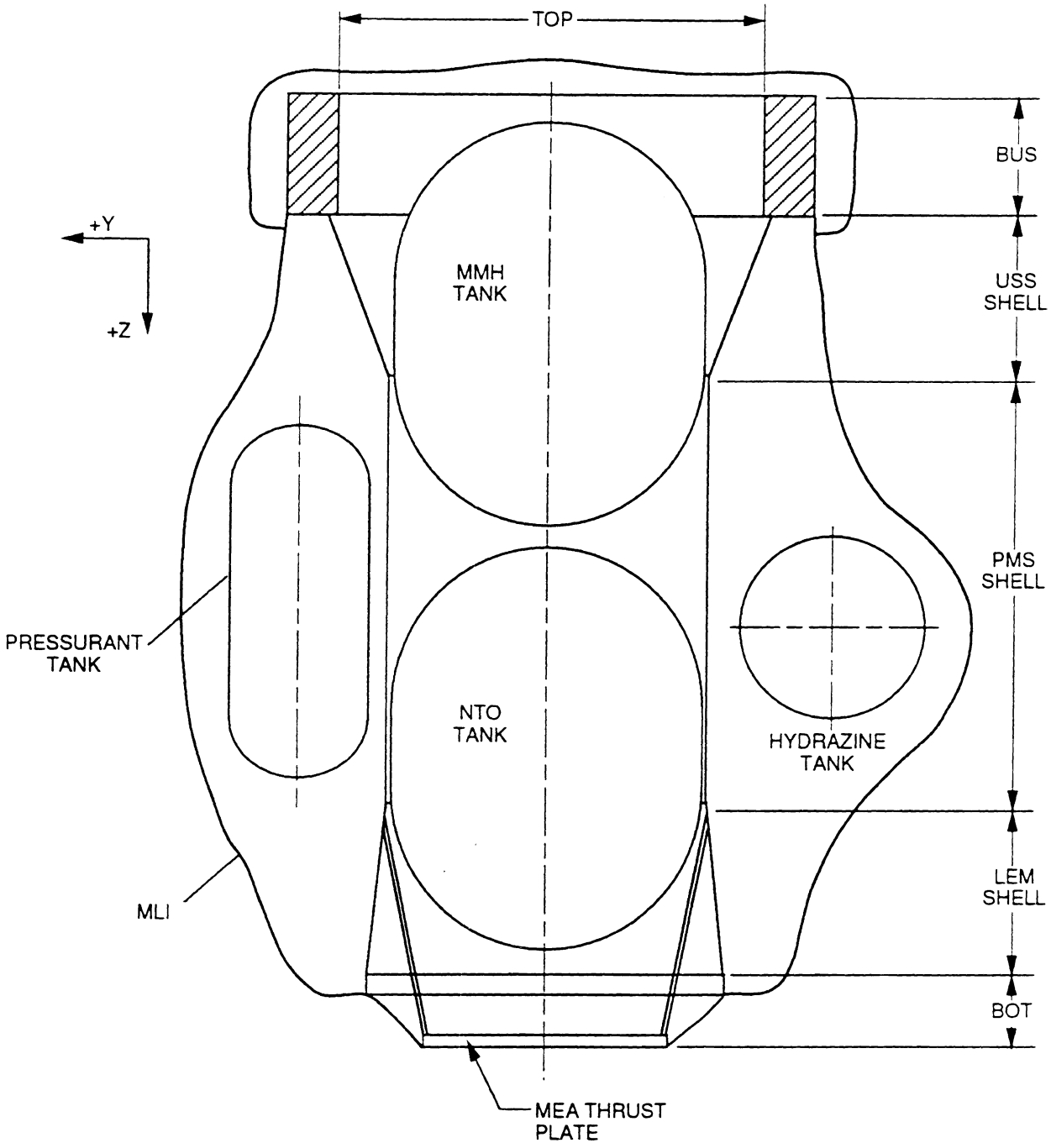

Figure 4-2 Critical Target Model

The best estimates for MIFs of the spacecraft tanks as a function of mission elapsed time (MET) before the Bayesian calibration are plotted in Figures 4-3 through 4-6. These graphs are for both missions, for the unspecified and Probe pointed orientations. The probabilities of failure of both halves of a critical engineering subsystem due to an MIF are shown in Figures 4-7 and 4-8. Because the bus receives little protection from the Probe in the ram-oriented case, the fluence estimates for the bus were performed for only the unspecified spacecraft orientation.

4.2.1.1.5 Micrometeoroid Model Uncertainties. Uncertainties in the environmental model, the protection evaluation models, and other data used in the calculations to predict MIF probabilities create uncertainties in the final results. The uncertainties in each part of the process were quantified and statistically combined, and were calibrated using the data discussed in Subsection 4.2.1.1.4.

The uncertainties are represented by a continuous distribution at each point in time on each MIF probability curve (see Figure 4-9 for a typical distribution). For each distribution, the conservative (84 percentile) value is 3.01 times the best estimate value and the non-conservative (16 percentile) value is 3.01-1 times the best estimate value.

4.2.1.2 ΔV Effects of a Micrometeoroid-Induced Failure. The anomalous ΔV resulting from a MIF depends upon which element of the spacecraft was damaged. A rupture of the bipropellant system will result in a much higher ΔV than a rupture of either the hydrazine or -pressurant tank. A micrometeoroid impact on the engineering bus will impart only a negligible ΔV.

4.2.1.2.1 ΔV Effects of a MIF of the Bipropellant System. An MIF of the TOP, BOT, USS, LEM, or PMS section of the spacecraft (See Figure 4-1) will result in a failure of one or both of the bipropellant tanks. The processes used to predict which of the tanks will burst and the resulting ΔVs are described below.

4.2.1.2.1.1 Bipropellant Tank Rupture Mechanisms. When one of the bipropellant tanks is ruptured by an MIF (i.e., a hole is formed in surface of the tank), the resulting ΔV is dependent upon whether or not the hole propagates. Very small ruptures of the tank surface [<0.01 m (0.4 in) diameter] will not propagate, and the fluids and gases in the tank will jet out through the pinhole. Holes larger than 0.01 meter in diameter will propagate, either disintegrating the entire tank or leaving a large hole with jagged edges. In this case, tank fragments will be created that may cause the other bipropellant tank to rupture.

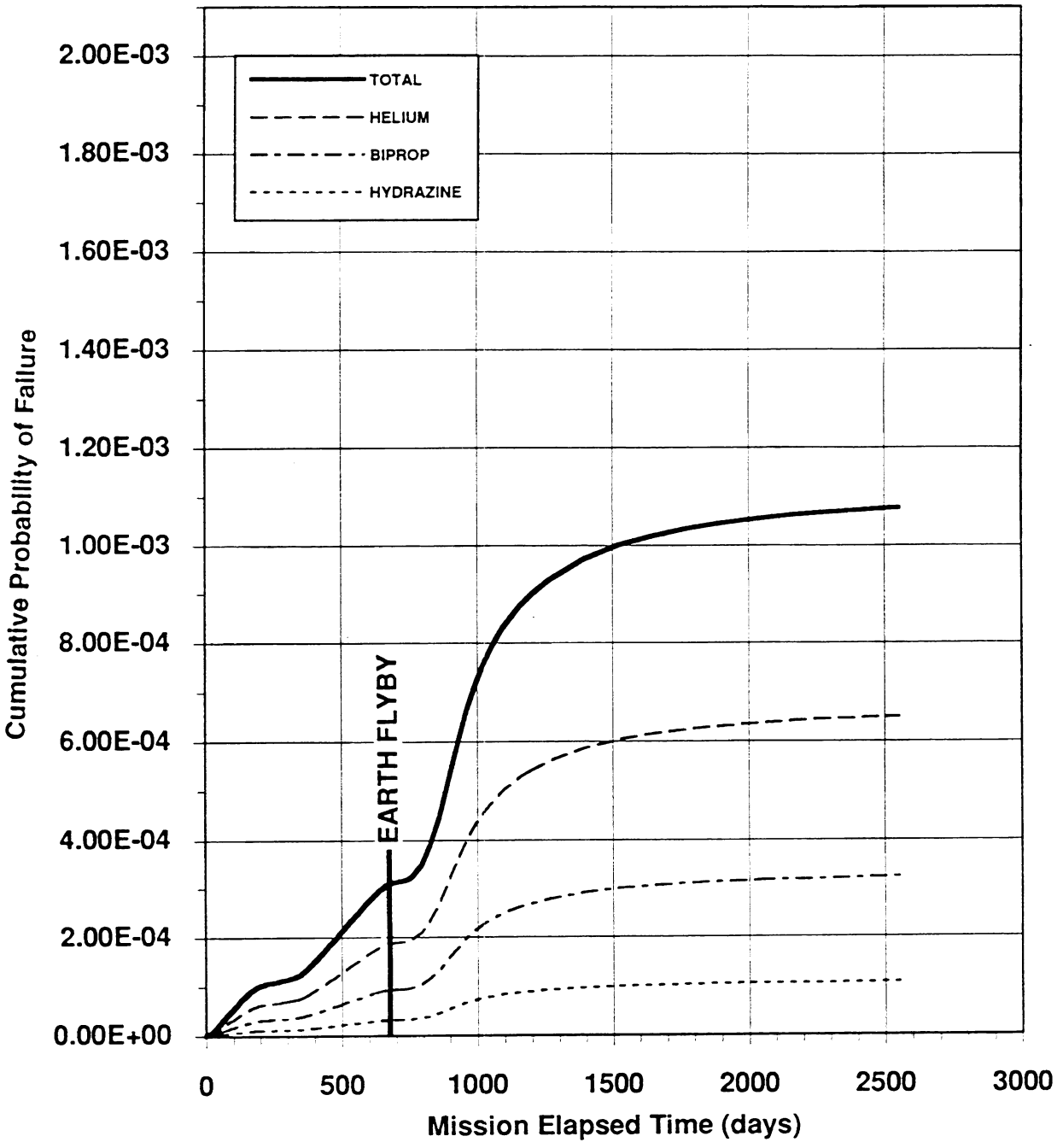

Figure 4-3 Best Estimate of the Cumulative Number of Micrometeoroid-Induced Tank Failures for the Primary Mission with the Nominal Spacecraft Orientation

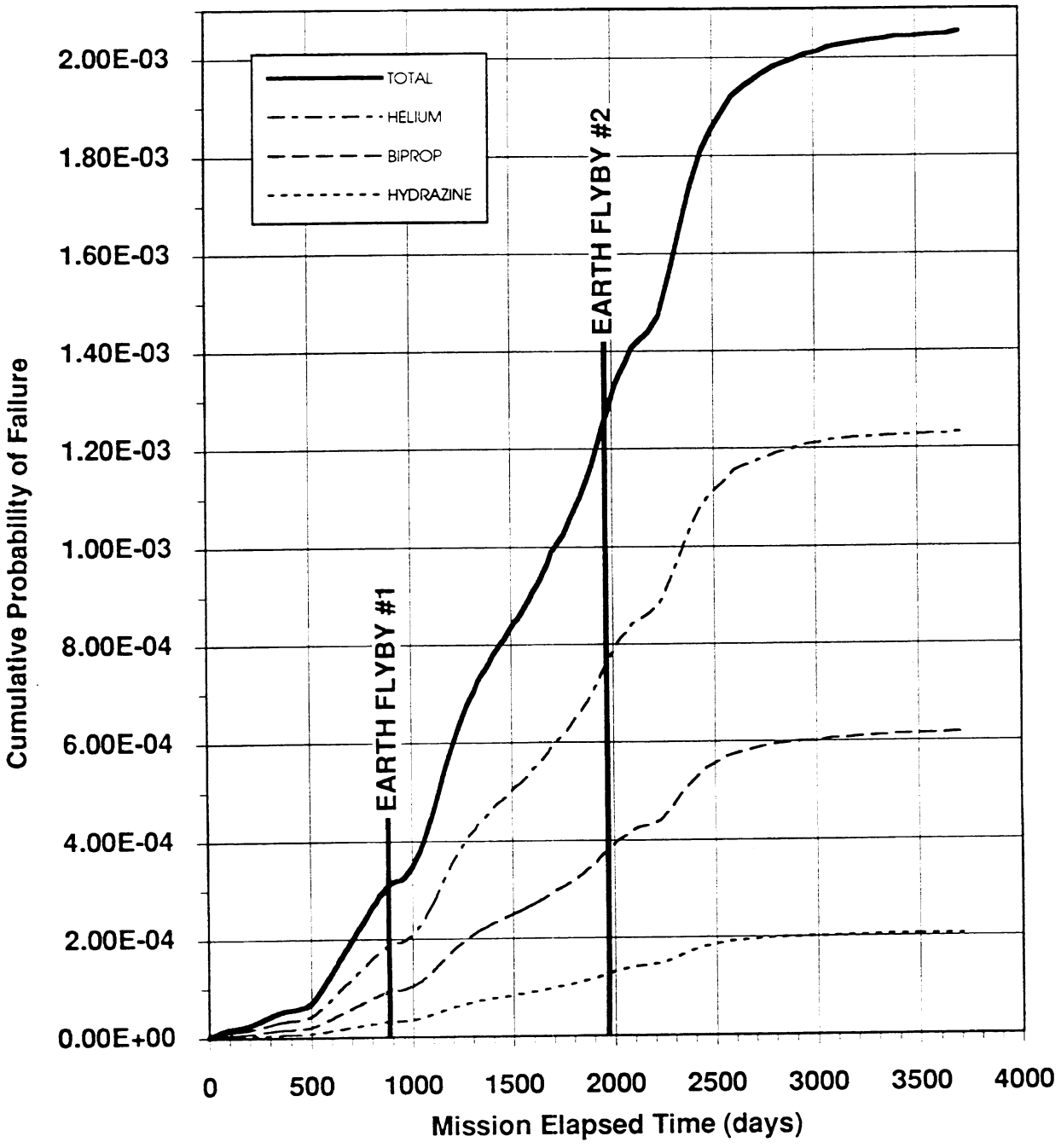

Figure 4-4 Best Estimate of the Cumulative Number of Micrometeoroid-Induced Tank Failures for the Backup Mission with the Nominal Spacecraft Orientation

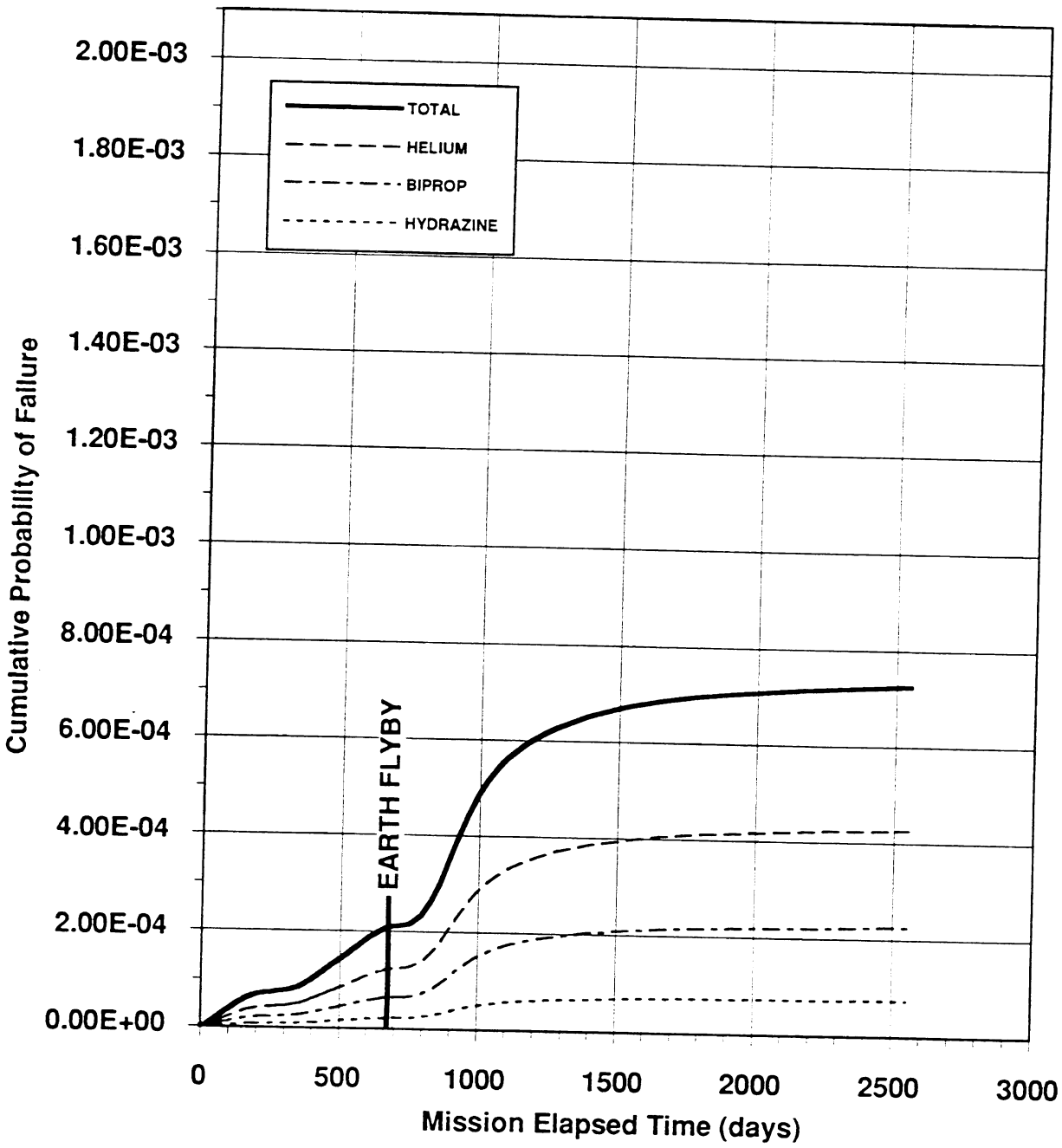

Figure 4-5 Best Estimate of the Cumulative Number of Micrometeoroid-Induced Tank Failures for the Primary Mission with the Probe Pointed in the Ram Direction

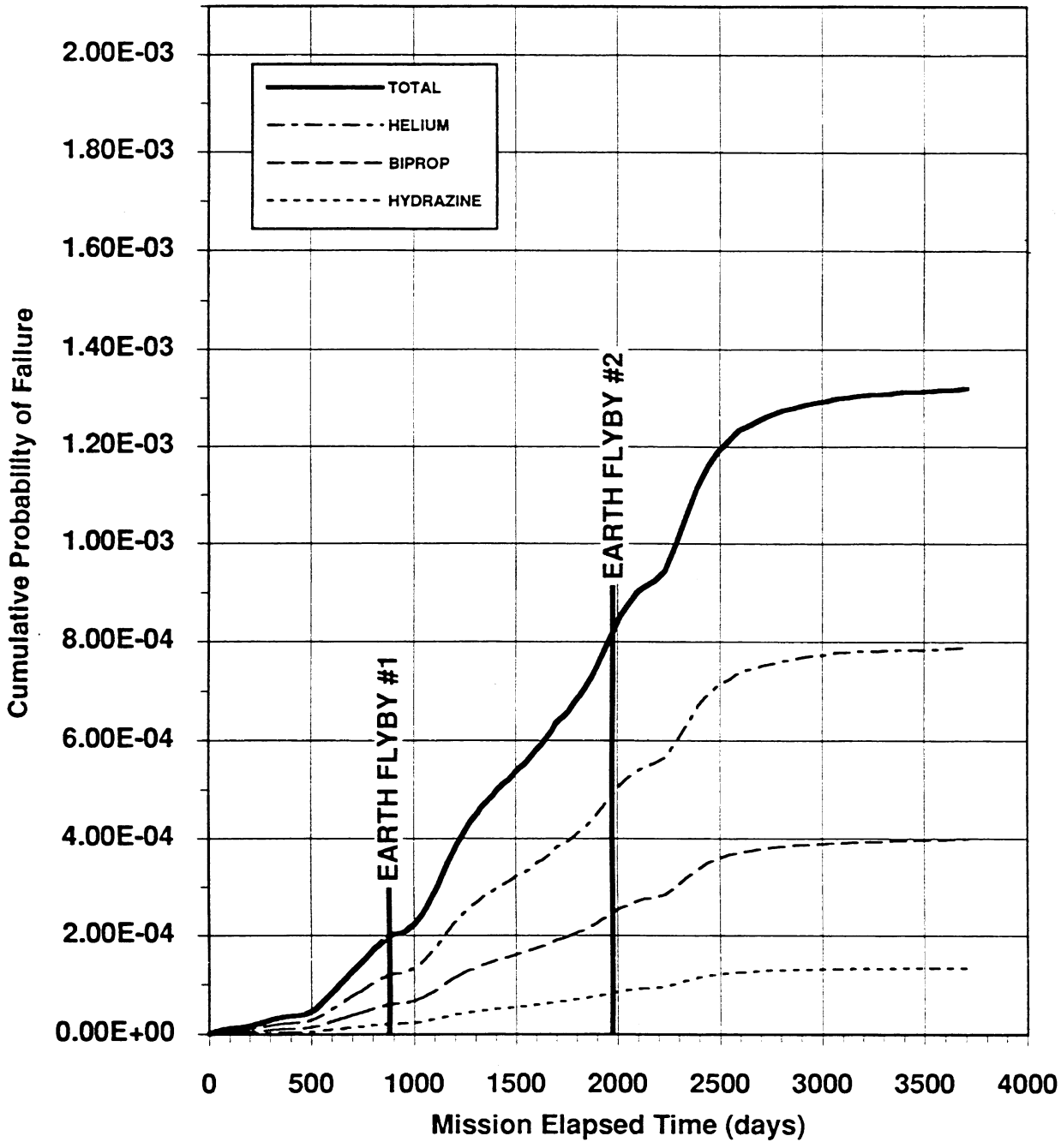

Figure 4-6 Best Estimate of the Cumulative Number of Micrometeoroid-Induced Tank Failures for the Backup Mission with the Probe Pointed in the Ram Direction

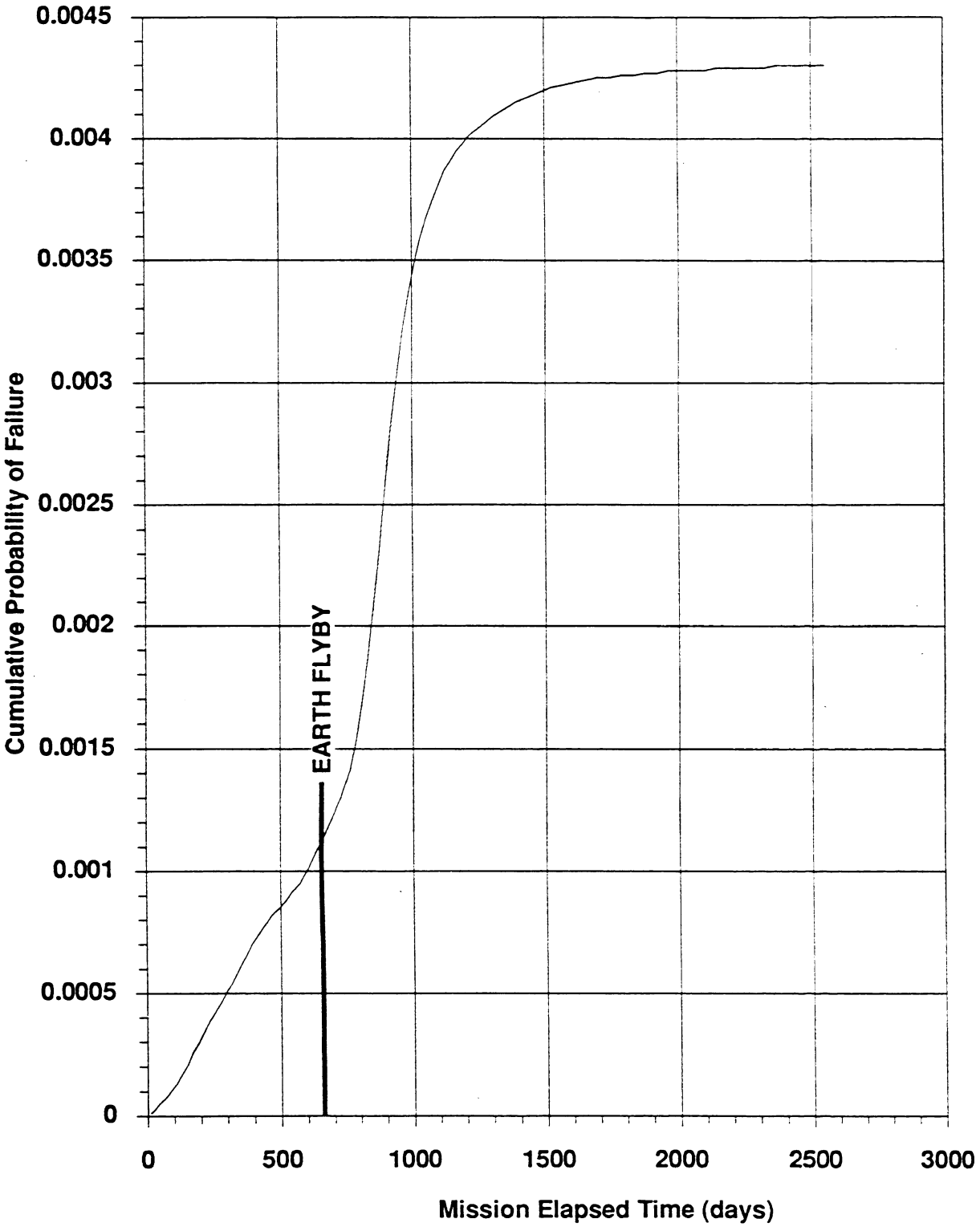

Figure 4-7 Best Estimate of the Cumulative Number of Micrometeoroid-Induced Engineering Bus Failures for the Primary Mission

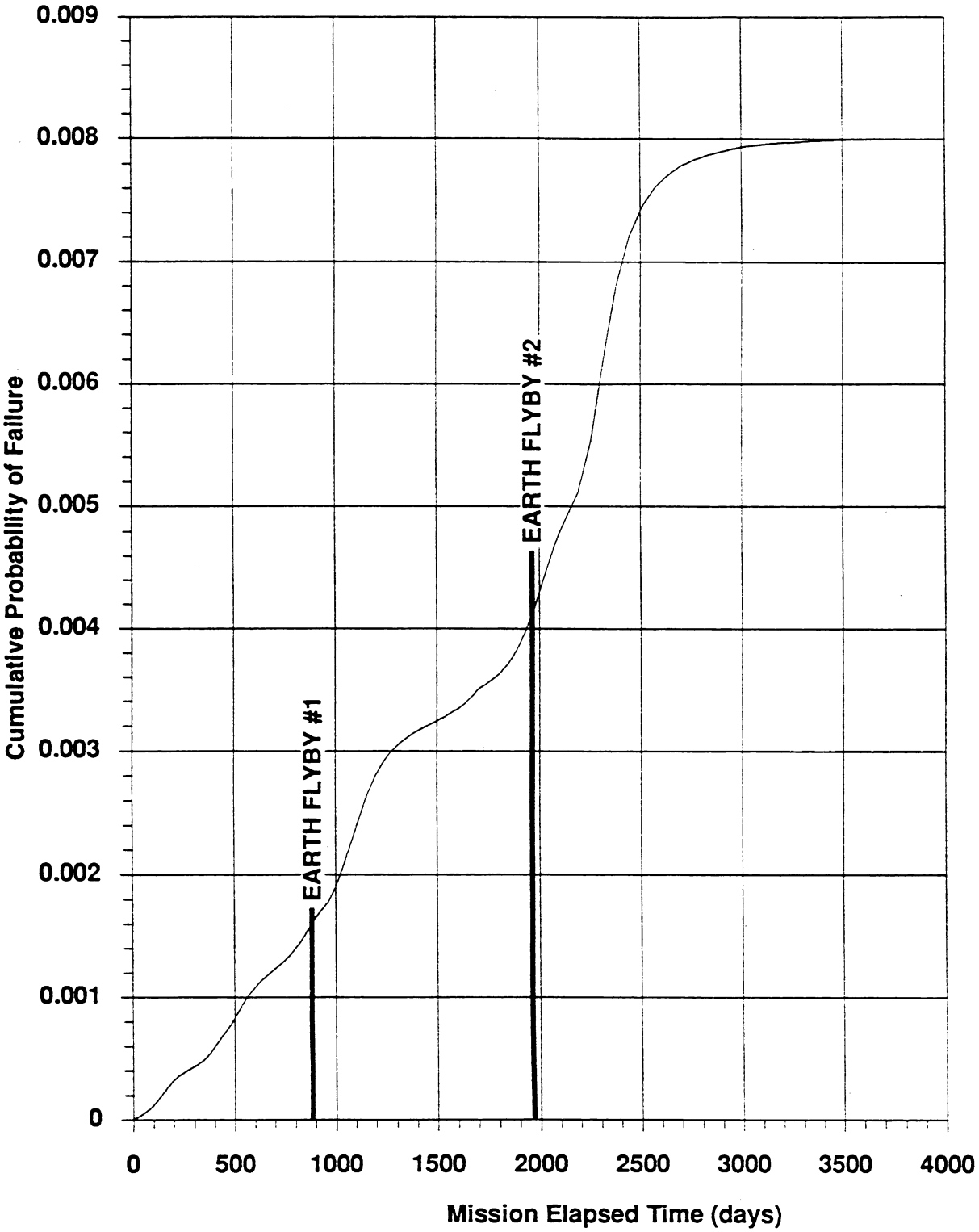

Figure 4-8 Best Estimate of the Cumulative Number of Micrometeoroid-Induced Engineering Bus Failures for the Backup Mission

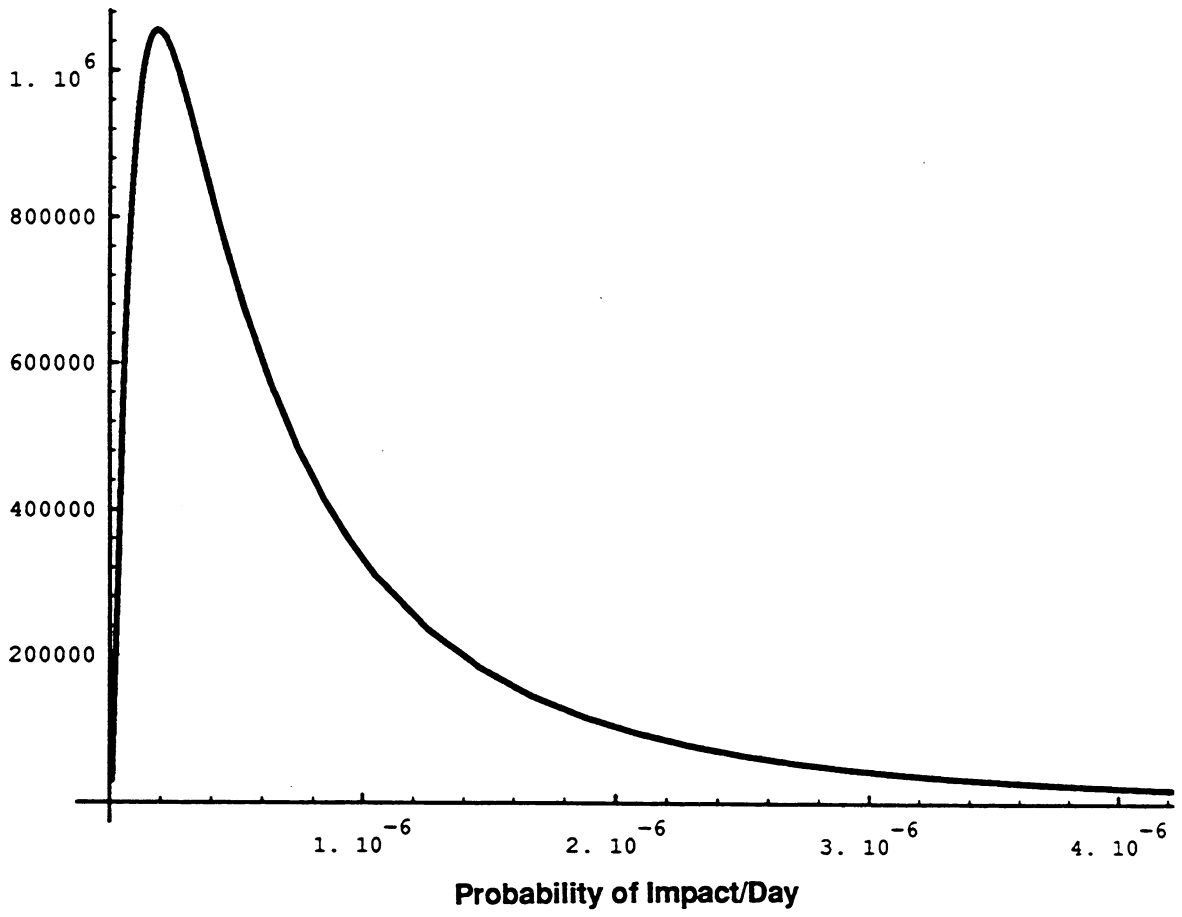

Figure 4-9 Example of Micrometeoroid Uncertainty Distribution

There are several possible physical mechanisms that can occur as a result of an MIF that will result in the rupture of a bipropellant tank. It is believed that all of these mechanisms will create holes in the tank surface with diameters greater than 0.01 meter, including failures due to spalling of the tank surface. All MIFs of one of the bipropellant tanks will therefore cause shattering or fragmentation of the tank.

4.2.1.2.1.2 Tank Rupture Scenario Determination. There are three scenarios that could result from a bipropellant MIF: the NTO tank could rupture, the MMH tank could rupture, or both tanks could rupture, resulting in combustion of NTO and MMH. The scenario that will occur depends upon what section of the spacecraft was impacted. Uncertainties about the physical processes occurring as a result of an MIF lead to uncertainties in predicting which scenario will occur. For the best estimate case, it is predicted that all impacts on the TOP and USS sections, and 3/8 of the impacts on the PMS section will result in destruction of the MMH tank. Similarly, all hits on the LEM and BOT sections, and 5/8 of the impacts on the PMS sections will destroy the NTO tank. Approximately 0.1 of all NTO or MMH tank ruptures will additionally cause rupture of the other tank, causing combustion. Uncertainties in the physical processes were modeled by varying the effects of hits on the various sections of the spacecraft (e.g., changing the ratio of PMS hits that will cause NTO rupture). The uncertainties in predicting which scenario will occur dominate the uncertainties in the total ΔV prediction process, and outweigh the uncertainties associated with the ΔV predictions for each scenario (described in Subsection 4.2.1.2.1.3).

The scenario probabilities are a function of the orientation of the spacecraft. When the spacecraft is oriented with the Probe in the ram direction, the likelihood of an MMH rupture versus an NTO rupture is increased because the Probe protects the NTO tank more than the MMH tank Tables 4-2 and 4-3 show the probabilities of occurrence for both spacecraft orientations.

Table 4-2 Relative Probabilities of Destruction of Bipropellant Tanks - Nominal Orientation

MMH	NTO	Both (Combustion)	Case
0.594	0.306	0.1	ΔV_{BE}
0.495	0.255	0.25	ΔV_{LL1}
0.165	0.085	0.75	ΔV_{LL2}

Table 4-3 Relative Probabilities of Destruction of Bipropellant Tanks - Probe-Pointed Orientation

MMH	NTO	Both (Combustion)	Case
0.661	0.239	0.1	ΔV_{BE}
0.55	0.2	0.25	ΔV_{LL1}
0.1835	0.0665	0.75	ΔV_{LL2}

4.2.1.2.1.3 ΔV Estimation Process for Bipropellant System Ruptures. The three scenarios described above will result in different ΔVs. For the scenarios where only one of the two tanks
ruptures, a ΔVwill be imparted as the propellant within the tank vaporizes and expands into the external vacuum. For the scenario where both tanks rupture, the NTO and the MMH released from the tanks will combust, releasing more energy than in the case of simple expansion.

4.2.1.2.1.4 Rupture of a Single Bipropellant Tank. Immediately following a tank rupture, the gas and liquid in the tank will begin to expand into the external vacuum. As previously noted, the tank will either entirely shatter, or will be left with a large hole with jagged edges. It must be noted that such a hole will not necessarily be located at the point of impact, but rather at some random point determined by tank flaws.

If the tank is completely shattered, the expanding gases and particles will react against the outer surface of the other tank, pushing the spacecraft in the opposite direction. For the case of a large hole, the net impulse due to the flow of gas and particles acts normal to the hole in the tank surface. In this case, the gases and particles will expand through the hole over a wide range of angles, with a considerable portion going backwards. For the ΔV estimation process, it was assumed that the center of the hole is equally likely to be anywhere on the upper hemisphere (for the MMH tank) or the lower hemisphere (for the NTO tank). Holes on the other hemispheres (lower for the MMH, upper for the NTO) will have the escaping fluid directed at the surface of the other tank, pushing the spacecraft away from center of the ruptured tank. The location of the hole was assumed to be equally likely anywhere about the z axis.

Experimental data examining the phenomena of hypergolic propellants escaping from containment vessels into vacuum is available from tests examining the rupture of small [8.25 cm (3.25 in)] glass spheres containing NTO and Aerozine-50 (similar to

MMH). The tests included NTO and Aerozine-50 filled spheres being burst alone, and then NTO and Aerozine-50 filled spheres being burst together (i.e., with combustion). Measurements of the impulse per unit area from these experiments for each scenario (NTO alone, Aerozine-50 alone, combustion) can be used to predict similar effects for much larger tank (sphere) sizes. The experimental results were scaled to the large-scale cases of Cassini bipropellant tank bursts (MMH alone, NTO alone, MMH and NTO together), using scaling rules obtained through dimensional analysis to obtain the total impulse imparted to the spacecraft in each scenario.

Once the impulse for each scenario was calculated, the equations of motion were solved, taking into account the time history of the impulse, the changing moments of inertia as the propellants leave Cassini, the rotation of the spacecraft during the impulse, etc. The direction and magnitude of the resultant velocity is dependent upon the location of the hole on the tank surface.

The results from this analysis provide a specific predicted magnitude for each possible tank hole location. However, due to variabilities in the parameters that influence the effects of a tank burst, there is, in reality, a range of possible ΔV magnitudes.

The variability of the ΔV was predicted from data obtained from tank burst tests performed in the 1960's. The PYRO test program examined the rupture of large pressurized tanks filled with liquid hydrogen and liquid oxygen. The tests were repeated for a number of conditions, with tests being performed for liquid hydrogen tanks alone, liquid oxygen tanks alone, and liquid oxygen and liquid hydrogen tanks together (combustion). The tests were performed enough times to predict that the variability in resultant ΔV for all three scenarios is approximately Gaussian in nature. The PYRO data was used to predict the variability of the ΔV because the small sphere tests were not repeated enough times to predict variability.

The singular ΔVs predicted in the first step of this analysis were modified to reflect the Gaussian nature of the bursts, using parameters calculated from the PYRO tests.

4.2.1.2.1.5 Rupture of Both Bipropellant Tanks. For the case of simultaneous NTO and MMH rupture, the escaping gases will combust. This process will occur in a region that is approximately spherical, and there will be a substantial cancellation of forces. For this case, an analysis similar to the ones performed for single tank ruptures (i.e., scaling up small scale test data, and modifying the result to be Gaussian in nature) was used. For this case, however, the location of the holes in the surfaces of the tanks is not important, and there no preferred direction of motion.

The equations presented in Appendix B (B.1 through B.3) predict the effects of single tank ruptures and combustion.

4.2.1.2.2 ΔV Effects of a MIF of the Hydrazine Tank. The ΔV imparted to the spacecraft due to a hydrazine tank burst was estimated using an analysis similar to the one performed for the rupture of a single bipropellant tank. If the hydrazine tank is ruptured, the tank will shatter, and the resultant impulse will act on the side of the spacecraft facing the tank. This phenomenon will bias the ΔV in the -Y direction, although there are random effects that will create uncertainties. The estimated ΔV for a hydrazine tank rupture is described in Appendix B.

When the hydrazine tank undergoes an MIF, there is a, fairly high chance that the failure will propagate into the bipropellant system. If the failure does propagate, the effects of a bipropellant failure are added to those of the hydrazine tan failure. Table 4-4 gives the probability of a hit on the hydrazine tank propagating into a bipropellant tank failure. As an example, the best estimate predicts that 0.5 of all helium tan ruptures will also rupture the bipropellant system, which then had different probabilities for causing each of the three bipropellant scenarios (NTO only, MMH only, MMH and NTO). The less likely scenarios have the same probability of rupturing the bipropellant system, but have different probabilities for each bipropellant scenario.

Table 4-4 Probability of Destruction of Bipropellant System Due to Hydrazine Tank Rupture

Probability of Hydrazine Rupture	Probability of Additional Bipropellant Rupture (Total)	MMH	NTO	Both (Combust.)	Case
1	0.5	0.225	0.225	0.05	ΔV_{BE}
1	0.5	0.1875	0.1875	0.125	ΔV_{LL1}
1	0.5	0.0625	0.0625	0.375	ΔV_{LL2}

4.2.1.2.3 ΔV Effects of a MIF of the Helium Tank. If the helium tank was ruptured by a micrometeoroid, the construction of the tank (fiber-wound graphite epoxy) would prevent the hole fro propagating and shattering the rest of the tank. The helium in the tank would jet out through the hole and impart a spacecraft torque and ΔV. The magnitude of this ΔV can be calculated from

momentum transfer based upon the initial pressure inside the tank, the mass of helium in the tank, the size of the hole, the mass of the spacecraft, etc. An analysis was performed to estimate the ΔV imparted by a helium tank rupture, and the results are presented in Appendix B. The direction of the imparted ΔV is a function of the location of the hole on the tank, which was assumed to have the same probability per unit area.

Similar to a hydrazine tank failure, there is a finite chance that a helium tank MIF will propagate into the bipropellant system. However, because the helium tank will not generate as much secondary debris when it fails, there is a much smaller likelihood of occurrence. Table 4-5 gives the probability of a hit on the helium tank propagating into a bipropellant tank failure. As an example, the best estimate predicts that 0.01 of all helium tank ruptures will also rupture the bipropellant system, which then has different probabilities for each of the three bipropellant scenarios (NTO only, MMH only, MMH and NTO). Less likely scenarios have different probabilities of rupturing the bipropellant system, with different ratios between the three bipropellant scenarios.

Table 4-5 Probability of Destruction of Bipropellant System Due to Helium Tank Rupture

Probability of Helium Rupture	Probability of Additional Bipropellant Rupture (Total)	MMH	NTO (Combust.)	Both	Case
1	0.01	4.95E-3	2.55E-3	2.5E-3	ΔV_{BE}
1	0.02	9.9E-3	5.lE-3	5E-3	ΔV_{LL1}
1	0.05	0.02475	0.01275	0.0125	ΔV_{LL2}

4.2.1.2.4 ΔV Effects of an MIF of the Engineering Bus. The ΔV imparted to the spacecraft by a micrometeoroid impact on the bus (via momentum transfer only) will be very small and does not affect the analysis.

4.2.1.3 Probability of No Recovery for MIFS.

4.2.1.3.1 Bipropellant Tanks. A rupture of either the NTO or MMH tank will result in a large sudden acceleration that may damage other spacecraft subsystems. Also, fragments generated

during the rupture may cause secondary damage, or the presence of relatively large amounts of NTO or MMH in the cloud resulting after the tank burst may cause damage to electronic subsystems, making them inoperable. It has been assumed that any rupture of the bipropellant tanks will-cause loss of spacecraft commandability.

4.2.1.3.2 Hydrazine Tank. Although the acceleration due to a rupture of the hydrazine tank is smaller than that of a bipropellant rupture, the fragments generated in the burst may damage other subsystems, or the resulting hydrazine cloud may damage electronics. Furthermore, the loss of the hydrazine system will cause loss of the ability to point the spacecraft. Therefore, it has been assumed that any rupture of the hydrazine tank will cause loss of spacecraft commandability.

4.2.1.3.3 Helium Tank. As previously noted, the helium tank will not necessarily shatter as a result of a micrometeoroid impact, and helium is an inert gas that will not damage the spacecraft electronics. After a helium tank rupture, sufficient pressurant will remain in both the hydrazine and bipropellant tanks to provide enough ΔV to remove the spacecraft from an impact trajectory. It has been assumed that a helium tank rupture will not render the spacecraft inoperable so long as it has not propagated to the other tanks, and thus the spacecraft can be placed onto a safe trajectory after failure (although the science mission will be lost).

4.2.1.3.4 Engineering Bus. Loss of a critical engineering subsystem results in the loss of spacecraft commandability, thereby prohibiting any chance of recovery from an undesirable trajectory (see Subsection 4.3.1).

4.2.2 Internal Spacecraft Failures

This subsection describes all of the ΔV inducing failures caused by spacecraft failures that have a significant contribution to the total probability of Earth impact. Also included is a list of those failures initially identified as possible contributors, but which were later eliminated due to their low probabilities of occurrence.

4.2.2.1 Stuck-Open RCS Thruster Valve. The flow of propellant to the spacecraft RCS thrusters is controlled by several valves. During launch, a latch valve isolates the propellant from the thrusters. After launch, the latch valve to the operating thruster branch is opened and remains open during long periods when the RCS thrusters are required for attitude control of the spacecraft. Fuel flow through the thrusters is controlled by valves contained in the thruster. Upon receipt of a firing command, a thruster valve will open for a specified duration, and then close. Commands to fire the thrusters can be generated by the ground or by onboard software.

If a thruster valve were to fail in the open position, excess thrust would be produced. A stuck-open thruster valve can occur at the end of any thruster firing. Detection and response to a stuck open thruster failure depends on whether the failure is an electrical failure or a mechanical failure.

Electrical Failure. The AACS continuously monitors the open/closed position of the latch valves using voltage and current measurements. This status is compared with the expected status for the commanded state, and a discrepancy will quickly initiate on-board fault protection to correct the fault.

Some electrical faults can be corrected quickly (several seconds) by turning off power to the thruster valves (which will automatically close upon loss of power), or by re-commanding closure of the thruster valve. Other electrical faults may require a fault protection sequence that switches thruster branches. This process could take seconds or several minutes and would increase the amount of anomalous ΔV produced before correction.

Mechanical Failure. A valve which fails to close due to mechanical failures cannot be detected via electrical monitoring. Failure detection will be observed by detecting uncommanded spacecraft motions as observed by gyro rates and stellar reference unit data. Small openings or leaks will be observed over longer periods by ground observation of the excessive use of an opposing thruster.

A detection of uncommanded motions, without observing a discrepancy in the electrical status comparison, would indicate a high probability of a mechanical failure. The corrective action is isolation of the thruster branch.

The time required to respond to a mechanical valve failure depends on the torques provided by the thruster and the limits built into the software that initiate fault-protection based on gyro or stellar reference unit data.

4.2.2.1.1 Probability of Failure of Stuck-Open Thrusters. JPL has conducted a survey of applicable spacecraft thruster flight experience from which failure probabilities can be estimated. Flight experience was derived from JPL experience, military and communications satellites, and several thruster ground qualification programs. Examining these programs, data is available for about 380,000 equivalent days of thruster operation. Failures which occurred during this period were:

- No JPL spacecraft/thruster failures.

- One defense satellite thruster failure; failed open valve attributed to failed driver electronics.

- Valve failure occurred in qualification tests; mechanical failure of a German thruster/valve.

- Four "catastrophic-leakage" events, causing total loss of attitude control gas in 5-30 days. However, these were gas-type thrusters. There probably would not have been any leakage in hydrazine (liquid) thrusters.

Examining the data, and assuming three failures of hydrazine thrusters in 380,000 thruster days yields a best estimate failure rate of approximately 7.5 X 10-6 failures/ operating day. The identification of one electrical and one mechanical failure lead to the assumption that each mode is equally likely, and the probability of failure was split evenly between the two modes. The PF.90 and PF.10 estimates are engineering judgments and consider the uncertainties in the failure database.

Estimates of the probability of failure for stuck-open thrusters are given in Table 4-1.

4.2.2.1.2 ΔV Estimates for Stuck-Open Thrusters. The net ΔV imparted to the spacecraft due to a stuck-open thruster will depend upon the orientation of the thruster and the length of time required to detect and correct the failure (depending upon whether it is an electrical or mechanical failure).

An uncommanded torque from a stuck-open Z-facing thruster will be compensated by firing an opposing Z-thruster to zero the spacecraft rate error. This will result in an undesired ΔV in the -Z direction. Torque from a stuck-open X-facing thruster will be compensated by firing a set of Z-facing coupled thrusters. A residual ΔV will be produced by the failed X-facing thruster, in addition to a ΔV in the -Z direction produced by the firing of the coupled thrusters.

Estimates for the ΔV induced by stuck-open thrusters were calculated using Newton's laws of motion. Estimated fault protection response times (based upon similar responses in other spacecraft) were used to predict the length of the additional acceleration, and thus the resultant ΔV. Uncertainties in the ΔV estimates were driven by uncertainties in the predicted response times, and were based upon engineering judgment.

Estimates of the ΔV produced by a stuck-open thruster are given in Table 4-1.

In the event of a RCS thruster valve failure, the spacecraft will be reconfigured to bring the redundant thruster branch into use, thereby restoring attitude control authority to the spacecraft.

4.2.2.2 Main Engine Valve Failures. The main engine system is somewhat similar to the RCS system. Two latch valves isolate the main engine from the bipropellant tanks (one each for the NTO and MMH lines). Propellant flow through the main engine is controlled by a pair of main engine valves. However, unlike the RCS system, the latch valves are closed between main engine firings, providing more protection against faults.

The important steps of a nominal main engine firing are:

(1) The main engine gimbal actuator is commanded to the correct orientation.

(2) The latch valves are opened to allow propellants to reach the main engine valves.

(3) The main engine valves are opened to permit combustion.

(4) The valves remain open until accelerometer data indicates the desired ΔV has been applied.

(5) The main engine valves are closed to terminate thrust.

(6) The latch valves are closed approximately one second after main engine valve closure to isolate the propellant tanks from the main engine valves.

Main engine firings can only occur when commanded by the ground.

If a main engine valve were to fail in the open position, excess thrust would be produced until the latch valves were closed and the propellant lines up to the latch valve were emptied. Detection and response to a stuck open main engine valve failure depends on whether the failure is an electrical failure or a mechanical failure.

Mechanical: The engine fuel and oxidizer valves are mechanically independent, and it is highly improbable that both valves will have simultaneous mechanical failures. If one of the two valves sticks open, excess thrust will be produced as one of the bipropellants continues to expand through the nozzle (without combustion) until the latch valves close and the propellant in the line downstream of the latch valve is expelled. The engine performance under these circumstances will be significantly reduced from the bipropellant thrust and specific impulse. Due to differences in the chemical nature of the NTO and MMH, the ΔVs imparted by each case is slightly different.

Electrical: Electrical power for both valves is provided by a single switch. It is thus possible for a single electrical failure to allow both the oxidizer and the fuel valve to remain open, thus permitting the continued flow of both MMH and NTD to the main engine. If this were to occur, the thrust of the engine would continue for approximately one second after the commanded shutoff (until the latch valves closed), and would continue until the expulsion of the fuel and oxidizer in the lines up to the latch valves was complete.

4.2.2.2.1 Probability of Failure Estimates for Main Engine Valve Failure. JPL has conducted a survey of applicable spacecraft main engine flight experience from JPL experience, military and communications satellites, and ground qualification programs. Data was available for about 6076 main engine starts. During this period, no flight failures were identified.

- No JPL spacecraft/main-engine failures.
- No identified main-engine failures in military or communications satellites.
- One valve qualification failure. German manufacturer made materials change to solve this problem.

Since no flight failures were identified for the main engine valve, the decision was made to base the failure rate on the larger database for thrusters. The electronic driver circuits and the valve mechanical elements are similar for latch valves, thruster valves, and main engine valves. Since the failure mechanisms which could cause a stuck-open failure are similar for the three valve applications, it seems reasonable to use the same failure rate per valve open/close operation for all three of the valves. Assuming that the success rate for closing thruster valves is applicable for main engine valves, the engine valve failure rate can be derived as follows:

Based upon Voyager experience and estimates for Cassini, an RCS thruster must open/close an average of 30 times per day. The thruster failure database includes 380,000 thruster days, which at 30 pulses per day, yields 11.4×10^6 openings and closings. The total (mechanical plus electrical) failure rate per firing (opening/closing), assuming the 3 failures indicated previously, is 0.26×10^{-6} failures per firing. Similar to thruster failures, this rate is assumed to be divided evenly between mechanical and electrical failures. Similar to thruster valve estimates, the $P_{F.90}$ and $P_{F.10}$ probabilities are based upon engineering judgment and consider large uncertainties in the failure database.

The estimated probabilities of main engine valve failure are given in Table 4-1.

4.2.2.2.2 ΔV Estimates for Main Engine Valve Failures. Similar to stuck-open thruster failures, the undesired ΔV resulting from a main engine valve failure can be estimated using basic equations of motion. The undesired thrust is a function of the time between main engine valve closure and latch valve closure, and the volume of propellant remaining in the upstream propellant lines after the latch valve is closed. Using this information, the total additional acceleration can be calculated .(for both electrical and mechanical failures), yielding the total ΔV. As the volume of the propellant remaining in the lines is well known, uncertainties in the length of time between main engine valve closure and latch valve closure dominate the total ΔV uncertainty. Estimates of the time between main engine valve closure and latch valve closure were predicted using engineering judgment based upon experience from other spacecraft and knowledge about the Cassini design.

The estimated values of ΔV for both types of main engine valve failure are given in Table 4-1.

In the event of a main engine valve failure, the spacecraft will be reconfigured to bring the redundant main engine into use, thereby allowing corrective maneuvers and continuation of the mission.

4.2.2.3 Accelerometer Failure. An accelerometer is used to measure the velocity change during a main engine burn and initiates main engine valve closure when the measured ΔV reaches the commanded value. This normal operation is backed-up by a timed shutoff at a maximum expected burn time predicted on the ground. Prior to the burn, the accelerometer is turned on, checked out and bias calibrated. Most accelerometer failures will be detected during this process, but some changes (e.g., low scale factor) are undetectable. A low accelerometer output will result in an underestimated ΔV, a long burn, and shutoff by the backup timer.

4.2.2.3.1 Probability of Failure Estimates for the Accelerometer. The probability of accelerometer failure was calculated in an analysis performed by the JPL Reliability Group. The analysis considered the Cassini accelerometer design, and was performed using standard military accepted practices. Electronics parts reliability data was taken from accepted reliability databases. Uncertainties in the probability of failure were generated using engineering judgment based upon past flight experience.

However, as the accelerometer is calibrated prior to a main engine burn, many of the possible accelerometer failures that may have happened since the previous main engine burn will be detected, and the planned maneuver will be aborted. It was assumed that 1/6 of the failures accumulated between main engine burns will not be detected during accelerometer calibration.

However, it was also assumed that any failure of the accelerometer occurring during a burn would result in an overburn. The probability of an accelerometer failure that would affect a main engine burn thus consists of two terms; the probability of failures accumulated between burns that cannot be detected during calibration, and the probability of failure accumulated during the burn. Due to the relatively short duration of main engine burns (on the order of minutes/hours) versus the relatively long period between main engine burns (on the order of days/weeks), the accumulated failure rate between maneuvers is the dominant part of the failure rate.

Estimates of the accelerometer failure rate (for both the period between maneuvers and the time during maneuvers) are given in Table 4-1.

4.2.2.3.2 ΔV Estimates for Accelerometer Failures. When the main engine is shutoff by a timer, the resulting velocity is a function of main engine performance characteristics and spacecraft mass parameters that are not precisely known. The probability of the additional ΔV associated with a timer shutoff of a main engine burn is predicted by a Gaussian function. The mean value of this Gaussian distribution is determined by the predicted main engine shutoff time calculated on the ground. This predicted shutoff time is not precisely specified, but will be approximately 5% of the desired burn magnitude. The uncertainties in the predicted shutoff time are reflected in Δ_{VLL}, and ΔV_{LL2}, and were determined using engineering judgment based upon similar systems used on other spacecraft.

Estimates of the ΔV error due to an accelerometer failure are given in Table 4-1.

It is possible to recover from an overburn due to accelerometer failure with a subsequent maneuver. However, since there is only one accelerometer, subsequent main engine burns are terminated with ground predicted burn times, and are performed with degraded magnitude accuracy.

4.2.2.4 Main Engine Gimbal Actuator Failure. Each main engine is mounted on non-redundant gimbals that allow for thrust vector control in the spacecraft X and Y directions. The engine can be gimbaled ±9° to place the thrust vector in line with the center of mass of the spacecraft, providing for rotation control about the X- and Y-axes during a burn. Roll control is handled by the attitude control thrusters. There are two non-redundant main engine gimbal linear actuators (EGAS) for each main engine, one for the X-direction and one for the Y-direction.

Prior to a main engine burn, the EGA is turned on and prepositioned so that the thrust line is through the spacecraft center of mass. Failure to respond to the preposition command would detect an already existing failure, and the maneuver would not execute. Failure of an actuator during the burn is thus the only concern. If the thrust line does not remain through the spacecraft center of mass, there will be an erroneous lateral acceleration and a torque that will cause an undesired rotation rate.

4.2.2.4.1 Probability of Failure Estimates for the Main Engine Gimbal Actuator. Estimates of the probability of failure of the engine gimbal actuator were created using engineering judgment based upon parts failure rate data and flight history. These estimates are shown in Table 4-1.

4.2.2.4.2 ΔV Estimates for Main Engine Gimbal Actuator Failures. When the thrust line does not pass through the center of mass, a torque is produced in which lateral and angular accelerations are proportional. The final lateral velocity that will imparted to the spacecraft (i.e., the anomalous ΔV) is a function of currently undefined fault protection responses. These fault protection responses will use spacecraft angular rate information to detect this type of failure. if fault protection terminates a maneuver after a spacecraft angular rate of l°/s (the current best estimate of the cutoff rate) has been reached, the anomalous ΔV is predicted by the best estimate value given in Table 4-1. The ΔV_{LL1} and ΔV_{LL2} estimates are based on different cutoff rates that could be implemented.

The axial velocity (i.e., in the commanded burn direction) accumulated between the fault and termination depends on the time required to detect the fault. However, termination due to a fault will always result in a maneuver underburn in the axial direction.

It is possible to recover from an EGA failure after swapping to the other main engine and its EGAS.

4.2.2.5 AACS Flight Software Coding Error. The PMS is commanded only from the RCS attitude control algorithm and the ΔV-control algorithm of the AACS software. A coding error within the AACS software could result in a spurious command to the PMS.

4.2.2.5.1 Probability of Failure Estimates for an AACS Flight Software Coding Error. Attitude control systems on the Magellan, Galileo, TOPEX, and Mars Observer spacecraft have a total of about 4000 days of in-flight use. Four significant software failures have been identified in these missions, none of which caused an erroneous maneuver. This yields an AACS software failure rate of 1E-3/day. However, the software used to command the thrusters and main engine represents only approximately 5% of the total AACS software. Thus, the best estimate of the probability of an error in the thruster and main engine control software is 5E-5. It has been conservatively assumed that any error in the thruster and

main engine control software will cause an undesired firing. Uncertainties in this estimate were estimated based upon engineering judgment considering uncertainties in the flight history database and the size of the thruster and main engine control algorithms.

Estimates of the probability of an AACS flight software error are presented in Table 4-1.

4.2.2.5.2 ΔV Estimates for an AACS Flight Software Coding Error. This type of failure is assumed to have a 50-50 chance of affecting the RCS or the main engine (though the main engine has more safeguards). The ΔV effect of the failure is found by assuming that one to four RCS thrusters or the main engine is turned on until fault protection identifies the error and terminates thrust. It is estimated that 0.25 to 2.0 seconds of thrust will be produced before the error is detected and corrected by fault protection. The resultant ΔV was calculated using the estimated uncertainties in time and the number of thrusters as inputs to the basic equations of motion. Table 4-1 shows the estimated ΔVs.

It is possible to recover from this failure mode by correcting the anomalous ΔV in a subsequent TCM.

4.2.2.6 CDS Flight Software Coding Error. CDS stores commands for all spacecraft subsystems (including AACS) in memory in the form of command sequences, and distributes those commands to the appropriate subsystems at times specified in the command sequence. Some of these command sequences initiate and control TCM maneuvers. A CDS coding error could result in erroneously issuing a stored maneuver command sequence to AACS at an inappropriate time, resulting in the premature execution of an planned maneuver, or in the re-execution of an already completed maneuver. A CDS software error of this sort is more likely to be introduced with a software change than to be latent in the launch software load.

4.2.2.6.1 Probability of Failure Estimates for a CDS Flight Software Coding Error. Estimations of the probability of a CDS flight software error are made by examining the individual steps required to cause an error, and then assigning probabilities of failure to each step. Table 4-6 shows the best estimate of the probabilities of failure for each step, and the total best estimate probability of failure.

Table 4-6 Predicted Probability of a CDS Flight Software Coding Error

Component	Probability per Sequence
a) Probability of error being introduced into flight code during 4000-day mission	2.5E-5/day (0.10 probability of error/mission)
b) Probability of erroneous flight code passing ground simulation check	0.10
c) Probability that CDS flight processor keeps functioning despite error	0.10
d) Probability that bad software erroneously executes a stored sequence	0.01
e) Probability that the stored sequence is a maneuver sequence	3.9E-3 (1/256)
Best estimate probability per day	1E-11

After the initial estimate of the probability of Earth impact was complete, the results were examined to determine the sensitivity of the Earth impact probability distribution to CDS flight software coding errors. By means of a technique for uplinking the planned maneuver parameters only 24 hours before execution, and then zeroing them out again after maneuver execution, the distribution was made insensitive to several order of magnitude variations in the probability of CDS software errors. As a result, the probability of CDS software errors was artificially increased by several orders of magnitude to eliminate any concerns about inaccuracies in the probability estimation process. These increased values are presented in Table 4-1.

4.2.2.6.2 ΔV Estimates for a CDS Flight Software Coding Error. The ΔV resulting from a CDS software error will be that specified in the erroneously initiated sequence. As the exact parameters for TCMs are developed after launch (based upon tracking data), the values of the parameters used in the erroneously executed sequence cannot be specified a priori. The magnitude of maneuvers performed prior to the final Earth swingby can be up to 170 m/s (558 ft/s), and could be executed in any direction in inertial space.

It is possible to recover from this error with a subsequent TCM.

4.2.2.7 Sun Search. If the spacecraft were to lose attitude knowledge, and the Sun is not within the Sun sensor's field of view (± 30°), the spacecraft will maneuver and perform a spiral

search of the whole sky. The search is terminated when the Sun is reacquired by the Sun sensor. The most likely cause of a Sun search is a loss of attitude knowledge while pointed off-Sun for a maneuver. A Sun search is not normally executed during the mission.

4.2.2.7.1 Probability of Failure Estimates for a Sun Search. The failure rate for a Sun search is conservatively based on the failure of either a stellar reference unit or an inertial reference unit. Loss of one of these components must occur during a period when the spacecraft is not oriented with the HGA pointed towards the Sun. The only time during the early part of the mission (prior to the final Earth swingby) that the spacecraft will not be Sun pointed is during maneuvers, and so the probability of a Sun search is estimated on a per maneuver basis. It has been assumed that fault detection and correction (i.e., swapping to redundant units) will not occur quickly enough to prevent loss of attitude knowledge.

The failure rates of the stellar reference units and the inertial reference unit were estimated using engineering judgment based upon parts failure rates and experience from other missions. The failure probabilities for each element were combined to predict the probability of one failure occurring during an off-sun period.

4.2.2.7.2 ΔV Estimates for a Sun Search. The ΔV imparted by a Sun search is determined by the length of time required to reacquire the Sun. Numerical simulations have been performed to predict the anomalous ΔV as a function of elapsed search time, and were approximated with a linear fit for this study. The best estimate of the imparted ΔV, ΔV_{BE}, was based upon the average search time required to reacquire the Sun. Uncertainties were estimated by predicting the ΔVs associated with long and short reacquisition times. The estimated ΔVs are shown in Table 4-1.

Maneuvers correcting the anomalous ΔV are possible after communication with the ground.

4.2.2.8 Non-Significant Spacecraft Failure Modes. The failures considered in the logic diagram are failures which provided a significant contribution to the total probability of Earth impact. A number of other spacecraft failures were also considered which did not significantly affect the total probability of Earth impact, due to their extremely low probabilities of occurrence (less than 1-10) These include:

(1) Rupture of the bipropellant tanks-due to overpressurization caused by excessive heat input.

(2) Radiation effects.

(3) Spacecraft charging.

(4) Erroneous star identification prior to a maneuver.

(5) Simultaneous main engine valve and latch valve failure.

(6) Memory failure resulting in thruster or main engine firing.

4.2.3 Ground-Induced Errors

This section deals with errors that are made on the ground by the spacecraft controllers, which are then sent to the spacecraft and executed. The Cassini uplink process is described in Subsection 3.4.

The details of the uplink process are currently under development, so it is not possible at this time to evaluate the individual procedures in detail. As the specific procedures are defined, they will be evaluated using human reliability methodology. If it appears that they are less reliable than estimated by an amount sufficient to cause the contribution of these errors to the total impact probability to become significant, actions (such as imposing more independent ground checks) will be taken to increase the reliability of the procedures.

There have been no significant incorrect velocity changes in any recent missions (Voyager, Galileo, Magellan, Mars Observer) due to ground-induced errors.

4.2.3.1 Erroneous Ground Command. The failure in this case is incorrectly sending a command which causes a ΔV. Failure to send a planned ΔV is not considered because such a failure could not result in the spacecraft acquiring an Earth impact trajectory.

There are two Cassini commands that can cause a ΔV: 7ENGINEBURN and 7RCSBURN, which cause a burn of the main engine or RCS, respectively. These are the only two Cassini commands which will contain the letter combinations "BURN" or, to prevent error, "BURM". Each command contains three parameters: the desired ΔV magnitude, a maximum burn time and a minimum burn time. Based on the maximum planned ΔV for a single maneuver, the maximum ΔV for the 7ENGINEBURN command is set at 1 km/s (0.62 mi/s); for 7RCSBURN, at 10 m/s (32.8 ft/s). The ground constraint checking software will reject a command with the ΔV exceeding the limit. In addition, the ground software will reject a command with maximum time less than minimum time. Both of the ΔV commands will be on the most restricted list of Cassini commands (see Subsection 3.4.1.3).

The BURN commands are normally sent up in conjunction with a number of set-up commands, including ones to position the spacecraft in the desired attitude. However, as currently defined, they can be executed individually, with defaults used for the missing set-up commands. In particular, the default burn attitude is the last inertial target in case of the 7ENGINEBURN and the last commanded attitude in case of the 7RCSBURN. It is possible that some of the set-up commands would also be sent with the BURN command. The only relevant effect of the set-up commands would be to change the direction of the burn; these commands would not affect the magnitude.

The spacecraft software assumes that all validity checks are done on the ground. As currently specified, a BURN command can be executed any time the spacecraft is in its nominal state. Therefore, if an erroneous ΔV command is transmitted, it will be executed.

There are two ways in which an erroneous command could be sent.

4.2.3.1.1 Sequenced or Planned Real-Time Command. The first method would be for someone to introduce an erroneous ΔV command into the nominal sequencing process. It could either be entered into the sequence to be stored in the on-board memory for later execution (see Subsection 3.4.1.4), or it could be planned to be sent up as a real-time command separate from the sequence (see Subsection 3.4.1.5). In either case, it would be subject to the full sequence review process, including software constraint checking and restricted command check. (See Subsection 3.4.3 for a description of the command generation and review process.) Under normal conditions the sequence generation process takes approximately two months. As described in Subsection 3.4.2, a single team is responsible for a sequence from the start of the generation process to execution.

The list of restricted commands, both sequenced and real-time, is distributed with the review package for the sequence. In order for the command to be sent, the reviewers of the restricted command list would either have to miss its presence or assume it was supposed to be there.

There is no way to insert a new command into the sequence after the checks have been made.

4.2.3.1.2 Unplanned Real-Time Command. The second method would be to introduce an erroneous ΔV command while generating a set of unplanned real-time commands. This is normally done only when a spacecraft anomaly has occurred requiring ground intervention, or when an instrument wants to change some characteristic of its data taking.

All unplanned real-time commands will be subjected to the same constraint checking and restricted command list checking as the planned real-time commands. An invalid ΔV command will be rejected; a valid ΔV command will appear on the restricted command list.

Each restricted unplanned real-time command must be generated by two people. The list of restricted commands in an unplanned real-time load will be small, because the loads themselves are significantly smaller than a sequence load; thus the chance of a reviewer missing a BURN command is very small. All operations personnel will be trained to recognize that BURN commands should never be sent as unplanned real-time commands. Thus, the probability of sending an unplanned real-time ΔV command is significantly less than that of sending a sequenced or planned real time ΔV command and it has been eliminated as a contributor.

4.2.3.1.3 Estimation of Erroneous Ground Command Failure Rates. There are three necessary components to the probability of transmission of an erroneous ΔV command: a) someone has to introduce an erroneous engineering command, b) it has to be a ΔV command, and c) it has to be passed through the review process.

The probability of the erroneous command being generated and transmitted is reasonably calculated on a per-sequence basis. The time of execution of the erroneous command is randomly distributed throughout the sequence execution period. Since there are approximately 50 days in each cruise sequence, the probability per sequence is divided by 50 to obtain the probability per day, which is used in the $P_{I/F}$ calculation.

For each of the three components, it was felt that the expected value (mean) and worst case value could be the most reliably estimated. Given the high level of uncertainty, a lognormal distribution was fit to these values, taking the "worst case" to be the 99% probability point. Best estimates of the probability of each of these events occurring were made based upon engineering judgment and experience with previous missions (in particular with the two Earth swingbys by Galileo).

A sequence may contain up to 300 kilobytes and includes the execution of a large number of different activities. Thus there is a high probability that in the early phases of command generation an erroneous command will be introduced. However, the cruise period is a relatively quiet period of the mission and the Earth swingby is a sufficiently long time prior to arrival at Saturn that the tour planning will not be taking significant attention away from cruise sequence development. During this time, therefore, most of the team members will be working only on this sequence. A value of 0.1 was adopted for the mean and 0.5 for the worst case.

Although the command list for Cassini has not been completely defined, based on previous missions it is likely to contain about 1000 commands. If the introduction of an erroneous command were random, the probability of it being one of the two BURN commands would be 0.002. However, the BURN commands should never be used as individual commands; they should only be included in maneuver sequences. Thus the probability of being introduced explicitly is very low. Because the letter combination "BURN" and "BURM" will not occur in any other commands, it is also unlikely a BURN command will be inserted in place of another command. Thus the probability of the erroneous command being a BURN command is significantly lower than random. A value of 10^{-4} was adopted for the mean and 10-3 for the worst case.

As discussed above and in Subsection 3.4.3, all sequenced and planned real-time commands are subject to several .independent reviews, both by software and inspection. Because the BURN commands should appear only during the few planned maneuvers, their presence in other places will be likely to be caught. In addition, they will appear on the list of restricted commands, which are reviewed by a number of people. operations personnel believe that there is virtually no chance of one of these commands getting through the review; however, a conservative value of 10^{-3} was adopted for the mean and 10^{-2} for the worst case.

The total probability was determined by using a Monte Carlo simulation to combine the errors from the three components. Table 4-7 shows the individual probabilities of failure for each step, and the total probability of failure.

Because the RCS is used for attitude control as well as trajectory changes, it is more likely that the erroneous planned command would be an RCS command rather than a main engine command, as the erroneous RCS command would be less likely to be caught in the review. It is estimated that 25% of the time an erroneous ΔV command would be a 7ENGINEBURN command and 75% of the time it would be a 7RCSBURN command.

A description of the ΔV effects of an erroneous ground command is given in Appendix B.

The execution of an erroneous ΔV ground command cannot ,cause the spacecraft to be unable to recover from a resulting impact trajectory.

Table 4-7 Probability of an Erroneous Ground Command

Component	Probability per Sequence
a) Probability of introducing an erroneous engineering command in a 50-day sequence (human error)	mean = 0.1 99% = 0.5
b) Probability of erroneous command being a valid ΔV command (10^{-3} not due to human error)	mean = 10^{-4} 99% = 10^{-3}
c) Probability of erroneous command not being caught in review (human error)	mean = 10^{-3} 99% = 10^{-2}
Total probability P_F per sequence	10%: 3.2×10^{-11} 50%: 6.6×10^{-10} mean: 9.5×10^{-9} 90%: 1.4×10^{-8}
Total probability PF per day	10%: 6.4×10^{-13} 50%: 1.1×10^{-11} mean: 1.9×10^{-10} 90%: 2.8×10^{-10}

4.2.3.2 Navigation Design Error. In the case of a navigational design error, a single error is made during the navigation design of the TCM that causes an error in the parameters for a planned maneuver.

The aim points of the maneuvers are determined far in advance and reviewed by a large number of people. There is a possibility, however, that the initial entry of the aimpoint into the software used for computing the maneuver parameters can be done incorrectly.

There is also a possibility that the initial state of the spacecraft is not known or input correctly. For the period prior to Earth swingby, any deviations from Sun-pointed attitude will be well known and members of the maneuver design group will explicitly check throughout the sequence generation process to ensure that the commanded spacecraft attitude is the same as the one used in the maneuver design. However, there is a small chance that an unplanned real-time commanded change in attitude might not be caught.

A maneuver is specified in terms of three parameters: the magnitude of the velocity change and two directional components, yaw and roll. After a maneuvers' parameters are calculated, a software simulation showing the trajectory resulting from the calculated

parameters is performed. Input to the simulation program will be the same electronic file that will be provided for command generation. For pre-Earth swingby maneuvers, the trajectory relative to the Earth will be shown. The proposed parameters and simulator outputs are reviewed by other representatives of the navigation and spacecraft elements of the ground operations team.

Once the maneuver parameters have been determined and validated, the file will be provided to software which will generate the commands necessary to execute the maneuver. This software will be thoroughly tested prior to its use. In addition, at least four maneuvers will have been done prior to the execution of any maneuver for which a navigation design error could lead to a credible probability of Earth impact. It is believed, therefore, that no errors will be introduced after the navigation design process.

There are two necessary components to the probability of a navigation design error affecting a TCM: a) someone has to make the error and b) it has to be passed through the review process. Similar to the process used to estimate the probability of an erroneous ground command, the probability of a navigation design error was estimated by examining the probability of failure for each step in the process, and then using a Monte Carlo simulation to combine the errors from the components.

As discussed above, the error source is more likely to be an entry error, rather than a knowledge error. This type of error would have a reasonable chance of being caught by the person making the error since there are only a few parameters involved. It also includes, however, the small possibility that a late change in spacecraft attitude is not caught. A value of 0.01 is adopted for the mean with a worst case of 0.1.

It is likely that for most maneuvers, the parameters will be calculated independently by two different people, although the same software may be used. Because of the extreme scrutiny of maneuvers and the use of simulations, it is likely that any errors will be caught. A value of 10-4 is adopted for the mean and 10-3 for the worst case.

Table 4-8 shows the individual probabilities of failure for each step and the total probability of failure.

Table 4-8 Probability of a Navigation Design Error

Component	Probability per TCM
a) Probability of making an error affecting the trajectory	mean = 10^{-2} 99% = $l0^{-1}$
b) Probability of error not being caught	mean = 10^{-4} 99% = 10^{-3}
Total probability P_F	10%: $6.9xl0^{-9}$ 50%: $1.lx10^{-7}$ mean: $9.3xl0^{-7}$ 90%: $1.7xl0^{-6}$

If an error occurs, it will most likely affect all three parameters: ΔV magnitude, roll orientation, and yaw orientation. The magnitude of the errors was estimated based on experience with navigation design and review. Because the importance of maneuvers to mission success causes them to be reviewed by a number of independent reviewers and because of the simulations, any large errors will be caught. The 10%/50%/90% probabilities were taken to be even distribution of error from zero to 1%/10%/100%, respectively.

The execution of an incorrectly designed TCM cannot cause the spacecraft to be unable to recover from a resulting impact trajectory.

4.2.3.3 Permanent Loss of Commandability Due to Incorrect Ground Commands. Loss of commandability with the spacecraft, including loss of communication, due to improper ground commanding was examined, but no credible failure modes were identified. Examples of failure modes that were identified but discarded for varying reasons are shown in Table 4-9.

Table 4-9 Non-Credible Ground Failures that Could Cause Permanent Loss of Spacecraft Commandability

Failure Mode	Rationale for elimination
Commands causing, the spacecraft to perform maneuvers that deplete the hydrazine	In addition to standard review and constraint checking there will be an automatic ground system software check that will disallow any RCS maneuver with a magnitude greater than 10 m/s (32.8 ft/s). Furthermore, the probability of sending an erroneous maneuver command (Table 4-7) is 5 orders of magnitude lower than the probability of losing commandability due to a spacecraft system failure (Figure 4-10).
Commands causing the spacecraft to acquire an inertial orientation that does not permit further uplinks	Communications analysis indicates that uplink will always be possible, independent of spacecraft orientation, when the spacecraft closes to within 0.6 AU of Earth. This provides sufficient time to regain control in the very unlikely circumstance that there is, first, an incorrect command sent to place the spacecraft in the wrong orientation and second, that there is a failure in the on-board fault protection. on-board fault protection will reorient the spacecraft to point the antennas at Earth or, if necessary, reacquire and. roll around the Sun (without using any previously uplinked data) after a specified time during which no commands have been received. [1 AU = 1.496×10^8 km (9.296×10^7 mi)]
Commands sent to spacecraft to an inertial orien-tation that causes bipropellant tanks to overheat and burst	Thermal analysis indicates that this cannot occur
Commands that turn off a critical subsystem	The Attitude and Articulation Control Subsystem (AACS) and Command and Data Subsystems (CDS) cannot be turned off without sending separate, real-time critical enable commands. There are no commands that will turn off the Power and Pyro Subsystem (PPS). Two levels of functionally redundant, on-board fault protection will repower the AACS, thruster valve driver circuits, CDS, PPS, and Radio Frequency Subsystems if they are turned off. Separate status commands have to be sent or generated by the spacecraft to intentionally keep a redundant half-subsystem turned off. The probability of permanently commanding off a critical subsystem is 5 orders of magnitude below the probability of losing commandability due to a spacecraft system failure. It is equal to the probability of an undesired command being introduced (10^{-2} per day, Table 4-7) times the probability of the command not being stopped during constraint checking (10^{-2}, Table 4-7) times the probability of two independent layers of onboard fault protection failing [10^{-3} estimated (for each layer)] times the probability of sending an incorrect real-time critical enable ($<10^{-1}$ for AACS and CDS commands), which is equal to or less than 10^{-10} per day

The Project is still in the process of defining its onboard fault protection. Preventing the loss of spacecraft commandability will be one of the primary factors considered during development of the on-board fault protection. Adverse effects due to other unidentified or overlooked design errors are taken into account by doubling the failure rate due to spacecraft system internal failures (see Subsection 4.3.8).

Temporary loss of commandability preventing the execution of a recovery maneuver is a concern during the time period when there is insufficient time to execute another maneuver, and is addressed in Subsection 4.5.2.

4.2.3.4 Non-significant Ground-Induced Failure Modes. Similar to spacecraft failures, there were several ground failures that were also considered which did not significantly affect the total probability (i.e., which had probabilities of occurrence less than 1-10). These include:

1) Uplink transmission error
2) Erroneous file transmission

4.3 PROBABILITY OF NO RECOVERY (PNR)

If the spacecraft were inadvertently placed on an Earth impact trajectory, the probability of being able to re-command the spacecraft onto a safe trajectory is a function of the type of failure and the time at which the failure occurs. Any failure which causes loss of spacecraft commandability (e.g., hydrazine tank rupture) would prevent recovery of the spacecraft. Other types of failures would require subsequent failures to prevent recovery, or must occur so near the time of the planned Earth swingby that there would be insufficient time to successfully recommand the spacecraft. Table 4-10 describes the different types of failures, as a function of time, which must occur to prevent recovery of the spacecraft. Table 4-11 shows representative failure modes and probabilities contributing to PNR around the three Earth swingbys.

4.3.1 P_{NR} for Failures Occurring Before E-39 Days

The nominal time for planning and executing a recovery maneuver is 30 days. A single failure that requires ground intervention should not preclude recovery if the recovery maneuver is executed at least 9 days before the swingby. Therefore, if the initial failure occurs prior to 39 days before swingby, the only reason not to be able to correct the trajectory would be loss of spacecraft commandability.

Table 4-10 Limiting Factors on Spacecraft Recovery as a Function of Time

Time of Initial Failure (days before swingby)	Limiting Factor on Recovery
39 or more	Spacecraft system or internal failure OR Micrometeoroid-induced failure of a propellant tank or electronic bus (Subsection 4.3.1)
2 to 39	Spacecraft system or internal failure OR Micrometeoroid-induced failure of a propellant tank or electronic bus OR 1 Non-catastrophic spacecraft failure requiring ground intervention to recover OR 1 Erroneous ground-induced error (Subsection 4.3.2)
0 to 2	No recovery possible (Subsection 4.3.3)

Table 4-11 Contributors to Probability of No Recovery

	Means		
Time	Spacecraft System Failures + Micro-Meteoroid-Induced Failures	S/C Failures Requiring Ground Intervention to Recover	Ground Error Preventing Maneuver
Primary E	$\approx 2.0 \times 10^{-5}$/day	$\approx 3.2 \times 10^{-4}$/day	10^{-5}
Backup E1	$\approx 2.0 \times 10^{-5}$/day	$\approx 2.7 \times 10^{-4}$/day	10^{-5}
Backup E2	$\approx 2.4 \times 10^{-5}$/day	$\approx 1.4 \times 10^{-4}$/day	10^{-5}

Loss of spacecraft commandability could be caused by a micrometeoroid rupture of either a bipropellant or hydrazine tan a micrometeoroid-induced failure of both halves of a critical engineering subsystem via a hit on the engineering bus, or as a result of a spacecraft system internal failure.

Propellant tank ruptures are discussed in Subsection 4.2.1, and are considered separately in the Earth impact calculations. The process used to predict the probability of a micrometeoroid induced failure of a critical subsystem is also discussed in Subsection 4.2.1, with the results presented in Figures 4-7 and 4-8. Spacecraft system internal failures are discussed below. During this period, the probabilities of MIFs of the engineering bus and spacecraft system internal failures must be combined to obtain the total probability of no recovery.

4.3.1.1 Spacecraft-System Internal Failures. This failure mode is loss of the ability to execute spacecraft maneuvers as a result of internal failures of the spacecraft system.

It is important to note that there has never been a loss of spacecraft commandability or total spacecraft failure on any of the six outer planetary spacecraft launched by NASA. These spacecraft, characterized by long design lifetimes and robust features, include the two Pioneers and two Voyagers (each of which has operated for more than 5000 days), and Galileo and Ulysses (each more than 1000 days). Similarly, there have been no permanent loss of commandability or system failures on any of the eight interplanetary spacecraft launched by JPL to the outer or inner planets since the late 1960's, that have been designed and built, as Cassini will be, using at least 90 percent Class S or Grade I parts.

The subsystems required to perform a maneuver are the Radio Frequency Subsystem for receiving commands, transmitting a carrier for tracking, and transmitting data for status monitoring; the Command and Data Subsystem for storing and executing commands and controlling the other subsystems; the Attitude and Articulation Control Subsystem for maintaining spacecraft attitude, and executing maneuver pointing; the Propulsion Module Subsystem to provide the ΔV's; and the Power and Pyrotechnics Subsystem for providing electrical power to the other subsystems.

All of these subsystems are redundant, and all require at least two component failures to disable the subsystem (with some high reliability exceptions, such as the reliance on a single cable harness). Some subsystems consist of several redundant components that are cross-strapped, referred to as subassemblies. The subsystems are designed so that internal failures are independent (i.e., that a failure in one half of a redundant subassembly does not propagate to the other half). Therefore, a total spacecraft failure occurs at time t when one half of a subassembly fails at some time $< t$, and the other half fails at time t, or when a design or implementation error in the hardware or software disables the system.

One of the reasons that the spacecraft reliability has been as high as it has been is that many of the functions necessary for performing and controlling a maneuver are not only component redundant but also functionally redundant.

Spacecraft control prior to a maneuver can be accomplished using the redundant reaction wheels or the redundant thrusters. During a maneuver, control about the X and Y axes can be exercised using either the main engine actuators or by pulsing the thrusters. Celestial reference can be maintained using either redundant gyros or a redundant set of sun sensor and stellar reference units. Uplink signals can be received over the high gain antenna or over one of the two low gain antennas.

Doppler can be accomplished using either X-band, S-band or K_a-band frequencies. The propulsion system can perform maneuvers in either a pressure-regulated mode or a blowdown mode. Thrust can be provided by either the main engines (primary) or the thrusters. The main engine shutoff signal is generated by an accelerometer and backed up by a timer. Protection against valve-open failures is provided by both closing isolation valves and by removing power from the engine valve coils.

In addition to the incorporated functional redundancy there are other programmatic steps that are taken to reduce the likelihood of common-mode failures. These include system, subsystem and sub-assembly level design reviews, a rigorous quality assurance program, thorough testing, and both system and subsystem failure mode effects analyses.

To calculate the predicted spacecraft system internal failure rates, consideration was given to random parts failures, design and implementation errors, and common-mode failures.

The calculation of random parts failure leading to loss of spacecraft maneuverability incorporated information from voyager mission flight experience (over 16 years of operating two spacecraft). The Voyager missions represent essentially all of the random parts failure experience of very-long life JPL spacecraft, and provide a sufficient database to derive meaningful results. For the Voyager mission, scaling laws were derived to relate the parts failure rates predicted from reliability databases (such as MIL-HDBK-217) to the actual rates occurring during flight. Voyager experience indicates a decreasing failure rate with time, and so a Weibull model was used to represent subassembly reliability, and was fit to the Voyager data. Cassini failure rates were then predicted using the same reliability databases, and the scaling laws derived for voyager were applied to these estimates to yield the final predictions.

Design and implementation errors, including common mode failures, are not included in the modeling of random parts failures, but can have the same consequences. A review of ground testing and

flight experience on the Voyagers, Vikings, Magellan, and Galileo showed that such errors represented approximately one half of all reported problems. As an approximation, the failure rate of the best estimate reliability model was doubled to incorporate the effects of design and implementation errors. This approximation enveloped a more detailed estimate that attempted to model design errors, specific common mode failures, and unpredicted common mode failures, based upon the JPL flight failure database covering Viking I and 2, Voyager 1 and 2, Magellan, Galileo, and Mars Observer. This estimate quantitatively modeled disabling errors on Cassini that are not protected by redundancy.

An overall process uncertainty of a factor of three was applied to the best estimate failure rate to arrive at the $P_{F.90}$ (x3) and $P_{F.10}$ (/3) failure rates. These uncertainty estimates were based upon engineering judgment and envelope the uncertainty derived from parameter variations of the models.

These calculations produce curves showing the cumulative probability of failure as a function of time, from launch to launch + 10 years. The curves are presented in Figure 4-10.

Loss of spacecraft commandability due to spacecraft system internal failures does not result in a ΔV. The spacecraft simply continues on its current course, unable to execute intentional ΔVs. However, because the spacecraft is no longer commendable, the spacecraft trajectory cannot be adjusted if the spacecraft is found to be on an Earth impact trajectory due to other errors.

4.3.2 P_{NR} for Failures Occurring Between E-39 Days and-E-2 Days

If the initial ΔV-inducing failure occurs from 39 days to 32 days prior to swingby, the nominal 30-day planning period can still be used. However, the recovery maneuver will be executed during the period starting 9 days before swingby, when recovery from a failure requiring ground intervention could prevent the successful execution of the initially planned recovery maneuver, and not allow enough time for the additional diagnosis and planning required for a new recovery maneuver. Failures requiring ground intervention include an erroneous ground command or a spacecraft electronics failure requiring ground intervention to recover.

If the initial failure occurs between 32 days and 9 days prior to the swingby, the schedule is contracted to allow the maneuver to occur 2 days before swingby.

If the initial failure occurs between 9 days and 2 days of the swingby, it is likely that the recovery maneuver will be executed within 2 days of the swingby.

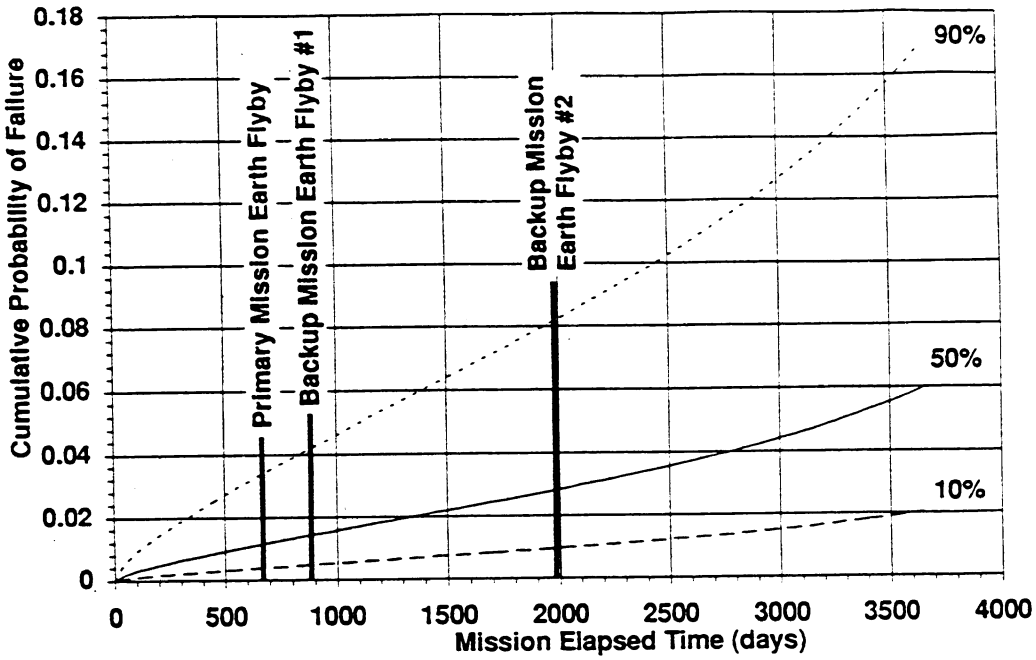

Figure 4-10 Cumulative Probability of Spacecraft System Internal Failure

For purposes of simplifying the calculations, without significantly affecting the impact probability during this period, a single set of assumptions was used in calculating P_{NR} for all initial failures occurring in the period from 39 days to 2 days.

It was conservatively assumed that the Ground System could not withstand any additional failures in the spacecraft (requiring ground intervention) if they fell within the recovery period and within nine days of encounter. It was further assumed that the Ground System could not withstand any additional ground-induced errors. Either was assumed to render the spacecraft non-recoverable.

4.3.2.1 Ground-Induced Error. There are a number of ways in which a ground-induced error could prevent recovery.

(1) The recovery maneuver sequence could be designed incorrectly, causing the spacecraft to remain on an impact trajectory.

(2) A real-time ground command could be sent up which prevented or modified the execution of the recovery maneuver.

(3) A command in the ongoing sequence could prevent or modify execution of the recovery maneuver.

(4) The failure causing the spacecraft to go on an impact trajectory is not correctly diagnosed or corrected.

(5) A DSN station is not available for uplink.

Some specific operational requirements are being imposed to decrease the probability of occurrence of the errors.

Error Source 1: Errors in the navigation design of the recovery maneuver are the most likely source of error. It is considered that because of the extreme scrutiny of the recovery maneuver, an error greater than 10% in any of the components will have a high probability of being detected. Therefore, recovery maneuvers within 39 days of swingby will be designed with large margins in each of the maneuver components to eliminate the possibility of a 10% error in one or more of the components from preventing a successful avoidance maneuver.

Error Sources 2 and 3: These errors could potentially cause an on-going recovery maneuver to terminate early or otherwise be modified in such a manner as to possibly leave the spacecraft on an impact trajectory. However, restrictions will be placed on the project that forbid any real-time commanding after the uplink of the recovery maneuver, unless necessary for Earth avoidance. In addition, the ongoing sequence will be halted as part of the recovery maneuver sequence.

Error Sources 3 and 4: No assumptions will be made about the state of the spacecraft when designing the recovery maneuver sequence. If the spacecraft needs to be in a particular state to execute the maneuver, commands should be included to put it in that state. Since the on-going sequence will be terminated, any necessary commands will be included in the maneuver recovery sequence.

Error Source 4: The spacecraft diagnosis and failure recovery should be very conservative at any time the spacecraft is on an Earth impact trajectory, but especially during the last 39 days. If there is any possibility a subsystem could have contributed to the spacecraft being on an impact trajectory, the redundant system will be swapped in. Because of the large number of people who would be involved in validating the recovery process, this failure is much less likely to occur than the others and will be ignored.

Error Source 5: Except for initial failures occurring just prior to two days before swingby, the recovery process will be performed to ensure uplink windows from at least two complexes (i.e., two geographical sites). The probability of two complexes being inoperable is virtually nil. Two of the three complexes

will have more than one antenna capable of uplinking the sequence. The probability of having the critical recovery period occur with an uplink window only over a single complex and having all antennas unavailable for a period of several hours is small enough to be ignored.

The only significant error sources left to be considered are thus navigation design error and real-time or sequenced command errors preventing execution. Because of JPL's lack of experience with having to do recovery maneuvers and because the recovery procedures are not well defined at the current time, it was considered impossible to evaluate each of the error sources in detail.

For each component, it was considered that the expected value (mean) and worst case value could be the most reliably estimated. Given the high level of uncertainty, a log-normal .distribution was fit to these values, taking the "worst case" to be the 99% probability point.

The probability of. making initial errors is higher for recovery than for normal operations because of the greater workload and stress. There will probably be overtime work for the regular personnel, and additional personnel will be brought in who may be less familiar with the operations. Therefore, the same probability for initial introduction of an error is adopted for recovery as for a nominal sequence even though the scope of the recovery activity is significantly smaller.

Most errors will not affect the capability of the spacecraft to get off an impact trajectory. The written procedures for recovery will explicitly cover any known potential errors. It is estimated that if any errors are introduced, the probability that one or more would prevent successful recovery if not caught is 0.01, with a worst case of 0.1.

Recovery activity will be subject to extreme scrutiny. It is likely that independent groups will be developing the command requests for the recovery. Thus, comparison of the results will eliminate most errors. In addition, there will be review by all of the knowledgeable people on the Project and possibly other personnel brought in from other assignments. However, because of the unpredictable nature of the recovery and the relatively short time scale compared to normal operations, an estimate of 0.01 with a worst case of 0.1 is adopted.

A Monte Carlo simulation was performed to combine the errors from the three components. Table 4-12 shows the individual probabilities of failure for each step, and the total probability of failure.

Table 4-12 Probability of a Ground-Induced Error Preventing Spacecraft Recovery

Component	Probability during period
a) Probability of the ground making an error which could affect a spacecraft engineering subsystem	mean = 0.1 99% = 0.5
b) Probability of it being an error which could prevent execution of a recovery maneuver	mean = 10^{-2} 99% = 10^{-1}
c) Probability of it not being corrected prior to execution of the recovery maneuver	mean = 10^{-2} 99% = 10^{-1}
Total probability	10%: 3.8×10^{-8} 50%: 7.5×10^{-7} mean: 1.0×10^{-5} 90%: 1.4×10^{-5}

4.3.2.2 Spacecraft Single Failure Contribution to P_{NR} for E-9 to E-2 Days. Some subsystem electronics failures require ground intervention to diagnose and correct the failure and return the spacecraft to normal operation. If such a failure were to occur, normal operation of the spacecraft would cease, and the spacecraft would place itself into a safe mode and wait for further instructions from the ground. A failure of this type could interrupt an Earth avoidance correction maneuver. If this were to occur between E-9 and E-2 days, there would be insufficient time to reconfigure the spacecraft and send another correction maneuver.

The model used to estimate the probability of spacecraft system internal failures (Subsection 4.3.1) was modified to include the probability of a single sub-assembly failure requiring ground intervention for recovery (also known as non-autonomously swapped failures) occurring during this period. The results of the model are presented in Figure 4-11.

4.3.3 P_{NR} for Failures Occurring Between E-2 Days and E-0 Days

If an anomalous ΔV were to place the spacecraft on an Earth impact trajectory between E-2 days and E-0 days, there would be insufficient time to create a recovery sequence using the nominal command generation process. Attempts would be made to create a recovery sequence, but due to the limited available time, complete review and constraint checking of

the commands would not be possible. The exact process that would be used is not predictable, and there is a high probability that a command sequence generated during this period would contain errors that would prevent recovery to a safe trajectory. Due to these uncertainties, it has been conservatively assumed that there is no chance to successfully command the spacecraft to recover from an anomalous Earth impact inducing ΔV occurring between E-2 days and E-0 days. This does not significantly affect the total probability of Earth impact due to the low probability of a failure occurring during this brief period.

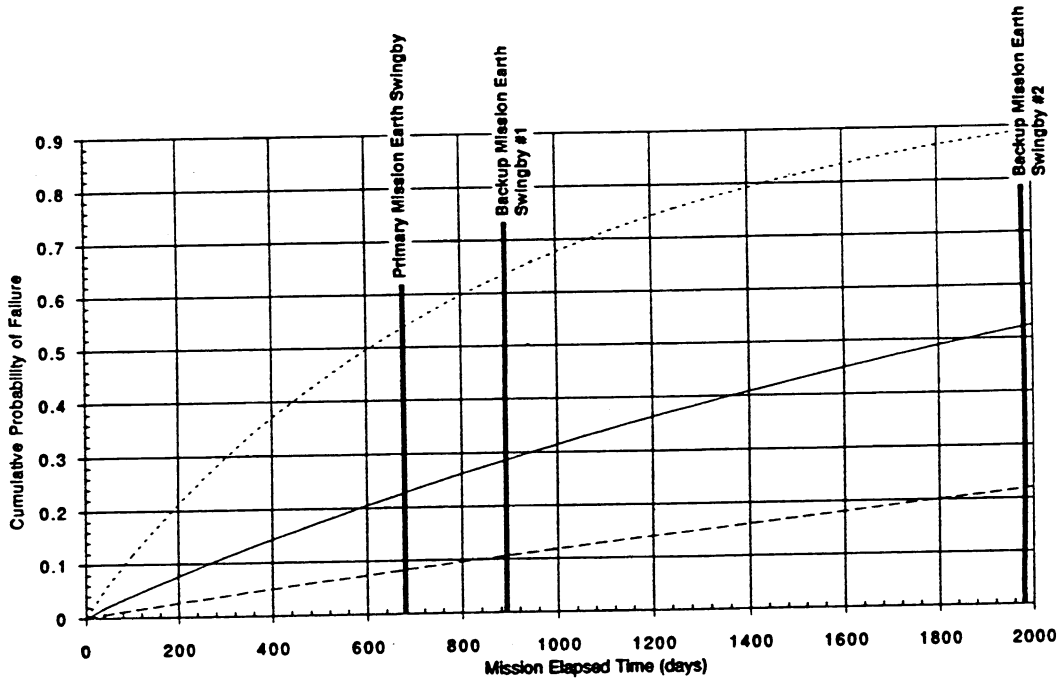

Figure 4-11 Probability of Spacecraft System Internal Failure, Including Single Sub-Assembly Failures Requiring Ground Intervention for Recovery

References

1) Divine, Neil, “Five Populations of Interplanetary Meteoroids,” Journal of Geophysical Research, Issue 98 E9, pp. 17029-17048, Sept. 25, 1993.

2) Titan Corporation Memorandum, Purchase Order #5A-865336, “Evaluation of Meteoroid Damage Potential to the Mariner Mark II Propulsion Module Subsystem,” from Hallock Swift, to R. Bamford, Jan. 19, 1990.

SECTION 5

SHORT-TERM EARTH IMPACT PROBABILITY

5.1 INTRODUCTION

This section presents the navigation strategy for designing and controlling the spacecraft trajectory between injection from Earth orbit and Earth swingby for the Cassini mission. It also provides estimates of the probability of impact on targeted Earth swingbys for the primary and backup trajectories.

The navigation strategy is driven by the requirement to control the trajectory so that the spacecraft can satisfy its mission objectives while maintaining a low probability of inadvertent Earth reentry. The navigation strategy discussed here is not concerned with the overall trajectory design, which is controlled by the launch vehicle capabilities and mission objectives (see Volume 1), but with the small variations in that trajectory.

This section is divided into nine parts. The next two parts, Subsections 5.2 and 5.3, define the problem and the solution technique, respectively. The following two parts, Subsections 5.4 and 5.5, define the navigation strategy and the reference trajectories, respectively. Subsection 5.6 describes the statistical technique used to provide a cumulative probability distribution for Earth impact, and the resulting overall Monte Carlo sampling. Most of the models are described in Section 4, but the navigation model is included in this subsection. Subsection 5.7 applies the navigation strategy and the spacecraft failure probabilities to the reference trajectories and computes the associated Earth impact probabilities. Subsection 5.8 condenses these results and presents the overall impact probability. Finally, Subsection 5.9 summarizes the results.

Only the Earth encounters designed into the reference trajectory are analyzed in this section. The possibility that the spacecraft might become disabled and have a later accidental encounter with the Earth is analyzed in the next section.

5.2 IMPACT OF FAILURES ON TRAJECTORY

Because the nominal trajectories include Earth swingbys, it is possible for the spacecraft to be on a trajectory which, if uncorrected, could result in Earth impact.

There are two general categories of uncertainties that can lead to an Earth-impacting trajectory. The first category results from uncertainties in the normal operation of the spacecraft and navigation system. For example, the actual ΔV

achieved during a maneuver* will differ slightly from the desired change. Likewise, the actual state (position and velocity) of the spacecraft will differ from the state estimated by the navigation system. Both of these uncertainties, if large enough and uncorrected, can lead to Earth impact. These are not failures, but expected variations in the operation of the systems. Ground Rules 1 and 2 of Subsection 5.4.1 below are designed to prevent any significant probability of impact resulting from these expected variations.

The second category of uncertainty is the result of spacecraft component failures, environmentally induced spacecraft failures, or operational errors that create conditions outside the expected operating conditions. These failures can be further divided into two types: (1) failures that do not impart a ΔV and (2) failures that do impart a ΔV, thus altering the trajectory.

The first failure type affects the performance of the spacecraft or supporting ground system, but does not alter the trajectory. An example of this category of failure, which does not impart a ΔV, would be the loss of uplink command capability due to a micrometeoroid hit on the engineering bus. If in the unlikely event the spacecraft were on an impacting trajectory prior to this failure, then this failure would preclude a corrective maneuver. Normally, if the spacecraft were determined to be on an impacting trajectory due to any cause, corrective action would be taken immediately. For the purposes of discussion, any failure that does not cause a ΔV will be designated a Type I failure.

The second type, where the failure may impart a ΔV to the spacecraft, will be designated a Type II failure. The ΔV resulting from the failure could be of sufficient magnitude and in the necessary direction to cause an Earth impacting trajectory. An example of this type is the rupture of a fuel tank with a ΔV being imparted by escaping propellant and/or pressurant. Depending on the particular failure, the spacecraft may or may not be able to recover from a Type II failure.

The effect of events in either category, off-nominal operation or failures, on the probability of the spacecraft impacting the Earth is strongly influenced by the spacecraft's ability to recover and apply a corrective maneuver. If, for example, a failure does not completely incapacitate the spacecraft, then the normal course of action is to command a recovery sequence to correct the trajectory and avoid Earth reentry. The following analysis of the effect of the failure modes will take into account the probabilities of taking corrective action.

* In this section, a maneuver is sometimes referred to as a Trajectory Correction Maneuver, or TCM.

As previously indicated, if the probability of a particular failure occurring is P_F, the probability of being on an impacting trajectory given the failure is $P_{I/F}$, and the probability of not being able to recover from this failure is P_{NR}, then the impact probability P_I resulting from this failure is:

$$P_I = P_F \, P_{I/F} \, P_{NR} \qquad (5\text{-}1)$$

For the purpose of defining the navigation strategy and impact probability calculations, each Type II failure can be further subdivided according to when the failure can occur. In particular, failures can occur during a maneuver, or at any time during cruise. This subdivision influences how the impact probabilities are computed, but in any case Equation 5-1 must be summed over all possible times and maneuvers to find the total probability of impact for this failure mode. Finally, the total probability of impact, P_I, is obtained by also summing over all the possible failure modes:

$$P_I = \sum_{\substack{\text{Failure} \\ \text{Modes}}} \sum_{\substack{\text{Time \&} \\ \text{Maneuvers}}} P_F \; P_{I/F} \; P_{NR} \qquad (5\text{-}2)$$

Refer to Table 4-1 for a summary of the spacecraft failure modes and the corresponding probabilities of failure. Refer to Subsection 4.5 for the recovery probabilities.

5.3 EARTH IMPACT AND PROBABILITIES

The trajectories from launch to Earth return are developed using a sequence of increasingly accurate models. The final trajectory specification is based on highly accurate double-precision numerical integration with an N-body model of the solar system, as well as detailed models for solar pressure and the gravitational fields of the planets. For perturbations of these trajectories by velocities resulting from the types of failures summarized in Table 4-1, two-body conic elements are used to describe the encounter conditions and linear perturbation techniques, with mapping-matrices called K-matrices used to relate changes in the encounter conditions to position and velocity along the trajectory. The K-matrices are generated using a fully integrated trajectory with the same models used to generate the design trajectories.

The hyperbolic orbit at the time of closest approach to the target body defines a coordinate system known as the B-plane (Figure 5-1). The point where the extended V_∞ vector intersects this plane is known as the miss parameter or b-vector. All of the swingby targets' encounter parameters will be expressed in this coordinate system. Typically, the b-vector is written as an ordered pair of its projections onto the R and T axes:

$$b = (b \cdot R, \, b \cdot T)$$

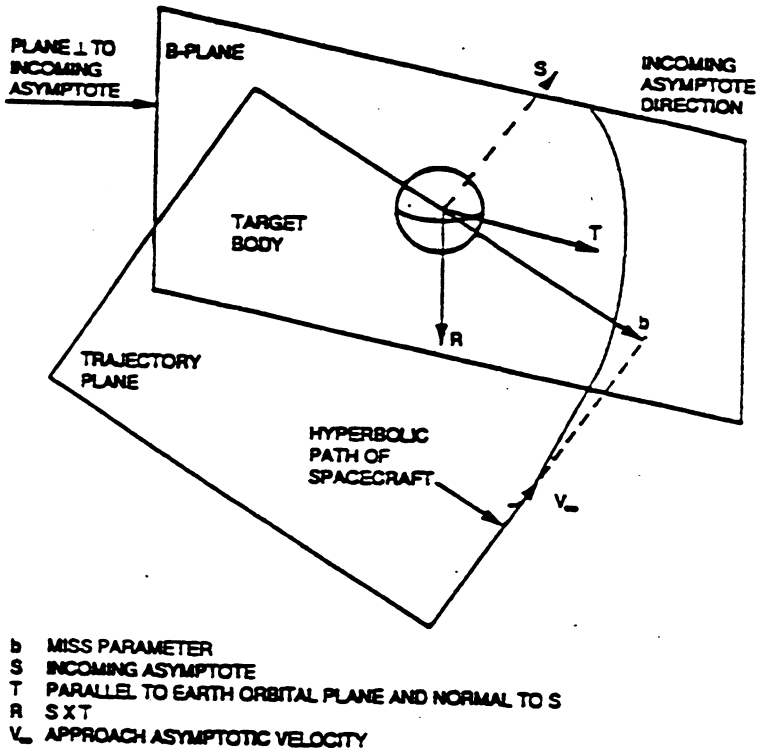

Figure 5-1 The B-Plane

Associated with any hyperbolic swingby, there is a distance from the origin in the B-plane known as the impact radius (Figure 5-2), such that if the miss parameter lies within that distance, impact with the target body will occur. In this context impact refers to any condition that causes reentry into the Earth's atmosphere and not necessarily impact with the surface. The assumption used to predict reentry into the Earth's atmosphere was any trajectory crossing a reference altitude of 122 km (400,000 feet) at ≥7°. The 7° limit is a best estimate with a poorly known uncertainty. However, the uncertainty would be expected to have only a small effect on the impact calculation For example, if a ±1° uncertainty were used the impact radius would have a variation of ±17 km (11 mi), which is a ±0.4% variation in the impact area, smaller than the navigation uncertainties. The effect of such a variation on the probability of impact would have been small, and was not included in this study.

The effective B_{IR} can be computed from the following relationship:

$$B_{IR} = R_E \left[\frac{2\mu}{R_E V_\infty^{\,2}} + 1 \right]^{1/2} \cos(\gamma_E) \qquad (5-3)$$

where R_E is the reference entry radius, μ is the Earth's gravitational constant, V_∞ is the hyperbolic excess velocity, and γ_E is the 7° entry flight path angle.

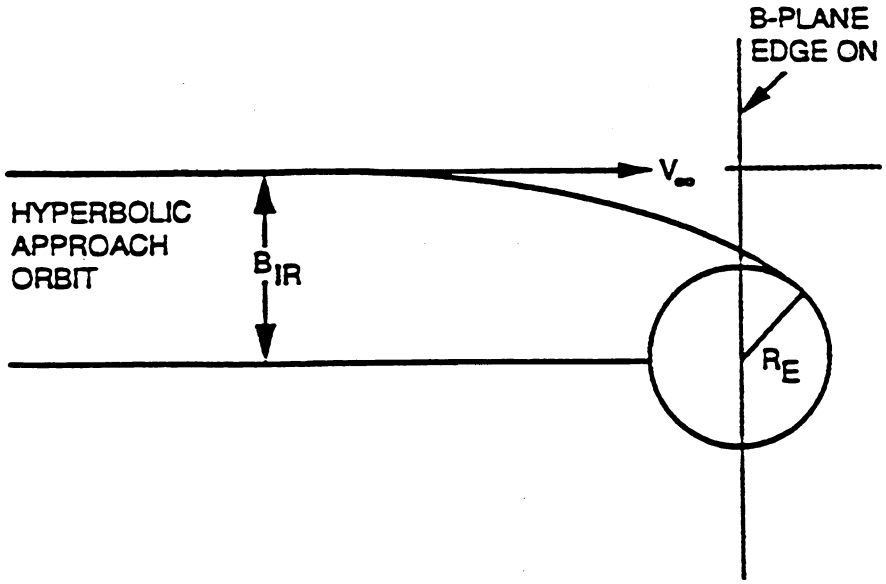

Figure 5-2 Impact Radius B_{IR}

For VVEJGA, the result is equivalent to an altitude of closest approach of 64 km (40 mi).

5.3.1 Calculation of Type I Failure Impact Probabilities

Given a Type I failure (a failure that does not impart a ΔV), an impact can only result if the spacecraft was on an impacting trajectory at the time of the failure. Hence the central calculation required is the probability of currently being on an Earth impact trajectory.

During the course of the mission, the exact conditions of the currently targeted swingby at Earth encounter will not be precisely known. This is the inevitable result of uncertainties in the orbit determination process, as well as variations in the performance of the propulsion system. At any particular point in the mission, for instance after the completion of a maneuver, the uncertainties in Earth encounter conditions are modeled by Gaussian distributions and can be graphically represented in the B-plane by a nominal swingby location (mean) and a dispersion (covariance) ellipse (Figure 5-3). Let b_0 denote the nominal swingby point and let Σ denote the covariance matrix, which numerically describes the error ellipse. As noted above, the only

dispersed points resulting in an impacting trajectory are those that are inside the impact circle, a circle of radius B_{IR} cent at the origin. Thus, the probability of being on an impacting trajectory when the failure occurs, $P_{I/F}$, given this mean aimpoint and dispersion, is the integral of the Gaussian density over the impact circle (Equation 5-3). Numerical techniques have been developed to accurately evaluate these values.

$$P_{I/F} = P_{I/F}(b_0, \Sigma) = \frac{1}{2\pi|\Sigma|^{1/2}} \iint_{|b| \le B_{IR}} \exp\left[-\tfrac{1}{2}(b - b_0)^T \Sigma^{-1}(b - b_0)\right] db \qquad (5-4)$$

Equation 5-4 then yields the probability of Earth impact given a Type I failure, for use in calculating the probability impact in either Equation 5-1 or 5-2.

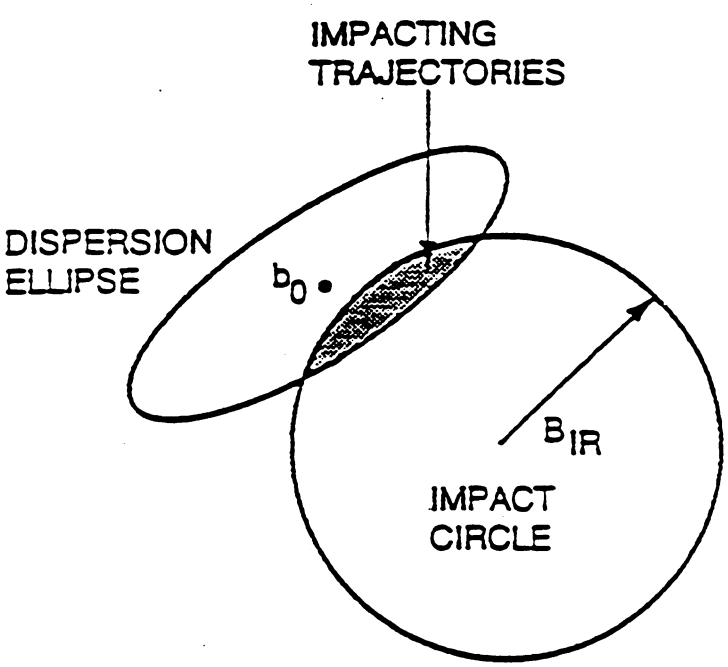

Figure 5-3 B-Plane Projections of Target, Impact Circle, and Sample Dispersion Ellipse

5.3.2 Calculation of Type II Failure Impact Probabilities

For each Type II failure (a failure that does impart a ΔV) discussed in Section 4, the analysis provides a probability of that failure occurring, as well as a description of the ΔV that could arise from that failure. Suppose that the current target of the spacecraft is $\bar{b}$ and that a spurious velocity, $\overline{\Delta V}$, has occurred, then an impacting trajectory will result if and only if

$$\left\| \bar{b} + K\overline{\Delta V} \right\| < B_{IR}$$

where K is the 2x3 K-matrix mapping the spurious velocity into the B-plane for the epoch of the velocity, $\overline{\Delta V}$ (Figure 5-4).

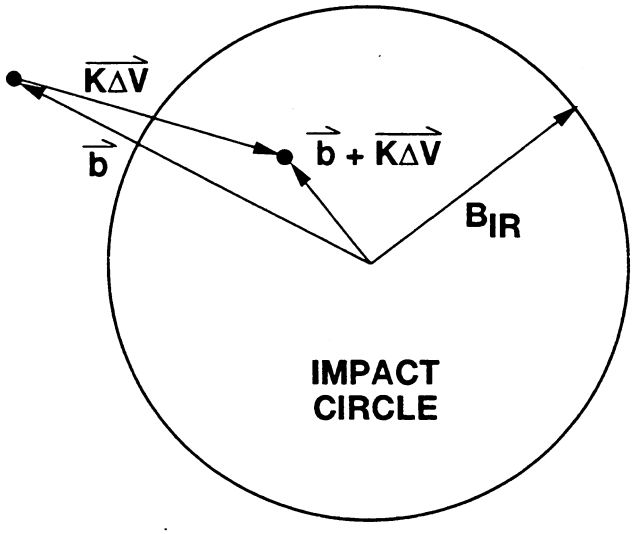

Figure 5-4 Velocity Error, ΔV, Which Causes an Impacting Trajectory

If the spurious velocities are distributed according to the probability density function $\phi(\overline{\Delta V})$, which is non zero only on a region S in velocity space, then the probability of impact, given that the $\overline{\Delta V}$ has occurred and that the spacecraft is currently targeted to $\bar{b}$ is

$$P_{I/\Delta V}(\bar{b}) = \int_S \chi(\bar{b} + K\overline{\Delta V})\phi(\overline{\Delta V})\, dV$$

where

$$\chi(\bar{b} + K\overline{\Delta V}) = \begin{cases} 1 & \text{if } \|\bar{b} + K\overline{\Delta V}\| < B_{IR} \\ 0 & \text{otherwise} \end{cases}$$

Taking into account the fact that the current target $\bar{b}$ of the spacecraft is itself a statistical quantity with mean $\bar{b}_0$ and covariance Σ, the total probability of impact, given that the specified failure has occurred, is

$$P_{I/F} = P_{I/F}(\phi, b_0, \Sigma) = \frac{1}{2\pi|\Sigma|^{1/2}} \int_{-\infty}^{\infty}\int_{-\infty}^{\infty} P_{I/\Delta V}(\bar{b}) \exp\left[-\tfrac{1}{2}(\bar{b} - \bar{b}_0)^T \Sigma^{-1}(\bar{b} - \bar{b}_0)\right] db \qquad (5-6)$$

If the probability of a particular failure occurring, again denoted by P_F, and the recovery probability P_{NR} are factored in, the probability of impact from this failure is also expressed by Equation 5-1. In this case, the probability of Earth impact from a Type II failure is simply the probability of the failure resulting in an impacting trajectory (Equation 5-6) times the probability of a failure occurring times the probability of no recovery. Note that, depending on the complexity of the evaluation of ϕ, the evaluation of Equation 5-6 can be a five-dimensional integral (three components of velocity and two components in the B-plane). Numerical techniques for accurate evaluation of Equation 5-6 have been developed.

A calculation of entry angle distribution was performed by iterative use of Equation 5-3 for reference entry angles different from 7°. By differencing the impact probabilities obtained by Equation 5-6, the probability of impact within a given range of entry angles was determined.

5.4 EARTH SWINGBY NAVIGATION STRATEGY

The primary objective of the navigation strategy between injection out of Earth orbit and the final Earth swingby for the Cassini mission is to deliver the spacecraft to the necessary Earth swingby conditions while maintaining the mean value of the total probability of Earth impact $<10^{-6}$. A secondary objective is to minimize the required propellant consumption.

To calculate the probability of Earth impact as given by Equation 5-2 requires a knowledge of three factors: the spacecraft failure probabilities and associated ΔVs, the uncertainties in the navigation process, and the characteristics of the spacecraft trajectory. For the purpose of defining an Earth swingby navigation strategy, steps are discussed below to minimize the effect of both spacecraft failures and navigation uncertainties. The navigation strategy focuses on specifying and controlling the spacecraft trajectory conditions assuming failure probabilities and navigation uncertainties.

In general, the impact probability decreases as the swingby altitude increases, so that impact avoidance requirements could be satisfied by simply raising the swingby altitude. However, the swingby conditions are needed to shape the trajectory, and the spacecraft cannot carry sufficient propellant to replace this effect (except possibly for a very small bias).

Fortunately, there is enough propellant to bring the trajectory in toward the Earth in several steps before the swingby. This technique has been used in past JPL interplanetary missions for planetary protection from biological contamination. The idea is to partition the trajectory into segments. The trajectory on each segment is targeted to swingby conditions that yield an acceptable impact probability under the conditions expected during that segment. Due to the navigation uncertainties and trajectory dynamics, this strategy allows at least the final segment to be targeted to the desired swingby conditions. Prior segments are targeted to-biased aimpoints that, if uncorrected, have higher swingby altitudes. The trajectory segments are joined by required spacecraft maneuvers.

The navigation strategy is, therefore, to break the overall trajectory to Earth encounter into segments where the Earth impact probability along each segment is controlled by a biased aimpoint. These aimpoints are chosen so that the sum of the impact probabilities over all such segments for the mission is kept low, to less than the overall requirement of 10^{-6}. As a secondary goal, the biased aimpoints are also chosen to minimize the ΔV required for impact avoidance.

Prior to launch, analysis is performed to determine both the duration and swingby conditions for each segment. After launch, the spacecraft is controlled to meet these conditions.

5.4.1 Ground Rules for Type I and Other Failures

In the design approach for Earth avoidance, two restrictions upon the aimpoint selection and maneuver strategies have been imposed:

(1) Ground Rule 1: At no point during the mission from injection out of Earth orbit to the final Earth swingby will the probability of being on an Earth impacting trajectory following the successful completion of a maneuver be greater than 10-6 (using the best estimate of navigation dispersions).

This Ground Rule helps to assure that the contribution of any failure to Earth impact will be small, by keeping the PI/F term of Equation 5-1 small. For a Type I failure it limits the $P_{I/F}$ term to $\leq 10^{-6}$. Thus the two Type I failure modes (Engineering Bus and Spacecraft System Internal Failure) both have low probabilities of impact (Table 5-6) for each encounter. In fact, the largest probability of impact for either of these failure modes is just 0.002×10^{-6}.

The figure of 10^{-6} also leads to a reasonable requirement for additional propellant consumption. At any time after launch, if the spacecraft were determined to be on a trajectory with an unacceptable impact probability due to navigation or other dispersions, the Navigation and Spacecraft Engineering teams would immediately design and implement a ΔV maneuver to correct this condition.

(2) Ground Rule 2: If, during the course of performing a maneuver, the maneuver were to inadvertently terminate early, the probability of a resulting Earth impacting trajectory will be no greater than that for a normal completed maneuver.

Rule 2 is an adjunct to the first rule in the sense that not only are the final target parameters for each maneuver constrained, but the path that the maneuver traces from initial to final aimpoint in the B-plane is also constrained. Rule 2 also implies that at no point during the course of a nominally designed maneuver will the path from the initial point to the desired target cross the impact circle. This ensures that if a maneuver fails to complete, there will be no increase in the possibility of an Earth impacting trajectory.

5.5 MANEUVER STRATEGY

The set of reference trajectories currently under consideration include either one or two Earth swingbys. Three Earth swingby trajectory segments have been studied in detail for this report: the Cassini Primary 1997 VVEJGA, plus both the Venus 2-Earth 1 (VE1) and the Earth 1-Earth 2 (E1E2) segment from the Cassini Backup 1999 VEEGA. The VVEJGA was chosen since it is the most likely candidate while the VEEGA is the backup trajectory. For both primary and backup trajectories, a launch date was chosen to provide the minimum altitude Earth swingby. This guarantees the analysis is valid over the launch period for each trajectory.

Analysis for each trajectory begins with the last maneuver before the planetary encounter preceding the Earth swingby. This maneuver achieves a chosen aimpoint at that preceding body to place the spacecraft on a trajectory that returns near the Earth. The preceding body's aimpoint is chosen such that the Earth avoidance criteria will be satisfied. Earlier trajectory segments will be targeted to the same preceding body's aimpoint, and failures during these segments have been found to contribute a negligible amount to the total short-term Earth impact probability. This is a result of the size of the delivery dispersions to the preceding body and the dispersive effects of the swingby. The beginning maneuver for the VVEJGA trajectory is 20 days prior to the second Venus swingby, and for the VEEGA trajectory is 20 days before the Venus swingby (for the VE1 segment) and 10 days before the Earth 1 swingby (for the E1E2 segment).

Mission design for minimal total ΔV usage to Saturn requires at least one Deep Space Maneuver (DSM) for most effective use of the encounter gravity assists. It is a deterministic maneuver required to achieve the nominal mission. If a DSM is included in the trajectory segment to the Earth, it provides a built-in Earth bias offset, usually large enough so that no trajectory bias is needed until after the DSM. The 1999 VEEGA trajectory has a DSM included in its E1E2 segment, which provides an adequate bias to the E2 Earth swingby. Therefore it is not necessary to bias the E1 swingby, but the DSM aimpoint will be appropriately biased to provide an Earth bias after the DSM. On the other hand, the 1997 VVEJGA trajectory does not have a DSM in its V2E segment. Therefore, the V2 encounter must be biased, to provide an adequate bias for the Earth swingby to follow.

In either case, following the swingby or DSM, the bias is gradually removed by a series of maneuvers targeted to biased aimpoints. The desired Earth swingby conditions are only achieved by the final maneuver 10 days prior to Earth swingby.

After the final Earth swingby, the trajectories for each mission proceed to separate destinations well away from Earth. The focus of the Earth avoidance navigation strategy is thus the control of each mission's trajectory prior to the final Earth swingby.

Table 5-1 presents the maneuver profile as well as the impact radii and other swingby parameters for the VVEJGA Earth encounter segment. The series of biased aimpoints is illustrated by the B-plane of Figure 5-5. Table 5-2 and Figure 5-6 present similar information for the VEEGA VE1 segment, while Table 5-3 and Figure 5-7 present the E1E2 segment information. As can be seen, the biased aimpoints all approach the final Earth swingby point from within ±90° of its radial direction, thus satisfying Ground Rule #2. The VVEJGA case was deliberately biased initially off this radial direction because it saved about 35% of the ΔV required for Earth avoidance. The VEEGA E1E2 case was biased off this radial direction primarily by the DSM.

Table 5-1 Cassini Primary Mission VVEJGA Earth Maneuver/Event Profile

Event	Epoch	Description	Earth Aimpoints (Earth mean orbit coordinates) b·R (km)	b·T (km)
V-20 day TCM	31-May-1999	Achieved desired Venus swingby conditions	150235	66258
Venus 2 Swingby	20-Jun-1999	Altitude * = 2270 km Vinf = 9.479 km/s |b| = 11,376 km B_{IR} * = 8966 km		
V+10 day TCM	3-Jun-1999	Correct Venus dispersions and particularly remove bias	14555	16000
E-30 day TCM	16-Jul-1999	Correct dispersions and partially remove bias	590	11325
E-10 day TCM	06-Aug-1999	Correct dispersions and remove bias	440	8324
Earth Swingby	16-Aug-1999	Altitude * = 439 km Vinf = 15.745 km/s |b| = 8336 km B_{IR} * = 7888 km V_{impact} = 19.28 km/s @122 km altitude		

*Altitude and impact radius are reported relative to a minimum safe altitude at closest approach. For Venus, a capture altitude of 100 km was assumed. For Earth, Equation 5-3 was used, yielding a safe altitude of 64 km.

1 km = 0.62 mi
1 km/s = 0.62 mi/s

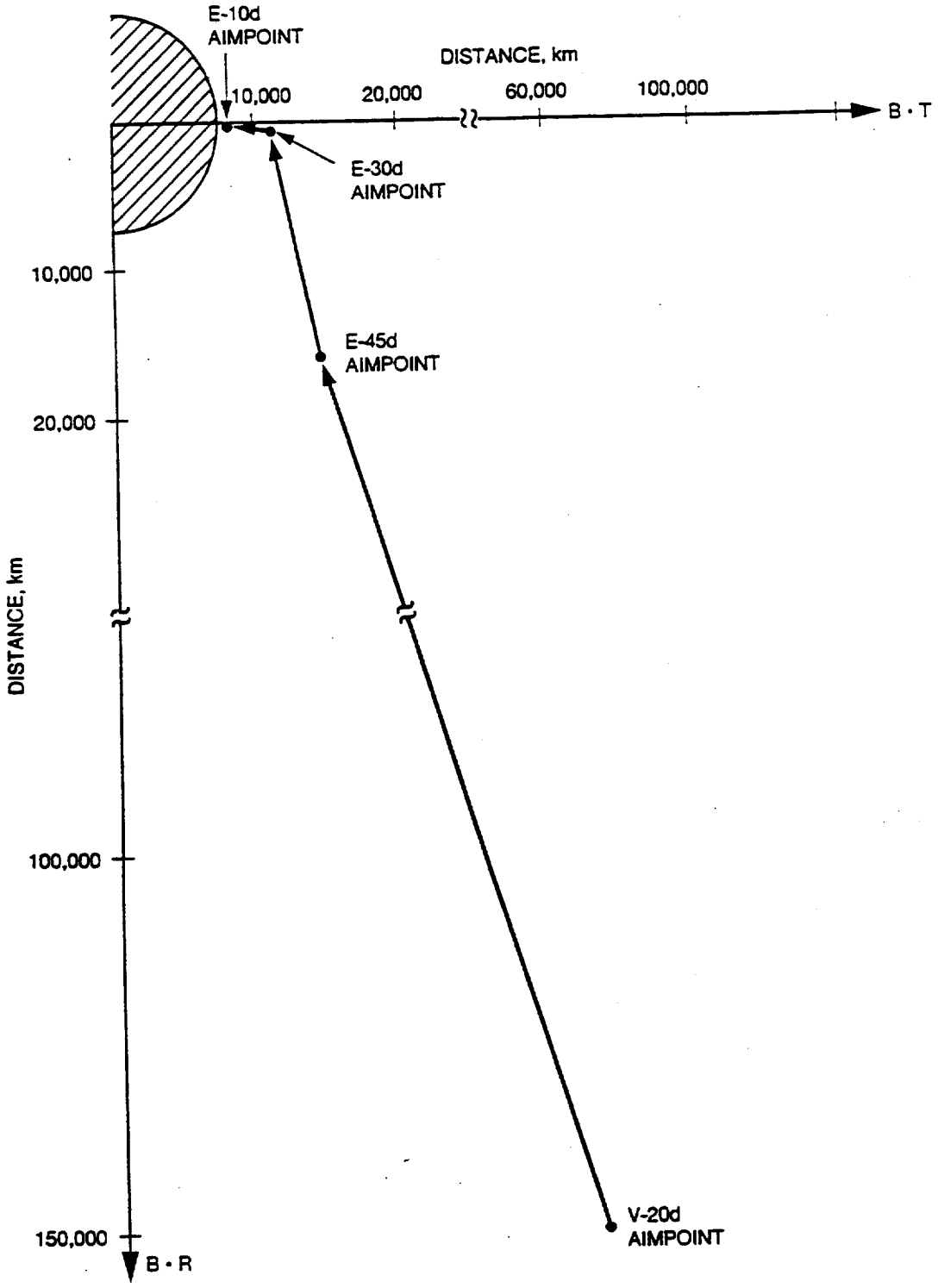

(1 km = 0.62 mi)

Figure 5-5 Cassini Primary Mission VVEJGA Trajectory
Earth B-Plane

Table 5-2 Cassini Backup Mission VEEGA Earth 1
Maneuver/Event Profile

Event	Epoch	Description	Earth Aimpoints (Earth mean orbit coordinates) b·R (km)	b·T (km)
V-20 day TCM	24-May-2000	Achieved desired Venus swingby conditions	-200000	-300000
Venus Swingby	13-Jun-2000	Altitude * = 1282 km Vinf = 8.1610 km/s |b| = 10173 km B_{IR} * = 9893 km		
V+40 day TCM	23-Jul-2000	Correct Venus dispersions	-200000	-300000
E1-200 day TCM	10-Feb-2001	Correct dispersions and partially remove bias	-100000	-150000
E-90 day TCM	31-May-2001	Correct dispersions and partially remove bias	-17000	-25000
E1-30 day TCM	30-Jul-2001	Same as above	-7400	-10700
E1-10 day TCM	19-Aug-2001	Achieved Desired Earth 1 swingby conditions	-5802	-8356
Earth Swingby	29-Aug-2001	Altitude * = 1464 km (Rel to a 60 km limit) Vinf = 12.205 km/s |b| = 10314 km B_{IR} * = 8712 km V_{impact} = 16.49 km/s @122 km altitude		

*Altitude and impact radius are reported relative to a minimum safe altitude at closest approach. For Venus, a capture altitude of 100 km was assumed. For Earth, Equation 5-3 was used, yielding a safe altitude of 60 km.

1 km = 0.62 mi
1 km/s = 0.62 mi/s

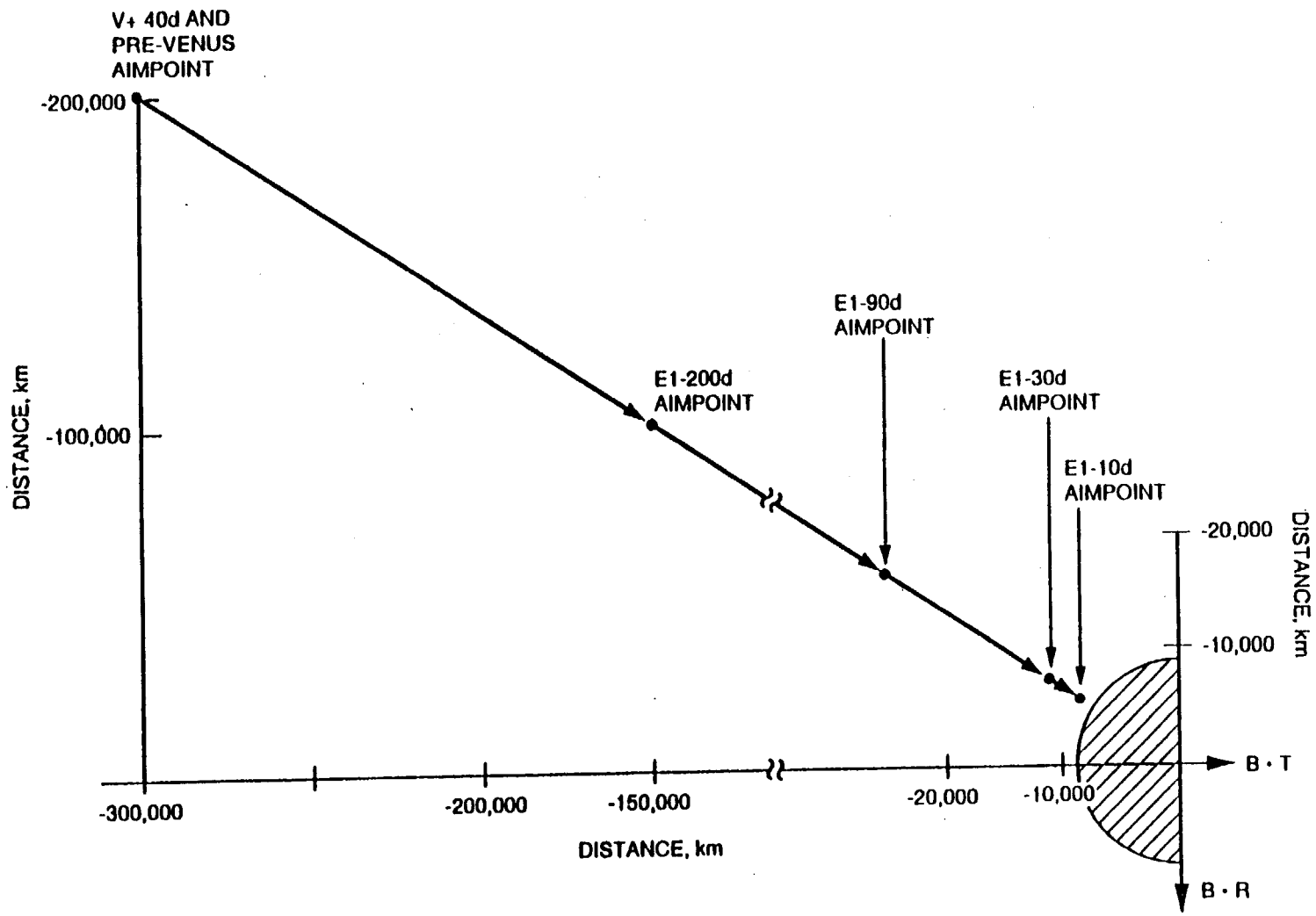

(1 km = 0.62 mi)

Figure 5-6 Cassini Backup Mission VEEGA E1 Earth B-Plane

Table 5-3 Cassini Backup Mission VEEGA Earth 2
Maneuver/Event Profile

Event	Epoch	Description	Earth Aimpoints (Earth mean orbit coordinates) b·R (km)	b·T (km)
E1-10 day TCM	19-Aug-2001	Achieved desired Earth 2 swingby conditions	394266	-3335485
Earth 1 swingby	29-Aug-2001	Altitude * = 1464 km (Rel to a 60 km limit) Vinf = 12.205 km/s |b| = 10314 km B_{IR} * = 8712 km		
E1+60 day TCM	28-Oct-2001	Correct Earth 2 dispersions	-394266	-3335485
E2-427 day TCM	24-Jun-2003	Perform DSM and partially remove bias	-100000	-200000
E2-390 day TCM	31-Jul-2003	Cleanup DSM and partially remove bias	-80000	-160000
E2-100 day TCM	16-May-2004	Correct dispersions and partially remove bias	-28000	-56882
E2-30 day TCM	25-Jul-2004	Same as above	-6000	-12007
E2-10 day TCM	14-Aug-2004	Achieved Desired Earth 2 swingby conditions	-3599	-8110
Earth Swingby	24-Aug-2004	Altitude * = 439 km (Rel to a 61 km limit) Vinf = 13.215 km/s |b| = 8873 km B_{IR} * = 8418 km V_{impact} = 17.28 km/s @122 km altitude		

*Altitude and impact radius are reported relative to a minimum safe altitude at closest approach. For Earth, Equation 5-3 was used, yielding a safe altitude of 60 km for E1 and 61 km for E2.

1 km = 0.62 mi
1 km/s = 0.62 mi/s

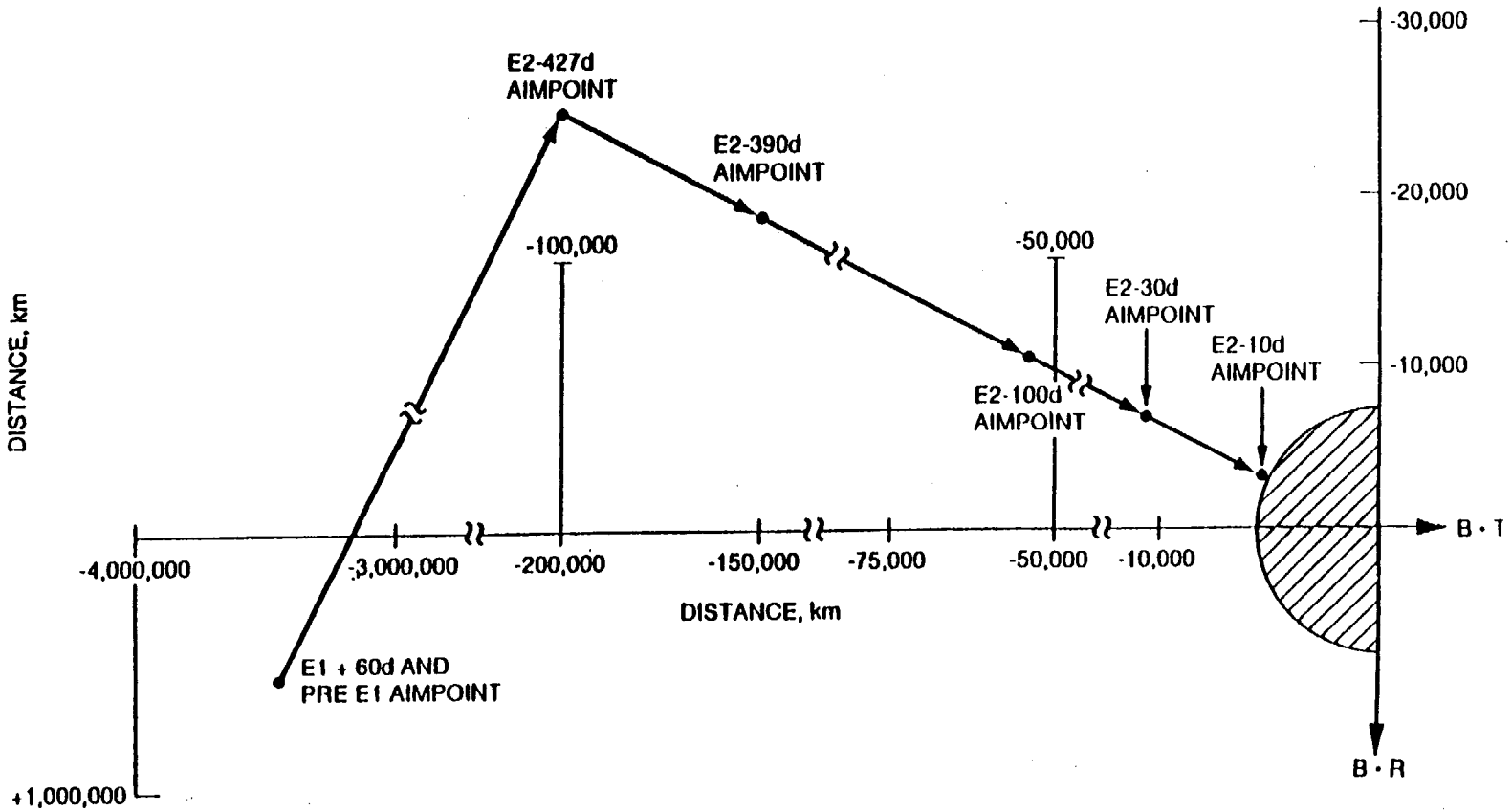

(1 km = 0.62 mi)

Figure 5-7 Cassini Backup Mission VEEGA E2 Earth B-Plane

5.6 METHOD OF COMPUTATION

The desired final result is an estimate of the probability that the spacecraft will impact the Earth given failures and other non-nominal conditions. This probability will be described in terms of not only its mean value but also the distribution about this mean. In order to achieve this result it is necessary to understand not only the best estimates of the various factors of Equation 5-2 but also the range of uncertainty in these best estimates.

5.6.1 Model and Process Uncertainty

In each of the spacecraft failure modes defined in Section 4, both the probability of failure, P_F, and the ΔV distribution resulting for the failure are described in terms of the best estimate (50% value) of the probability of failure and of the distribution of the resulting ΔV. In addition to these best estimates, the expected variations in the best estimate are provided. For example, for the CDS Flight Software failure mode, the best estimate of the probability of failure is $1x10^{-5}$ per day (the 50% value) and it is estimated that there is a 10% chance that the probability of failure might be as low as $1x10^{-6}$ per day and a 10% chance that the probability of failure could be as high as $1x10^{-4}$ per day.

The variations in the probability levels are designed to reflect the uncertainty in the value of the best estimate that arises from uncertainties in the process or the data used to construct the best estimate. Given a full understanding of the processes and the uncertainty in the models of these processes, it would have been possible to generate complete probability distributions statistically describing these variations. However, in most cases this level of information was not available and it was necessary to approximate the full distribution by the best estimate, upper bound, and lower bound as described above.

For a micrometeoroid-induced failure it was possible to generate a continuous distribution, since its probability is a sum over products of several terms (some in the flux and some in the penetration model). Each of these terms has a three-point distribution as above; their combination allowed the generation of a continuous distribution for the model uncertainty.

These variations were developed for each of the parameters that influence the overall probability of Earth impact. The spacecraft failure probability statistics are provided in Section 4 along with the statistics defining the probability of executing a recovery maneuver. The navigation accuracy statistics are provided in Subsection 5.6.3.

5. 6.2 Impact Probability Estimation Process

The previous subsection noted that each of the parameters that contribute to the overall probability of impact is described by a statistical distribution. The computation of the statistical distribution of the probability of Earth impact is, conceptually, accomplished in two steps.

First, the probability of impact given failure, $P_{I/F}$, is computed for each of the failure modes which contribute to the final result, using the ΔV data at each of the three probability levels. For example, assuming an accelerometer failure, the probability of impact given failure is computed using Equation 5-6 at each of the maneuver times using one of the three density functions, ϕ, of the ΔV resulting from the failure, along with three levels of navigation uncertainties. This process results in nine separate estimates of the probability of impact given an accelerometer failure. This yields a set of individual impact probabilities, one at each time step or maneuver point depending upon the type of failure.

The second step is to conduct a Monte Carlo simulation of the mission segment under consideration. Each Monte Carlo sample is in itself a complete simulation of the mission segment, with all failure modes sampled over all time steps. For each failure mode the simulation includes:

(1) The time-ordered set of probability of impact given failure (at three levels for Type I failures and nine for Type II).

(2) The probability of failure, P_F. For all of the failures except the micrometeroid impact induced failures, the probability of failure is given at three discrete probability levels, 10%, 50%, and 90%, representing the best estimate of the failure probability and the upper and lower values. For the micrometeroid impact induced failure, the probability of failure is given as a continuous distribution. The failure probabilities are defined in Section 4 and may be either constant or time varying.

(3) The probability of not being able to accomplish a recovery maneuver, P_{NR}. This is a time-varying probability also specified at the three probability levels, 10%, 50%, and 90%, in Section 4.

The Monte Carlo simulation then simulates the results for a large number of missions (1000 samples were adequate to accurately calculate the mean value and characterize the tails of the distribution). Each simulated mission is broken down into a number of time steps. Each time step represents either a time interval during the cruise phase between maneuvers or a maneuver. The size of the cruise time interval varies over the trajectory.

At each time step the simulation computes the probability of impact for each failure mode using Equation 5-1. Except for the micrometeoroid impact failure mode, the value of each of the three factors in Equation 5-1 is selected in a random fashion from one of the three input distributions. A value for the 50% best estimate distribution is selected in 40% of the samples with the remaining 60% equally split between the 10% and 90% distributions. This sampling ratio provides the same mean and standard deviation as a normal distribution with the given 10%, 50%, and 90% values. The micrometeoroid failure mode is handled in a similar fashion except that the probability of failure is sampled from a continuous distribution. PNR was calculated as described in Subsection 4.5.

The three individual factors are multiplied together to obtain a probability of impact PI for the failure mode during the time interval (or maneuver). These individual impact probabilities are then summed over both the duration of the mission segment and across all of the failure modes to obtain one Monte Carlo sample of the total distribution of the probability of impact for the mission segment as required by Equation 5-2.

Finally, when all the Monte Carlo samples have been calculated, the resulting overall cumulative probability and probability density curve are also calculated, along with the mean value and a breakdown into the contribution due to each failure mode.

5.6.3 Navigation Models

The three inputs which can change the navigation dispersions are the influence matrices (K-matrices), the TCM execution uncertainties, and the orbit determination uncertainties. K-matrices model the linearized influence of a perturbation on the trajectory, and should be fixed. In practice some degree of error creeps into the calculation of K-matrices, especially near the end of a long or complex trajectory segment. However this variation is small compared to the variation due to the orbit determination and TCM execution uncertainties.

TCM execution uncertainties have been published as 3σ requirement levels, as given in Table 5-4. The corresponding 1σ values were used for the 50% model. Those numbers were then multiplied by 1/2 to obtain a 10% model and by 2 to obtain a 90% model.

Table 5-4 TCMExecution Errors (3σ)

Error Type	Main Engine	RCS System
Proportional Magnitude	1.0%	6.0%
Proportional Pointing	20.0 millirad	25.5 millirad
Fixed Magnitude	32.4 mm/s	10.0 mm/s
Fixed Pointing	50.0 mm/s	10.0 mm/s

1 mm = 0.03937 in

B-plane orbit uncertainty was estimated using detailed study results when available. A long-term non-gravitational uncertainty model was used at all other times to estimate the three probability levels of orbit determination uncertainty. The dominant term in the covariance matrix is the B-plane uncertainty, usually modeled as circular for this study. Thus, one number will approximately describe the orbit uncertainty for each case. The resulting orbit determination uncertainties are given in Table 5-5 below, for each TCM leading to an Earth encounter.

Table 5-5 Orbit Uncertainty in B-Plane Position
(10%, 50%, 90%, in km*)

TCM (days from Enc.)	VVEJGA, VE	VEEGA, VE1	E1E2
V-20d	7.0, 10.0, 18.0	6.0, 10.0, 18.0	
E1-10d			2.0, 3.7, 8.0
Previous	Encounter		
E1+60d			1904, 3570, 7042
V+40d		351, 658, 1302	
E2-427d			328, 615, 1214
E2-390d			278, 521, 1028
E1-200d		82.7, 155, 306	
E2-100d			20.8, 38.9, 76.7
E1-90d		18.3, 34.3, 67.5	
E-45d	9.0, 10.0, 12.0		
E,E1,E2-30d	15.0, 18.0, 40.0	6.0, 8.0, 10.0	6.0, 8.0, 10.0
E,E1,E2-10d	2.0, 3.7, 8.0	2.0, 3.7, 8.0	2.0, 3.7, 8.0
Earth	Encounter		

*1 km = 0.62 mi

Separate Monte Carlo simulations were performed for the 10%, 50%, and 90% models of TCM execution/orbit determination uncertainties, and the resulting delivery uncertainties for each TCM were used as inputs for the overall Monte Carlo simulation.

5.6.4 Other Calculations

Calculations were also performed to find the distribution of spacecraft entry angles and latitudes, given impact. These have been requested for use in assessing the potential danger of an Earth impact should one occur.

The spacecraft entry angle distribution was calculated by providing a corresponding Earth B-plane radius for each entry angle boundary desired, and then calculating the number of Earth impact cases inside that radius. The number of Earth impacts for any elevation angle zone was merely the difference between two of these calculations.

The impact latitude distribution was estimated by fitting the entry angle distribution (which had already been calculated) with models of the expected impact-scatter chosen for each case. Two models were used: First, a uniform distribution was used where impact was assumed to be equally likely at any point in the B-plane. Second, a two-dimensional Gaussian distribution was used centered about the final Earth approach aimpoint. The uniform distribution model was found to fit the VEEGA E1 swingby entry angle distribution very well all by itself. The other two encounters required a tailored combination of both models to match the entry angle distribution. Given a distribution of impact points and the approach declination, the latitude of each simulated impact point was computed and the latitude distribution determined.

5.7 EARTH IMPACT PROBABILITIES

The total short-term probability of Earth impact resulting from inflight spacecraft and operational failures is the sum of the contributions from each failure. This subsection examines each of the failure modes analyzed in Section 4, and computes the fraction of the total impact probability resulting from that failure mode. If the result is less than 10^{-12}, it will be replaced by "nil", since it over represents the accuracy of the analysis. The failure rates and resulting ΔV distributions are given in Table 4-1, and its organization into I. Environmental, II. Spacecraft, and III. Ground failures will be retained.

The fractional impact probability for each continuous failure mode has been computed at 5-day intervals (except for 1-day intervals for the last 20 days and 1-hour intervals for the last day before encounter) and summed over the entire trajectory segment. For Type II failures occurring during discrete maneuver events, the fractional impact probability is a sum over all such events in the segment. The segment totals for each failure mode are presented below.

For Type II failures that occur during maneuvers, the failure is assumed to occur at the end of the maneuver. If the failure occurs after the desired ΔV has been achieved, the resulting aimpoint will be closer to the Earth (Ground Rule #2) leading to higher impact probabilities. Most of these failures can occur at any time during the execution of the maneuver, hence this is a conservative assumption.

I. Environmental Failures

1.) Micrometeoroid

The only significant environmental failures are those caused by micrometeoroid impact. The space environment bombards the spacecraft with particles (micrometeoroids) which can rupture sensitive elements. When a micrometeoroid of sufficient energy impacts one of the spacecraft's propellant tanks, there is a probability of catastrophic failure that not only imparts a ΔV to

the spacecraft but also precludes any corrective maneuvers (except for helium tank failure). The cumulative failure probability due to collision with micrometeoroids is cited in Subsection 4.2.1, Figures 4.3 through 4.9 for the primary and backup trajectories. For each time interval to be analyzed the corresponding cumulative probability curve was differenced to obtain the probability of failure in that time interval.

For the micrometeoroid-induced failures, the model uncertainties are specified by a continuous, time-dependent log-normal distribution as discussed in Subsection 4.2.2.

For each of these failures, the resulting ΔV is analyzed in Subsection 4.2.3. If the spacecraft bus protection is defeated, the resulting ΔV is assumed to be zero, but the probability of no recovery is assumed to be 1.0.

Because of the tank construction, helium tank rupture is not very likely to cause rupture of any other tank, as shown in Table 4-5. Thus it may not prevent recovery (i. e. a blowdown mode may be used), which lowers the probability of impact due to helium tank rupture.

The micrometeoroid mean fractional impact probability for the Cassini primary trajectory is 1.95×10^{-7} and for the backup trajectory it is 2.04×10^{-7} for the E1 encounter and 4.02×10^{-7} for the E2 encounter. Comparison of these numbers with the total impact probabilities of Table 5-6 shows that micrometeoroid induced failures are the dominant failure mode for causing possible Earth impact.

II. Spacecraft Failures

Internal failures in the spacecraft can be caused by malfunction in any important piece of hardware or software. The malfunction in turn can be due to a marginally faulty part, to aging/cycling, to a design error not found in testing, etc. Subsection 4.3 gives a detailed analysis of these failure modes.

1) Stuck-Open Thruster Valve

An electronic or hardware fault can cause an anomalous ΔV when the spacecraft is using the monopropellant system to control the spacecraft attitude. While the spacecraft periodically may use the reaction wheels for attitude control during the cruise period, these short periods will be ignored. The spacecraft can recover from this failure. The stuck thruster fractional mean impact probability for the Cassini primary trajectory is 2.86×10^{-10} and for the backup trajectory is nil for the E1 encounter and nil for the E2 encounter.

2) Stuck-Open Main Engine Valve

If the main engine valve fails to close at the commanded termination of a main engine maneuver, then an overburn of the maneuver will result. This is a failure that occurs only during maneuvers, so the direction of the erroneous ΔV will be the same as the maneuver direction. The spacecraft can recover from this failure. The stuck-open main engine valve mean fractional impact probability for the Cassini primary trajectory is nil, and for the backup trajectory is nil for the E1 encounter and nil for the E2 encounter.

3) Accelerometer Failure

Failure of the main engine accelerometer can result in an anomalous overburn ΔV. The magnitude depends upon the setting of the backup maneuver termination command and the accuracy of the propulsion system modeling. If the accelerometer fails during a main engine burn, the termination command will be sent by a backup timer, set to nominal maneuver duration time plus 5%. Modeling accuracy for the timer is assumed to be normally distributed with a zero mean and a 3σ variance of 5% of the commanded ΔV magnitude. This is a failure that is discovered only during maneuvers, so the direction of the erroneous ΔV will be the same as the maneuver direction. The spacecraft can recover from this failure.

The accelerometer failure mean fractional impact probability for the Cassini primary trajectory is 2.45×10^{-10} and for the backup trajectory it is nil for the E1 encounter and 7.17×10^{-9} for the E2 encounter.

4) Main Engine Gimbal Actuator Failure

Failure of the main engine gimbal actuator during a maneuver will cause the main engine to slew to an improper orientation. Spacecraft fault protection will terminate the maneuver if this failure happens but not before an erroneous ΔV occurs. The spacecraft can recover by using the monopropellant system. The main engine gimbal actuator failure mean fractional impact probability for the Cassini primary trajectory is 2.07×10^{-1} and for the backup trajectory is nil for the E1 encounter and 2.66×10^{-12} for the E2 encounter.

5) AACS Flight Software Coding Error

An error in the AACS flight software could result in an unplanned maneuver. The spacecraft can recover from this failure. The AACS flight software coding error mean fractional impact probability for the Cassini primary trajectory is 3.00×10^{-12}, and for the backup trajectory is nil for the E1 encounter and nil for the E2 encounter.

6) CDS Flight Software Error

A CDS software failure is the result of the CDS sending an erroneous command to the AACS which, in turn, executes an unplanned maneuver. The spacecraft can recover from this error. The CDS flight software error mean fractional impact probability for the Cassini primary trajectory is nil, and for the backup it is nil for the E1 encounter and 1.60×10^{-9} for the E2 encounter.

7) Anomalous Sun Search

If attitude knowledge is lost and the Sun is not seen by the Sun sensor, then a spiral-search of the whole sky is started, which is terminated when the Sun is reaquired. The anomalous Sun search error mean fractional impact probability for the Cassini primary trajectory is 1.35×10^{-11}, and for the backup trajectory is nil for the E1 encounter and nil for the E2 encounter.

8) Spacecraft System Internal Failure

The paragraphs above emphasize Type II failure analysis (i.e., one causing a spacecraft ΔV). If a failure occurs but no change is made to the trajectory - a Type I failure - then the only added danger is due to the possibility that the failure makes it impossible to do a recovery maneuver. This amounts to an end to the mission. With careful design, including redundancy, the probability of this happening is very low. Ground Rules 1 and 2 (discussed in Subsection 5.4.1) are designed to keep the fractional impact probability low for this failure type.

The probability of failure was estimated in Subsection 4.3.8 and the result is shown in Figure 4-10. There is no associated ΔV and no probability of recovery. The spacecraft system internal failure mode mean fractional impact probability for the Cassini primary trajectory is 1.93×10^{-9} and for the backup trajectory is nil for the E1 encounter and 2.90×10^{-11} for the E2 encounter.

III. Ground Failures

Since overall control of the spacecraft is done from the ground, failures can occur as a result of errors induced by the controlling process. These errors can occur as a result of mission planning, operations, and commanding (generation, transmission, and reception).

1) Erroneous Ground Command

There is a Cassini command for main engine burn and another for RCS burn. Each contains a desired $|\Delta V|$ plus maximum and minimum burn times. There is also a default burn attitude of the last inertial target for the main engine, and the last commanded attitude for the RCS system. Either of these commands could be sent as part of a planned uplink sequence or as part of a series of uplinked real time commands. The spacecraft can recover

from this failure. The erroneous ground command mean fractional impact probability for the Cassini primary is 1.76×10^{-10}, and for the backup trajectory it is 1.92×10^{-10} for the E1 encounter and 3.04×10^{-10} for the E2 encounter.

2) Navigation Design Error

This failure mode assumes that an erroneous value for the maneuver was computed as a result of the navigation maneuver design process, and that the error is not found and corrected during the maneuver review process. Estimates were made in Subsection 4.4.2 of the mean value and upper limit probability for each of these events happening, assuming that a large error is easier to detect than a small one, and that an error is equally likely in roll, yaw, or $|\Delta V|$. Log-normal distributions were fitted to each mean value/upper limit set and a Monte Carlo simulation run to estimate statistics on the product. The spacecraft can recover from this error.

The navigation design error mean fractional impact probability for the Cassini primary trajectory is 6.94×10^{-10}, and for the backup trajectory it is 4.11×10^{-10} for the E1 encounter and 2.40×10^{-10} for the E2 encounter.

5.8 NUMERICAL RESULTS

A final summary of the short-term mean impact probabilities is given in Table 5-6. In many cases the impact probability computations lead to very small values, which over represent the accuracy of the analysis. Rather than listing these small values, they are denoted by "Nil" (whenever the calculated value is $<10^{-12}$).

The total mean probability of short-term Earth impact is 0.20×10^{-6} for the primary trajectory and 0.61×10^{-6} for the backup trajectory (0.20×10^{-6} for the E1 swingby and 0.41×10^{-6} for the E2 swingby). These probabilities are very much dominated by the contribution due to the micrometeoroid failure type.

Variation in the models permits collection of other statistics in addition to the mean values. Figure 5-8 shows the complementary cumulative probability curve for the probability of impact on the primary trajectory, and Figure 5-9 shows the corresponding frequency distribution. Figures 5-10 and 5-11 show the same information for the backup trajectory.

One other numerical study performed was to calculate the distribution of entry angles, assuming that an Earth reentry does occur. Entry angles less than 7° were assumed to lead to skipping back out of the atmosphere and were not included in the results. Figures 5-12, 5-14, and 5-16 give the frequency distribution of entry angle for the primary trajectory Earth swingby and the backup trajectory El and E2 swingbys, respectively. Figures 5-13, 5-15, and 5-17 show the corresponding cumulative probability

distributions. The VEEGA E1 swingby was found to have a nearly uniform distribution of impacts per unit area on the Earth disk. For this case, Figure 5-14 shows a falloff of probability near 90' because the area in the middle annulus is small. It also shows a falloff near 7° because the transformation from entry angle to equivalent radius gives a very narrow annulus. The frequency distributions for VVEJGA and for VEEGA E2 tend to be largest near the low entry angles, because the impacts are concentrated toward the point below the final Earth swingby aimpoint.

The nominal velocity of reentry was computed at the reference altitude of 122 km (76 mi), and is 19.25 km/s (11.96 mi/s) for the primary trajectory, and 16.48 km/s (10.24 mi/s) for the E1 encounter and 17.24 km/s (10.71 mi/s) for the E2 encounter on the backup trajectory. Some variation in these nominal values can occur if the failure mode includes a ΔV and/or if the failure occurs early in the trajectory segment.

Finally, the results of the study of latitude distribution given impact are shown in Figures 5-18, 5-19, and 5-20. As expected, the distribution spread is smallest for the VEEGA E2 swingby with its low altitude swingby and maximum biasing of the trajectory. The VEEGA E1 swingby has the greatest spread since it is a relatively high swingby with less trajectory biasing. The primary VVEJGA swingby falls in between since it is a low swingby with less than maximum trajectory biasing. Each distribution is centered over the latitude underneath the final swingby aimpoint.

All longitudes should be considered equally likely for these studies, since the Earth swingby date varies as a function of the launch date. Over the primary VVEJGA launch period the nominal Earth swingby time changes by 1.4 days. Over the backup VEEGA launch period the nominal Earth swingby time changes by 1.3 days. Thus any longitude could become the most likely one. Even after launch, a micrometeoroid-caused failure could result in a substantial change in the swingby time. As an upper bound, a bipropellant tank failure right after the Venus swingby on the backup VEEGA trajectory could cause up to a one day change in the E1 swingby time.

5.9 SUMMARY

A strategy has been developed for satisfying the navigation Earth swingby reliability requirement. Three Earth swingbys were analyzed, representing the primary VVEJGA trajectory and the backup VEEGA trajectory (E1 and E2 swingbys) from the set of current trajectory candidates. Launch dates were chosen to provide minimum altitude Earth swingbys, guaranteeing a result valid over the launch period.

Subsection 5.7 computed fractional Earth impact probabilities resulting from the spacecraft failure modes specified in Section 4 by using the maneuver strategy specified in Subsection 5.5. The sum of the individual contributions yields the total probability of Earth impact from injection to Earth

swingby. Table 5-6 presents the summation for both the Cassini primary and Cassini backup Earth swingbys. Please note that the very small probabilities shown in Table 5-6 are not just the failure mode probabilities. They are rather the final result of multiplying failure mode probabilities by Earth impact probabilities given failure mode occurrences and then multiplying by probabilities of non-recovery in accordance with Equation 5-1.

These summaries show that the short-term impact probability has been held to a fraction of the total Earth impact probability requirement. The mean values of 0.20×10^{-6} total impact probability for VVEJGA and 0.61×10^{-6} total impact probability for VEEGA are both within the total impact probability requirement of 1.0×10^{-6}, and will be added to the long-term impact probabilities computed in the next section.

Table 5-6 Short-Term Mean Earth Impact Probabilities

Section	Failure Mode	Primary (VVEJGA)	Backup (VEEGA)	
			Earth1	Earth2
I Environmental Failures				
1) Micrometeoroid (The only significant environment failure mode.)				
A)	Bipropellant Tank	1.01×10^{-7}	1.37×10^{-7}	2.79×10^{-7}
B)	Hydrazine Tank	7.54×10^{-8}	5.40×10^{-8}	9.40×10^{-8}
C)	Helium Tank	1.82×10^{-8}	1.29×10^{-8}	2.87×10^{-8}
D)	Engineering Bus	2.21×10^{-10}	Nil	1.03×10^{-12}
II Major Spacecraft Failures				
1) Stuck-Open Thruster Valve				
A) Z Thruster				
1)	Mechanical Failure	1.37×10^{-12}	Nil	Nil
2)	Electrical Failure	3.23×10^{-12}	Nil	Nil
B) X Thruster				
1)	Mechanical Failure	2.33×10^{-10}	Nil	Nil
2)	Electrical Failure	4.86×10^{-11}	Nil	Nil
2) Stuck-Open Main Engine Valve				
A) Mechanical Failure				
1)	Oxidizer Valve	Nil	Nil	Nil
2)	Fuel Valve	Nil	Nil	Nil
B) Electrical Failure		Nil	Nil	Nil
3)	Accelerometer Failure	2.45×10^{-10}	Nil	7.17×10^{-9}
4)	Main Engine Gimbal Actuator Failure	2.07×10^{-12}	Nil	2.66×10^{-12}
5)	AACS Flight Software Error	3.00×10^{-12}	Nil	Nil
6)	CDS Flight Software Error	Nil	Nil	1.60×10^{-9}
7)	Anomalous Sun Search	1.35×10^{-11}	Nil	Nil
8)	Spacecraft System Internal Failure	1.93×10^{-9}	Nil	2.90×10^{-11}
III Ground -Induced Errors				
1)	Erroneous Ground* Command	1.76×10^{-10}	1.92×10^{-10}	3.04×10^{-10}
2)	Navigation Design** Error	6.94×10^{-10}	4.11×10^{-10}	2.40×10^{-10}
	TOTAL:	1.98×10^{-7}	2.04×10^{-7}	4.11×10^{-7}

* Computed as a bound by setting $P_{I/F} = 1.0$

** Computed as a bound by setting ΔV toward the Earth.

Notes: Nil indicates mean fractional Earth impact probability $<10^{-12}$;
Three-digit precision is retained to facilitate adding.

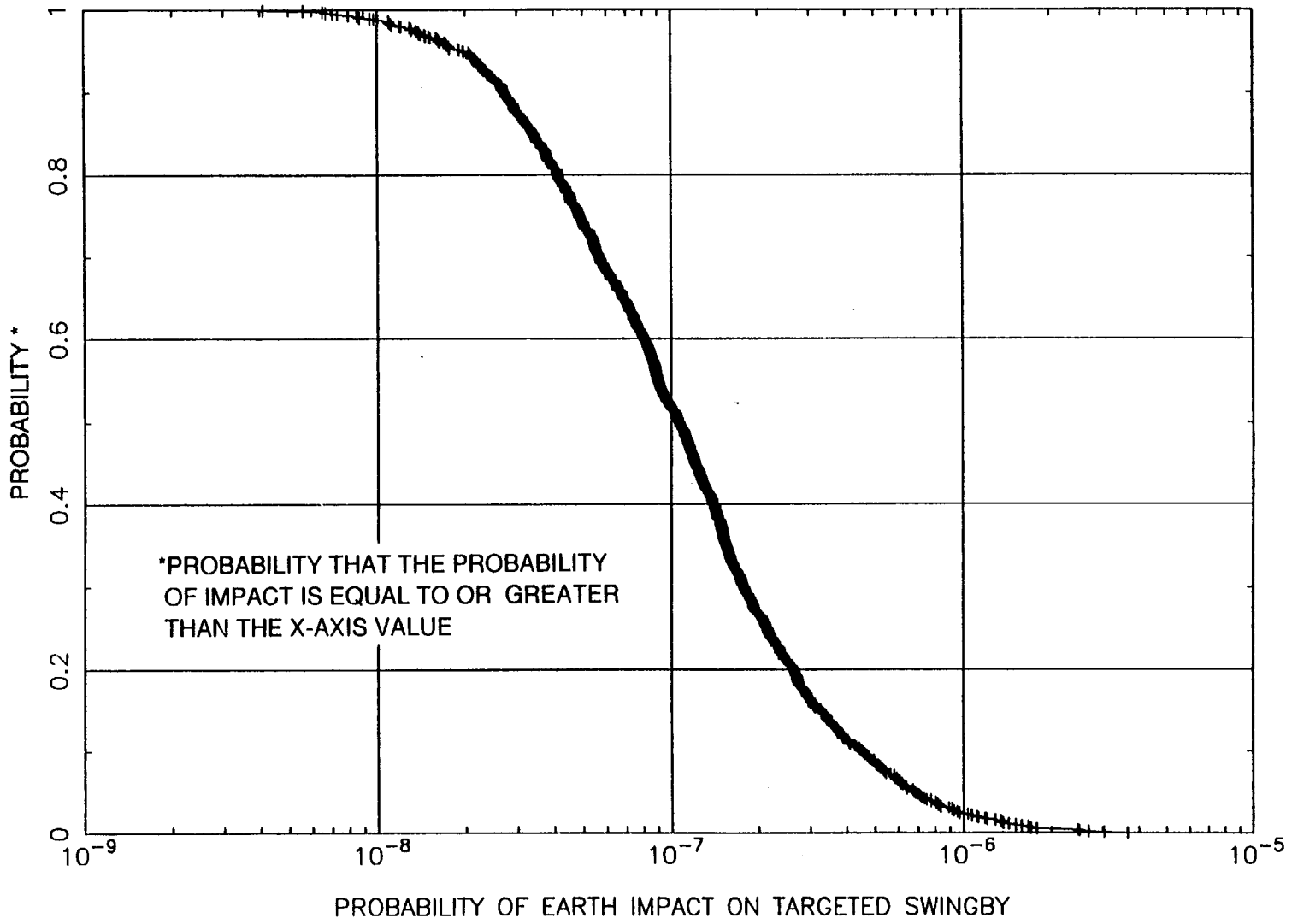

Figure 5-8 Primary Mission: Complementary Cumulative Probability

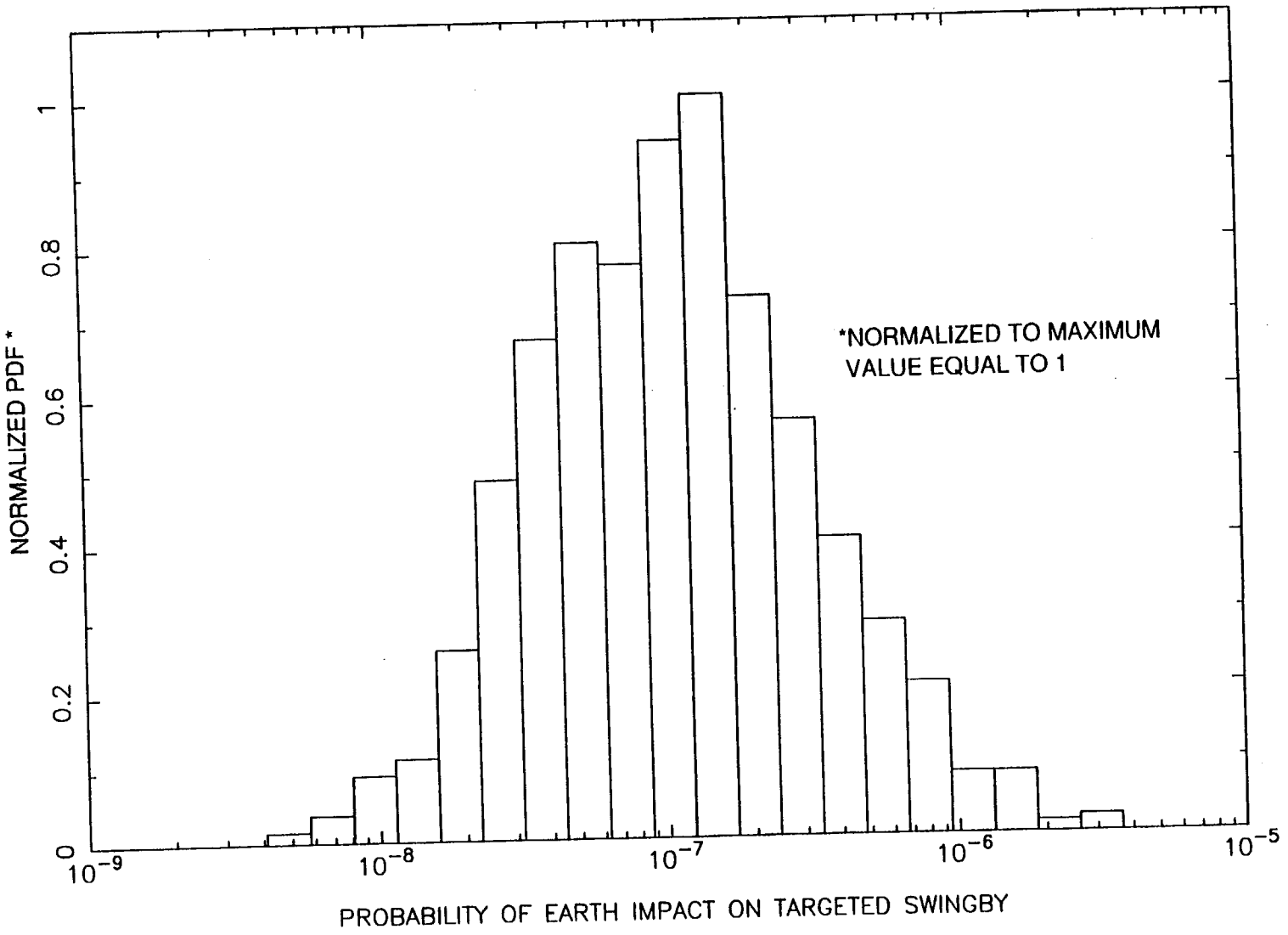

Figure 5-9 Primary Mission: Probability Density Function

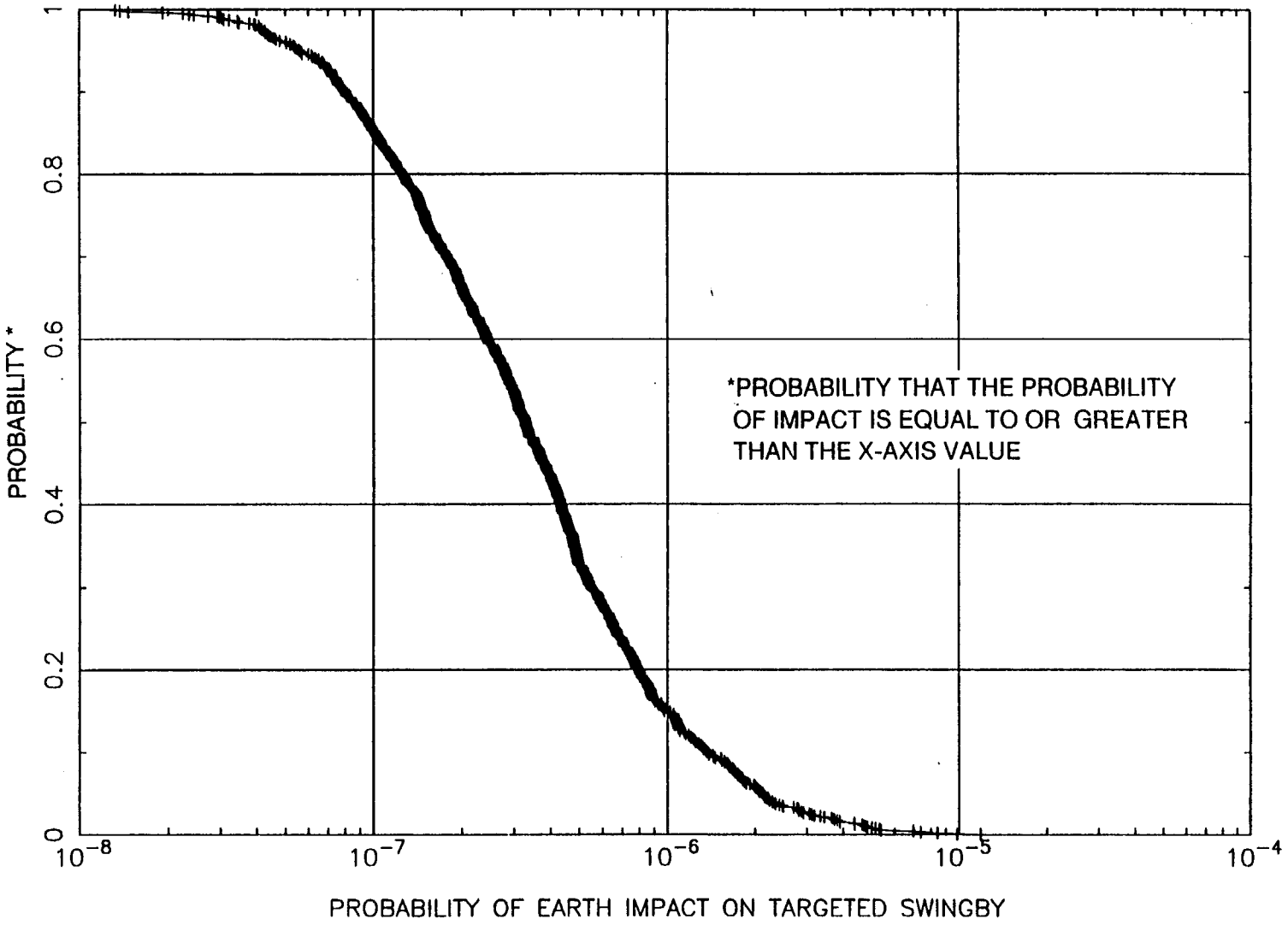

Figure 5-10 Backup Mission: Complementary Cumulative Probability

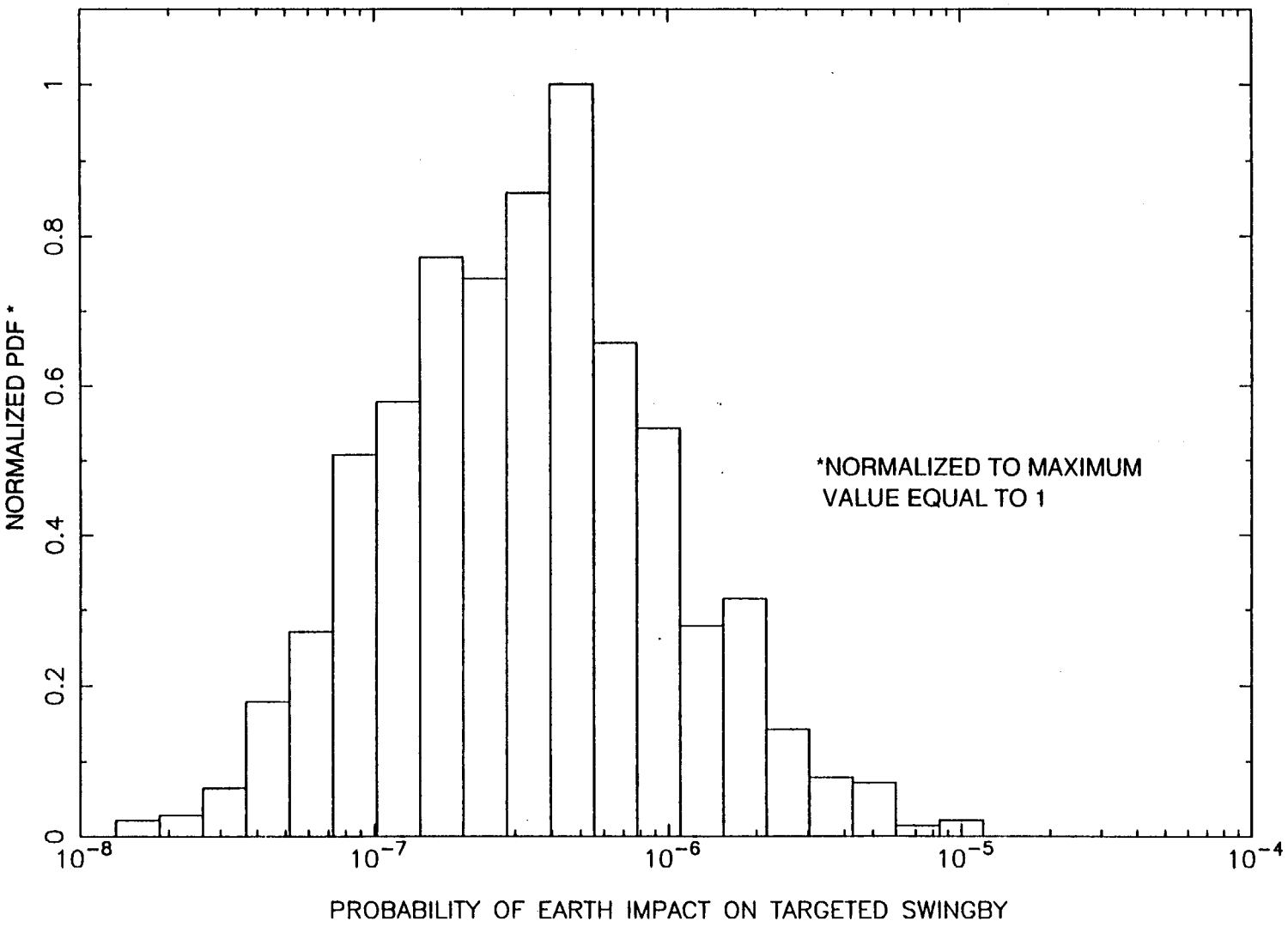

Figure 5-11 Backup Mission: Probability Density Function

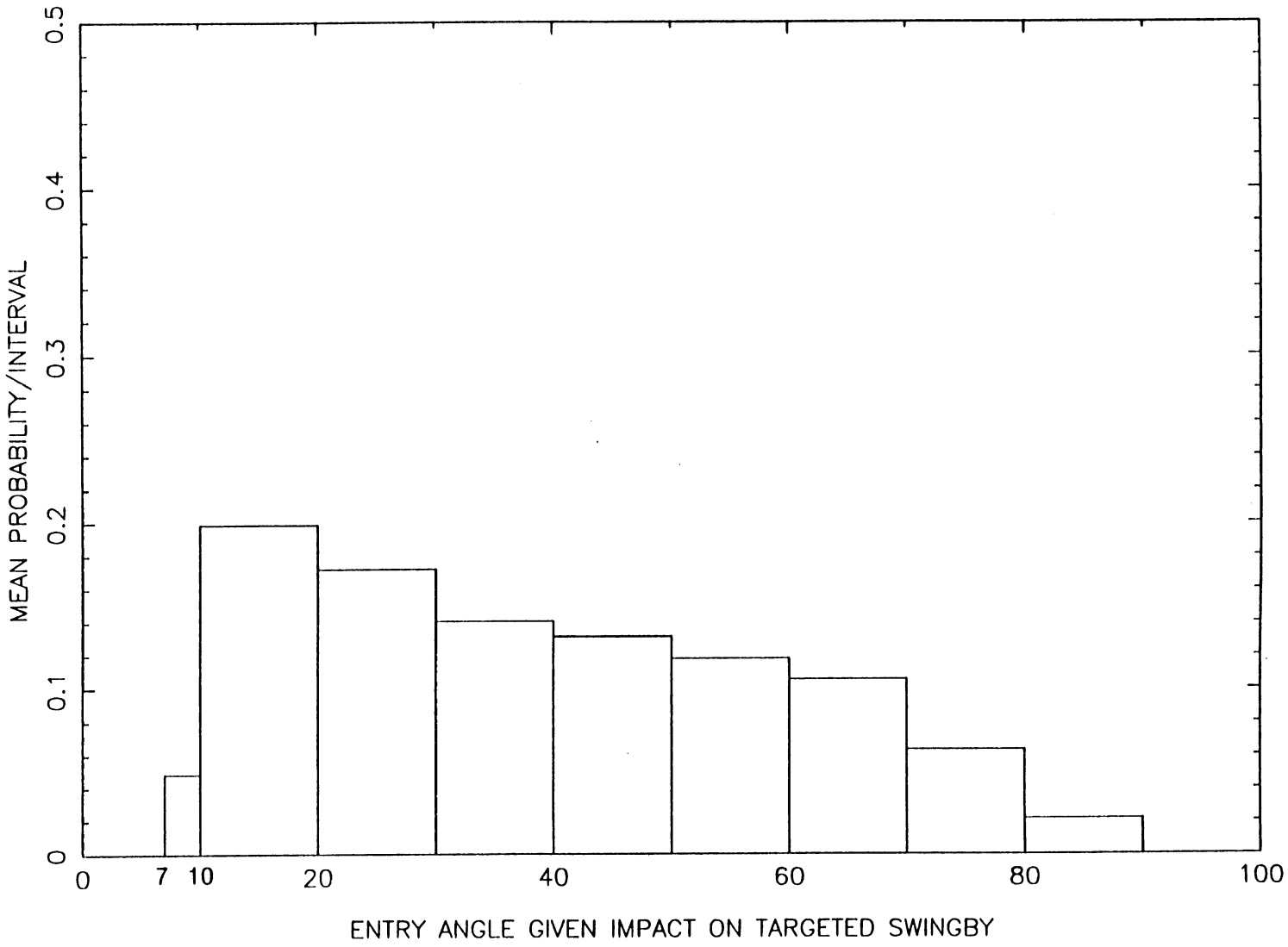

Figure 5-12 Primary: Probability vs Entry Angle

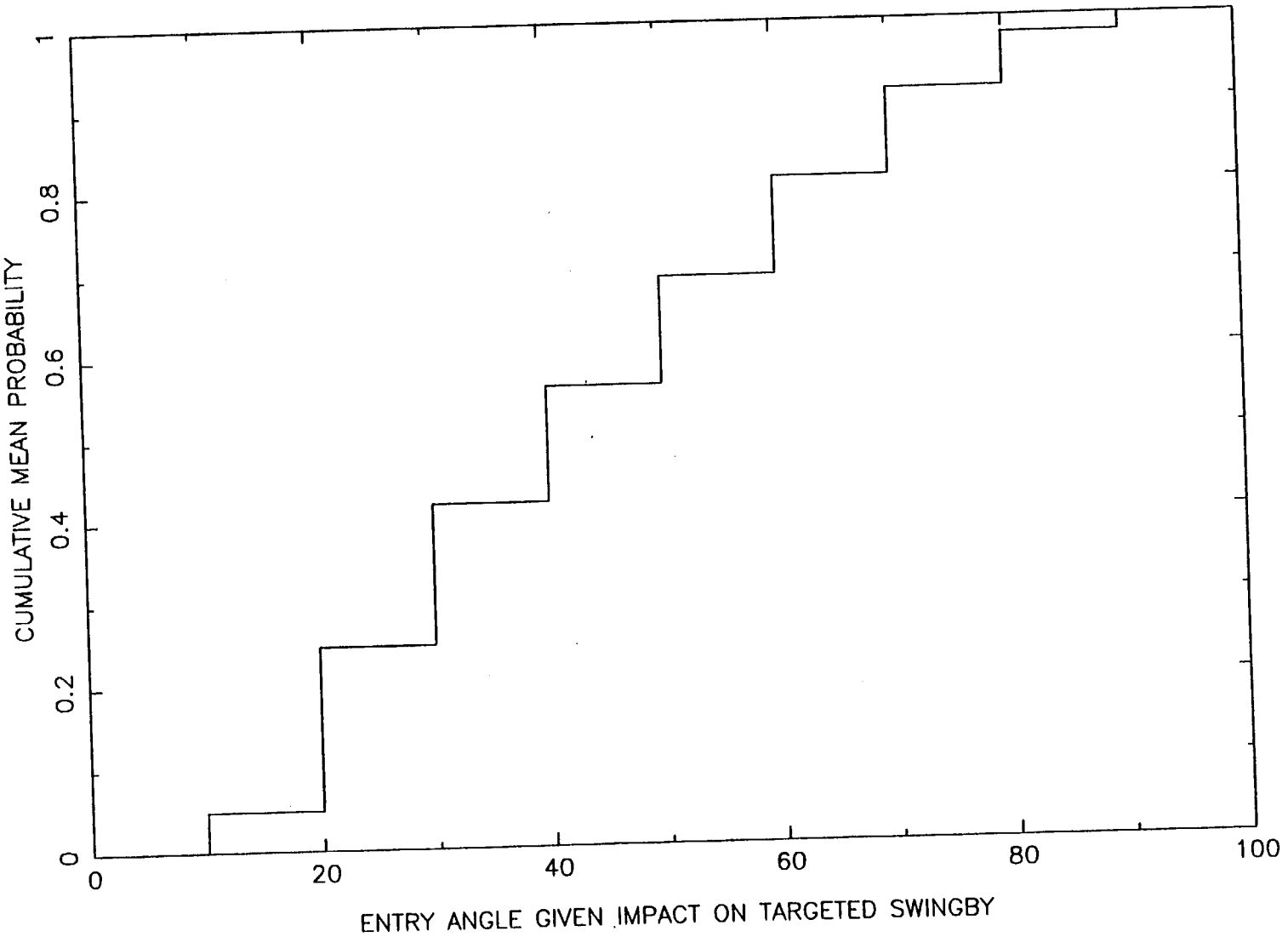

Figure 5-13 Primary: Entry Angle Cumulative Probability

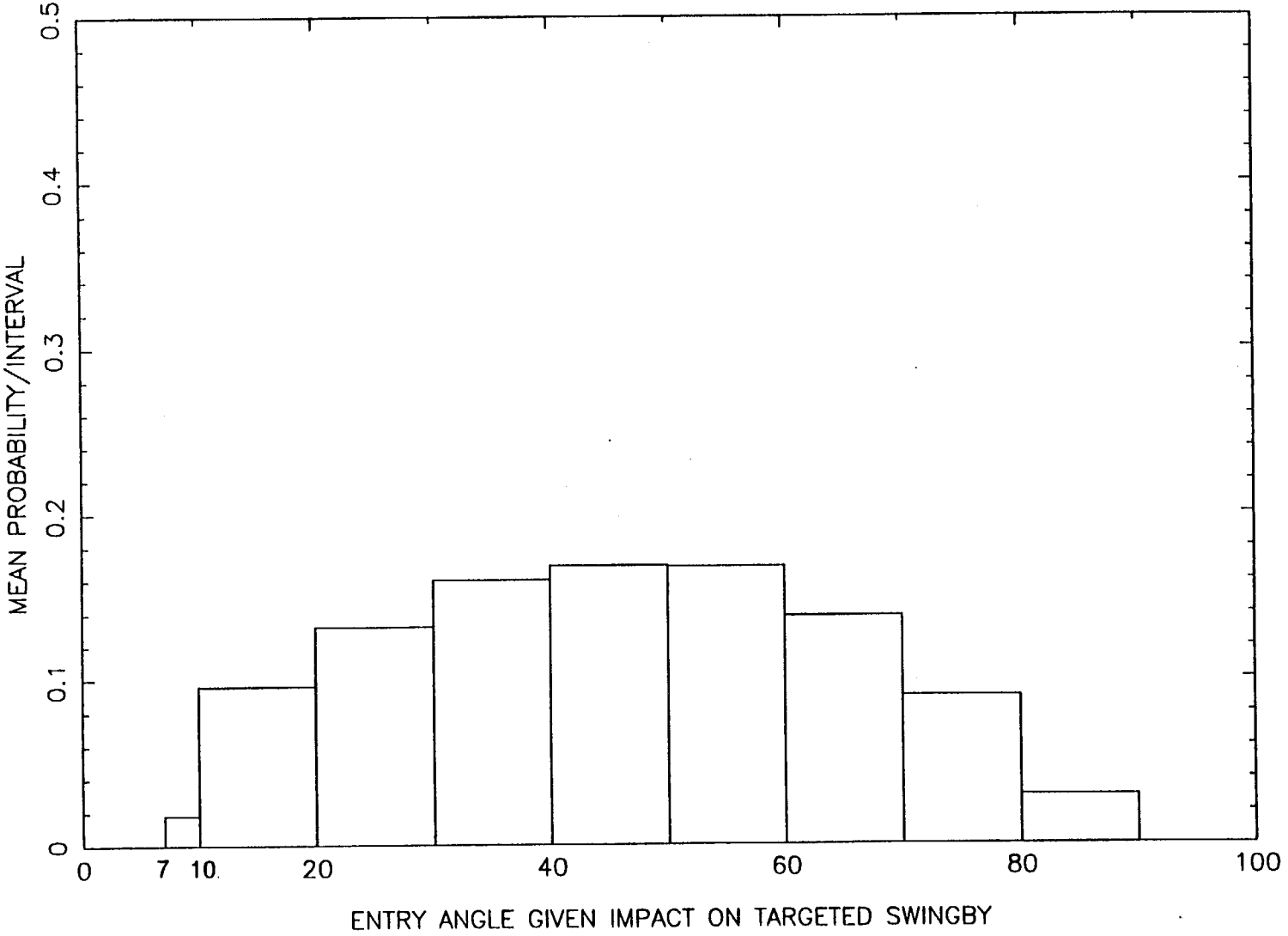

Figure 5-14 Backup--E1: Probability vs Entry Angle

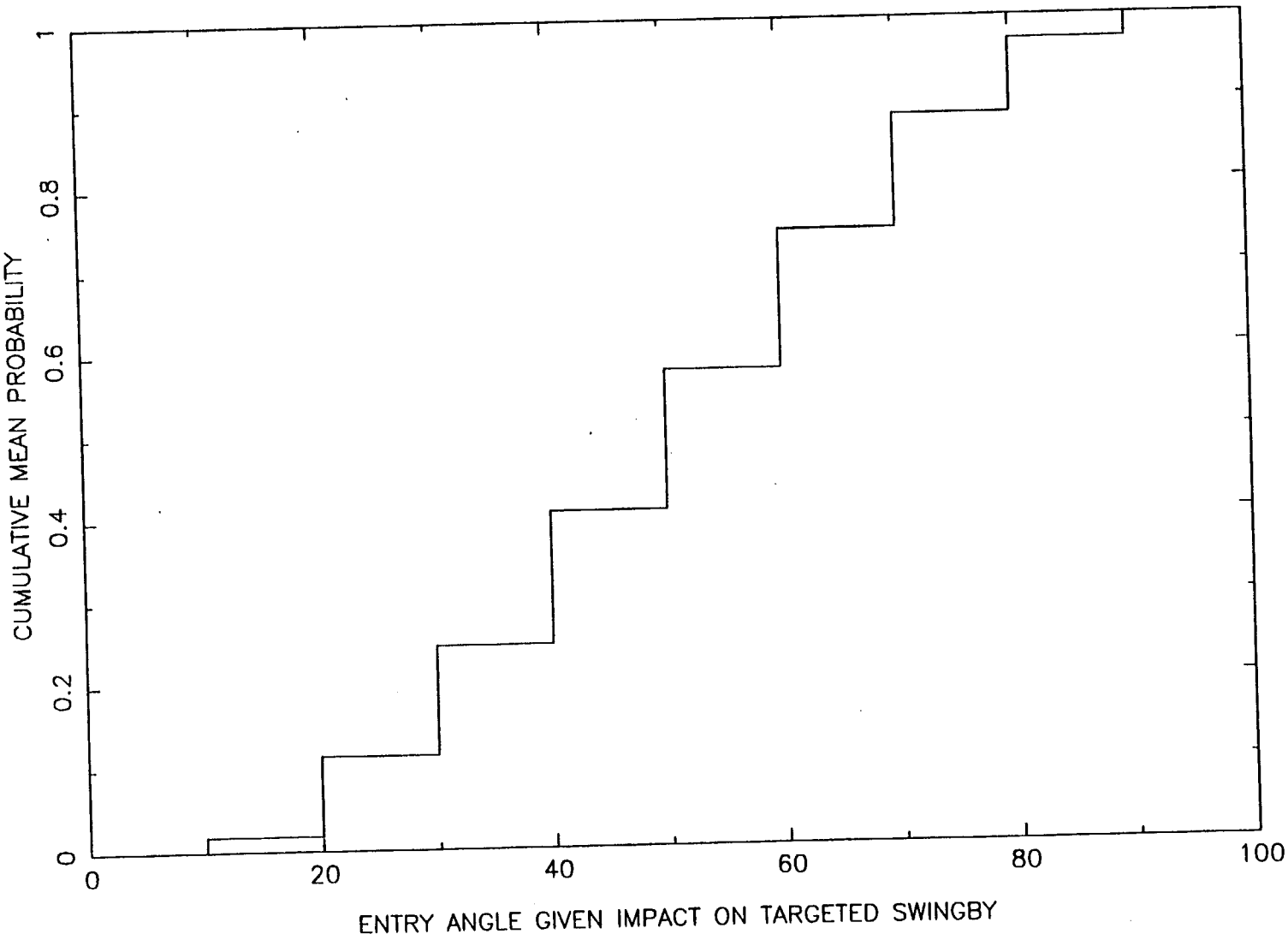

Figure 5-15 Backup--E1: Entry Angle Cumulative Probability

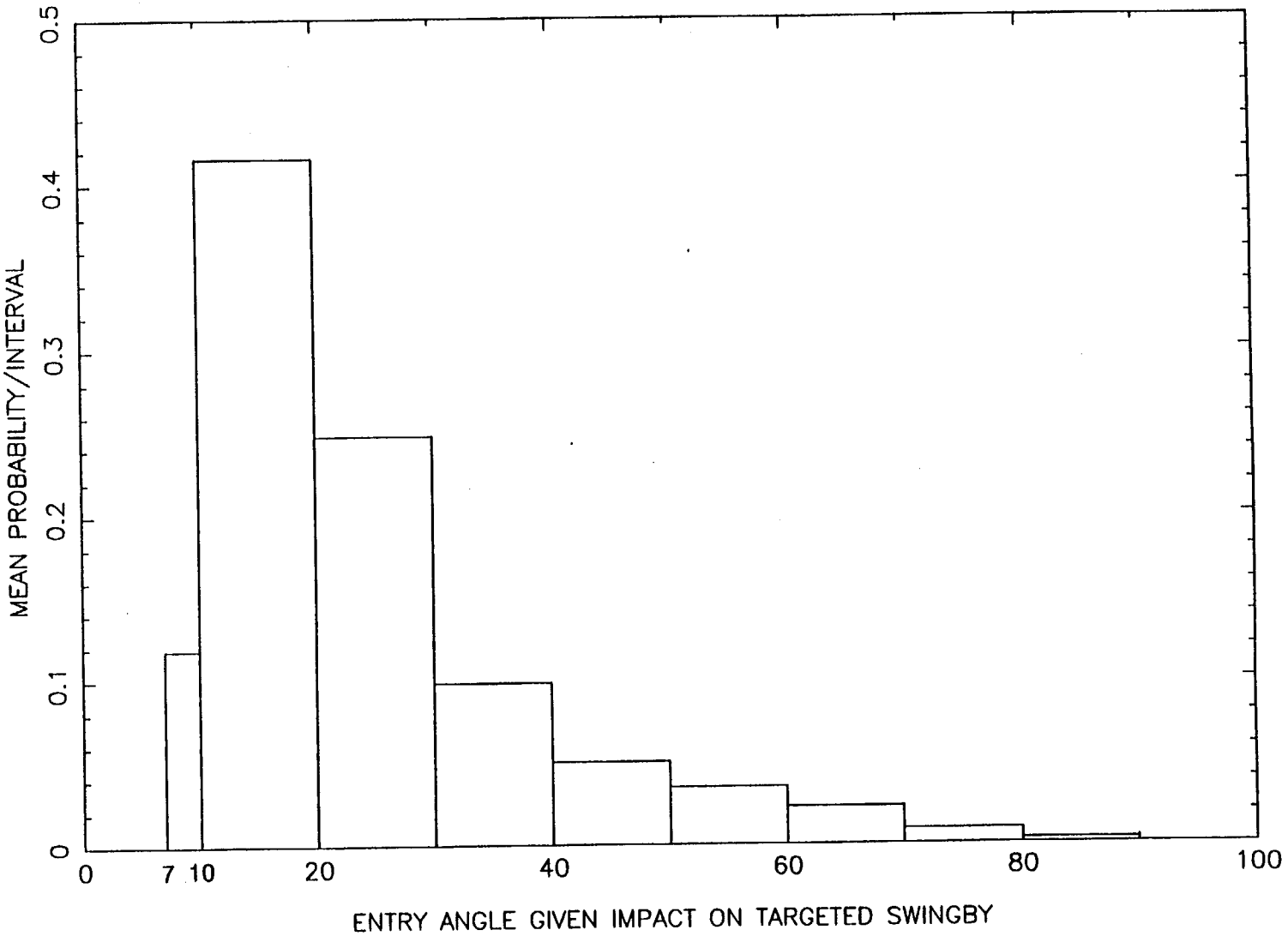

Figure 5-16 Backup--E2: Probability vs Entry Angle

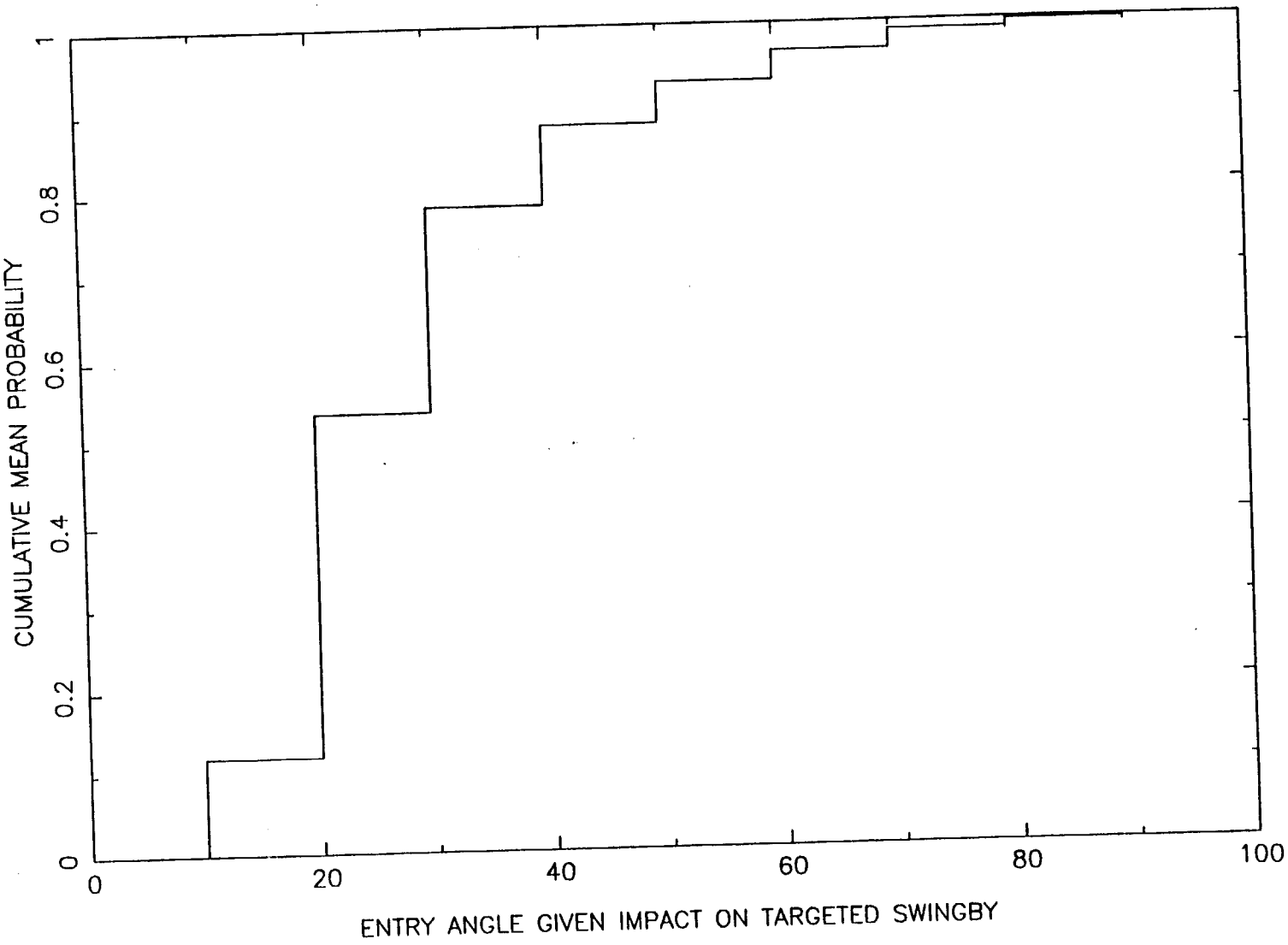

Figure 5-17 Backup--E2: Entry Angle Cumulative Probability

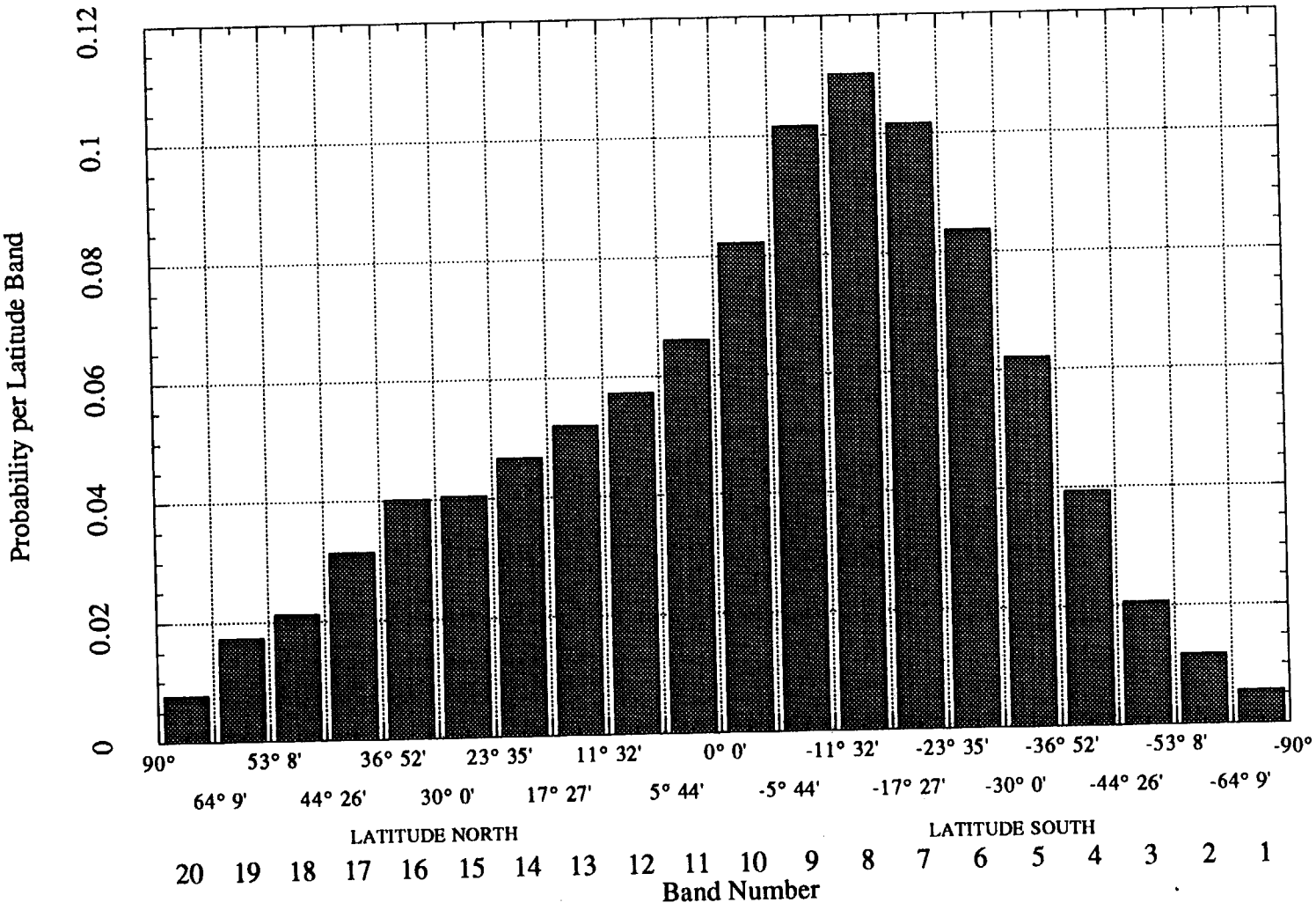

Figure 5-18 Primary: Entry Latitude Probability Distribution

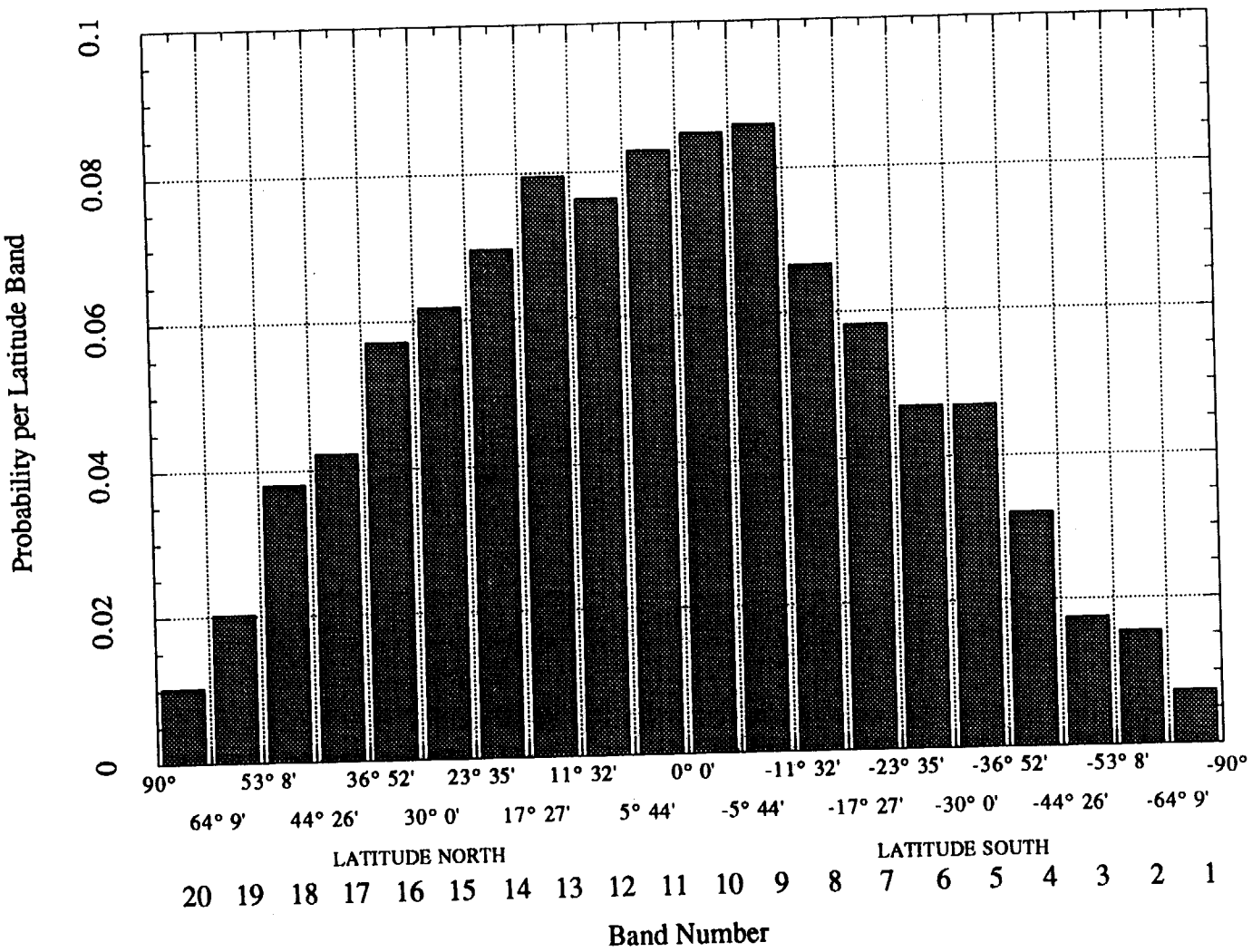

Figure 5-19 Backup--E1: Entry Latitude Probability Distribution

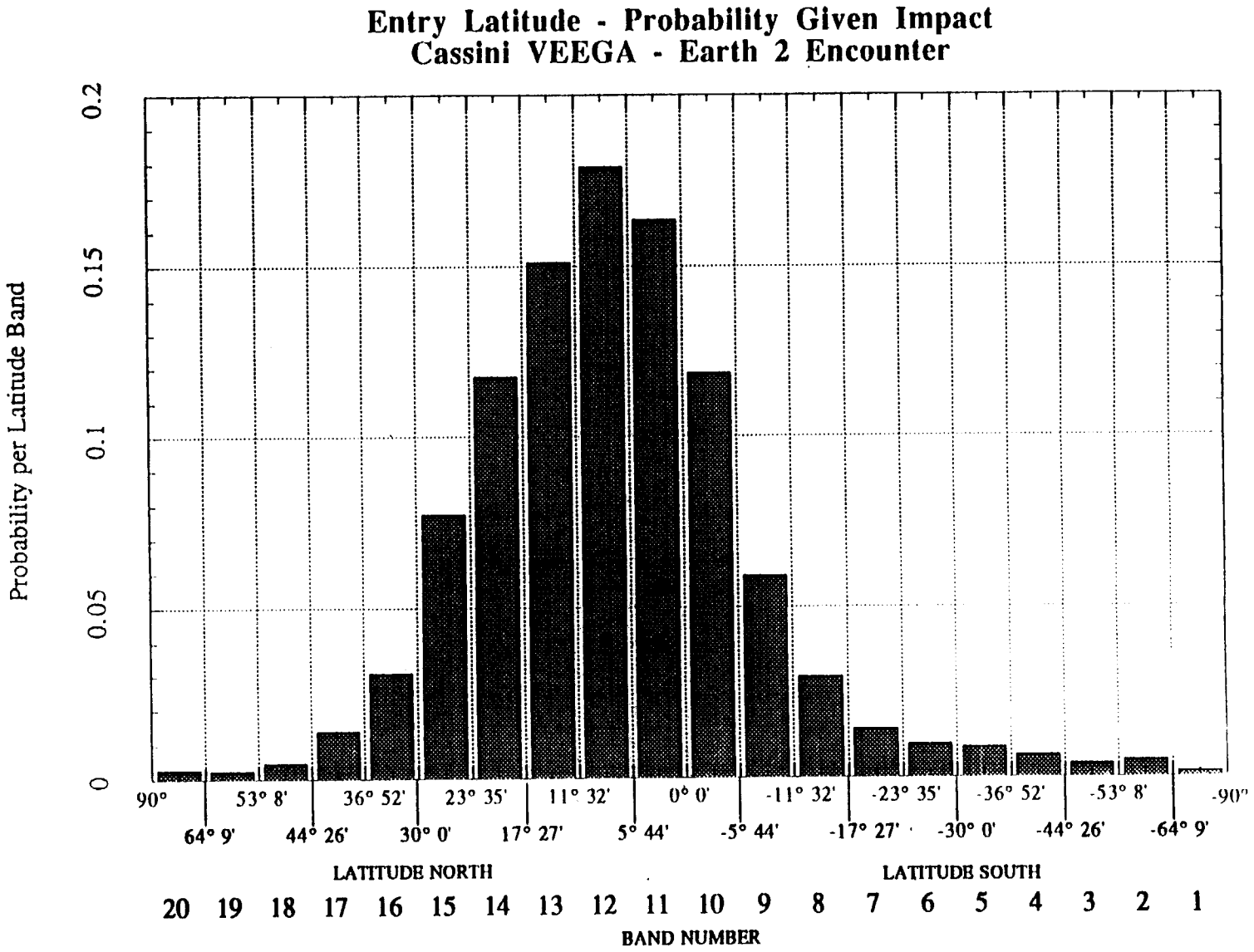

Figure 5-20 Backup--E2: Entry Latitude Probability Distribution

SECTION 6

LONG-TERM EARTH IMPACT PROBABILITY

6.1 INTRODUCTION

During the Cassini mission, there exists the possibility that the spacecraft might become unmaneuverable after successful insertion into its interplanetary cruise trajectory. The short-term impact analysis presented in Section 5 establishes that the probability of Earth impact during a targeted Earth swingby is extremely small. However, if the spacecraft becomes unmaneuverable before SOI and does not impact the Earth during a targeted swingby, there is still a remote possibility that long-term perturbations to the orbit could cause the spacecraft to eventually reencounter the Earth. The long-term analysis described in this section computes the probability of Earth impact by a non-targeted swingby from the time of spacecraft failure to 100 years beyond the planned SOI date.

To compute the probability of Earth impact, a knowledge of the spacecraft failure probabilities and associated ΔVs, the uncertainties in the navigation process, and the long-term motion of the spacecraft is required. Use was made of a large body of work refined over the past forty years to estimate the probability of impact by Earth-crossing asteroids. Existing theory which was applicable to lifetime analysis of asteroids and comets was modified to apply to this spacecraft impact analysis.

The primary purpose of this section is to document the computation of a PDF of the long-term component of the Earth impact probability for the primary VVEJGA and backup VEEGA Cassini missions. The short and long-term PDFs are then combined into a single PDF, as described in Section 7. Additional information is also presented on the long-term entry angle, entry velocity, and entry latitude characteristics. The change to Earth impact probability when considering a 1000-year time period, rather than a 100-year period, is discussed to illustrate very long-term behavior.

6.2 METHOD

The following method is used to compute the long-term Earth impact probability for both the primary and backup trajectories. An important defining equation for Earth impact probability, which was presented in Subsection 2.1, is as follows:

$$P_I = \Sigma_{FAIL}\Sigma_{TIME}\, P_F(i)\, P_{I/F}(i)\, P_{NR}(i) \qquad (6\text{-}1)$$

where

P_I	=	probability of Earth impact
Σ_{FAIL}	=	summation over all i failure modes
Σ_{TIME}	=	summation over long-term time period (~100 years)
$P_F(i)$	=	probability of failure for ith failure mode
$P_{I/F}(i)$	=	probability of a resultant Earth impact given an ith failure mode
$P_{NR}(i)$	=	probability of no recovery for the ith failure mode given the time to impact

Only those failures which would cause the spacecraft to become unmaneuverable with no chance of recovery are appropriate for the long-term analysis. If the spacecraft could recover, it would permanently enter Saturn orbit at SOI at the end of interplanetary cruise precluding any chance of Earth impact. The P_{NR} term is therefore always equal to 1 for the long-term analysis.

A logic diagram that illustrates which conditions must be satisfied in order for a long-term Earth impact to occur is discussed in Subsection 2.3 and shown in Figure 2-3. Referring to the logic diagram, in order for an Earth impact to occur, the spacecraft must fail during cruise ($P_F(i)$ term) and the spacecraft's orbital geometry must be such that an Earth impact ($P_{I/F}(i)$ term) occurs in the next 100 years. The significant failure modes for the long-term analysis are spacecraft system internal failure and micro-meteoroid impact as shown in the logic diagram. Micrometeoroid impact can result in a ΔV if a propellant tank is ruptured, although this occurs for only a small subset of the micrometeoroid failure cases.

Since a single spacecraft trajectory propagation would not be representative of the range of possible trajectories that could result given a failure any time during interplanetary cruise, a Monte Carlo analysis was performed using thousands of trajectories considering a wide range of failure times and any associated ΔVs. The primary and backup Cassini trajectories were each evaluated using -5000 failure cases. Most of the failures are due to spacecraft system internal failure. About one tenth are from micrometeoroid hits and of these about one-fifth are propellant tank hits which result in AV. Associated with each case is an initial spacecraft orbital state, which is perturbed by navigation uncertainty, and any ΔVs associated

with the failure. Each state is then propagated for 100 years in the analysis.

For the long-term analysis, probability distributions for the $P_F(i)$ and $P_{I/F}(i)$ terms, which are representative of the entire interplanetary cruise, are computed separately and are then combined to yield the Earth impact, P_I, probability distribution. Spacecraft failure probabilities documented in Section 4 were used to compute a probability distribution for the $P_F(i)$ term representative of the entire interplanetary cruise for each mission. The failure probability distribution was obtained by randomly sampling the cumulative failure probability distributions as many times as required until ~5000 failure times during cruise were obtained (see Subsection 6.2.1). only failures during cruise need to be considered since at the end of nominal cruise, the spacecraft enters Saturn orbit.

If the spacecraft becomes unmaneuverable, the orbital geometry of the spacecraft must be such that an Earth impact occurs in the next 100 years. To determine the probability of Earth impact given a failure, $P_{I/F}(i)$, use was made of existing theory used to estimate the probability of impact by Earth-crossing asteroids. In this method, the number of passages of the spacecraft through the torus swept out by the Earth as it orbits the Sun is used to compute the probability of Earth impact. In order for an impact to occur, the spacecraft must cross through the Earth torus, and at the time of the crossing, the Earth must be at a position within the torus to cause impact. This intersection geometry is illustrated in Figure 6-1. The term $P_{I/F}(i)$ is computed as the product of two terms as follows:

$$P_{I/F}(i) = \Sigma_{TIME} \left(N_{CRX} / N_{CASE}\right) P_{I/CRX} \qquad (6\text{-}2)$$

where

$P_{I/F}(i)$ = probability of a resultant Earth impact given an occurrence of the ith failure mode

Σ_{TIME} = summation over long-term time period (~100 years)

N_{CRX} = number of Earth torus crossings encountered in all Monte Carlo cases propagated 100 years

N_{CASE} = number of Monte Carlo cases (initial trajectory states at spacecraft failure times) propagated 100 years

$P_{I/CRX}$ = probability of Earth impact given that spacecraft has passed through torus

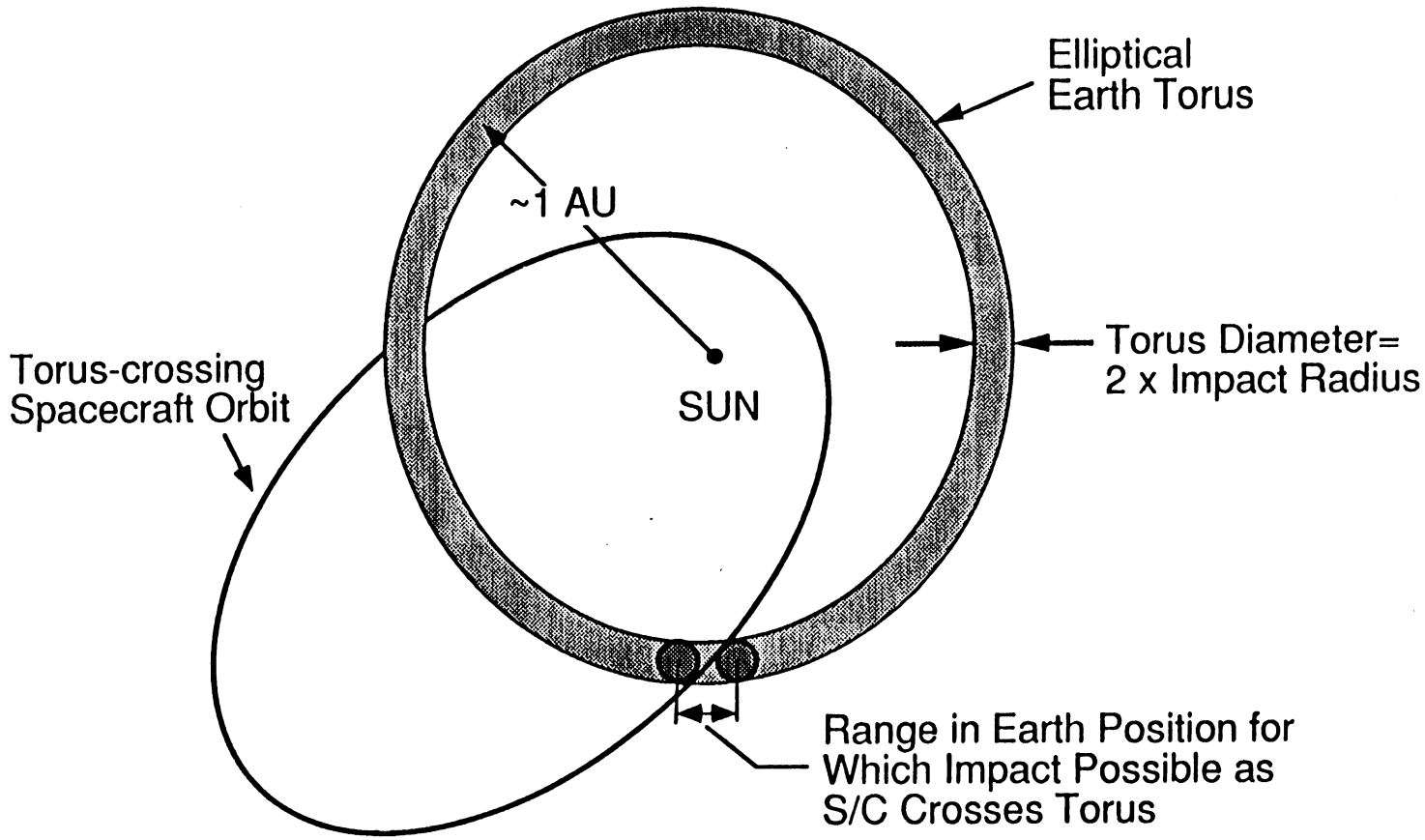

Figure 6-1 Orbit Geometry And Phasing Required For Earth Impact

The first term, N_{CRX}/N_{CASE}, in Equation 6-2 yields the expected number of torus crossings per Monte Carlo case. The second term, $P_{I/CRX}$, is the probability that the Earth occupies the same portion of the torus as the spacecraft at the time the spacecraft crosses the torus. Substitution of Equation 6-2 into Equation 6-1 yields Equation 6-3, which is used to compute the long-term Earth impact probability. Since $P_{NR} = 1$ for the long-term, this term is omitted from Equation 6-3.

$$P_I = \Sigma_{FAIL}\Sigma_{TIME}\, P_F(i) \quad (N_{CRX} / N_{CASE}) \quad P_{I/CRX} \tag{6-3}$$

The process for computing the required data for the NCASE Monte Carlo cases is illustrated in Figure 6-2. The process for computing the trajectory initial conditions depicted in the top half of Figure 6-2 has already been briefly discussed and is treated in more detail in Subsection 6.2.1. The process for computing best estimates of N_{CRX} and $P_{I/CRX}$ is described below.

The number of torus crossings for all cases were computed by propagating the initial conditions for each case using a high-precision numerical integration program, and counting each passage through the Earth torus. This procedure was used rather than the analytical model for long-term orbital motion used in most Earth-crossing asteroid analyses, since the assumptions inherent in the analytical expressions proved inadequate for the Cassini time frame and orbital characteristics. An uncertainty on the number of torus crossings per case was determined and a distribution for the N_{CRX}/N_{CASE} term was constructed assuming a normal (Gaussian) distribution.

Standard Earth-crossing asteroid theory was used to compute the $P_{I/CRX}$ term. The value of $P_{I/CRX}$ is slightly different for each torus crossing and thus an average value was used to compute a best estimate value representative of all torus crossings. An uncertainty in the value of $P_{I/CRX}$ was estimated and a distribution for this term constructed assuming a log-normal distribution.

The distributions for the N_{CRX}/N_{CASE} and $P_{I/CRX}$ terms were combined with the distributions for the $P_F(i)$ term to yield a PDF for the long-term Earth impact probability, P_I. The velocity vector of the spacecraft relative to the Earth was estimated at each torus crossing assuming that the Earth was in the position required for impact in order to estimate the likely range of entry velocities and entry latitudes for

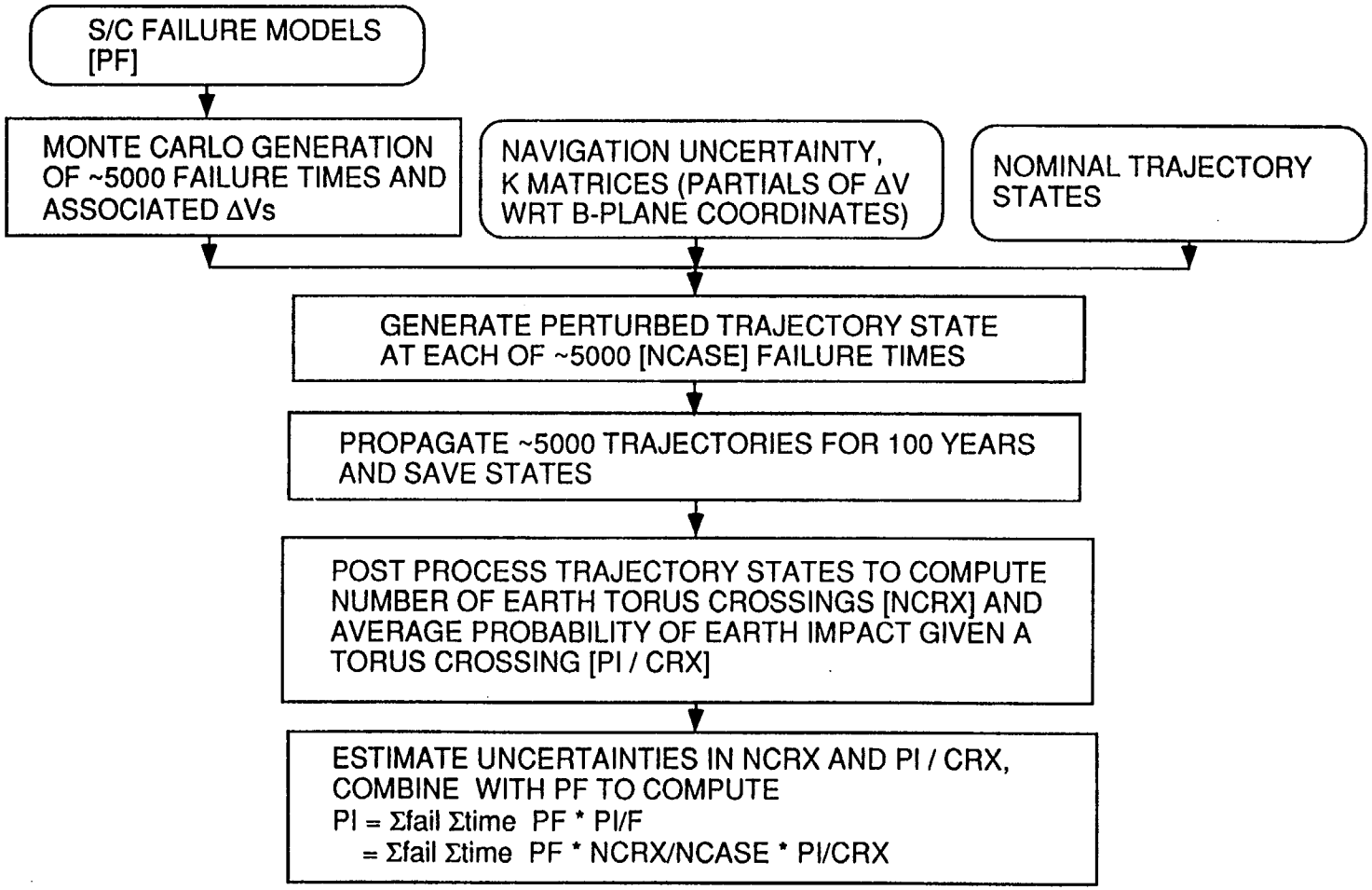

Figure 6-2 Process for Computing Long-Term Earth Impact Probability for Each Mission

the long term. The entry latitude distribution can be estimated given the likely range of magnitudes and declinations of the Earth-relative velocities. An entry angle distribution is computed assuming that the spacecraft aimpoint is equally likely to lie anywhere within the Earth impact circle. A subset (~20%) of the Monte Carlo cases were also propagated for 1000 years to study the very long-term probability of Earth impact. The same methodology as used for the 100-year propagation was used for these 1000-year cases.

Portions of the above methodology are described in greater detail in the following subsections.

6.2.1 Monte Carlo Case Formulation

If exact knowledge of the spacecraft state at failure were available and the ability to precisely predict the spacecraft trajectory 100 years into the future existed, to determine if the spacecraft were to impact the Earth, the trajectory would simply be propagated 100 years beyond the failure time and checked for Earth impact. However, exact knowledge of the spacecraft state is never available due to orbit determination uncertainty and maneuver execution errors. Also, if a ΔV is associated with the spacecraft failure, exact knowledge of the ΔV magnitude and direction is not available, further corrupting knowledge of the initial state. In addition, the ability to accurately model the physical universe for such long time spans does not exist, since the long-term trajectory is extremely sensitive to small differences in the initial spacecraft state and the force modeling used to propagate the trajectory does not exactly model the actual perturbations experienced by the spacecraft. The time at which a failure could occur is specified in a probabilistic sense and thus a failure could occur anytime during cruise although failures are more likely at certain times than others.

Therefore, a small number of trajectories is not representative of the range of possible spacecraft trajectories which could result given a failure anytime during the interplanetary cruise. The solution adopted in this analysis is to perform a Monte Carlo analysis of thousands of trajectories. The primary and backup Cassini trajectories were each evaluated using ~5000 failure cases. The failure probability distribution was obtained by randomly sampling the cumulative failure probability distributions as many times as required until ~5000 failure times during cruise were obtained. The ~5000 cases resulted in sufficient numbers of torus crossings and sampling of the navigation dispersion ellipses to provide confidence in the results. The influence of the number of cases run is discussed further

in Subsection 6.3.1. Associated with each Monte Carlo case is an initial spacecraft orbital state which has been perturbed by navigation uncertainty and any ΔVs associated with the failure.

Given a failure time and any associated ΔV, the initial conditions for the spacecraft state were obtained in the following manner. Navigation uncertainty encompassing both orbit determination and maneuver execution errors is typically expressed in terms of la dispersion ellipses centered at the planetary swingby aimpoint. A different dispersion ellipse is supplied for times following each maneuver. The last aimpoint dispersion ellipse before the failure time was randomly sampled to yield a perturbed swingby state which was then used as the initial state for the trajectory propagation. Thus, the initial conditions for the Monte Carlo cases occur at planetary swingbys. The perturbed aimpoint coordinates could have been mapped backward in time to the failure epoch, but the resulting trajectories would be the same. Furthermore, examination of perturbed swingby states yields more intuitive information. For the small subset of failure times between a planetary swingby and the next maneuver, the next maneuver dispersion ellipse was sampled. This is required since the dispersion corresponding to the previous maneuver is changed by the planetary swingby. The number of failure times which fall into this category is small since maneuvers are intentionally placed shortly after planetary swingbys.

For failure times between a planetary swingby and a major deep space maneuver, the perturbed aimpoint coordinates were mapped back to the deep space maneuver epoch. The initial conditions for these failure times are specified at the deep space maneuver date. This was required since the aimpoint dispersion ellipses at the planetary swingby assume that the deep space maneuver has been executed, which will not be true if the spacecraft fails before the maneuver. The primary and backup missions each have a single deep space maneuver and thus only one portion of the trajectory requires this procedure.

Any probabilistic ΔV associated with the failure is mapped to the next planetary swingby epoch or the deep space maneuver epoch as appropriate, and then added to the initial spacecraft state already perturbed by navigation uncertainty. The ΔVs are mapped by a standard method using K-matrices which are partials of next planetary body aimpoint coordinates with respect to spacecraft state at a given epoch. K-matrices were generated every few days for both the primary and backup trajectories. The K-matrix closest to the failure time was used to map the ΔV to the required epoch.

For failures on a trajectory leg where the next targeted swingby was not Earth, impact with the targeted body sometimes occurred. Most of these impacts occurred at the first Venus encounter of each mission. These cases were identified but not propagated. Impact with targeted Earth encounters is avoided by the strategy described in Subsections 5.4 and 5.5.

6.2.2 Orbital Geometry Required For Impact

For a given spacecraft trajectory corresponding to a failure event, the required orbital geometry for an Earth impact is addressed in the right-hand portion of the long-term logic diagram (Figure 2-3). The most likely scenario is that if the spacecraft fails, it will never reencounter the Earth in 100 years. To determine the probability of Earth impact given a failure ($P_{I/F}(i)$ in Equation 6-3), use was made of theory used to estimate the probability of impact by Earth-crossing asteroids.

In order for any chance of Earth impact, the spacecraft must be present in the solar system. For nearly all failures during the second half of the interplanetary cruise, the spacecraft is ejected from the solar system by the strong Saturn gravity assist, precluding any possibility of Earth impact. If the spacecraft is present in the solar system, in order for an Earth impact to occur, the spacecraft must pass through the Earth torus. The spacecraft may be on an Earth torus-crossing orbit at the failure time or may eventually be put on one by orbital perturbations such as gravitational perturbations by the planets and solar radiation pressure. Distant non-targeted gravity assists are actually quite common for some trajectory legs. These conditions are shown in the lower right-hand portion of the logic diagram (Figure 2-3).

6.2.2.1 Application of Earth-Crossing Asteroid Theory. If the spacecraft crosses through the Earth torus, Earth-crossing asteroid theory is applied to compute the probability of impact. A fundamental paper was written in 1951 on the subject by Opik[1], who subsequently revised and extended his work[2,3]. Further research was done by Arnold[4,5] in the 1960's and more recently this topic has been addressed by Shoemaker, Wetherill, and others[6-10]. In this theory, the probability that the spacecraft is within the torus swept out by the Earth as it orbits the Sun is used to compute the probability of Earth impact. An advantage to this method is that passage of the spacecraft through the Earth's torus is a more likely event than an actual collision with the Earth and thus provides a statistically significant set of data. A prohibitive number of Monte Carlo cases would probably have

to be evaluated in order for a single Earth impact to result within 100 years. No Earth impacts were detected for any of the ~5000 trajectory propagations conducted for each of the missions investigated.

In Earth-crossing asteroid theory, the average probability that the spacecraft is within the Earth torus over extremely long time spans is computed using very approximate analytical expressions (equivalent to the N_{CRX}/N_{CASE} term in Equation 6-3). This probability is multiplied by the probability that the Earth is in the correct position in its orbit at the time the spacecraft crosses through the Earth torus ($P_{I/CRX}$) to compute the probability of Earth impact. This intersection geometry was discussed in Subsection 6.2 and is illustrated in Figure 6-1. The diameter of the Earth torus is twice the impact radius of the Earth, which is slightly larger than the Earth radius due to gravitational focusing. The Earth impact radius is a function of the velocity of the spacecraft relative to the Earth and the mass of the Earth.

Figure 6-1 shows that in order for an impact to occur, the spacecraft must cross through the Earth torus, and at the time of the crossing, the Earth must be at a position within the torus to cause impact. The probability that the spacecraft passes through the torus **is** computed differently than in the referenced Earth-crossing asteroid theories since the analytical expressions used to model the long-term orbital motion proved inadequate for the Cassini time frame and orbital characteristics. The analytic expressions used in these theories are only valid when considering time spans approaching millions of years for a restricted class of orbits and do not accurately depict what is likely to occur for Cassini trajectories in 100 years. In this analysis, the probability that the spacecraft passes through the Earth torus was computed by numerically integrating each of the Monte Carlo cases using a high-precision trajectory propagation program and then counting the number of times the spacecraft actually passed through the Earth torus during these propagations. The total number of torus crossings (N_{CRX}) divided by the total number of Monte Carlo cases (N_{CASE}) yields the likelihood that the spacecraft will be within the torus during the interplanetary cruise. The estimated uncertainty in this torus-crossing frequency is discussed in Subsection 6.3.1.

Numerical integration of the trajectory provides the most realistic model of long-term orbital motion. Forces modeled included the gravity of all the planets and solar radiation pressure. Trajectory states were archived at least every 6 months for each 100-year propagation and then post-processed to determine the number of spacecraft crossings through the Earth torus. Crossings were detected by a

numerical method that stepped through the spacecraft orbit when in the vicinity of the Earth torus, checking at each position whether the spacecraft was within the volume occupied by the torus. The impact radius assumed for each torus crossing was different and was based on the velocity of the spacecraft relative to the Earth assuming that the Earth was in an impact position for that crossing. An elliptical torus was used whose shape was identical to that of the actual orbit of the Earth at epoch January 1, 2000. The slight change in the Earth's orbit over 100 years does not significantly change the number of torus crossings detected, since a small shift in the torus position tends to add or subtract torus crossings with equal probability.

Earth-crossing asteroid theory was used to analytically compute $P_{I/CRX}$ for each torus crossing. The $P_{I/CRX}$ term is a function of the velocity vector of the spacecraft relative to the Earth at impact and is slightly different for each torus crossing; therefore, an average value was used to compute a best estimate value representative of all torus crossings. The theory may be used to compute $P_{I/CRX}$ because no assumptions about long-term perturbations are made in this calculation. A basic assumption in the computation is that the Earth is equally likely to be anywhere in its orbit at the time of the crossing. This assumption is valid for the long-term time period and is discussed in Subsection 6.3.1. Derivation of the analytic expression used is provided in the following Subsection 6.2.2.2.

6.2.2.2 Derivation of $P_{I/CRX}$ Expression. The following derivation assumes that the spacecraft will pass through the Earth torus during a particular orbit. For spacecraft orbits inclined with respect to the Earth's orbit, an elliptical intersection region is formed by the intersection of the plane of the spacecraft's orbit and the Earth torus (see Figure 6-3). The velocity of the spacecraft relative to the Earth orbit node determines the time spent by the spacecraft within this intersection ellipse during a spacecraft orbit, which contributes to the probability of Earth impact.

The average probability of impact, P, for passage through the elliptical intersection zone by the spacecraft per spacecraft revolution is:

$$P = \pi/4\ P' \qquad (6\text{-}4)$$

where P' is the average probability of collision with the Earth for a spacecraft trajectory which passes through the center of the elliptical intersection zone. It is assumed that the relative probability of a collision is proportional to the length of the chord of the intersection

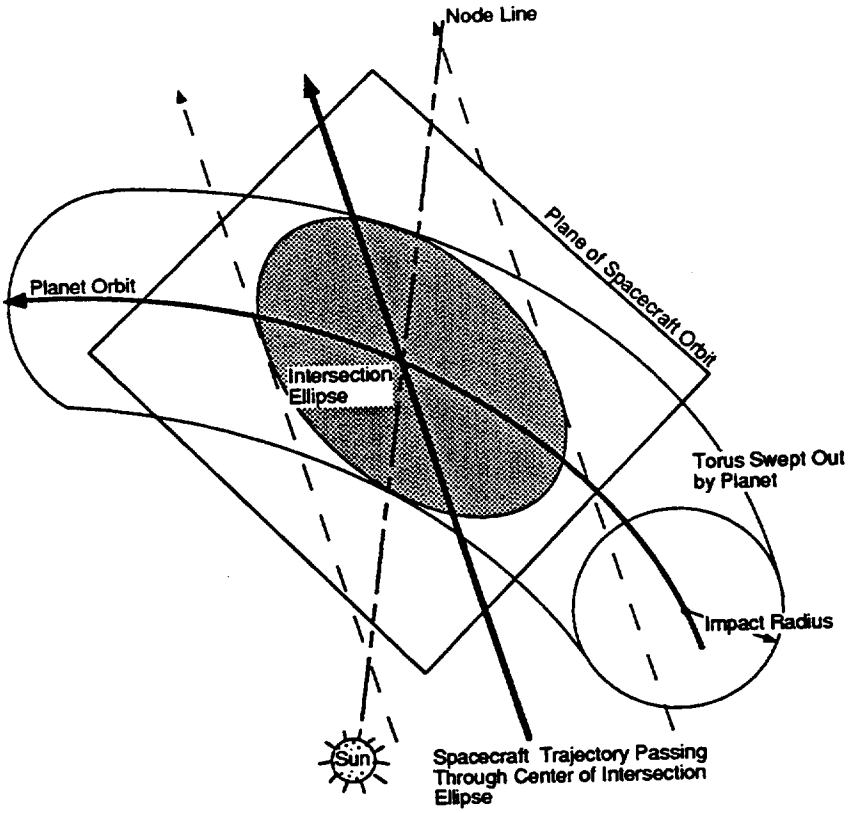

Figure 6-3 Spacecraft and Earth Orbit Intersection Geometry

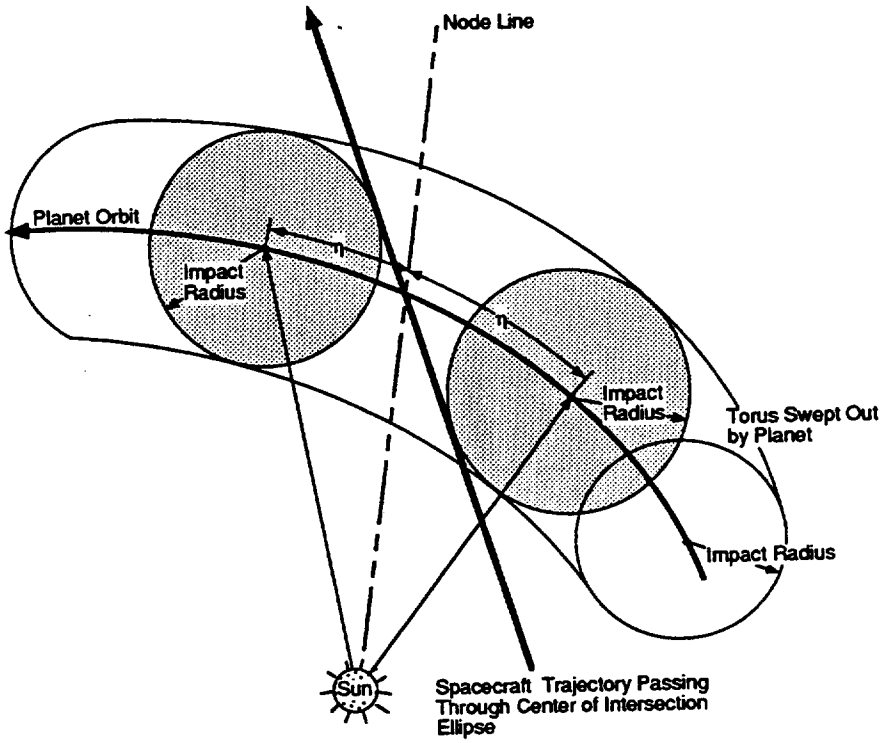

Figure 6-4 Range of Planet Motion for Which Intersection Is Possible

ellipse (which determines the time spent in the intersection zone). The average chord length is $\pi/4$ times the maximum chord length, which is the distance traversed by the spacecraft if it passes through the center of the ellipse.

For a collision to occur, the Earth and spacecraft must be present within the intersection ellipse at the same time. The average probability of collision, P', is proportional to the arc distance measured along the Earth's orbit for which any part of the Earth lies within the intersection ellipse (see Figure 6-4). This arc distance normalized by the heliocentric distance of the Earth is:

$$\eta = \tau \, |U| / \text{sqrt}[U_X^2 + U_Z^2] \qquad (6\text{-}5)$$

where τ is the impact radius, divided by the heliocentric distance of the Earth , $|U|$ is the magnitude of the velocity of the spacecraft relative to the Earth divided by the heliocentric velocity of the Earth , U_X is the radial (Sun to Earth direction) component of U, and U_Z is the component of U normal to the Earth orbit plane direction. For these calculations, the Earth is assumed to be at an impact position. The value η defines the range in Earth motion for which an impact is possible. The average probability of collision is simply 2η divided by the circumference of the Earth's orbit, which when normalized by the Earth's heliocentric distance is:

$$P' = |\eta| / \pi \qquad (6\text{-}6)$$

Equation 6-6 assumes that the Earth is equally likely to be anywhere in its orbit at the time of a torus crossing. For the long time spans considered in Earth-crossing asteroid theory and in this long-term analysis, this assumption is valid. Resonance between the spacecraft orbital period and that of the Earth can sometimes cause the Earth to be more or less likely to be in certain portions of its orbit at a torus crossing. These effects were studied as part of the uncertainty analysis presented in Subsection 6.3.1.

If the spacecraft's orbit partially crosses the Earth's orbit, collision is only possible within the fraction of the Earth's orbit crossed by the spacecraft. The spacecraft's orbit “partially crosses” the Earth's orbit if the spacecraft's perihelion or aphelion lies between Earth's perihelion and aphelion. In this case, the value of P' obtained from Equation 6-6 must be multiplied by this fraction to obtain the probability of impact per spacecraft revolution.

By combining Equations 6-4, 6-5, and 6-6, the probability of impact within a spacecraft revolution is obtained:

$$P_{I/CRX} = f \tau |U| / (4 \text{ sqrt}[U_X^2 + U_Z^2]) \quad (6\text{-}7)$$

Passage of the spacecraft through the intersection ellipse often occurs for multiple revolutions of the spacecraft until orbital perturbations move the spacecraft orbit away from the Earth torus.

6.3 RESULTS

The probability of long-term Earth impact is presented and discussed in this subsection. Other long-term characteristics pertinent to the Earth impact analysis are also presented.

An uncertainty analysis is first described which yields uncertainties for the torus-crossing frequency (N_{CRX}/N_{CASE}) and probability of Earth impact given a torus crossing ($P_{I/CRX}$), terms which are required to compute the long-term Earth impact PDF (see Equation 6-3). The contribution to Earth impact probability will be shown to be influenced by the interplanetary trajectory characteristics at the failure time. Long-term entry angle, entry velocity, and entry latitude probability distributions are presented. The mean probability of Earth impact over 1000 years is also analyzed.

6.3.1 Uncertainty Analysis

Several parameter and model uncertainties enter into the long-term impact probability calculation. They are the spacecraft system internal failure uncertainty, the micrometeoroid failure model uncertainty, the Earth torus-crossing frequency uncertainty, and (given a torus crossing) the Earth impact probability uncertainty. All of the uncertainties take the form of a log-normal distribution, except the torus-crossing frequency uncertainty, which is a normal (Gaussian) distribution. Probability distributions for each term in the long-term Earth impact Equation 6-3 are combined to yield a single long-term PDF as described in Subsection 6.3.2. Probability distributions for the probability of failure, $P_F(i)$, are detailed in Section 4 for each failure mode. Probability distributions for the N_{CRX}/N_{CASE} and $P_{I/CRX}$ terms were constructed as follows using empirical analysis and engineering judgment.

The mean value of N_{CRX}/N_{CASE} was computed by counting the torus crossings detected for all Monte Carlo cases. A normal distribution for this torus-crossing frequency was constructed by estimating a sigma due to all uncertainties. The dominant uncertainties in the computation of the torus-crossing frequency are listed in Table 6-1. One a uncertainties are listed in terms of the percentage of the mean value of N_{CRX}/N_{CASE} and were root-sum-squared to yield a final sigma.

Table 6-1 Dominant Contributors to N_{CRX}/N_{CASE} and $P_{I/CRX}$ Uncertainties

Term	Source of Uncertainty	VVEJGA Uncertainty	VEEGA Uncertainty
N_{CRX}/N_{CASE}		Uncert. = 1sigma / mean	
	Navigation	0.2	0.2
	Solar Radiation Pressure	0.15	0.15
	Sample Size	0.05	0.03
$P_{I/CRX}$		5% Confidence = Median/Uncert. 95% Confid. = Median x Uncert.	
	Random Earth Location at Torus Crossing	5	6

Navigation uncertainty results from orbit determination and maneuver execution uncertainty, and enters into the computation of the initial trajectory states for each Monte Carlo case as described in Subsection 6.2.1. The contribution due to navigation uncertainty was estimated by evaluating trajectory legs which had significant numbers of torus crossings using 10%, 50%, and 90% navigation uncertainties to generate the initial states. One σ variations in the number of torus crossings were then computed by comparing the difference in the torus-crossing counts for each navigation uncertainty. The analysis showed that the lσ variation in the number of torus crossings approaches 20% of the mean total. The 50% navigation uncertainty was used to compute the mean torus-crossing frequency for the nominal study. The uncertainty due to solar radiation pressure force modeling in the trajectory propagation was computed in a similar manner. The nominal solar radiation pressure force was scaled to higher and lower values and certain trajectory legs propagated again. The

variation in the number of torus crossings was then used to compute the uncertainty.

The uncertainty in the number of torus crossings due to the number of Monte Carlo cases considered is roughly equal to the square root of the number of torus crossings detected. For example, if 100 torus crossings were detected in 300 cases, the uncertainty would be ~10/300. The torus-crossing frequency was not sensitive to whether a ΔV was associated with spacecraft failure (only ~2% of all failure cases involved a ΔV).

The median value of the probability of Earth impact given a torus crossing, $P_{I/CRX}$, was computed as the average of all values computed at each torus crossing. A sigma for this term was estimated in order to construct a log-normal distribution. The dominant uncertainty in $P_{I/CRX}$ is due to the assumption that the Earth is equally likely to be anywhere in its orbit at the time of a torus crossing. Uncertainties due to navigation, solar radiation pressure, sample size, and failure ΔV were found to be negligible compared to the random Earth location assumption.

For the long time spans considered in Earth-crossing asteroid theory and in this long-term analysis, the assumption that Earth is equally likely to be anywhere in its orbit is valid. The trajectory can be predicted for the first few years, but predictive accuracy quickly degrades due to lack of precise knowledge of the initial spacecraft state and an inability to exactly model the physical universe. Resonance between the spacecraft orbital period and that of the Earth can sometimes cause the Earth to be more or less likely to be in certain portions in its orbit at a torus crossing. These effects were studied as part of the uncertainty analysis. The uncertainty analysis did not invalidate the relation but resulted in the specification of a large uncertainty for the $P_{I/CRX}$ term. The uncertainty is slightly different for each mission since the degree to which orbital resonance plays a role is a function of the trajectory characteristics. Uncertainty values are listed in Table 6-1 as a multiplication or division factor to the mean. For example, for the VVEJGA trajectory, 5% of the $P_{I/CRX}$ values are estimated to possibly be beyond 5 times the median value and 5% are estimated to be below the median value divided by 5. The uncertainty values were based both on empirical analysis of the location of the Earth in its orbit at each torus crossing and engineering judgment as to the accuracy of the Earth-crossing asteroid theory used.

6.3.2 Long-Term Earth Impact Probability

Distributions for each term in Equation 6-3 used to compute P_I were combined to yield a long-term probability density function (PDF) for the primary VVEJGA and backup VEEGA trajectories. All of the uncertainties take the form of a log-normal distribution, except for the torus-crossing frequency, which is a normal (Gaussian) distribution. A lognormal distribution is expected to arise when several variables with independent distributions are multiplied, especially when most of those distributions are themselves log-normal. These distributions were combined using a Monte Carlo simulation (separate from the Monte Carlo analysis which produced the data) of 1000 points for both the primary and backup trajectories. 1000 points are sufficient to generate a distribution within the accuracy of the analysis. A maximum-likelihood fit was made to a log-normal distribution. The simulation data was used to produce PDF and complementary cumulative distributions for each mission as shown in Figures 6-5 to 6-8. The points plotted are fractions of the 1000 simulations of the long-term impact probability, and the solid curves are the fit log-normal distributions. The mean value of the long-term Earth impact probability, P_I is 3.7×10^{-8} for the primary and 3.6×10^{-7} for the backup mission.

The mean value of each term used to compute Earth impact probability, P_I, is listed in Table 6-2 for each . trajectory leg to illustrate that the probability of Earth impact is a function of the trajectory characteristics at failure. The orbital characteristics change significantly at planetary swingbys or major deep space maneuvers. The percentage of the cruise duration that the spacecraft spends on each leg is also shown. Recall that the interplanetary cruise duration is 6.7 years for the VVEJGA trajectory and 9.8 years for the VEEGA trajectory.

The number of Monte Carlo cases (N_{CASE}) evaluated for each trajectory leg is listed as well as the number of torus crossings (mean N_{CRX}) detected during the 100-year propagations of these cases. A median value of $P_{I/CRX}$ was computed based on the average values computed at each torus crossing. The mean value of $P_{I/CRX}$ is then computed using the uncertainty estimates listed in Table 6-1 and is shown in Table 6-2. The mean values of $P_{I/CRX}$ are about 1.6 to 1.8 times higher than the median values. The mean value of P_I is then computed using Equation 6-3. The number of cases for which the spacecraft was eventually ejected from the solar system is shown in the last column.

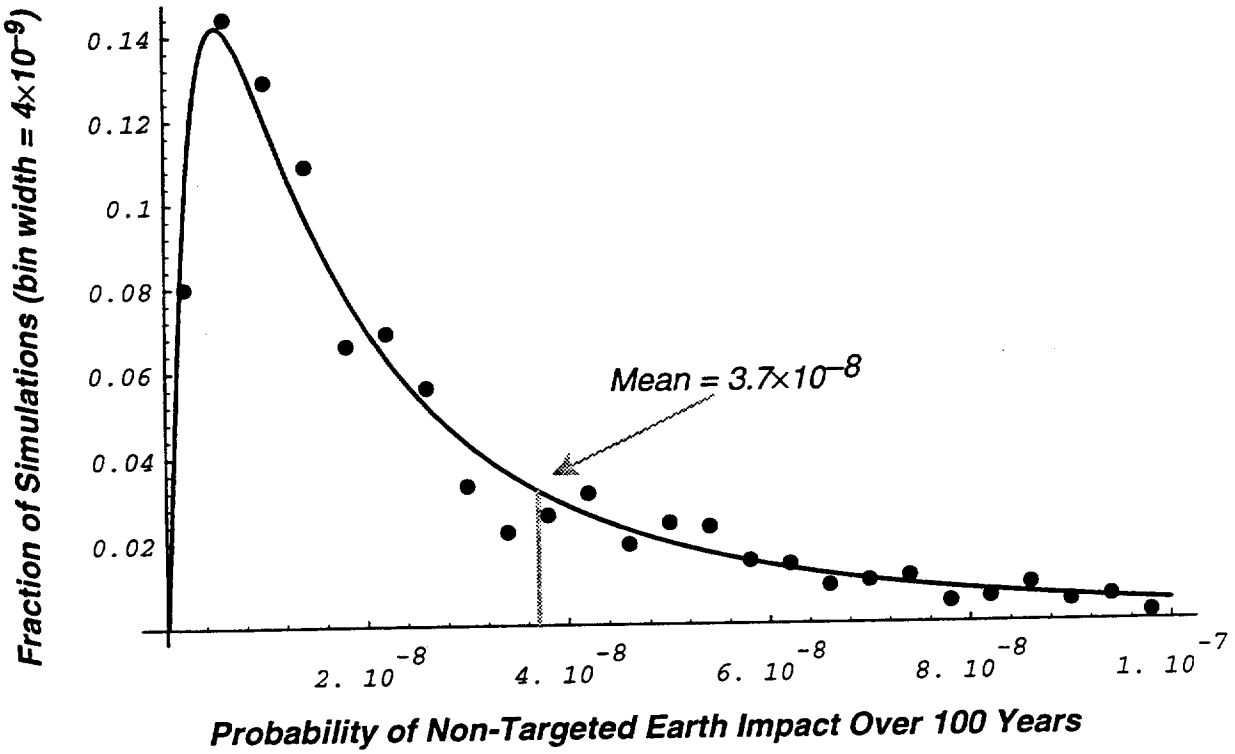

Figure 6-5 Long-Term Earth Impact Probability Density Function for Primary Mission

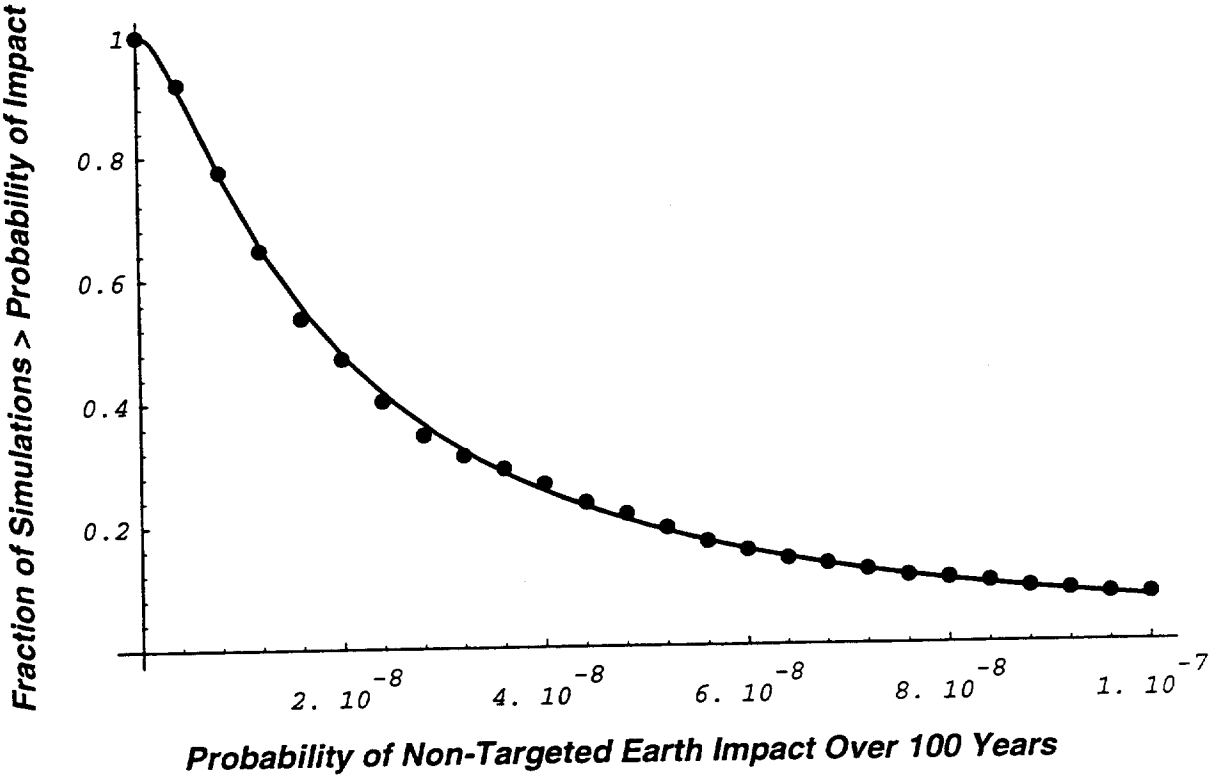

Figure 6-6 Long-Term Earth Impact Complementary Cumulative Distribution for Primary Mission

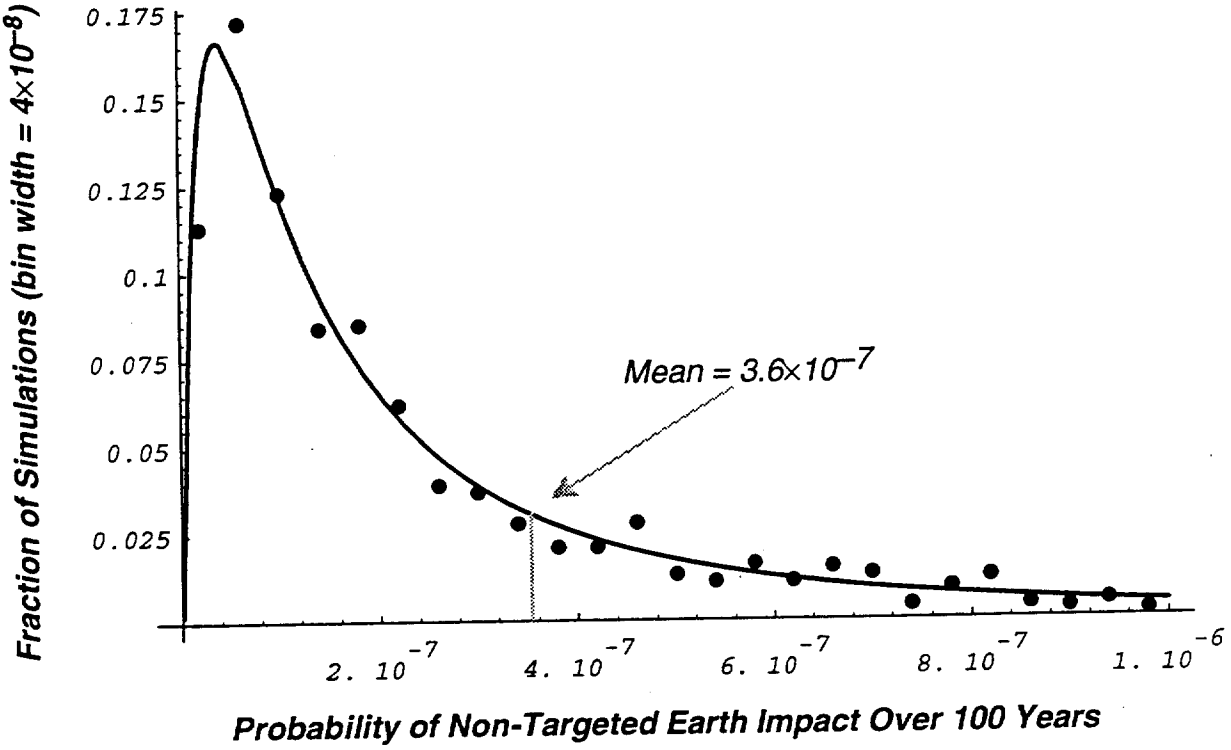

Figure 6-7 Long-Term Earth Impact Probability Density Function for Backup Mission

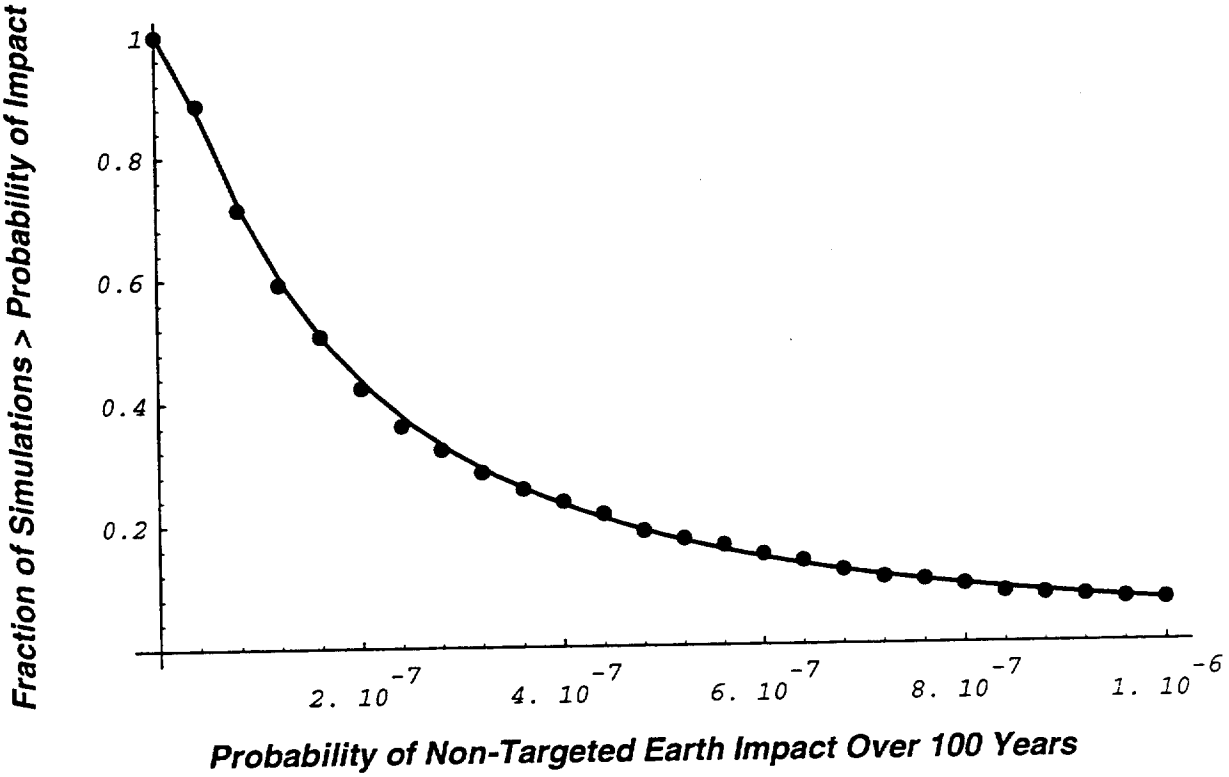

Figure 6-8 Long-Term Earth Impact Complementary Cumulative Distribution for Backup Mission

Table 6-2 Mean Estimate of Earth Impact Probability

Trajectory Leg	Leg Duration in % of Cruise Duration	Mean PF (%)	N_{CASE}	Mean N_{CRX}	Mean $P_{I/CRX}$ ($x10^{-5}$)	Mean P_I	% NCASE Ejected From Solar System
VVEJGA							
Launch-V1	7.9	0.69	563	9	2.9	N/A	<1
V1-DSM	8.8	0.49	453	0	N/A	N/A	0
DSM-V2	8.4	0.43	417	155	2.1	N/A	2
V2-E	2.2	0.12	101	0	N/A	N/A	1
E-J	20.5	1.21	1225	0	N/A	N/A	0
J-S	52.2	2.33	2239	0	N/A	N/A	99.8
Launch-S	10.0	5.27	4998	164	12.1	$3.7x10^{-8}$	45
VEEGA							
Launch-V	12.7	1.26	670	29	3.1	N/A	4
V-El	12.4	0.92	550	573	2.6	N/A	3
El-DSM	18.6	1.36	818	0	N/A	N/A	0
DSM-E2	12.0	0.88	529	57	2.8	N/A	<1
E2-S	44.3	4.34	1882	0	N/A	N/A	99.9
Launch-S	100	8.76	4449	659	2.7	$3.6x10^{-7}$	43

Note from Table 6-2 that the number of torus crossings is influenced by the trajectory geometry at failure. The size of the aimpoint dispersion at the next targeted swingby determines the scatter in the post-swingby trajectories when a failure occurs on that leg. Most of the trajectories for failures on a leg targeted for an Earth swingby tend to be quite similar whereas failures on a leg targeted for a Venus swingby tend to result in dispersed trajectories. An aimpoint biasing strategy is used to reduce the probability of Earth impact for the targeted Earth swingbys and does influence the long-term behavior, but since the long-term behavior is very difficult to predict, use of aimpoint biasing to control long-term impact probability is probably not feasible.

Failures on legs targeted to Venus or Earth swingbys tend to result in trajectories which remain in the vicinity of Earth's orbit. Legs on which the most torus crossings occur are ones in which the spacecraft receives the proper targeted gravity assists to place the spacecraft in the vicinity of the Earth. The spacecraft can receive multiple targeted gravity assists even after failure if no major maneuvers are required and the aimpoint dispersions are

sufficiently small. Note that when failure occurs just before a deep space maneuver, no torus crossings were obtained. The most likely explanation for this absence of torus crossings is that if the deep space maneuver is missed, the spacecraft misses the targeted swingbys that keep it in the vicinity of Earth.

Failures on legs targeted to Jupiter or Saturn tend to result in trajectories which never return to the vicinity of Earth's orbit. For failures on the VVEJGA trajectory after the targeted Earth swingby (1.8 years after launch), the spacecraft is always targeted to the vicinity of Jupiter where it receives a powerful gravity assist that raises the distance at the nearest point in the spacecraft orbit to the Sun to greater than 1.4 AU [2.09×10^8 km (1.30×10^8 mi)] . The periapsis radius remains above this initial value for the duration of the long-term analysis. For failures on the Jupiter to Saturn leg, the Saturn aimpoint dispersion is located such that ejection from the solar system by the massive Saturn gravity assist almost always occurs. From Table 6-2, 99.8% of cases on this leg are ejected from the solar system. The few trajectories whose arrival conditions are outside the ejection region have their orbit periapses raised above 5 AU [7.49×10^8 km (4.65×10^8 mi)] by the Saturn swingby. Ejection from the solar system results 99.9% of the time for failures on the Earth-2 to Saturn leg of the VEEGA trajectory for. the same reasons. Note that these trajectory legs occupy a considerable portion of the entire cruise duration. Thus gravity assists by the massive outer planets virtually assure that failures during the last 73% of the primary and last 44% of the backup interplanetary cruise do not result in Earth impact.

Only about 20% of the torus crossings occur within 10 years after the nominal SOI date for both the primary and backup missions. Therefore, torus crossing orbits usually are the result of long-term perturbations that modify the spacecraft orbit.. The majority of the torus crossings occurred within the first 50 years for both the primary and backup missions.

Although torus crossings occur within the first 100 years, the mean time to impact is much greater. A rough estimate of the mean time to impact can be computed using theory presented in Reference 1. The mean time to impact is a function of the spacecraft orbit's semi-major axis, the torus crossing frequency (N_{CRX}/N_{CASE}) , and the probability of impact given a torus crossing ($P_{I/CRX}$) . The mean time to impact was estimated for each trajectory segment and ranges from 105 to beyond 106 years. Within the first few thousand years, the likelihood of torus crossings is greater since the spacecraft is targeted for at least one Earth swingby during the interplanetary cruise, resulting in a spacecraft orbit which is initially in the vicinity of Earth's orbit. Long-

term perturbations tend to move the spacecraft orbit away from its initial orientation, but over millennia the torus crossing geometry can be reestablished by long-term orbital perturbations.

6.3.3 Entry Angle, Velocity, and Latitude Distribution

The flight path angle, γ, is the angle between the local spacecraft velocity vector and the plane tangent to the Earth's atmosphere. For the spacecraft to impact Earth, the spacecraft's aimpoint relative to Earth must lie within a circle of radius (Ri), called the "impact circle". In addition, the entry angle must be greater than 7° for impact to occur, because the spacecraft will skip out of the atmosphere if the entry angle is less than this value. The determination of Ri accounts for this behavior; that is, a trajectory aimed at a point along the circle of radius (Ri) enters the atmosphere at an angle of 7°.

When considering long-term Earth impacts, the spacecraft aimpoint can be considered to be equally likely to be at any point within the impact circle. The probability distribution function (the probability that the entry angle is between 70 and any given value γ) and its derivative, the PDF, can be easily computed using an analytic expression which is solely a function of γ. The long-term entry angle PDF and cumulative probability distribution are shown in Figures 6-9 and 6-10. The velocity vector of the spacecraft relative to the Earth (referred to as the V_∞ vector) was estimated at each torus crossing, assuming that the Earth was in a position to cause impact in order to estimate the likely range of entry velocities and entry latitudes for the long-term. Given the $\mathbf{V}_\infty$ magnitude, the entry velocity can be computed at any distance from the Earth. For the entry velocity calculations in this section, Earth impact is assumed to occur at an altitude of 122 km (76 mi). Entry velocity PDFs for the primary and backup missions are shown in Figures 6-11 and 6-12. Since a single segment of the interplanetary trajectory was responsible for most torus crossings in each mission, the entry velocities tended to group near similar values for each mission. For the primary mission, most entry velocities were between 19 and 20 km/s (11.8 and 12.4 mi/s) and for the backup mission, most entry velocities were between 16 and 17 km/s (9.9 and 10.6 mi/s).

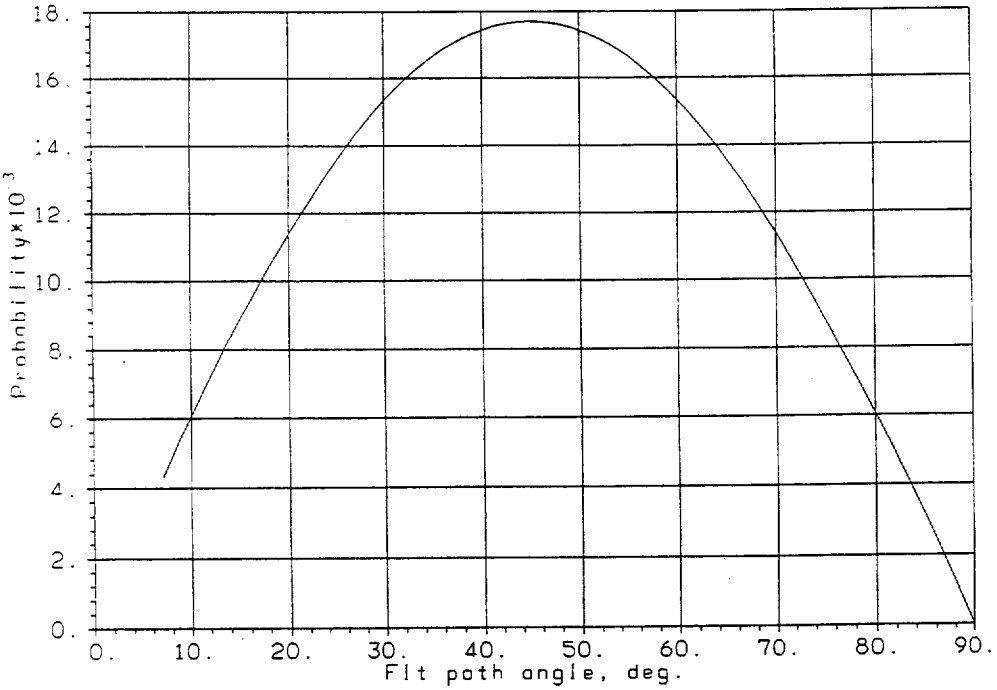

Figure 6-9 Long-Term Entry Angle Probability Density Function

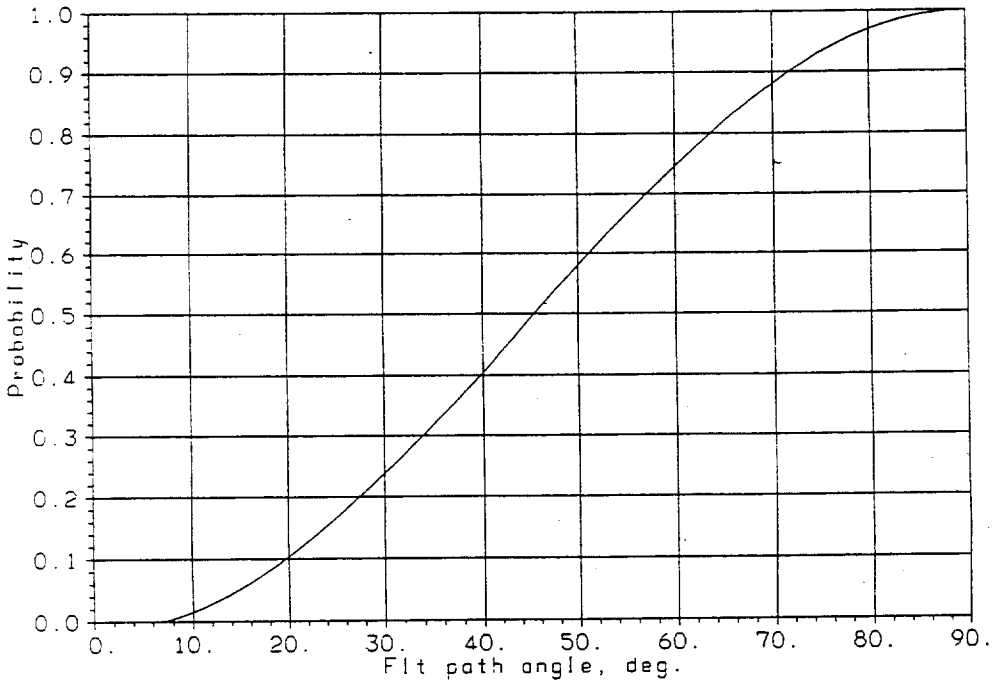

Figure 6-10 Long-Term Entry Angle Complementary Cumulative Distribution

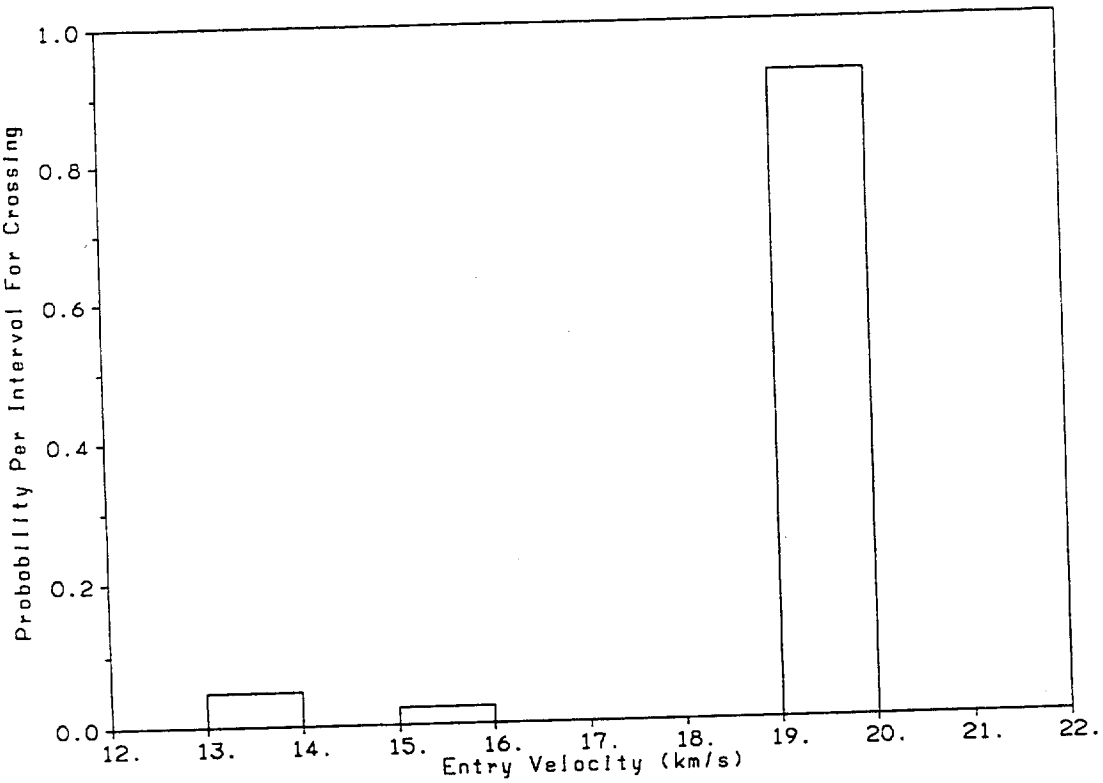

Figure 6-11 Long-Term Entry Velocity Probability Density Function for Primary Mission

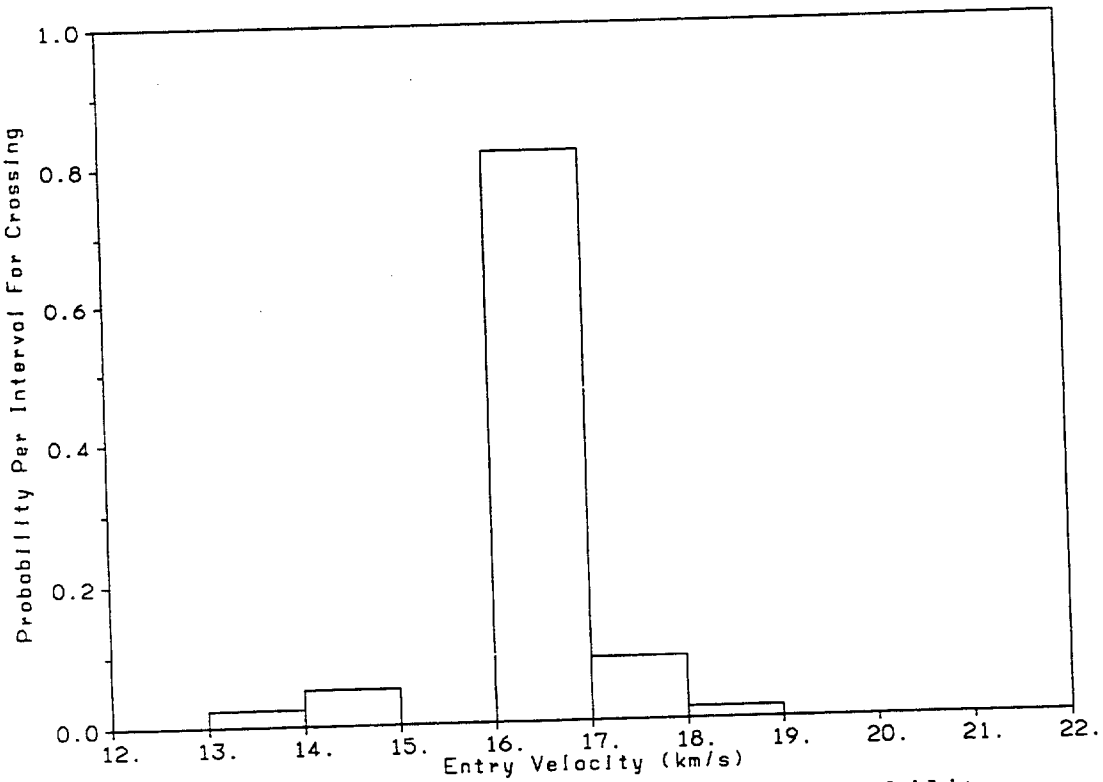

Figure 6-12 Long-Term Entry Velocity Probability Density Function for Backup Mission

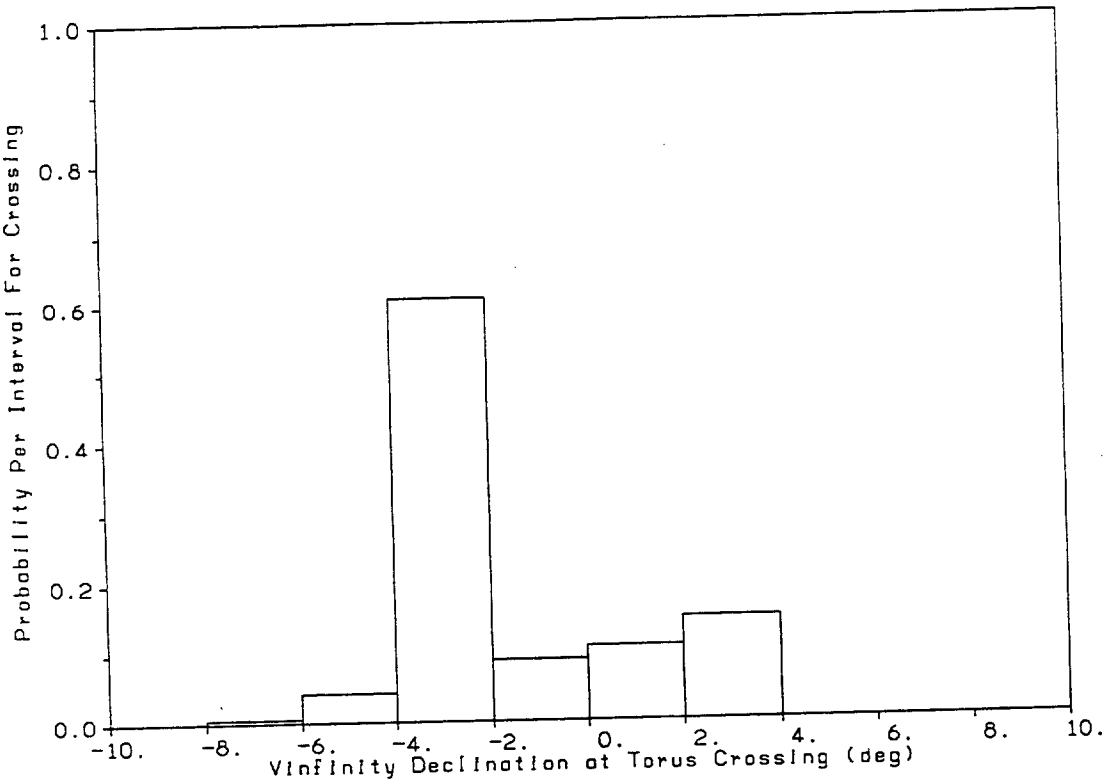

Figure 6-13 Long-Term V_∞ Declination Probability Density Function for Primary Mission

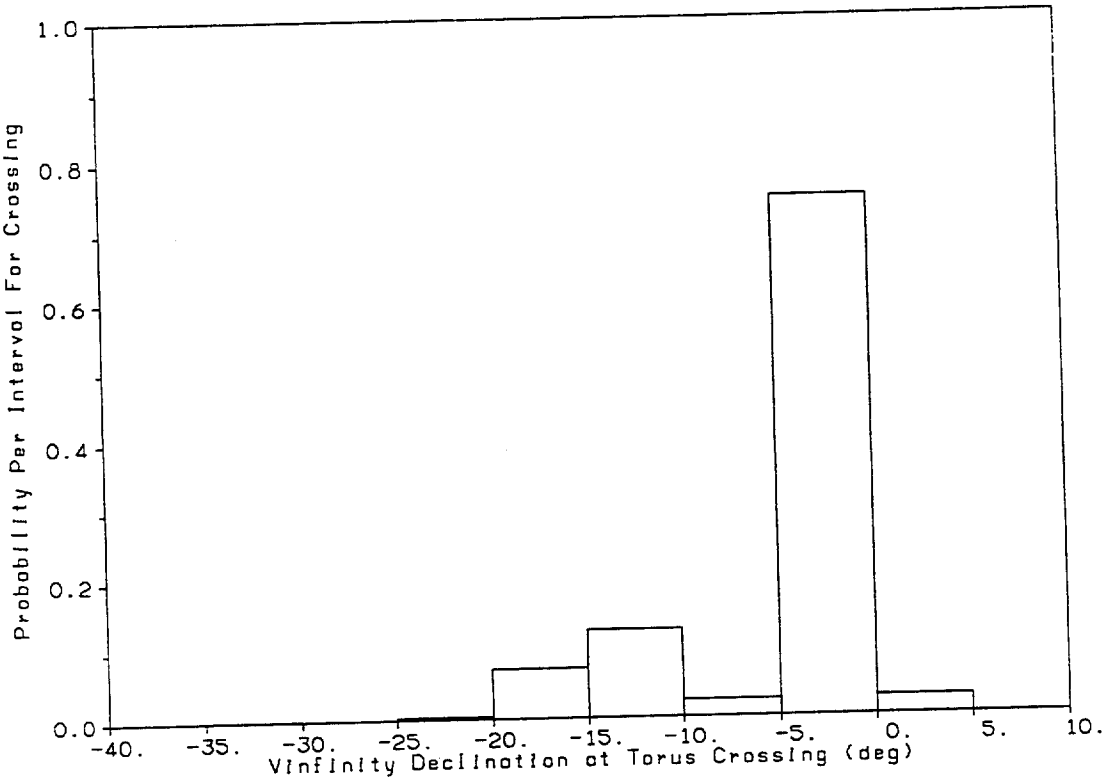

Figure 6-14 Long-Term V_∞ Declination Probability Density Function for Backup Mission

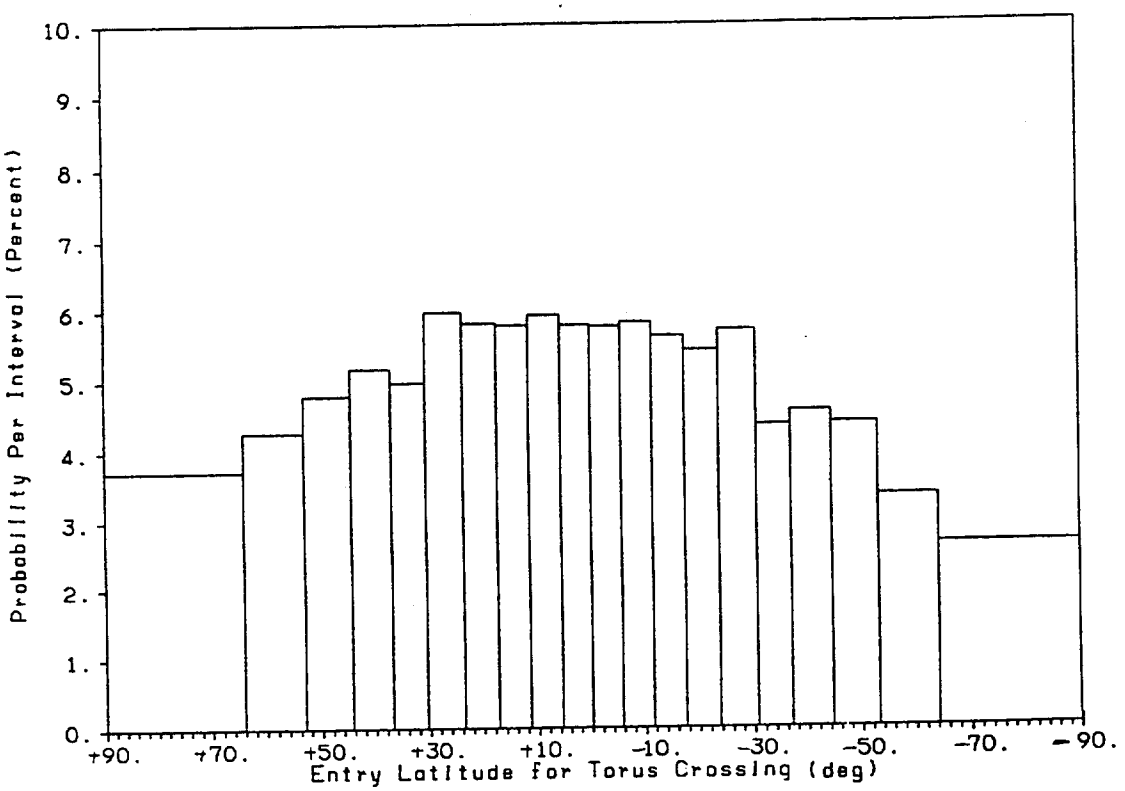

Figure 6-15 Long-Term Entry Latitude Probability Density Function

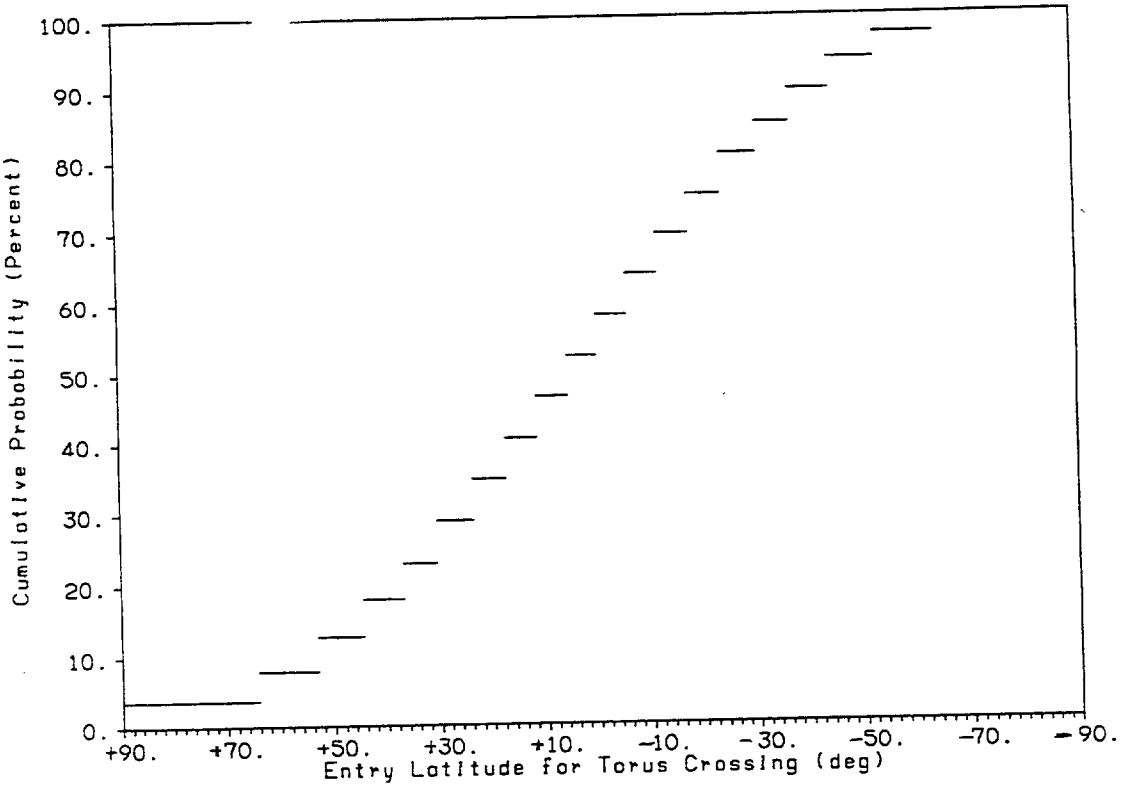

Figure 6-16 Long-Term Entry Latitude Cumulative Distribution

The $\mathbf{V}_\infty$ vector computed at each torus crossing in the above manner is also used to estimate the entry latitude distribution. At Earth entry, the spacecraft aimpoint is considered to be likely to be at any point within the impact circle, as assumed in the entry angle distribution computation. The declination of the $\mathbf{V}_\infty$ then determines the latitude distribution. For example, if the spacecraft approaches from Earth's North Pole, the probability of impacting the South polar region is near zero. The PDF of $\mathbf{V}_\infty$ declination with respect to the Earth equator at torus crossings is shown in Figure 6-13 for the primary and Figure 6-14 for the backup mission. An entry latitude PDF and cumulative probability for a $\mathbf{V}_\infty$ **o** declination of -30 is shown in Figures 6-15 and 6-16 and are representative of the long-term behavior for both missions. The latitude bins in Figure 6-15 delineate equal areas on the Earth's surface. A declination of -3° is characteristic of both missions as shown in Figures 6-13 and 6-14 and the latitude distributions are relatively insensitive to $\mathbf{V}_\infty$ magnitude. Since $\mathbf{V}_\infty$ declinations were near zero for both missions, long-term entry latitude is nearly evenly distributed among latitude bands delineating equal areas on the surface.

6.3.4 Very Long-Term Earth Impact Analysis

A random subset (~20%) of the ~5000 Monte Carlo cases evaluated for each mission were also propagated for 1000 years to study the very long-term probability of Earth impact. The same methodology used for the 100-year cases was used for these 1000-year cases. The probability of spacecraft failure is unchanged since the spacecraft must still fail before SOI or it will be permanently placed in Saturn orbit. When considering 1000 rather than 100 years, the mean $P_{I/CRX}$ did not change significantly, while the number of torus crossings detected increased as expected. The mean probability of Earth impact over 1000 years is ~2.5 times higher for the primary mission and ~1.5 times higher for the backup mission than that for a 100-year time period. Most torus crossings occurred within the first few centuries.

6.4 CONCLUSIONS

This analysis computed the probability of Earth impact by a non-targeted Earth swingby within 100 years past the planned SOI date. PDFs for the long-term probability of Earth impact were generated for the primary and backup missions. The mean probability of Earth impact for the long-term is 3.7×10^{-8} for the primary mission and 3.6×10^{-7} for the backup mission. For trajectories for which long-term impact

is possible, the mean time to impact is estimated to range from 10^5 to beyond 10^6 years.

The significant spacecraft failure mode for the long-term is spacecraft system internal failure. The probability of impact given failure is influenced by the trajectory characteristics of the spacecraft at the time of failure. Gravity assists by the massive outer planets virtually assure that failures during the last 73% of the primary and last 44% of the backup interplanetary cruise do not result in Earth impact.

By applying the same methodology used to compute impact probabilities for 100 years, the mean probability of Earth impact over 1000 years is estimated to be ~2.5 times higher for the primary mission and ~1.5 times higher for the backup mission. Most torus crossings occurred within the first few centuries following injection.

REFERENCES

6-1 Opik. E.J., "Collision Probabilities With the Planets and Distribution of Interplanetary Matter", Proceedings of the Royal Irish Academy vol. 54A, 1951.

6-2 Opik, E.J., "The Dynamical Aspects of the origin of Comets", Liege Mem. vol. 8, Ser. 5, 12 (Armagh Observatory Contributions, vol. 53), 1966.

6-3 Opik, E.J., Interplanetary Encounters: Close-Range Gravitational Interactions, Scientific Publishing Company, Amsterdam, 1976.

6-4 Arnold, J.R., The Origin of Meteorites as Small Bodies, in Isotopic and Cosmic Chemistry, Craig, H., S.L., Miller and G.J. Wasserburg, ed., North Holland Publishing Co., Amsterdam, pp. 347-364, 1964.

6-5 Arnold, J.R., The Origin of Meteorites as Small Bodies, II and III, Astrophysical. J. 141: 1536-1547; 1548-1556, 1965.

6-6 Shoemaker, E.M., J.G. Williams, E.F. Helin, and R.F. Wolfe, "Earth Crossing Asteroids: Orbital Classes, Collision Rates With Earth, and Origin", in Asteroids, T. Gehrels, ed., University of Arizona Press, Tuscon, 1979.

6-7 Shoemaker, E.M., R.F. Wolfe, and C.S. Shoemaker, "Asteroid and Comet Flux in the Neighborhood of Earth", Geological Society of America special paper 247, 1990.

6-8 Wetherill, G.W. and Shoemaker, E.M, "Collision of Astronomically Observable Bodies with the Earth", Geological Society of America Special Paper 190, in Geological Implications of Impacts of Large Asteroids and Comets on the Earth, Silver, L.T., and H.T. Schultz, eds., Boulder, CO, 1982.

6-9 Friedlander, A.L., and D.R. Davis, "Long-Term Risk Analysis Associated with Nuclear Waste Disposal in Space", AAS Paper 79-175, presented at the AAS/AIAA Astrodynamics Specialist Conference, Provincetown, MA, 1979.

6-10 Greenberg, R. and M.C. Nolan, "Delivery of Asteroids and Meteorites to the Inner Solar System", in Asteroids 2, T. Gehrels, ed., University of Arizona Press, Tuscon, 1989.

SECTION 7

EARTH IMPACT PROBABILITY ASSESSMENT

The short-term probability of Earth impact and the long-term probability of Earth impact were combined probabilistically for both the primary and backup trajectories. The data from the 1000 Monte Carlo simulations for the short-term impact probability on the primary trajectory calculated in Section 5 were added point-by-point to the data from the 1000 Monte Carlo simulations for the long-term impact probability on the primary trajectory calculated in Section 6. This provided a 1000-point Monte Carlo simulation for the total probability distribution for Earth impact on the primary trajectory. The same procedure was used for the backup trajectory.

The PDF and complementary cumulative probabilities for the primary and backup trajectories are presented in Figures 7-1 thru 7-4. The points plotted are fractions of the 1000 simulations of the probability of impact. The mean values of these distributions are 2.4×10^{-7} for the primary trajectory and 9.7×10^{-7} for the backup trajectory. Since the means of both distributions are less than 10^{-6}, the Project Earth impact requirement is satisfied for both missions. For reference, Figures 7-2 and 7-4 also indicate values below which 90% of the possible Earth impact probabilities lie.

To facilitate further analyses, maximum likelihood fits of log-normal distributions to the 1000-point distributions were generated for primary and backup probabilities of Earth impact, and are shown as the solid curves in Figures 7-1 thru 7-4. The complementary cumulative graphs show the closeness of fit between the data points and the log-normal curve. For the primary trajectory the fit median Earth impact probability is $l.4 \times 10^{-1}$ and the fit $l\sigma$ spread is 2.6. For the backup trajectory the fit median Earth impact probability is 6.0×10^{-1} and the fit $l\sigma$ spread is 2.6.

As the probability distributions for the short-term and long-term probabilities were largely but not completely independent, Monte Carlo simulations were run to test the effects of correlation. Correlation was demonstrated to have no significant effect on the results.

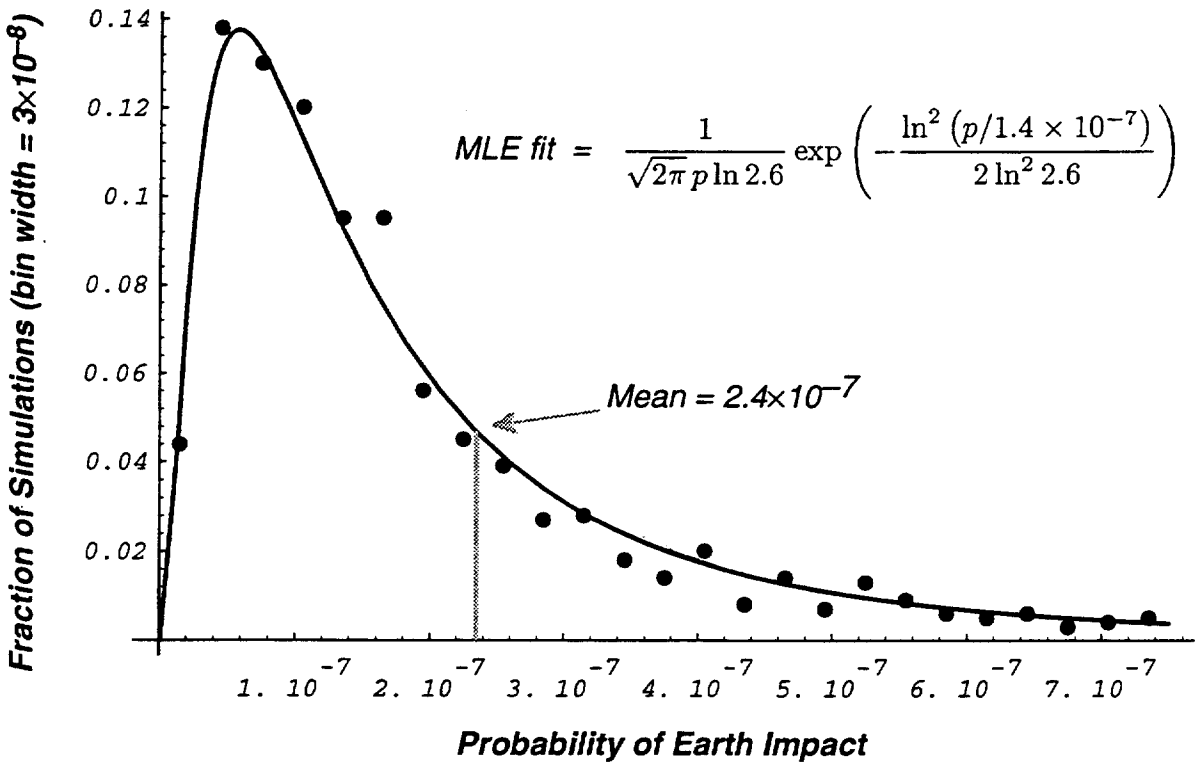

Figure 7-1 Primary Mission Probability Density Function

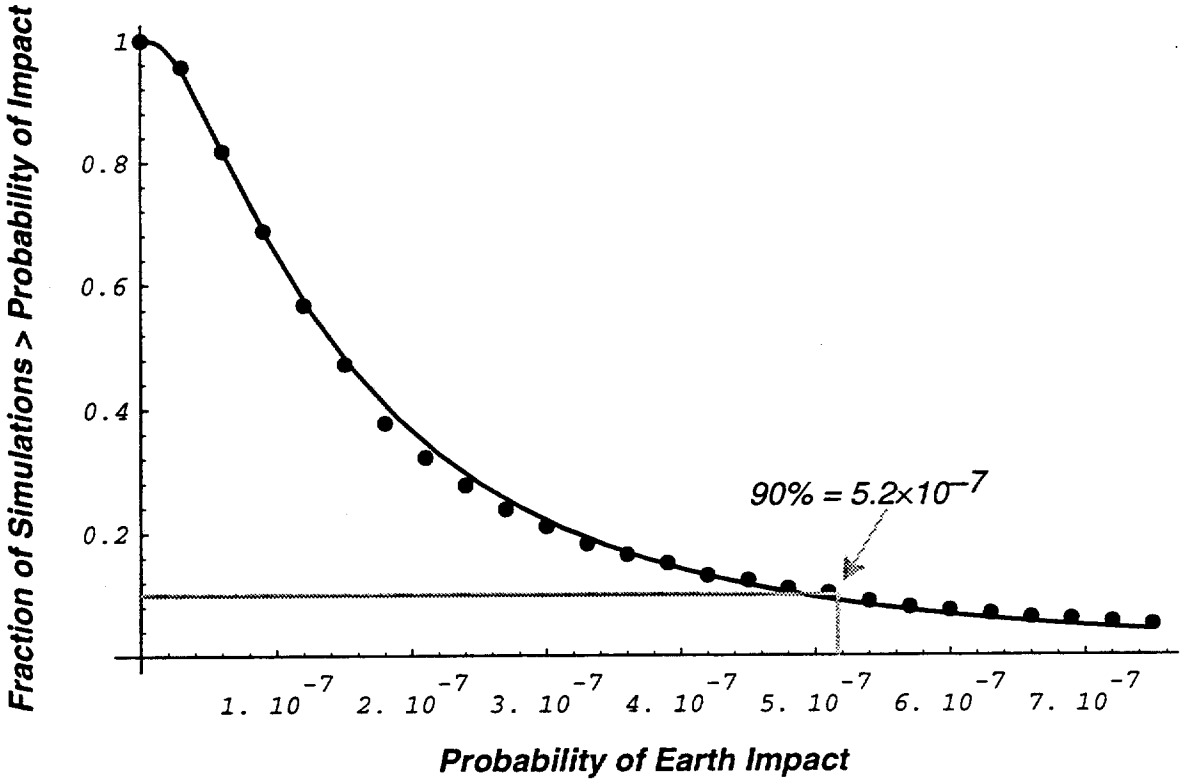

Figure 7-2 Primary Mission Complementary Cumulative Probability

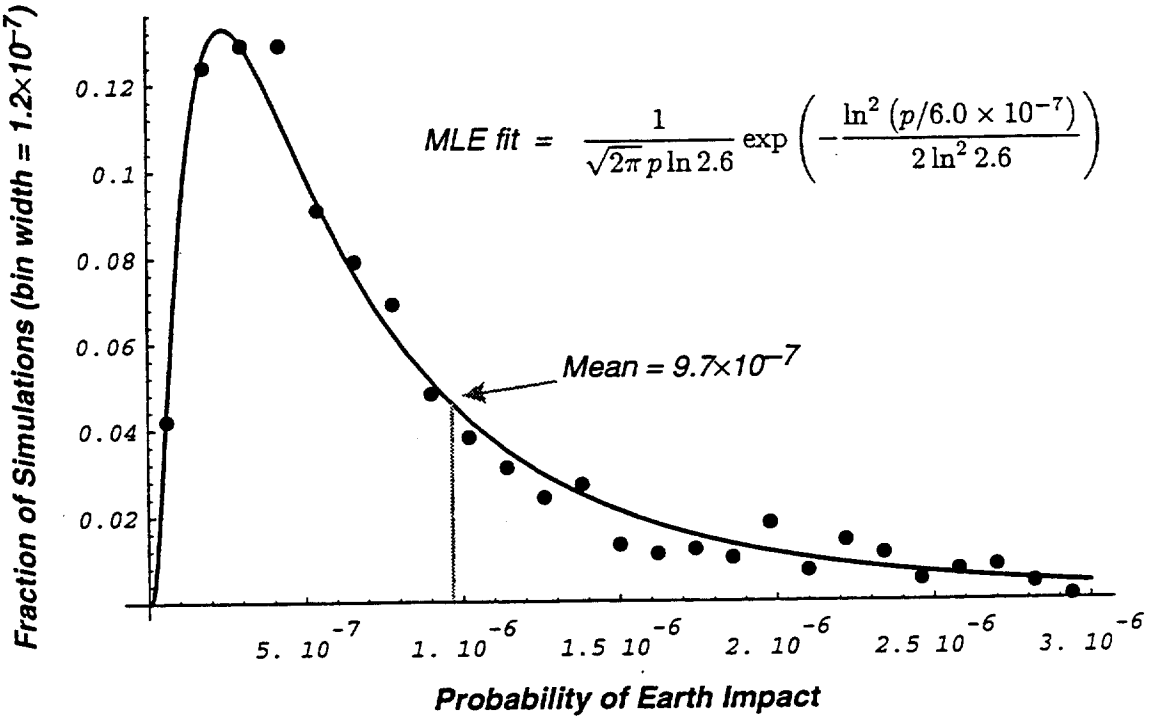

Figure 7-3 Backup Mission Probability Density Function

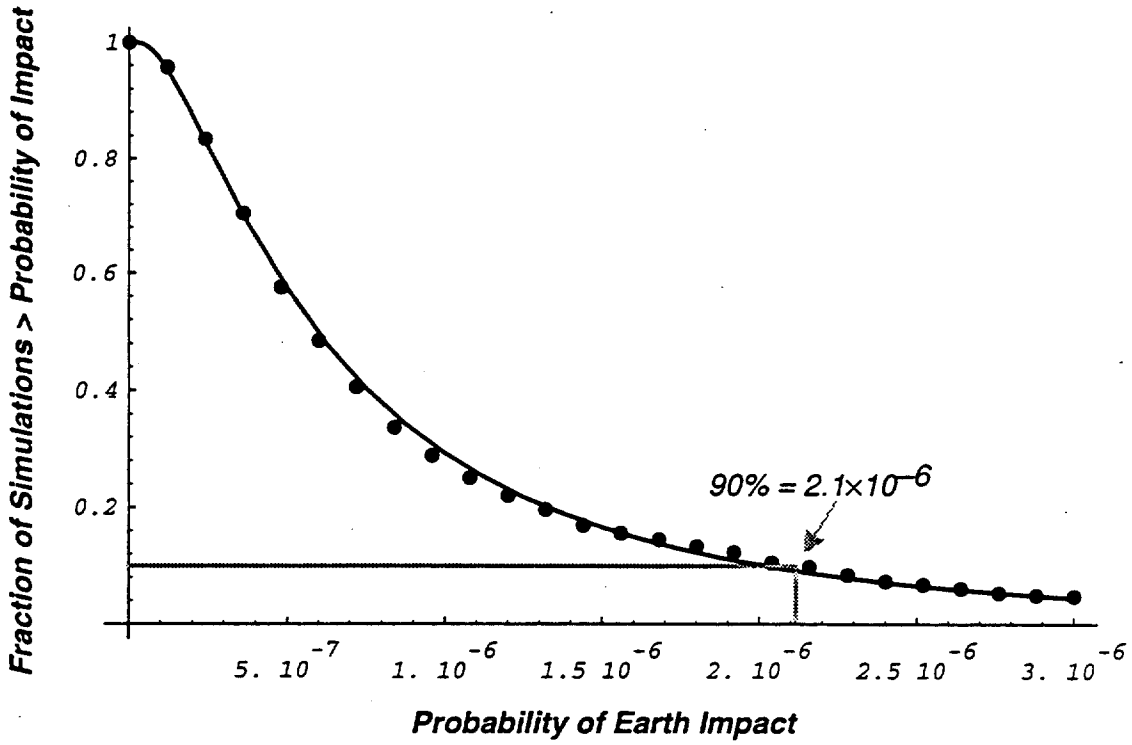

Figure 7-4 Backup Mission Complementary Cumulative Probability

APPENDIX A

BAYESIAN CALIBRATION OF THE MICROMETEOROID MODEL

This appendix describes in more detail the Bayesian calibration of the process by which the probability of disabling micrometeoroid hits are calculated. The basic method is to construct a prior distribution over model uncertainty for hits on Voyagers 1 and 2 and Galileo, and to use Bayes' theorem to combine that with the likelihood of the observation (zero hits on those missions) to get a posterior prediction for the number of hits. The change from the prior to the posterior is applied to the Cassini uncalibrated calculation of disabling hits. This is shown diagrammatically in Figure A-1.

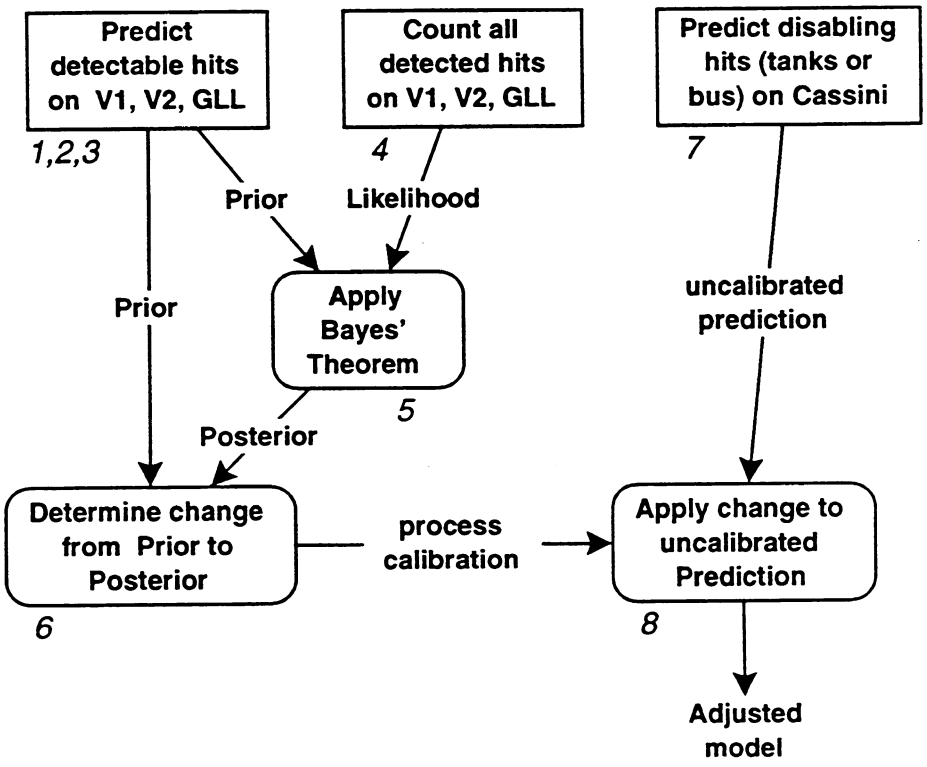

Figure A-1 Calibration Method

The illustrated method is to 1) develop Voyager and Galileo spacecraft models relative to micrometeoroid protection using the standard JPL penetration models, 2) predict the micrometeoroid environment for the respective missions using the Project's environmental model, 3) predict the detectable number of hits on those missions by combining (1) and (2), 4) determine the number of Voyager and Galileo detected hits from the flight problem failure reports, 5) combine the prior (3) and likelihood (4)using Bayes' theorem to get the posterior distribution on the

predicted number of detectable hits for those missions, 6) determine the change in the median and spread of the prediction distribution over model uncertainty between the prior and posterior, 7) predict the Cassini disabling hit probabilities using the same process as in (1), (2), and (3) above, and 8) apply the changes determined in (6) to the results of (7) to get the final calibrated prediction over model uncertainty.

The result of step 3 above is a log-normal distribution over the model uncertainty with a mean of 0.99 hits total for the three missions, and a spread (1σ multiplying factor) of 3.9. The 0.99 is the sum of 0.46 for each of the Voyager missions and 0.07 for Galileo to date. The result of step 4 is zero detected hits, giving a likelihood of *h* predicted hits of e^{-h} (from the Poisson distribution).

Step 5 is performed using Bayes' Theorem:

$$\text{posterior}(h) = \text{prior}(h \mid \text{model}) \times \text{likelihood}(h \mid \text{observation}) / \text{normalization}$$

where the denominator (normalization) is the integral of the numerator to make the posterior integrate to one, so that it is a proper probability density function. The posterior is then fit to a new log-normal distribution (which it fits very closely). The prior and posterior distributions of predicted hits over the model uncertainty, and the likelihood curve of the predicted hits are shown graphically in Figure A-2.

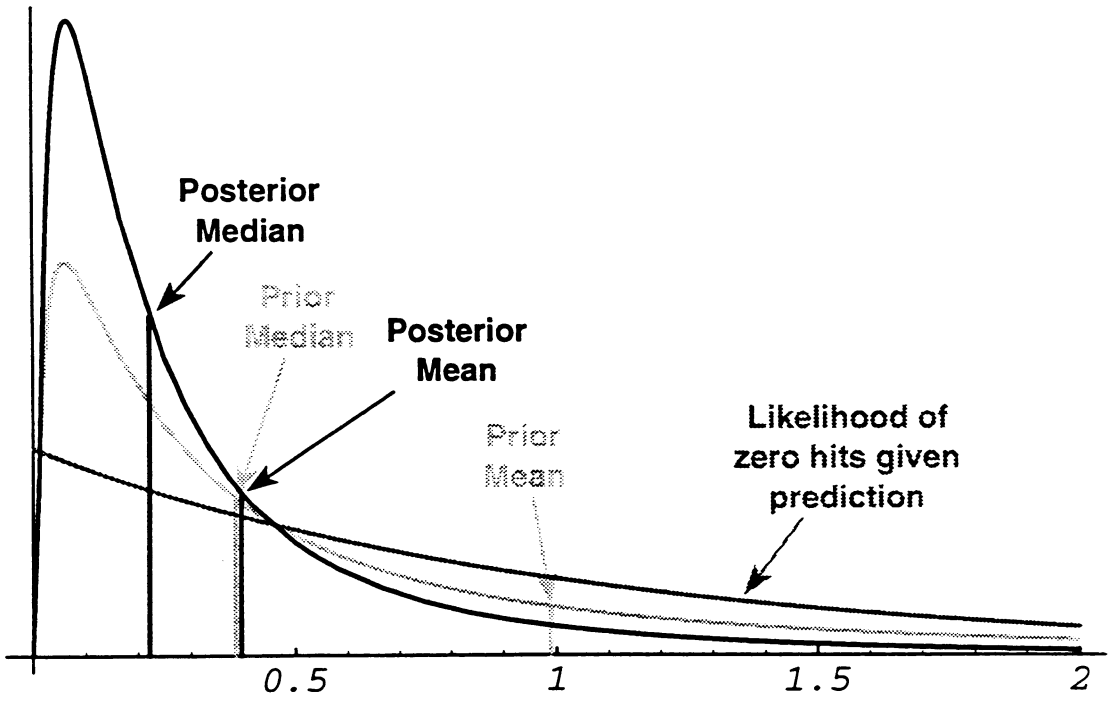

Figure A-2 Prior Distribution, Likelihood, and Posterior Distribution

Numerically what happens in the normalization is that the tail of the distribution is sharply depressed which pushes the total unit probability more towards zero hits. Since most of the mean is in the tail of a log-normal, the mean is reduced by more than a factor of two. Also, the spread of the distribution is reduced slightly by bringing in the tail.

The result for step 6 above is obtained by comparing the prior and fit posterior log-normal curves. The median is reduced by 1.8, and the spread goes from 3.9 to 3.0, which gives a reduction of the mean number of hits from 0.99 to 0.40.

The same uncalibrated machinery is used to calculate tank penetration probabilities and disabling spacecraft bus hit probabilities as a function of time for the primary and backup missions. This calculation also gives a log-normal spread of 3.9, since the model uncertainties are the same. Those median curves then have the above factor applied, and the spread is reduced to 3.0 for the final distributions on hit probabilities.

See the Mars Observer appendix (Appendix C) for the effect of assuming one experienced hit instead of zero.

APPENDIX B

ANOMALOUS ΔV EFFECTS FOR MICROMETEOROID- AND GROUND-INDUCED FAILURES

This appendix describes the anomalous ΔV effects associated with micrometeoroid-induced failures of the PMS and with erroneous ground commands.

B.1 ΔV EFFECTS OF A MMH TANK RUPTURE

Based upon the analysis described in Subsection 4.2.1.2.1.1, the following equations were generated to predict the ΔV distribution for a MMH tank rupture. For each possible location of the hole on the tank surface, there is a specific Gaussian distribution that is used to predict the ΔV resulting from a hole in that location.

The location of the center of a hole on the tank surface is denoted by the angle α_1, (see Figure B-1). Immediately following the rupture; which produces the hole, the MMH in the tank will begin to expand through the hole. The escaping gases/liquids impart a torque and ΔV to the spacecraft. The torque will cause the spacecraft to rotate and will change the direction of the ΔV imparted by the gases that continue to escape. The direction of the final net ΔV is thus not in the original direction of the hole on the tank surface. The final direction of the velocity vector is denoted by θ_1 (see Figure B-1). Based upon the equations of motion, spacecraft properties, etc., the relation between θ_1 and α_1 is predicted to be:

$$\theta_1 = 0.918 * \alpha_1$$

For each possible location of the hole, the mean value of the Gaussian distribution used to predict ΔV magnitude is a function of the final net ΔV direction, θ_1. The mean value of each distribution, V_m is predicted by the following equation:

$$V_m(\theta_1) = 1.64 - 0.00061*\theta_1 - 0.0115*\theta_1^2 + 0.00554*\theta_1^3$$

The standard deviation of each distribution is a function of V_m and a constant derived from the 1960's PYRO tests, and is given by the following equation, where k = 0.564:

$$\sigma = k * V_m(\theta_1)$$

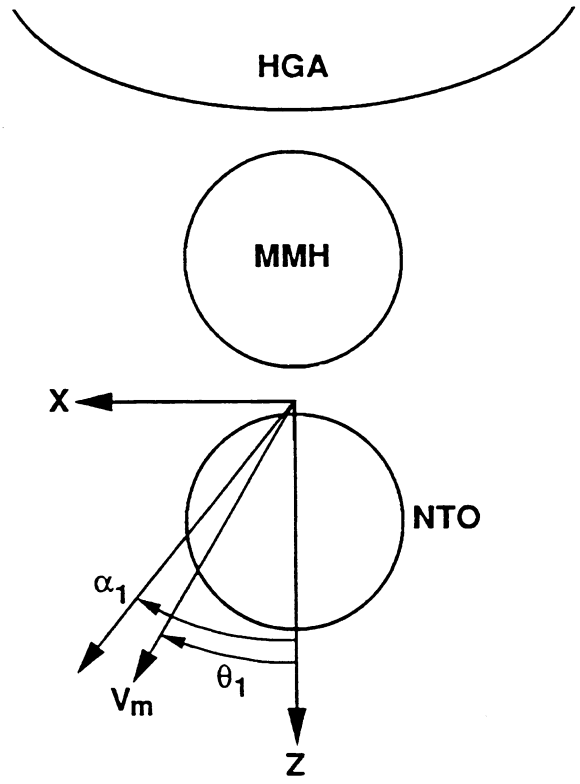

Figure B-1 Definition of MMH Rupture Angles

For the navigation analysis used to predict the probability of impact, it was desirable to predict the probability of the imparted **ΔV** being greater or equal to some magnitude, V, for each given θ_1. Combining the equations noted above with the form of Gaussian distributions, the probability density of the imparted **ΔV** at magnitude V is given by:

$$P_1(V,\theta_1) = \sin(\alpha_1) * \frac{\exp\left\{(-0.5) * \left[\frac{V - V_m(\theta_1)}{k * V_m(\theta_1)}\right]^2\right\}}{0.962 * \sqrt{2\pi} * k * V_m(\theta_1)}$$

with the total probability of all possible events being:

$$\int_0^{\infty} \int_0^{\theta_{2\,max}} P_2(V,\theta_2)\, d\theta_2 \; dV = 1$$

B.2 ΔV EFFECTS OF A NTO TANK RUPTURE

The process used to predict the effects of a NTO tank rupture was identical to that used for the MMH scenario. The equations are different due to NTO having different chemical properties than MMH. Due to differing geometry, the definition of the angles used in this case are different than those used for the MMH case. The new angles, θ_2 and α_2 are illustrated in Figure B-2. Similar to before, the direction of the final net ΔV, θ_2, is a direct function of the initial location of the hole on the tank surface, and is predicted by:

$$\theta_2 = 0.538 * \alpha_2 + 0.131 * \alpha_2^2$$

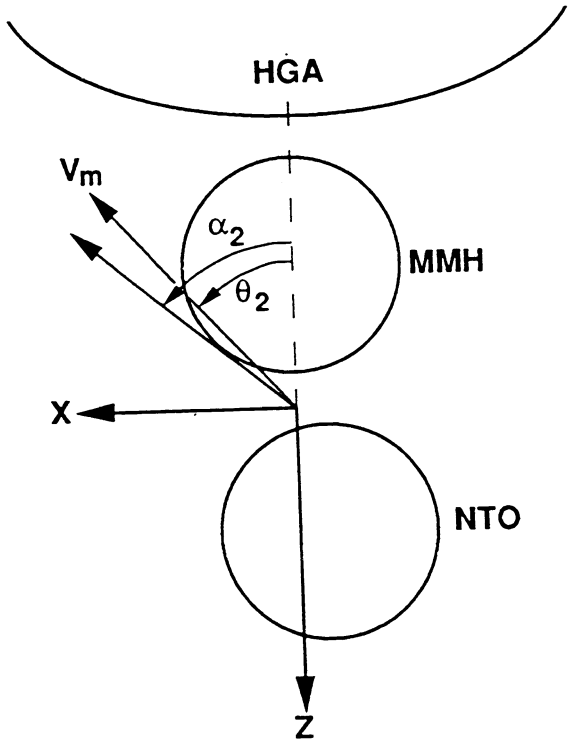

Figure B-2 Definition of NTO Rupture Angles

The mean value of the ΔV magnitude for each tank hole location is predicted by:

$$V_m(\theta_2) = 7.18 + 0.0157 * \theta_2 - 1.82 * \theta_2^2 + 1.91 * \theta_2^3 - 0.564 * \theta_2^4$$

The standard deviation is still a function of the hole location and the parameter derived from the PYRO experiments:

$$\sigma = k * Vm\ (\theta_2)$$

(where k = 0.564)

Combining equations again yields an equation which predicts the probability density of the imparted ΔV at some magnitude, V:

$$P_2(V,\theta_2) = \sin(\alpha_2) * \frac{\exp\left\{(-0.5) * \left[\frac{V - V_m(\theta_2)}{k * V_m(\theta_2)}\right]^2\right\}}{0.962 * \sqrt{2\pi} * k * V_m(\theta_2)}$$

with the total probability of all possible events being:

$$\int_0^{\infty} \int_0^{\theta_{2max}} P_2(V,\theta_2)\, d\theta_2\ dV = 1$$

B.3 ΔV EFFECTS OF A SIMULTANEOUS MMH & NTO TANK RUPTURE

When both tanks shatter, the MMH and NTO will mix and combust. The effects of the combustion will be approximately spherically symmetric and there will be no preferential direction of motion. In addition, there will be a large cancellation of forces acting on the spacecraft, offsetting the greater release in energy due to the combustion.

The location of the holes in the tank surfaces do not effect the magnitude or direction of the imparted ΔV. For all cases of combustion, the distribution of possible ΔV magnitudes is represented by a single Gaussian distribution with a mean value of 1.0 m/s (3-3 ft/s) (obtained through numerical experiment), and a standard deviation of 0.564. Combining equations provides the equation that predicts the probability density of the imparted ΔV, at some value, V:

$$P_3(V) = \frac{\exp\left\{(-0.5) * \left[\frac{V-1}{k}\right]^2\right\}}{0.962 * \sqrt{2\pi} * k}$$

(where k = 0.564) and:

$$\int_0^\infty P_3(V)\, dV = 1$$

The direction of the imparted ΔV is equally likely to occur in any direction and can be thought of as being randomly distributed over a full sphere with equal probability.

B.4 ΔV EFFECTS OF A HYDRAZINE TANK RUPTURE

Similar to the NTO or MMH tanks, the hydrazine tank will shatter when ruptured. However, the location of the hydrazine tank (on the +Y face of the spacecraft) dictates that the impulse induced by a rupture of the tank will have a preferred direction (i.e., the escaping gases will expand away from the spacecraft, pushing the spacecraft in the other direction). The smaller amount of fuel contained in than the hydrazine tank relative to the MMH/NTO tanks yields a smaller predicted velocity. The following equations predict the ΔV distribution for a hydrazine tank rupture:

$$\overline{V}_{mag} = -0.137\overline{y} + V_r\,\overline{r}$$

where the probability of the magnitude V_r is given by:

$$P_4(V_r) = \frac{\exp\left\{(-0.5) * \left[\frac{V - V_m}{k * V_m}\right]^2\right\}}{0.962 * \sqrt{2\pi} * k * V_m}\, r$$

(where V_m = 0.0126 m/s (.0413 ft/s) and k = 0.564)

It is a good approximation to ignore the $\bar{V}_r$ term and consider only the first term. Here, $\bar{y}$ is the unit vector along the y axis and $\bar{r}$ is a unit vector in a uniformly random direction with coordinates θand ϕ, as defined in Figure B-3.

B.5 ΔV EFFECTS OF A HELIUM TANK RUPTURE

The predicted velocity for a helium tank rupture is represented by the following equations. The polar coordinate system used to describe directions was mapped into a Cartesian system for computational reasons. The variable x = cos (θ) goes from -1 to 1 as the polar angle θ goes from +π (in the Z direction) to 0. The angle ϕ, extending from -π to π defines a scaled variable y = ϕ/π which goes from -1 to 1. The area of the surface of the sphere is mapped onto a sphere as shown in Figure B-3. The probability is uniformly distributed in the square with x and y varying from -1 to +1, the spacecraft velocity vector is given in terms of x and y.

$$V_{mag} = 1.86 + 0.115\, x^2 + 0.715 * y^2 - 0.741 * x^2 * y^2$$

$$\theta = 1.57 + 0.979 * x - 0.388 * x^3 - 0.856 * x^5$$

Where $V_{mag}(x, y) = V_{mag}(x, -1 - y)$ for $y < -1/2$
$V_{mag}(x, y) = V_{mag}(x, 1 - y)$ for $y > 1/2$

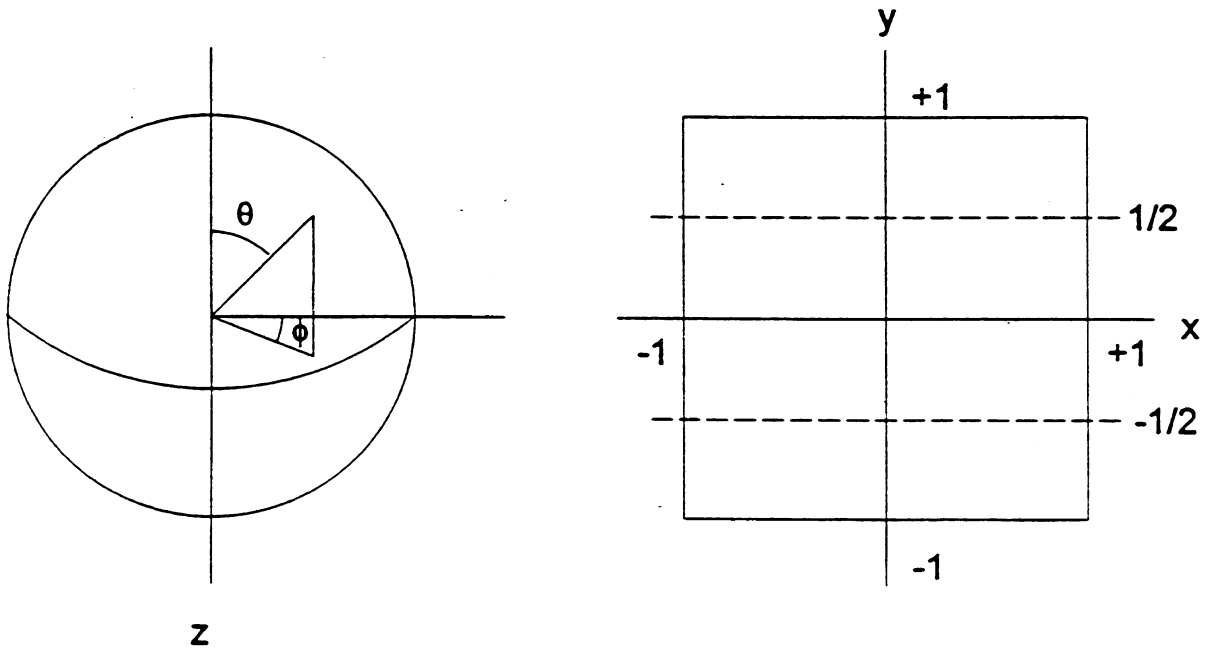

Figure B-3 Definition of Helium Tank Coordinates

B.6 ΔV EFFECTS OF AN ERRONEOUS GROUND COMMAND

Magnitude

There are two independent components to the ΔV magnitude from an erroneous ΔV command.

Component 1: The ΔV resulting from a randomly generated command: a uniform distribution from zero to the maximum allowed ΔV for the particular command (See Subsection 4.2.3.1).

Component 2: The ΔV resulting from inserting a previously generated valid command: a narrow distribution around the ΔV values expected for each of the TCMs executed prior to the time of the error and for the next TCM to be executed. The specific distribution for each TCM is developed as part of the calculation of $P_{I/F}$.

The best estimate (50% value) is:

(10% of the time) Component 1
(90% of the time) Component 2

These estimates take into account the fact that many of the randomly generated commands will be rejected on the ground because of parameter constraint violation (e.g., minimum time > maximum time).

The 10% value is:

(1% of the time) Component 1
(99% of the time) Component 2

The 90% value is:

(90% of the time) Component 1
(10% of the time) Component 2

Direction

When the error is a single BURN command without any accompanying spacecraft positioning commands, the direction effect of both ΔV components is the same. The default for the 7ENGINEBURN command is the last commanded inertial target; for the 7RCSBURN it is the last commanded attitude.

During the pre-Earth cruise phase, the spacecraft will be Sun-pointed to within 2' with small excursions (<8 hrs/week), primarily for ground communication with the high gain antenna. Since the high gain antenna is on the spacecraft axis, Earth-pointing of the antenna is equivalent to Earth-pointing of the ΔV direction.

The probability for Earth-point incorporates the small probability that turn commands were sent with the ΔV command. This probability is small because the more incorrect commands there are, the more likely it is that they will be discovered and questioned by reviewers. Earth-point is the worst-case direction for an erroneous burn.

The directional effects will be approximated (50% value) as:

(3%) Earth-pointed
(97%) Uniform within 2° of Sun-point

The 10% value is:

(1%) Earth-pointed
(99%) Uniform within 2° of Sun-point

The 90% value is:

(5%) Earth-pointed
(95%) Uniform within 2° of Sun-point

APPENDIX C

MARS OBSERVER IMPLICATIONS

C.1 INTRODUCTION

At the same time the technical analyses of this study were being completed, communications were lost with the Mars Observer spacecraft, approximately eleven months after launch. Since the Cassini Earth impact probability calculation depends strongly on assumptions of Cassini spacecraft reliability in the first two to three years after launch, it was considered prudent to assess the implications of the Mars Observer failure on the assumptions that supported the analysis presented in this volume.

This assessment takes a broad overview of the possible failures that could have led to the Mars Observer loss of communications. The reason is partly that the Mars Observer investigations will not be complete by the time this volume is published, but even more so is that we may never know with certainty what caused the Mars Observer loss, since it happened during a planned communications outage with the spacecraft.

C.2 APPROACH

The basic approach to this assessment is to define several general categories of causes for the loss, and for each category to assume that it was the cause, and then to see if and how that might change the assumptions used for Cassini. If that category does affect the assumptions significantly and is considered a credible one, we can reevaluate the Earth impact probability for Cassini.

Once the Mars observer investigations are complete, the Earth impact probability for Cassini and the assumptions that fed into it will be reconsidered to see if the results need to be reevaluated. This assessment was done to reduce the chance that a later reevaluation will be necessary and was aided by some early insight into the investigation board's leading candidates for possible causes of the Mars Observer loss.

Figure C-1 shows the general failure categories and how each was addressed for Cassini. The basic categories are: an externally induced failure caused by a micrometeoroid impact, random internal failures, a design or implementation error, or a ground operations error.

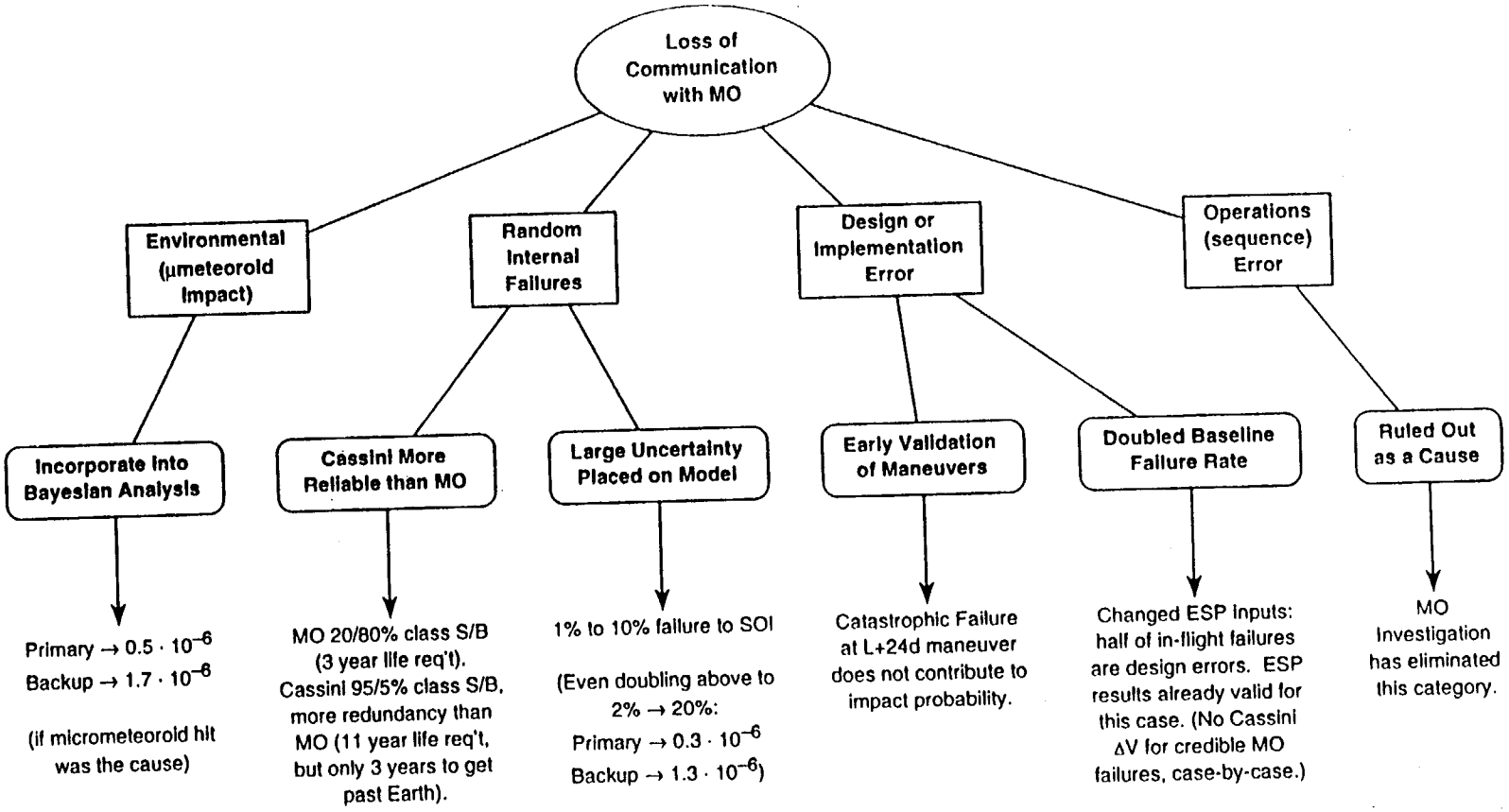

Figure C-1 Addressing Mars Observer Failure Categories

C.3 ENVIRONMENTAL

The process used to predict the probability of a disabling micrometeoroid hit on Cassini was calibrated using the flight experience of zero detected micrometeoroid hits on several outer planet missions (Voyagers 1 and 2, and Galileo; see Appendix A). If we assume that the Mars Observer loss of communications was due to a micrometeoroid, then we could add it to the set, increasing the number of detected hits to one. This has a significant effect on the Bayesian calibration of the process, approximately doubling the mean probabilities of a disabling impact. In order to examine the sensitivity, the Earth impact probabilities were recomputed with this assumption. On the primary, the baseline mean of 2.4×10^{-7} increased to 4.9×10^{-7}; the backup's baseline mean increased from 9.7×10^{-7} to 1.7×10^{-6}. However, this category has a very low probability of being the cause of the Mars Observer failure, based on calculations of the expected flux combined with immediate and latent damage models. Hence, this assumption was not made part of the baseline for the Cassini Earth impact calculation.

C.4 RANDOM INTERNAL FAILURES

The second category is random internal failures. A model of Cassini random part failures was constructed and calibrated to the Voyager parts failure experience. If we assume that the loss of Mars Observer was caused by a parts failure, this would not necessarily compel a change in the Cassini reliability model. one reason **is** that the Mars Observer mission was only three years in length, whereas Cassini is designed for an elevenyear mission and only needs to work for two (primary) to three years (backup) to get past the last Earth swingby. As a result, Mars Observer was designed with less redundancy and-with lower reliability parts (20% / 80% Class S/B parts) than Cassini (95% / 5% Class S/B parts). Just the parts class ratios results in approximately a factor of four difference in the parts-failure time scales between Mars Observer and Cassini. There are other differences in practices for very long-life missions like Cassini, such as in testing and parts qualification. Furthermore, the Cassini reliability model used in this study has a very large uncertainty already built into it to take into account our lack of data on and understanding of random part failures. The probability of Cassini failing to make it to SOI on the primary mission (6.7 years after launch) is estimated to be 1% to 10% - an order of magnitude of uncertainty.

Even considering the large uncertainty, the sensitivity to increasing those failure probabilities by a factor of two (up to an approximately 2% to 20% failure probability by SOI) was determined. This took the primary mean from 2.4×10^{-7} to 2.8×10^{-7} and the backup mean from 9.7×10^{-7} to 1.3×10^{-6}.

Aside from the purposes of the Mars Observer assessment, it is interesting to note the sensitivities of the Earth impact probability calculation to the above changes in the most critical failure modes: disabling micrometeoroid impacts and spacecraft system internal failure. In both cases the large change did not take the primary Earth impact probability above 10^{-6}, but did take the backup over (it was close to begin with). If a reevaluation is needed that results in increases like those above, there are approaches to adjusting the backup trajectory that would reduce the total probability of impact on that trajectory back below 10-6. These approaches include raising the altitude of the Earth-2 swingby and rebiasing the backup trajectory. This would levy a ΔV cost and thus would have some impact on the resulting mission science.

C.5 DESIGN OR IMPLEMENTATION ERROR

The third category of failures is design and implementation errors. After reviewing some early investigation board scenarios, it became clear that design and implementation errors are credible causes for the Mars Observer failure. A review of a large set of past flight problem reports on many spacecraft revealed that approximately half could be assigned to design or implementation error. This insight was incorporated into the Cassini reliability model simply by doubling the system failure rate derived by modelling random part failures. This approximation is probably conservative since the consequences of the design and implementation errors were not examined, and most do not result in system failure. However, if the Mars Observer loss was due to a design or implementation error, then there would be at least one example of that.

This change was made part of the baseline calculation for the Cassini Earth impact probability, and so the reported results of 2.4×10^{-7} for the primary and 9.7×10^{-7} for the backup already include the assumption of a design or implementation error on Mars Observer.

There still remains the possibility of a design or implementation error resulting in an anomalous ΔV failure, and that type of error is not covered by the above increase in the spacecraft system failure rate. However, each Mars Observer failure scenario that results in such a ΔV (all in the propulsion system) can be addressed by assessing whether or not a similar failure could occur on Cassini. Many design and procedural steps are taken on Cassini to avoid these errors; these steps are detailed in Table C-1 for each specific Mars Observer ΔV failure mode. Furthermore, and perhaps more importantly, the Cassini mission validates much of the design and implementation of its propulsion system with a system pressurization and a main engine maneuver only 24 days after launch. A catastrophic failure at that early maneuver does not contribute significantly to Earth impact probability. Failure modes that take time to build up or that are thermally dependent are not validated by the early maneuver., but such modes relevant to Mars Observer are addressed in Table C-1.

Table C-1 Examples of Postulated Mars Observer Failure Modes That Add ΔV (Page 1 of 2)

POTENTIAL MO FAILURE MODE	COMMENTS
1. External or Internal contamination plugs redundant gas regulator sensing ports causing regulator to malfunction during pressurization, resulting in over-pressurization and burst of downstream propellant tank. 2. NTO leaks and permeates into gas lines upstream of check valve and during pressurization gets driven into MMH system causing chemical reaction or combustion and resultant burst of lines or tank.	Cassini on-board fault protection will detect problem and isolate pressurant tank before any serious overpressurization could occur. Flexibility coming from use of latch valves will allow system to be pressurized long before critical earth swingby sequence. Cassini Isolates both the NTO and MMH tanks with latch valves. Cassini is using Galileo check valves with leak rates 100X lower than the Mars Observer specification. Use of latch valves will allow system to be pressurized long before critical Earth swingby sequence. Need for improving reliability still further by adding limited number of pyro valves for better isolation and improving thermal control of feed lines to minimize permeation and condensation will be assessed following release of MO report.

Table C-1 Examples of Postulated Mars Observer Failure Modes That Add ΔV (Page 2 of 2)

POTENTIAL MO FAILURE MODE	COMMENTS
3. NTO leaks and permeates into gas lines upstream of check valve, condenses, gets accelerated when gas tank squib valve opens and generates shock waves and ruptures lines when suddenly decelerated in downstream flow restriction	Same as above.
4. Unintentional sympathetic firing of redundant pyro valve squib initiator ruptures and propels first initiator into adjacent MMH tank.	Cassini tests all squib valves with redundant initiators in place. Problem appears unique to titanium pyro values. Cassini can use stainless steel versions if needed. Based on MO report additional protection for critical hardware will be taken if warranted.

C.6 OPERATIONS ERROR

The fourth and final category of Mars Observer failures is ground operations errors. This is the one case where real data exists - the records of the ground commanding performed on Mars Observer. However, this category has been ruled out after an examination of the ground command data. Therefore, no adjustments to the Cassini ground system reliability were warranted.

C.7 CONCLUSION

The implications of all credible Mars Observer failure scenarios for the Cassini Earth impact calculation have been assessed, and with one change (i.e., taking into account design and implementation errors), the assumptions used in the calculation of the impact probability are expected to hold up in light of the possible conclusions of the Mars Observer failure investigations. If it turns out that a change in the current assumptions is needed, and if that change brings the mean impact probability on the backup trajectory over 10^{-6}, then that probability can be brought back below 10^{-6} by changing the swingby altitudes and rebiasing the trajectory, albeit at some cost to the backup mission science return.

APPENDIX D

PERSEIDS METEOR SHOWER IMPLICATIONS

D.1 INTRODUCTION

Every year around August 12 the Earth passes within 150,000 km (93,210 mi) of the orbit of the comet Swift-Tuttle. Particles left in the comet orbit enter our atmosphere as the Earth passes by the comet orbit creating the annual event know as the Perseids meteor shower. During this year's Perseids meteor shower, the Russian space station Mir I is said to have experienced as many as 60 to 70 micrometeoroid hits (Reference D-1).

The Earth swingby date for the primary trajectory is August 16, 1999. Consequently, the Cassini spacecraft will pass by the orbit of Swift-Tuttle at a distance of about 4 million km (2.5 million mi) on August 13, 1999. A heliocentric diagram of the Cassini spacecraft trajectory and the comet orbit is shown in Figure D-1. Note that the orbit of Swift-Tuttle is highly inclined. The two Earth swingbys for the backup trajectory also occur in late August, yielding comet-orbit miss distances of about 18 million km (11.2 million mi) and 11 million km (6.8 million mi).

Russian experience with Mir 1 alerted the study team to the need for assessing the environmental implications of Earth swingbys during the month of August for Cassini.

D.2 PRELIMINARY ASSESSMENT

The flux of the Perseid micrometeoroids is thought to reach a maximum within several years of Swift-Tuttle’s passage through the Earth's orbit on its 130-year journey around the Sun. The comet passed the Earth's orbit in 1991 and the micrometeoroids have not yet peaked or “stormed.” Expectations are that this will occur within the next two years.

Since at the time of release of this report there is not sufficient information to predict what flux will exist in 1999, it was conservatively assumed equal to the "130-year storm level." Likewise, it was not known how to predict the decrease in flux that occurs as distance increases from the center of the orbit. Again, values were conservatively considered equal to Earth-based measurements (150,000 km from the orbit compared to 4 million km for Cassini).

Best estimates were made of the density [0.5 grams/ cc (0.3 oz/cubic inch)] and velocity (60 km/sec) of the micrometeoroids and of the equivalent width and time of passage (4 hours) through the densest part of the belt.

The most important remaining parameter of concern was the size of the micrometeoroid particles. Conclusions have been drawn using the minimum size that could be observed from Earth, yet some uncertainty remains. Variation of size with frequency was assumed equal to that observed within the solar system in general and consistent with the Neil Divine Model (Section 4). Based on this, the specific micrometeoroid mass that would penetrate the double-shielded tanks, the flux, and the time-integrated fluence were all calculated. Finally, the effect on the overall probabilities of a micrometeoroid failure was estimated. The results range from 35% (conservative) to 250% (very conservative) above the mean values reported in Section 4.

It should be noted that these estimates are not outside the range of assumed uncertainties. If they are proven valid, the Earth impact probability for the primary mission would still not exceed 10^{-6}. The Earth impact probability for the backup mission would probably exceed 10^{-6}, however, more data needs to be collected before a definitive conclusion can be reached.

The geometry and shielding of the Mir space station and the size and frequency of the micrometeoroid hits must be determined. Also, the particle flux must be better characterized as functions of micrometeoroid mass, distance from the comet orbit, and time.

After the data are collected and evaluated, modifications to the spacecraft's micrometeoroid shielding or Earth swingby distance will be made, if necessary, to keep the mean Earth impact probabilities for the primary and backup missions below 10^{-6}. These modifications will come at the expense of additional propellant consumption and mission science.

D-1 Lenorovitz, Jeffrey M., “Russia May Hold Space Station Key,” *Aviation Week Space Technology*, pp. 22-24, August 23, 1993.

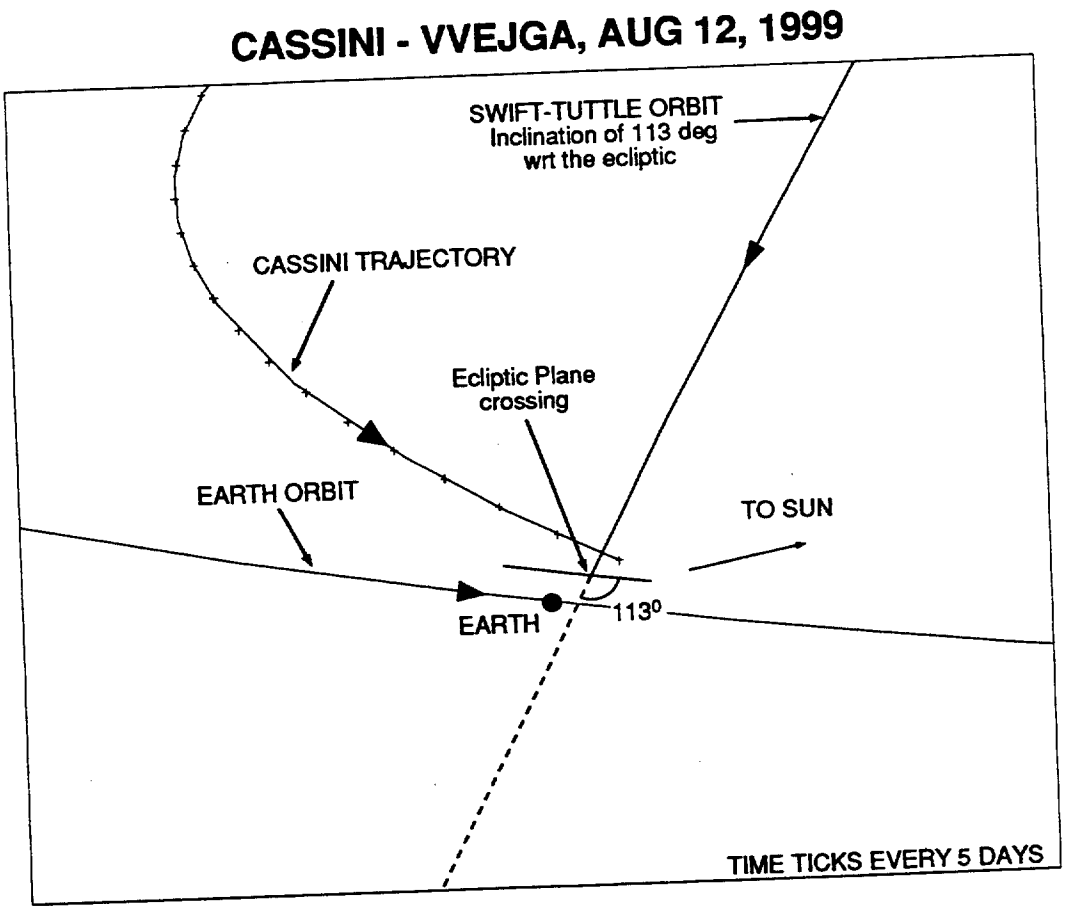

Figure D-1 Geometry Between Cassini Trajectory and Swift-Tuttle Orbit

APPENDIX E

EARTH-ESCAPE CENTAUR FAILURES

E.1 INTRODUCTION

The short- and long-term analyses in Sections 5 and 6, respectively, assume nominal injection by the Centaur upper stage. This Volume does not address the probability of Earth impact as a result of failures during the launch phase (it will be addressed as part of the total Environmental Impact Statement), but there are two potential Centaur failures which could leave the spacecraft (or possibly a Centaur/spacecraft combination) in an Earth-escape trajectory with initial conditions significantly different from the nominal injection conditions. The probability of Earth impact associated with these Centaur failures is addressed in this appendix.

The short-term probability of Earth impact due to such Centaur failures is zero, since there would be no targeted Earth swingbys to navigate for those trajectories whose injection conditions were significantly different than nominal. Therefore, only non-targeted Earth swingbys over a long-term time period are possible. The time period considered is 100 years past the nominal injection date.

E.2 METHOD

A method similar to that used to compute the long-term Earth impact probability (see Subsection 6.2) is used to compute Earth impact probability due to Centaur failures. A Monte Carlo analysis was not conducted due to its complexity and the computer resources required; instead, conservative values were assumed for these terms in order to estimate an upper bound for the Earth impact probability.

The logic diagram for Earth impact due to Centaur failure is given in Figure E-1. The two required conditions for impact are an uncommandable spacecraft (see left-hand branch of logic diagram) and satisfaction of orbit geometry and phasing requirements for Earth impact (see right-hand branch of logic diagram). The logic diagram is similar to the long-term Earth impact logic diagram discussed in Subsection 2.3 (see Figure 2-3) except that all scenarios leading to an uncommandable spacecraft involve a Centaur failure, which significantly changes the nominal injection conditions.

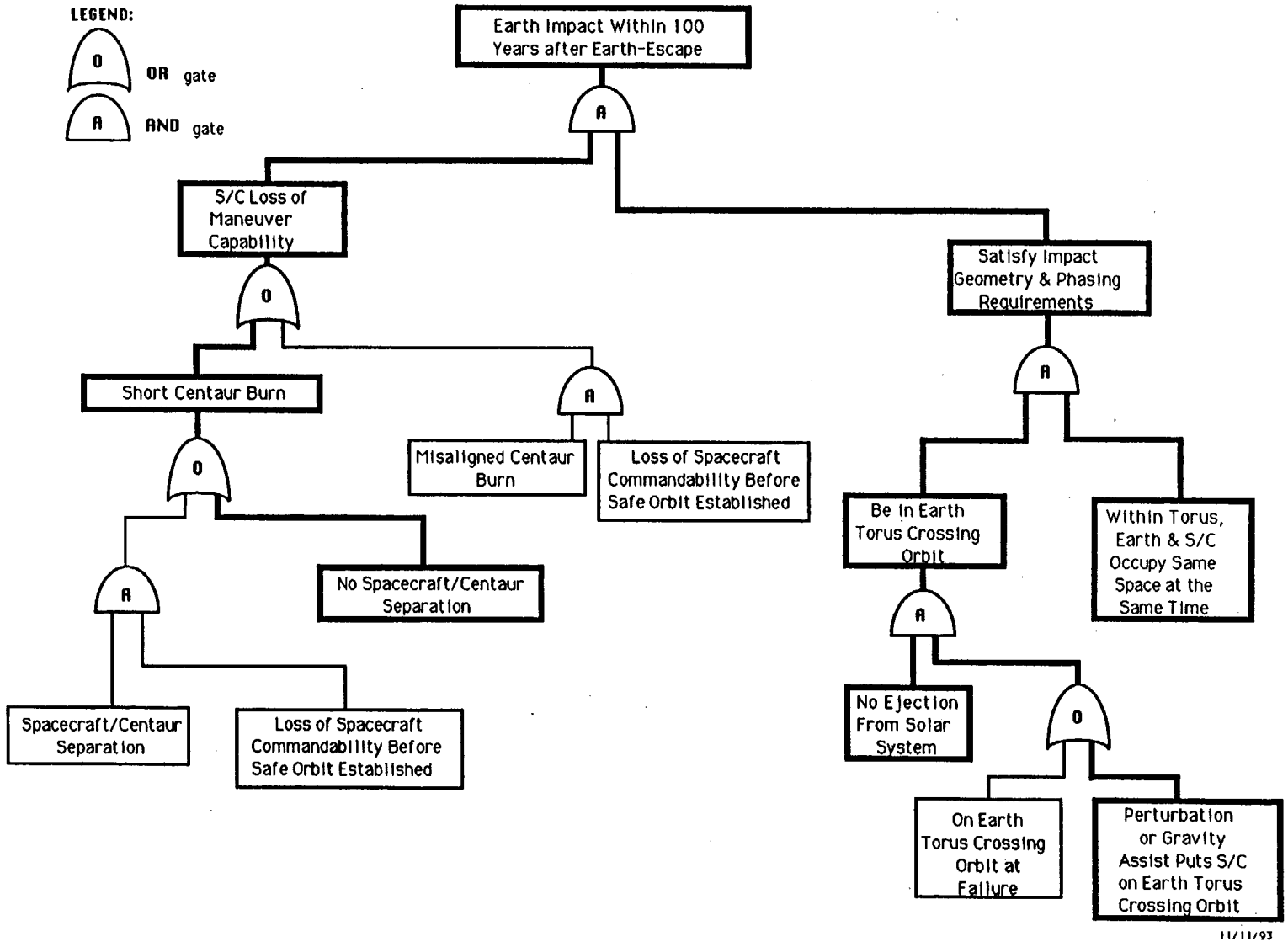

Figure E-1 Earth-Escape Centaur Failure Logic Diagram

The first Centaur failure considered is a short Centaur burn in which the flight path is nominal but the thrust is prematurely terminated. The mean probability of this failure injecting the spacecraft onto an Earth-escape trajectory is 3.2×10^{-3} (Reference E-1) The Centaur may or may not separate from the spacecraft. The probability that the Centaur will not separate from the spacecraft is assumed to be less than 0.05 for this study. Analysis is currently underway to finalize this value. Should such analysis show that this probability exceeds 0.05, the results of this appendix will be reevaluated. If the spacecraft remains attached to the Centaur, it is considered to be disabled.

If a short Centaur burn occurs and the spacecraft is commendable, the entire 3000 kg (6614 lb) bipropellant load can be used to achieve a heliocentric orbit that satisfies Earth impact protection requirements. This safe orbit scenario is therefore not included in the logic diagram (Figure E-1) since it can not lead to Earth impact. A long-term Earth impact is only possible if the spacecraft fails before a safe orbit can be established. A time period of 30 days past injection is assumed to be required to design and execute a maneuver resulting in a safe heliocentric orbit. The probability of spacecraft failure within the first 30 days is roughly 10^{-3} (see Section 4).

The second Centaur failure considered is a misaligned Centaur burn in which nominal thrust is attained but in an off-nominal direction. Separation of the spacecraft from the Centaur is unaffected. The mean probability of an Earth-escape trajectory is 4.3×10^{-5} (Reference E-1). In order for this failure to contribute to the Earth impact probability, the spacecraft must also fail within 30 days before a safe orbit can be established.

An upper bound on the mean Earth impact probability for each scenario depicted in the logic diagram (Figure E-1) is computed. The fundamental equation used to compute Earth impact probability (see Subsection 2.1) is multiplied by an additional term, P_{CF}, which models the probability of Centaur failure, to compute the impact probability for the Earth-escape cases as follows:

$$P_I = P_{CF} \, \Sigma_{FAIL} \Sigma_{TIME} \, P_F(i) \, P_{I/F}(i) \, P_{NR}(i) \qquad \text{(E-1)}$$

where

P_I = probability of Earth impact

P_{CF} = probability of Centaur failure

Σ_{FAIL} = summation over all i spacecraft failure modes

Σ_{TIME} = summation over time (~100 years)

$P_F(i)$ = probability of failure for ith spacecraft failure mode

$P_{I/F}(i)$ = probability of a resultant Earth impact trajectory given an ith spacecraft failure

$P_{NR}(i)$ = probability of no recovery given the ith spacecraft failure mode and the time to impact (=1 for long-term)

Note that $P_{NR}(i)$ is equal to 1, since only spacecraft failures that render it permanently uncommandable are considered. The $P_{I/F}(i)$ term is subdivided into further terms as shown by Equation 6-2 from Subsection 6.2. See Subsection 6.2 for detailed definition and discussion of the terms used in Equation E-1.

Since a Monte Carlo analysis was not conducted for the Centaur failures, values were assigned for the $P_{I/CRX}$ and N_{CRX}/N_{CASE} terms used to compute $P_{I/F}(i)$ (see Equation 6-2). A typical mean value of $3x10^{-5}$ was assigned to the $P_{I/CRX}$ term (see Table 6-2), and the value from a Monte Carlo analysis should be quite similar. Since an estimate of the torus crossing frequency (N_{CRX}/N_{CASE} terms) is more difficult to obtain, a conservatively high value of 1 is assumed (see Table 6-2). Therefore, a value of $3x10^{-5}$ was used for $P_{I/F}(i)$ for all cases considered.

E.3 RESULTS

An upper bound for the Earth impact probability for scenarios associated with Centaur failures is computed and illustrated in Table E-1. Scenario A in Table E-1 is a short Centaur burn in which the spacecraft separates from the Centaur. The probability of Centaur failure, PCF, is the product of the probability of a short burn, $3.2x10^{-3}$, and the probability of spacecraft/Centaur separation, 0.95.

Scenario B in Table E-1 is a short Centaur burn in which the spacecraft fails to separate from the Centaur. The probability of Centaur failure, P_{CF}, is the product of the probability of a short burn, $3.2xl0^{-3}$, and the probability of

no spacecraft/Centaur separation, 0.05. In this case, the spacecraft is uncommandable and thus $P_F(i)$ is 1. Scenario C in Table E-1 is a misaligned Centaur burn. Spacecraft/Centaur separation is unaffected in this scenario.

Table E-1 Long-term Earth Impact Probabilities Associated With Centaur Failure

Centaur Failure Scenario	P_F	P_{CF}	$P_{I/F}$	P_I
A) Short Centaur Burn Spacecraft/Centaur Separation, Spacecraft Active 30 Days	$30x10^{-3}$	10^{-3}	$3x10^{-5}$	$9x10^{-11}$
B) Short Centaur Burn, No Spacecraft/Centaur Separation, Spacecraft Disabled	$106x10^{-4}$	1	$3x10^{-5}$	$5x10^{-9}$
C) Misaligned Centaur Burn, Spacecraft Active 30 Days	$4.3x10^{-5}$	10^{-3}	$3x10^{-5}$	$1x10^{-12}$

E.4 CONCLUSIONS

For all Centaur failures which significantly alter injection conditions while still injecting the spacecraft on an Earth-escape trajectory, the probability of Earth impact within 100 years after injection is less than $5x10^{-9}$. Therefore, this result does not affect the Earth impact probability assessment. There is no short-term component to the impact probability since no targeted Earth swingbys exist for significantly perturbed injection conditions.

REFERENCES

E-1 Titan IV CRAF/Cassini Databook, MCR-91-2581, Dec. 1991, pages 10-17.

Cassini Environmental Impact Statement
Supporting Studies

Executive Summary

Volume 1 - Program Description

Volume 2 - Alternate Mission and Power Study

Volume 3 - Earth Swingby Plan

Earth Swingby Plan Supplement